Modification and experimental calibration of ADM1 for modelling the anaerobic digestion of solid wastes in demand driven applications

Davide Antonio Poggio

Submitted in accordance with the requirements for the degree of Doctor of Philosophy

The University of Leeds

School of Chemical and Process Engineering

October 2015

Declaration

The candidate confirms that the work submitted is his/her own, except where work which has formed part of jointly-authored publications has been included. The contribution of the candidate and the other authors to this work has been explicitly indicated below. The candidate confirms that appropriate credit has been given within the thesis where reference has been made to the work of others.

The work which appears in the jointly authored publications (with Davide Poggio as the lead author) appears in chapters 3, 4 and 6, the details of the publications are as follows:

> Poggio, D., Walker, M., Nimmo, W., & Pourkashanian, M. (2013). "Estimation of the kinetic model parameters of anaerobic digestion of waste materials using semi-continuous laboratory scale digesters". International Conference on Advances in Energy Research, IITB, Mumbai, India.
>
> Poggio, D., Walker, M., Nimmo, W., & Pourkashanian, M. (2013). "Model based evaluation of control strategies for the operation of anaerobic digesters in a microgrid with variable biogas demand". In: 13th World Congress on Anaerobic Digestion: Recovering (bio) Resources for the World, 25-28 June 2013

In these cases the work was directly attributable to the lead author with the co-authors performing supervisory roles in the research.

The work which appears in the jointly authored publication (with Davide Poggio as a co-author) appears in chapter 6, the details of the publication are as follows:

> Castellanos, J., Nimmo, W., Walker, M., Poggio, D., & Pourkashanian, M. (2014). "Modelling an off-grid integrated renewable energy system for rural electrification in India using photovoltaics and anaerobic digestion". Renewable Energy, 74, 390-398.

In this case the work was performed by Juan Castellanos as part of an MSc project and the role of Davide Poggio was in formulation of the original research concept and supervision and mentoring.

Acknowledgement

I would like to thank my supervisors Professor Mohamed Pourkashanian, Professor Derek Ingham and Dr Bill Nimmo for their valuable guidance, encouragement and for the appreciated independence gifted to me in exploring the pleasures and risks of research. Thanks to Dr Mark Walker for all the advices, generous support and frank discussions during the various stages and discovers we went through.

Thanks to Rokiah Yaman and the AD-LEAP team, for all the support and for the necessary perspectives to enrich scientific research.

Thanks to EPSRC for the financial support.

Conferences and publications

Journal Paper

Castellanos, J., Nimmo, W., Walker, M., Poggio, D., & Pourkashanian, M. (2014). “Modelling an off-grid integrated renewable energy system for rural electrification in India using photovoltaics and anaerobic digestion”. Renewable Energy, 74, 390-398.

Conferences

Poggio, D., Walker, M., Nimmo, W., & Pourkashanian, M. (2013). “Estimation of the kinetic model parameters of anaerobic digestion of waste materials using semi-continuous laboratory scale digesters”. International Conference on Advances in Energy Research, IITB, Mumbai, India.
[Award for second best paper]

Poggio, D., Walker, M., Nimmo, W., & Pourkashanian, M. (2013). “Model based evaluation of control strategies for the operation of anaerobic digesters in a microgrid with variable biogas demand”. In: 13th World Congress on Anaerobic Digestion: Recovering (bio) Resources for the World, 25-28 June 2013

Poggio, D., Walker, M., Nimmo, W., & Pourkashanian, M. (2015) “Integration of AD into microgrid”. The AD Network Early Career Researcher Event. Warwick University 29/30th June 2015

Abstract

This thesis is an exploration into the modelling of anaerobic digestion (AD) with a focus on its integration into a microgrid for rural electrification. The work investigated the improvement of Anaerobic Digestion Model No 1 (ADM1) in order to better describe the kinetics of biogas production in an AD system with particular focus on substrate characterisation, codigestion and the mechanisms of inhibition. The resulting model was used to investigate the possible role of AD in microgrid systems.

A novel biochemical and kinetic fractionation method was developed in order to fully characterise any substrate and produce the required input parameters into the a modified version of ADM1. The method uses a combination of analytical and digestion batch tests and was applied to food waste, green waste, pig manure and oat processing residues. The fractionation method was validated using measurements from semi-continuous laboratory scale digesters, operated with varying substrate combinations and loading rates. The model was able to suitably predict the methane production rate and the typical off-line measurements in AD systems, except during periods of high organic loading rate where biochemical inhibition became an important phenomenon. Possible inhibiting mechanisms were investigated by model based analysis of the experimental data characterised by inhibition, and a possible inhibition mechanism was proposed and integrated in the ADM1 model.

Microgrid modelling software HOMER was used alongside the updated version of ADM1 in order to perform a benchmark of various operational and control strategies for the demand-driven operation of an AD system integrated in a microgrid. Different biogas demand profiles were considered. In the case of a biogas demand profile with low variability it was found that simple operational strategies could be used, with limited required biogas storage buffer and without causing process instabilities. With more variable demand profiles, an expert control system was needed in order to reduce the biogas storage requirements and guarantee process stability.

Table of Contents

List of Figures

List of Tables

Nomenclature

Symbols

Alk_{IC}	Alternative notation for partial alkalinity (PA)
Alk_{IC}	Alternative notation for partial alkalinity (IA)
C_i	Carbon content of biochemical fraction (i) in ADM1
C_i	Generci concentration term
$C_nH_aO_bN_c$	General chemical formula for organic matter
$CH_yO_zN_v^u$	General chemical formula for organic matter (alternative)
f	Stoichiometric yield (general)
$f_{x,y}$	Stoichiometric yield of substance y from substance x
f_{ch}	Protein/amino acid fraction of f_d
f_d	Degradable fraction of substrate
f_{li}	Lipid/fat fraction of f_d
f_{pr}	Protein/amino acid fraction of f_d
f_s	Soluble fraction of f_d
f_{Xr}	Readily degradable fraction of f_d
i	Integrated gain (of controller)
I	Inhibition factor or function
$I_{in,Ci}$	Inlet loading of component C_i
K_a	Acid base dissociation constant
k_{CNT}	Contois maximum uptake rate
k_{dis}	Disintegration constant
k_{hyd}	Hydrolysis constant for particulate fraction
K_H	Henry's constant
K_I, K_i	Inhibition constant (general)
$K_{I,x,y}$	Inhibition constant (of species x on process y)
k_La	Gas liquid transfer rate
k_m	Monod maximum uptake rate
K_s	Monod saturation constant
$K_{s,CNT}$	Contois saturation constant
lb	Loading bias (of controller)
N_i	Nitrogen content of biochemical fraction (i) in ADM1
N_{org}	Organic Nitrogen
p	Proportional gain (of controller)
P	Volume of methane
P_0	Specific methane potential of substrate

pHs	pH safety point
p_{gas}	Partial pressure of gas
p_{kW}	Dissociation constant for water
Q_{in}	Volume flow rate at inlet
Q_{out}	Volume flow rate at outlet
R^2	Coefficient of determination
rAE	Relative absolute error
S	Soluble substrate concentration
$sc_{k,l}$	Scaling factor applied in multivariate estimation
t_{res}	Difference in residence time of solid and liquid fractions
V_R	Digester working volume (liquid)
X	Particulate substrate concentration as per ADM1
X	Microorganism concentration as per ADM1 (subscript is substrate)
y_m	Generic measured data point
y	Generic data point (model)
α	Charge per unit COD for ionic balance
χ^2	Chi-Squared (sum of square of residuals)
ρ	Biochemical reaction rate
ρ_T	Gas-liquid transfer rate
σ	Mean

Subscripts

Notes;

1. In some cases, e.g. using certain software packages, subscripts were unavailable and therefore alternative notations denoting subscripts were used e.g. either _ or lower case letters. As an example the following terms should be considered equivalent throughout: $X_{ch,}$ X_ch and Xch.
2. Multiple subscripts are often used to uniquely describe a parameter or variable which should be self-explanatory e.g. $K_{a,ac}$ refers to the acid base dissociation constant (K_a) of acetic acid.
3. Subscripts which are a standard chemical formula or a whole word descriptor are not listed since their usage is clear.

a	Molar hydrogen in $C_nH_aO_bN_c$
aa	Amino acid (soluble)
ac	Acetic acid

acid	Acidogenic processes
an	Anion
b	Molar oxygen in $C_nH_aO_bN_c$
biomass	Microorganisms (i.e. X_{ac}, X_{pro}, X_{c4}, X_{aa}, X_{fa}, X_{su}, X_{h2})
bu	Butyric acid
c	Composite organic matter (from biomass decay)
c	Molar nitrogen in $C_nH_aO_bN_c$
cat	Cation
ch	Carbohydrate (particulate)
CNT	Contois
dis	Disintegration
fa	Fat (soluble)
hyd	Hydrolysis
I	Inert (non-biodegradable)
IC	Inorganic carbon (CO_2 + HCO_3^- + CO_3^{2-})
in	Inlet, influent
IN	Inorganic nitrogen (NH_3 + NH_4^+)
ini	Initial (initial conditions of simulation or experiment)
li	Lipid (particulate)
m	Monod (as in k_m denoting Monod maximum uptake rate)
n	Molar carbon in $C_nH_aO_bN_c$
out	Outlet, effluent
pr	Protein (particulate)
pro	Propionic acid
r	Readily degradable fraction
s	Slowly degradable fraction (as in $k_{hyd,s}$)
S	Saturation (as in k_S denoting Monod saturation constant)
su	Sugar
va	Valeric acid

Acronyms/abbreviations

AA	Amino acids
ADM1	Anaerobic Digestion Model no. 1
BCA	Bicinchoninic acid
COD	Chemical oxygen demand
COE	Cost of electricity
DSM	Demand side management

FW	Food waste
GSA	Global sensitivity analysis
GW	Green waste
HRT	Hydraulic retention time
HVFA	Undissociated volatile fatty acids
IA	Intermediate alkalinity
IC	Ion chromatography
ISR	Inoculum substrate ratio
IWA	International Water Association
LCFA	Long chain fatty acids
LOLP	Loss of load probability
MS	Monosaccharides
MT	Microturbine
NPC	Net present cost
OAT	Oat processing residues
OFMSW	Organic fraction of municipal solid waste
OLR	Organic loading rate
PA	Partial alkalinity
PM	Pig manure
PV	Photovoltaic(s) (shorthand for PV panels)
STP	Standard temperature and pressure
STR	Scientific and Technical Report
TAN	Total ammoniacal nitrogen
thOD	Theoretical oxygen demand
TOC	Total organic carbon
TKN	Total Kjeldahl Nitrogen
UASB	Upflow anaerobic sludge blanket
TS	Total solids
TSS	Total suspended solids
VFA	Volatile fatty acids
VS	Volatile solids
VSS	Volatile suspended solids
X	Single particulate substrate fractionation mode
XS	Single particulate and soluble substrate fractionation model
XX	Two-particulate substrate fractionation model
XXS	Two-particulate and single soluble substrate fractionation model

1 Introduction

Anaerobic digestion (AD) is an energy technology which converts organic matter to a methane-rich biogas through the action of a microbial community (Batstone and Jensen, 2011). The AD process has received much attention due to its ability to convert a variety of organic feedstocks, which would pose challenges for thermal conversion technologies due to the moisture content, to a gaseous biofuel. One novel application of AD is in rural electrification in the developing world and this idea was developed by the research project BioCPV[1] as part of the BURD (Bridging the Urban and Rural Divide) program: a joint UK/India initiative that aims to address the challenge of poverty reduction in rural regions of India.

Decentralised hybrid power plants with different renewable technologies can provide efficient, cheap and sustainable options for rural electrification (Bajpai and Dash, 2012, Gao et al.) and the main concept of the BioCPV project was to develop such a system with the capability to meet the energy needs of an off-grid community in rural India. The proposed system included concentrating photovoltaics (CPV) and AD in order to use the main energy resources available locally, sunlight and biomass, and is shown in figure 1.1 (Astals et al., 2013). The work presented in this thesis forms part of the BioCPV project, and focuses on the role that AD can play in small scale microgrid systems and the associated challenges that this may present.

1.1 Microgrid energy systems and AD integration

Generally, a microgrid is a combination of the following elements:

- a set of dispatchable generators (ie. generators that can be turned on or off or can adjust their power output in a relatively short amount of time, such as turbines, reciprocating engines, fuel cells) and non-dispatchable generators (ie. generators whose electrical output is not continuously available due to factors outside direct control, such as wind turbines, PV and wave energy converters).
- electrical and thermal energy storage.
- heat and electrical local distribution infrastructure.

[1] See biocpv.ex.ac.uk for more information.

- a connection with the macro-grid for import and export of electricity.
- a control system for the operation of the microgrid.

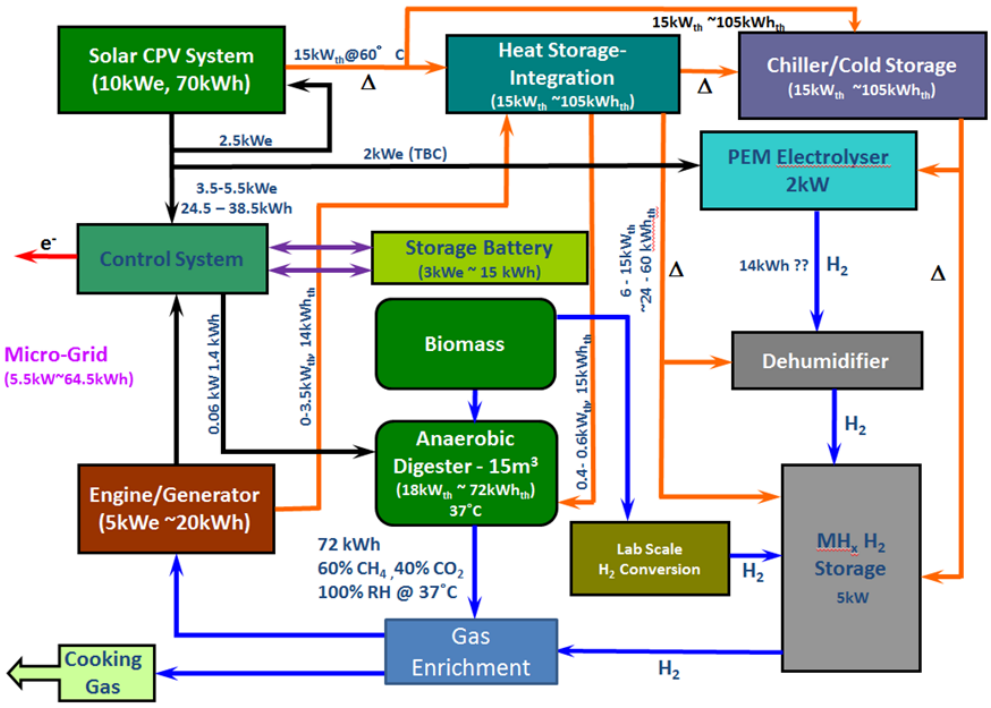

Figure 1.1 Schematic of the proposed BioCPV off-grid energy system, from Mallick et al. (2013).

Microgrids allow power quality and reliability, sustainability and economic benefits and may run continuously in off-grid or on-grid mode, as well as in dual mode by changing the grid connection status. When operated in grid-connected mode, the micro-grid can import deficit and export excess electricity to the macro-grid. The operation in island mode (ie. in isolation from the national or local electricity distribution network) is more challenging, because electricity demand must be met exactly and any excess electricity production would be dumped with clear economical inefficiencies. Island operation mode is typical for electrification of rural villages and remote regions (Kanase-Patil et al., 2010), and therefore in this thesis it is considered as the principal mode of operation for a micro-grid.

The integration of wind and solar generation into a microgrid poses some technical challenges, principally for their intermittency. Intermittency comprises two separate elements: non-controllable variability and partial unpredictability (Pérez-Arriaga and Batlle, 2012). There are various approaches to match energy demand and supply, when considering autonomous systems with a high penetration of intermittent renewable energy technologies (Delucchi and Jacobson, 2011, Rae and Bradley, 2012):

- The use of demand side management (DSM) and control techniques whose aim is to alter the characteristics of the demand profile according to the generated energy profile.
- The use of energy storage systems which store excess energy when supply exceeds demand, for later use.
- The integration of variable energy sources (such as wind and PV) with non-variable energy sources (hydroelectric, biomass, etc.).
- The increase in the dispatchability of the system, i.e. the ability of the system to increase and/or decrease output quickly following demand variations.
- The forecast of the weather and therefore of the future energy supplied by the variable energy sources, in order to better plan the operation of the system.

In the context of the BioCPV project, DSM is not addressed and the focus is put on storage and energy sources integration. In this regard, the integration of an AD system into a renewable-based micro-grid presents specific advantages and challenges:

- The renewable energy produced by AD (biogas) can be stored in a cost-effective way, e.g. in a low pressure gasometer (see Figure 1.2).
- The storage of biogas permits the system to be dispatchable, i.e. to respond quickly to demand variations (limited by the amount of biogas stored and the dynamics of the engine-generator set).
- The AD system can be considered as a non-variable system, i.e. its production of biogas can be predicted within a small range of variation.

Figure 1.2 Biogas storage gasometer with capacity 20 m^3 installed as part of BioCPV project

The operation of the engine-generator set has to cope with more cycling to compensate for the fluctuations in the intermittent generation: on/off operation, low-load cycling operations and load following (Pérez-Arriaga and Batlle, 2012). Depending on the technology adopted for the engine-generator set, higher maintenance expenditures and increased wear and tear, with respect to base-load operation, could be a consequence.

AD systems can compensate energy fluctuations in two ways:

- In the short term (hours), using the biogas that has been stored in the external storage.
- In the long term (days), changing the loading rate of the digester in order to increase the biogas produced and restoring the biogas reserve in the external storage. Change in the loading rate can be realized by an increase in the mass loading rate or by a change in the composition of the feed, allowing a higher ratio of degradable and energy-rich substrates (Hahn et al., 2014).

The relative importance of these two strategies (biogas storage and change in loading rate) depends on the characteristics (length and amplitude) of the fluctuations that the AD system needs to compensate: eventually it is possible to imagine a storage that is big enough to compensate the fluctuations while the AD reactor is run at steady state.

When changing the organic load to the AD plant, challenges regarding the stability of the plant after changes in the loading rate or composition of the feedstock become important. The AD process is based on a multistep process, where the rate of formation of organic acids (hydrolysis and fermentation) must be in balance with the rate of consumption of acids by methanogenesis. When the production of acids exceeds the capacity of the methanogenic conversion, the pH drops and the reactor acidifies (Figure 1.3). This phenomenon requires a reduction in the loading rate of the digester, or in extreme cases even the emptying of the digester and a new start-up with fresh inoculum and substrate: both processes represent a high cost for the AD plant owner and that is why digesters are usually operated with a low-risk strategy, far from the theoretical optimum.

Control systems can be used to determine the state of the digester, therefore allowing the operator to optimize the loading rate with higher probabilities of improving the performance of the plant. However, control systems for optimization

of the plant operation require a certain degree of sophistication. As previously stated, AD process are affected by changes in loading rate and substrate composition, but the effect on the process (the gain, in control terminology) is dependent on the type, magnitude, duration and frequency of the change (Leitao et al., 2006). Anaerobic systems have large time constants when operated at a stable steady state point; however they react faster (shorter time constant) and are highly non-linear when operated in dynamic mode out of steady state points and close to overload conditions.

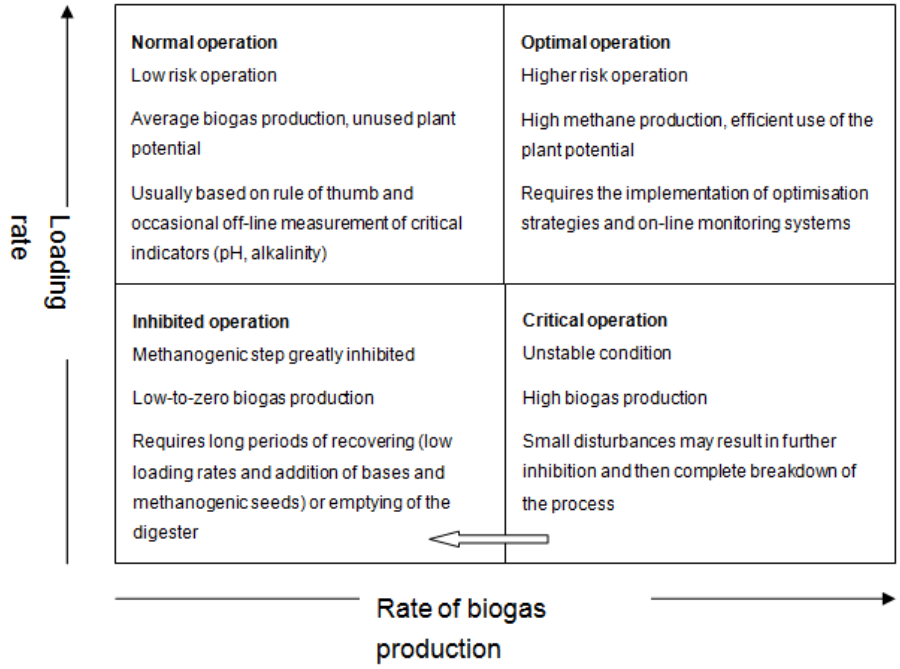

Figure 1.3 Different operational states in AD plants.

1.2 Anaerobic digestion modelling

In order to address the issues of the integration of AD into a microgrid system, such as that proposed in the BioCPV project, including its flexible operation and biogas demand matching and codigestion of different available biomass feedstocks, modelling for process analysis and evaluation is used in this thesis. For a model to be useful in this scenario it must have the following characteristics:

- To allow good characterisation of solid biomass feedstocks relating to their biochemical composition and degradation behaviour in an AD system, and allow the simulation of their codigestion.

- To reproduce accurately the important process kinetics, such as degradation of the biomass feedstock and biogas production such that demand matching on short timescales can be assessed.
- To give reliable prediction of process stability, mainly focussing on instabilities and/or inhibition caused by fluctuations in organic load when attempting to match a particular biogas demand.

Almost all current research into AD process modelling involves the use of the International Water Association (IWA) Anaerobic Digestion Model No. 1 (Batstone et al., 2002) with the subsequent improvements and modifications made by Rosen and Jeppsson (2006). There have since been hundreds of published journal articles that use, adapt or develop ADM1, including its application to a wide variety of substrates, as a tool for optimisation, and its modifications to specific situations or substrates (Lauwers et al., 2013). In fact particular focus has been on modelling the AD of solid substrates (Mairet et al., 2011, Galí et al., 2009, Ramirez et al., 2009) and distributed parameter versions have been developed for particular situations (Mu et al., 2008).

Despite many developments, there are still topics that require more research work and that have specific relevance to the work in this thesis:

- A recent review identified that feedstock characterisation for use as model inputs was still a bottleneck to a broader adoption of ADM1, with more work being required on this topic (Batstone et al., 2015). While some methods do exist for characterisation, they are still not well developed or generally adopted.
- In another review paper, Mata-Alvarez et al. (2011) identified that there were relatively few research papers that explored the issue of anaerobic codigestion, where a mixture of substrates are digested together.
- A third review paper, exploring the various inhibition causes and effects in AD processes (Chen et al., 2008), highlights the deficiency of this part of ADM1 in which only a handful of the inhibition mechanisms are included.

Meanwhile there is a growing area of study surrounding the benchmarking of operational and control strategies for biological systems which is fairly mature for wastewater treatment (Mottet et al., 2013), but it is still relatively undeveloped for AD systems, with only a few studies so far (Alferes, 2012, Alferes et al., 2012, Batstone and Steyer, 2007).

1.3 Aims and objectives

From the identified requirements and deficiencies of AD models, and considering the demand driven operation of an AD system integrated into a microgrid, the following aims of this research can be formed:

AIM: To improve the capabilities of ADM1 in order to use it as a tool for the analysis and design of operational strategies of an AD system integrated into a microgrid energy system.

In order to fulfil the aim a number of objectives have been defined as follows:

1) To develop a methodology which allows characterisation of any substrate for its input into ADM1.
2) To assess different ADM1 substrate degradation mechanisms, which allow accurate description of the biogas production kinetics from the characterised substrates from 1).
3) To use the method from 1) and the updated model developed in 2) to assess the capability of ADM1 to predict the output of an AD system fed on a different substrates with temporal variations in codigestion mixtures.
4) To use experimental data to assess the possible mechanisms for inhibition that are relevant to AD systems with fluctuating/intermittent loading rates and to incorporate them into the updated version of ADM1 from 2)
5) To use the updated version of ADM1 from 4) to performed *in silico* assessment of the performance of an AD system in a hypothetical microgrid energy system with regards to operational strategies, potential control systems and reactor designs.

1.4 Thesis structure

The subsequent content of this thesis is split into the following chapters:

- Chapter 2 Literature review – This section is a review of the important literature regarding the AD process and AD process modelling, including the biochemical and physiochemical aspects. It goes on to discuss the input data requirements of ADM1 and existing methods of how this data can be obtained.
- Chapter 3 Methodology – In this section the methods used throughout chapters 4-6 are described. Both the modelling and experimental

approaches are described. The chapter goes on to describe the development of the methodology for substrate characterisation (both biochemical and kinetic) **(Objective 1)** and how the codigestion process is managed from a modelling perspective.

- Chapter 4 Substrate fractionation – This chapter presents and discusses the results from the substrate biochemical and kinetic fractionation based on both batch and continuous experimental results **(Objective 1)**. Different substrate degradation model structures, within ADM1, are compared and discussed **(Objective 2).**
- Chapter 5 Codigestion and inhibition modelling – The first half of this chapter includes results and discussion of the codigestion experimental and modelling work, including the assessment of the modified ADM1 model to accurately describe codigestion **(Objective 3)**. Inhibition mechanisms are explored in the second half of this chapter, including selection of the most important inhibition functions **(Objective 4)** for inclusion in the updated ADM1 model for use in Chapter 6.
- Chapter 6 Modelling microgrid energy systems containing anaerobic digesters – This chapter includes the modelling of the microgrid energy system in HOMER and goes on to assess (*in silico*) a variety of operational strategies and control systems to allow an AD system to meet the biogas demands of the microgrid **(Objective 5)**.
- Chapter 7 – Conclusions and future work.

2 Literature review

2.1 The AD process

Anaerobic digestion (AD) is a complex process carried out by a consortium of different microorganisms. During the process, biodegradable organic substrate is converted to methane, carbon dioxide and biomass; organic nitrogen and sulphur are reduced to ammonia and sulphides respectively. It occurs naturally in environments such as such as landfills, rice fields, sediments, and intestinal tracts of animals where light and inorganic electron acceptors (oxygen, nitrate, sulphate, iron, etc.) are not present or limiting (Angelidaki et al., 2011). In contrast to aerobic processes, where the reactions are driven by the presence of oxygen as an external electron acceptor, anaerobic digestion processes are driven by the presence of internal electron acceptors: gaseous and dissolved products (mainly methane and carbon dioxide) have the same combined carbon-oxidation state as the primary substrates (Batstone and Jensen, 2011).

The microbial ecology present in a digester is complex and consists of a sequence of interrelated reactions (Batstone and Jensen, 2011):

1. Hydrolysis, during which biopolymers are solubilised by extracellular enzymes.
2. Acidogenesis, during which soluble substrate such as sugars and amino acids are converted through fermentation largely to organic acids and alcohols.
3. Acetogenesis, during which fermentation products are converted to acetate and hydrogen using hydrogen ions or bicarbonate as electron acceptors.
4. Homoacetogenesis, during which hydrogen is used to reduce carbon dioxide to acetate, and its reverse reaction which oxidise acetate to carbon dioxide and hydrogen.
5. Hydrogen-utilising methanogenesis (hydrogenotrophic), during which hydrogen and formate are converted with carbon dioxide to methane.
6. Acetoclastic methanogenesis, during which acetate is cleaved to form methane from the methyl group and carbon dioxide from the carboxyl group in a fermentation reaction.

Acetogenic reactions occur due to a syntrophic relationship with hydrogen-utilising organisms (Figure 2.1): interspecies hydrogen transfer between these two groups maintains hydrogen concentration to a level that is thermodynamically favourable for the occurrence of acetogenic reactions (Schink, 1997). Homoacetogenic reactions have usually minimum impact in mesophilic reactors and therefore are neglected in most AD models (Batstone et al., 2002). However in certain conditions, such as with inhibition of hydrogenotrophic methanogenesis in biohydrogen production (Siriwongrungson et al., 2007) and in psychrophilic conditions (Conrad et al., 1989), or with ammonia inhibition of acetoclastic methanogenesis (Schnürer and Nordberg, 2008), the homoacetogenic rate increases and its impact should be considered.

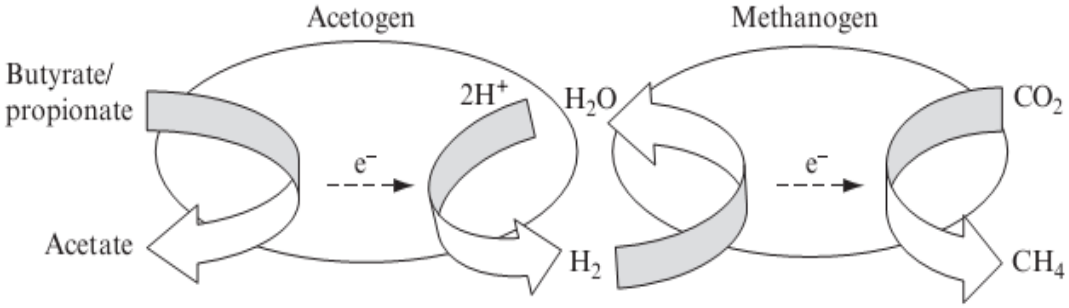

Figure 2.1. Syntrophic relationship between acetogenic and hydrogen-utilising microorganism. Adapted from Angelidaki et al. (2011).

Depending on the feedstock characteristics, and on the initial conditions in batch operation, a rate limiting mechanism, which kinetically limits the production of methane, can usually be identified (Donoso-Bravo and Mairet, 2012). The most common controlling mechanisms are hydrolysis and methanogenesis, and on this basis a simple classification of anaerobic systems is often proposed (Batstone and Jensen, 2011):

- Methanogenesis controlled systems. This apply to systems that are fed mostly with soluble substrate or where the resulting buffering is poor: the rate of methane production is limited by the growth rate of methanogenic microorganisms. A decrease in the performance of the system is indicated by an increased concentration of volatile fatty acids (VFA) in liquid phase and of H2 in the liquid and the gas phase; severe reductions of pH and gas flow indicates process failure.

- Hydrolysis controlled systems. This applies to systems that are fed mostly with particulate substrate and where the release of ammonia from protein degradation ensures a robust buffering system. The rate of methane production is limited by the hydrolytic solubilisation of particulate matter; the rate of methane production is therefore governed by the retention time of solids in the system. The poor performance is indicated by an increase of solids concentration in the effluent.

In some cases this classification is not straightforward, as in the case of particulate substrates which contain/produce inhibitory compounds of the methanogenic steps (e.g. manure which can often produce ammonia inhibition). In this case a more complex modelling of the process can assist in the analysis and design of the AD system. Further details about the AD processes and biochemistry is included in Section 2.3, where the AD modelling is described.

2.2 Reactors for AD

Several configurations exist for the engineering and designing of the reactors for anaerobic digestion (Figure 2.2): anaerobic digesters can differ depending on their loading regime, temperature of operation, solids content in the reaction phase, spatial separation of the digestion stages, flow characteristics and mixing, differential retention time for the biomass, etc. These configurations may be combined between them and therefore many different AD reactors can be devised and implemented (Table 2.1).

The selection of the reactor type depends primarily on the characteristics of the influent, mostly its solids content and the relative abundance of soluble to particulate solids. A rough classification can be made between (1) reactors which treat mostly soluble wastewaters and must provide beneficial conditions for the methanogens, and (2) reactors that treat particulate substrate and must provide beneficial conditions for the efficient solubilisation of the substrate.

In the context of the BioCPV project, the selection of the reactor configuration was taken after the assessment of the substrate availability and on the basis of other context specific characteristics. Given the high moisture content of some of the proposed substrates (aquatic weed and manure), and the local available expertise, a wet mixed tank was finally proposed.

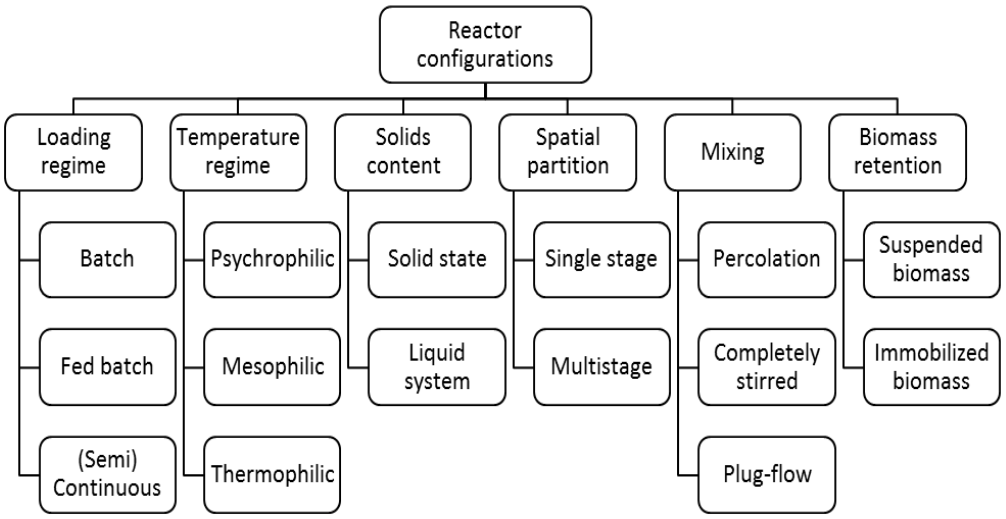

Figure 2.2 Schematic of different reactors configuration.

2.2.1 Design of AD reactors

Empirical, recommended values for design of AD reactors are available for common substrates whose composition can be assumed fairly constant across different systems: for instance, recommended values for manure can be found in Wellinger (1999), while for sewage sludge recommended values can be found in wastewater reference texts (Tchobanoglous et al., 2003). These values ensure low-risk operation of the digester with an average methane yield of the substrate.

In the simplest modelling approach, the process dynamics is approximated with the rate-limiting concept; then the respective kinetics is selected and calibrated (usually first-order for hydrolysis limited and Monod for methanogenic limited). A mass balance around the digester provides the equations for the temporal evolution of the substrate and biomass in the system; it is then possible to optimize the operational parameters (e.g. retention time, temperature, recycle ratio) with respect to the selected indicators of performance in steady state (e.g. volumetric productivity of the digester, substrate removal efficiency, etc.). The minimum retention time to avoid wash out can also be calculated, usually taking into account a safety factor. The described approach can be found in environmental engineering reference texts (Rittmann and McCarty, 2001).

Technology	Principle	Advantages	Disadvantages	Max OLR kg COD m^{-3} d^{-1}
High rate digester	Biomass is retained in the reactor through granules formation or attachment to carriers	High OLR Low footprint Low capital cost Resilient to shocks Low strength effluent	Clogging or malfunctioning when particulate is present in the influent Long start up time	10-15
Anaerobic pond	Large retention time in unmixed lagoons	Low capital cost Technological simple and robust	High footprint Low degassing effect Low OLR Needs periodic desludging	0.1
Mixed tank	Dilution to 3-6% and continuous feed into an agitated tank	Established technology Continuous gas production A good degree of control is possible	Effluent is in liquid form and might need dewatering High consumption of energy Expensive tanks	1-3
Liquid plug flow	Influent solids concentration around 15%	High loading rates Continuous gas production	Poor contact between substrate and biomass Liquid effluent	5
Batch solid state	Solid concentration higher that 15%. System is loaded, enclosed, and leachate circulated over the solid bed.	Very high loading rates Pre-treatment requirement of biomass is lower Solid digestate	Gas production is non- constant Loading and unloading of substrate can be cumbersome Difficulty in sealing properly the reactors Conversion of the substrate may be lower	6-10
Solid state plug flow	Solid concentration higher that 15%. Continuous feed, with leachate or effluent recirculation as inoculum	Very high loading rate Continuous gas production Solid digestate	Very high capital cost Complicated mechanical system	10

Table 2.1 Anaerobic digestion technologies, adapted from Batstone and Jensen (2011) and Nizami and Murphy (2010).

The rate limiting approach fails when more complex substrates, which contain both easily and slowly degradable components, are fed to the digester; or when highly dynamics operations could be expected. In this case a more complex and dynamic process modelling is required.

2.3 Modelling and simulation of AD

A mathematical model is a set of one or more equations that describe the input/output transformation of a system, for the purpose of understanding, predicting or communicating the system behaviour. Generally, a mathematical model can be classified as empirical (black-box) or mechanistic (white-box) model. A black-box model is an empirical model based on an experimental data set and which is able to represent the apparent relationship between input and output of a system. For instance, in an AD process, a simple relationship between the substrate influent flow and the biogas production rate can be considered as a black-box model. The generality of a black box model depends on the amount of and type of experimental data; model applications are usually limited to small changes in the operational parameters and plant inputs. They can be used for formulating rule of thumbs for design and operation.

A white-box mechanistic model is a mathematical description of a system in terms of its constituent parts and mechanisms. For example, in anaerobic digestion, the main constituents are the substrate, the microbial biomass and the reactor volume and headspace, substrate and gas flows, while the main mechanisms are microbial growth and heat and mass transfer. Mechanistic models are built on deterministic principles, which permit the prediction of future system states based on the given initial conditions.

Mechanistic models usually offer better extrapolation capabilities than empirical models. Extrapolation capabilities are essential in process modelling, where it is important to investigate the process performance under different operating conditions. Different process scenarios can be simulated *in silico*, and at a later stage extra data can be collected to validate the most promising scenarios from the simulation (Gernaey et al., 2010). Mechanistic models can also be seen as methods for structurally and systematically collecting and storing process knowledge obtained at laboratory, pilot and full scale.

In this thesis, mechanistic models are prevalently used for the design of the AD process and the simulation of scenarios with different control and operational strategies. Black box models could be used to map the input - (state of the system) - output relationship of the experimental full-scale plant and then using this map as an input for the control of the plant. For instance, Gaida et al. (2012) used advanced pattern recognition techniques to predict the state of the system from basic online measurements of the outputs (such as biogas production, CH_4 and CO_2 content in the biogas, pH value) and of the input (mass flow of different substrates). In this case, the black box was trained using synthetic data created with a mechanistic model simulating over a wide range of possible plant operating regions, thus showing an interesting combination between mechanistic and empirical models.

2.3.1 Models for anaerobic digestion

The modelling of AD processes is particularly challenging, given its intrinsic characteristics:

- Multiple reactions, occurring in series and in parallel, mediated by different groups of microorganisms.
- Feedback relations between the physicochemical and biological system
- Highly non-linear behaviour, in particular of the pH regulation and microbial inhibitions.
- Temporal adaptation of the biomass to the reaction conditions, with resulting changes in the observed activity rates (Palatsi et al., 2010). Living cells are in fact able to alter the rate and the nature of their biochemical reaction to maintain their homeostasis after changes in the environment.
- Difficulty in collecting experimental data to describe the state of the process (e.g. biomass concentration).

The structure and complexity of a mathematical model is principally dictated by its purpose definition, which represents the first step in the model building (Table 2.2).

AD models can be classified based on their complexities, i.e. on the number of reactions and phenomena they take into account in their structure. A review on the history of AD modelling with detailed description of the different model structures can be found in Gavala et al. (2003). In general the models have differences related to:

- The number of biomass groups.
- The number of steps and intermediates: from limiting step (usually hydrolysis or methanogenesis) to multistep.
- The form of kinetic laws inhibition functions adopted.
- The inclusion of physicochemical processes.
- The characterisation of substrate: from dedicated models (e.g. for manure or sewage sludge) to generic models (with fractionation in biochemical compounds: protein, lipids, carbohydrates, VFAs and inerts).

Purpose and context	**Application**	**Model characteristics**
Process design	Design of a new, full scale system.	A validated parameter set for a similar process is needed. Hydraulic and particle behaviour is required.
Analysis and improvement of existing system	Optimization of the operational parameters of an existing system.	The required parameter set has to be sourced directly from the process. The model needs to describe the mechanisms that are influenced by the investigated operational parameters.
Technology development	Development and assessment of new specific applications (mixing system, substrate pre-treatment, inoculum efficacy, etc.).	The model needs to include detailed mechanistic relationships relative to the investigated applications (e.g. impact of the mixing system on mass transfer).
Model based control	Development of a control algorithm.	The model tends to be minimal, with many approximations, including only relevant variables for control.
Control and operation system benchmarking	*In silico* testing and evaluation of new control hardware and operational strategies.	Complex and realistic models are required, including intermediate species, inhibition, nonlinear kinetics.

Table 2.2 Overview of different models characteristics and purposes. Adapted from Batstone et al. (2006).

As a response to the need of a standard model, the IWA Task Group for Mathematical Modelling of Anaerobic Digestion developed the generic Anaerobic Digestion Model No. 1 (Batstone et al., 2002), which would allow a common basis for further model development and comparison of different studies. In its original version, the model describes the dynamics of 7 biomass groups, 12 soluble compounds, 5 particulate compounds, interrelated by 19 biochemical kinetic processes, 7 physicochemical equilibrium processes, and 3 gas-liquid mass transfer processes. The high number of parameters, and therefore the related identifiability problem, is the major criticism for such a structured model. One of the interesting peculiarities of the ADM1 is that it allows the description of the relations between the biochemical, physicochemical and hydraulic processes that occur in an anaerobic digester, such as:

- Biochemical reactions produce weak acids and bases that modify the pH of the liquid phase.
- High and low pH values inhibit the biological activity.
- The undissociated form (function of the pH) of certain products such as ammonia and hydrogen sulphide, has inhibitory effects on biological activity.
- Gas-liquid interactions between the headspace and liquid phase of a reactor.
- Biochemical reactions produce gases whose transfer to the gas phase is influenced by the hydrodynamics conditions.
- Low mixing or high solids content can limit the mass transfer rate in the liquid phase, thus limiting the overall degradation rate.

Figure 2.3 shows the classification of the main influential processes for AD and under this framework they are described in the next sections. Figure 2.4 gives a “map” of the principal reactions considered in ADM1.

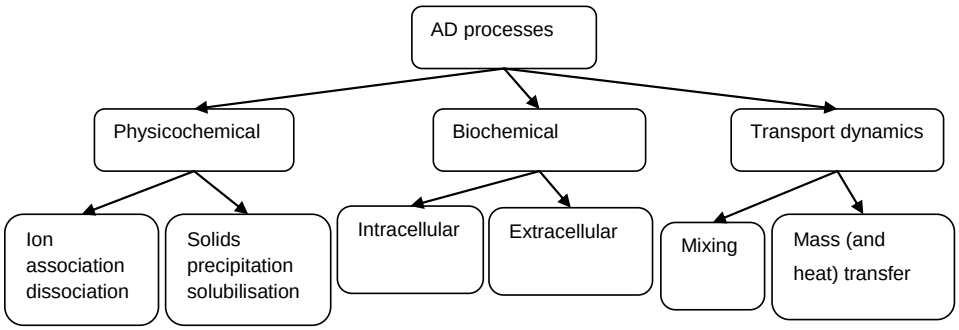

Figure 2.3. Principal processes considered for AD modelling

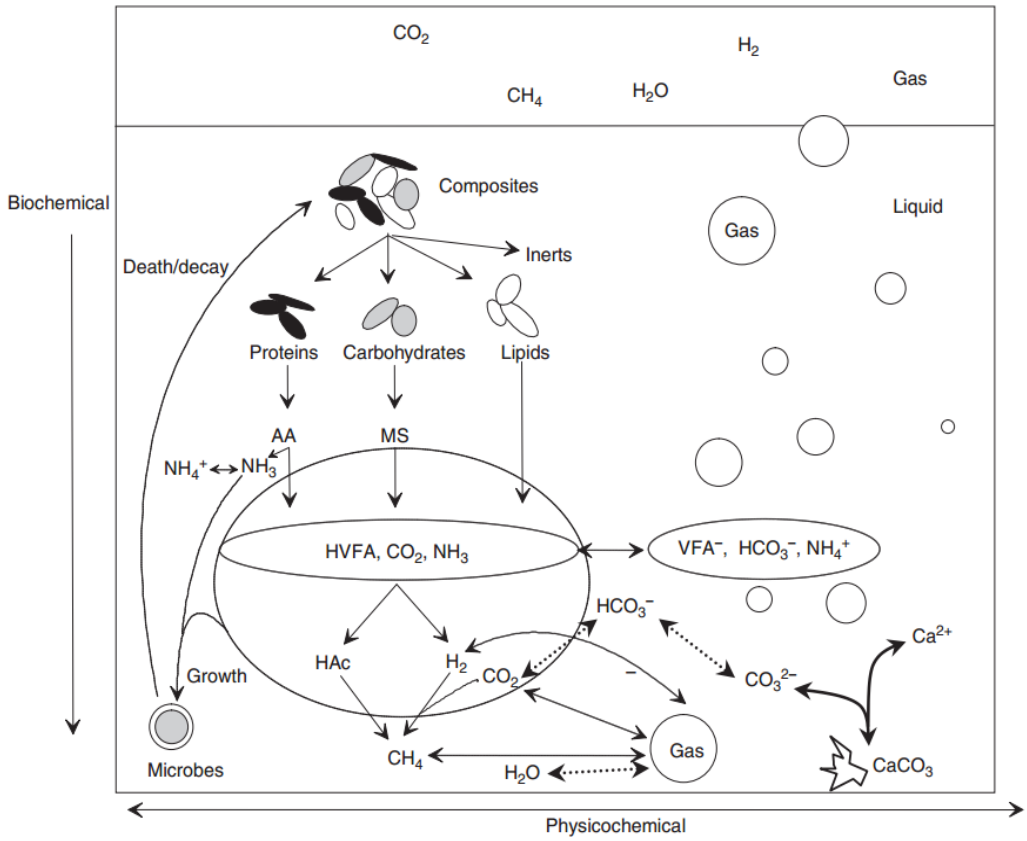

Figure 2.4. Biochemical and physicochemical processes considered in ADM1. AA: amino acids; MS: monosaccharides. Adapted from Batstone et al. (2002).

Methodologies have been proposed that allow the selection of the structure of a mass balance based model, i.e. the maximum number of biomasses groups and steps necessary to reproduce an available data set (Rodríguez et al., 2008, Bernard et al., 2006). For instance, in some cases high complex models such as ADM1 can be simplified to simpler models with fewer biomass groups, still maintaining an equivalent simulation accuracy (Rodríguez et al., 2008). Such simplification methodologies can be useful when more manageable models are necessary for implementing control algorithms in already existing AD plants. However, considering the objectives of this research, such as scenario simulations for comparing different control strategies, it appears how the framework offered by ADM1 does represent a better model structure with respect to simpler models. For this reason, in the following paragraphs, which describe the various AD processes, a focus is maintained on the ADM1 implementation.

ADM1 has received wide attention since its introduction, and many researchers have used it for simulating different AD systems, also proposing ad-hoc updates and modifications to the original version (Batstone et al., 2006). Some of the reviewed applications are detailed in Table 2.3.

2.4 Modelling the biochemical processes in anaerobic digestion

Most AD models use a kinetic-based approach to describe the biological experimental behavior, incorporating inhibition terms to describe the dependence of the reaction rate on environmental factors. In ADM1, first-order kinetics is used to model extracellular reactions (degradation and hydrolysis) while Monod kinetics is used to model intracellular reactions (acidogenesis, acetogenesis and methanogenesis). The Monod equation is the most frequently used expression for intracellular reactions. However it is only valid for balanced growth and should not be applied with rapidly changing growth conditions.

Biochemical reactions are described as substrate uptake and not as biomass growth. Substrate uptake considers both biomass growth and maintenance and is related to biomass growth through a yield coefficient. Microbial diversity in a mechanistic model can be taken into account through the description of the kinetics parameters with probability distributions. It has been shown that this kind of approach can better simulate the dynamics of the process under inhibiting conditions, e.g. overloading, toxic influent, etc. (Ramirez and Steyer 2008).

The biochemical processes considered in ADM1 are represented in Figure 2.5. It is observed that the uptake of substrate, growth and decay of biomass are interrelated: the microorganisms decay process results in new substrates that are available for growth, and this regeneration approach makes the model analysis more complex.

Table 2.3. A selection of ADM1 implementations from the literature.

Purpose for the model	Reactor and substrate	Discussion	Reference
Evaluation of different feeding regimes (continuous or split) on methane yield. Simulation of net energy produced and self-heating potential of the digester.	Pilot scale CSTR (3.5 m3), co-digesting cow manure and energy crops. Flow-through lab reactor (36 L), co-digesting cow manure and rape-oil.	The model permitted the identification of the best feeding regimes, which were functions of the composition of the feeding. However the results depend on the hydrodynamics of the reactor and cannot be considered to be general. The heat released by every reaction was computed and then added to the standard ADM1 simulation: in this way a detailed energy balance of the system and the influence of different substrates on the digester self-heating could be gained.	(Lübken et al., 2007)
Evaluation of acid dosing in order to decrease $CaCO_3$ precipitation in the reactor.	UASB, treating paper mill wastewater.	Simulations allowed the prediction of the effect of acid dosing on the biochemical reactions. Predictions were made on steady state: the process dynamics were ignored. Calcium carbonate precipitation was described with three new state variables added to the standard model. Simulations showed that acid dosing has little influence on the $CaCO_3$ inventory and methane production.	(Batstone and Keller, 2003)
Evaluation of change to thermophilic operation, in order to: reduce ammonia inhibition and related acid dosing costs; increase hydrolysis and uptake rates.	CSTR, mesophilic, treating solids and concentrated liquid streams from gelatine processing.	The Van't Hoff equation was used to model the influence of temperature on physicochemical parameters. Simulations showed that a change to thermophilic operation has little impact on reactor stability or increased methane production (because of the change in the ammonia dissociation constant and in the half saturation constant for acetate uptake reaction).	(Batstone and Keller, 2003)

Table 2.3 (continued) A selection of ADM1 implementations from the literature.

Evaluation of different feeding regimes, substrate strength, cycle lengths and temperatures in a wastewater treatment plant	Two anaerobic sequential batch reactors. (ASBR) coupled with sludge enrichment reactors (SER).	Simulations showed that thermophilic operation could handle a much higher OLR than mesophilic operation, considering both pH and ammonia inhibition. The optimum cycle length for ASBR was identified, but with negligible differences in relation to other simulated cycle lengths. Parallel and serial operations were compared regarding the maximum tolerable OLR and methane yield achievable.	(Rönner-Holm et al., 2012)
Prediction of biogas production and inhibition effects; optimization of co-digestion ratio between different substrates.	Batch and continuous lab scale, treating different agro-residues.	The methane potential (and therefore inert fractions) and degradation kinetics were identified for various agro-wastes in batch reactors. Using these parameters, ADM1 was used to predict the co-digestion effects and performance in continuous reactors with good accuracy respect to experimental values.	(Galí et al., 2009)
Determination of the SRT in the reactor: during calibration the value for t_{res} is determined. Prediction of long time operation on selected outputs (VFA, TS and VS accumulations). Evaluation of the recirculation rate between reactors on VFA and TS accumulation in the reactors.	2-stage CSTR (312 L each), mesophilic, digesting grass silage	The model permitted the estimation of the difference between SRT and HRT, thus allowing a prediction of solids accumulation in the reactor. Validation of the model using TS values in the reactor was complex due to samplings non-homogeneity (stratification occurring in the reactor). The same set of parameter was used in the two reactors, even if different conditions were occurring.	(Thamsiriroj and Murphy, 2011)

Table 2.3 (continued) A selection of ADM1 implementations from the literature.

Identification of the causes of reduced methane production and solid accumulation in long term operation (340 days) of the digester	2-stage CSTR (312 L each), mesophilic, digesting grass silage	ADM1 was extended including the lactate path from glucose fermentation and the acetogenic lactate degraders. Results from simulation, which showed lactate accumulation, suggested that inhibition of lactate acetogenesis was the origin of process failure. However, results from the simulations and the related interpretation were not validated rigorously as lactate measurements were not available.	(Thamsiriroj et al., 2012)
Process design	Anaerobic septic tank, treating concentrated sewage sludge	A simplified version of ADM1 was used to assess the effect of HRT and temperature on the COD removal efficiency and desludging interval of the system.	(Elmitwalli et al., 2003)
Process design	2-stage pilot scale high solid anaerobic digester (HSAD) and UASB treating food waste. HSAD is mechanically mixed in the upper zone with floating particulate solids and unmixed in the lower zone with prevalently soluble solids.	HSAD is assumed to operate with a perfect separation of particulate solids between upper and lower zones: upper zone was modelled as CSTR and lower zone as advective-diffusive reactor (ADR). UASB was modelled as ADR as well. Model was validated with HSAD operated in batch mode. The validated model was used to predict the influence of the recycle rate, UASB geometry and retention of methanogens in UASB on various performance indicators. The difference between calibration in batch mode and prediction in continuous mode was not addressed.	(Yu et al., 2012)

Table 2.3 (continued) A selection of ADM1 implementations from the literature.

Decision-making, Planning-Support tool Co-digestion	Lab-scale continuous digester, treating different mixes of cow manure, corn silage, rapeseed oil and grass silage.	The model is calibrated on a specific mixture (cow manure and corn silage). The calibrated model is then used as a virtual plant to predict the behaviour of the reactor with different feeding mixes (different substrate, different percentages, and different OLRs). The simulation with different substrate mixtures (with respect to calibration) is questionable, as some of the biological parameters might change. No experimental data were available to compare the validity of the simulated data, except comparison with literature data range.	(Zhou et al., 2011)
Co-digestion optimisation		The modified version of the ADM1 model developed by Galí et al. (2009) predicted correctly the co-substrate degradation of pig manure and glycerine, specially, considering the final biogas production.	(Astals et al., 2011)

The Petersen matrix is often employed to represent biochemical reactions in mechanistic models (Gernaey et al., 2010), and ADM1 is also presented in this way (Batstone et al., 2002). COD, carbon and nitrogen lost from reactants must flow to the products. The matrix representation allows for straight verification of COD, carbon and nitrogen conservation: the stoichiometric coefficients for each row should add up to zero. Before implementing the model, stoichiometric parameters and carbon and nitrogen content of every compound should be checked in a spreadsheet and changed consequently to allow material conservation (Batstone et al., 2002). The substrate might contain a specific compound whose degradation dynamics is of interest: in these cases, the matrix can be updated with the new state variable and its related stoichiometric and kinetic parameters. For instance, Batstone et al. (2004) included ethanol oxidation to simulate the degradation of winery wastewater; Thamsiriroj et al. (2012) included lactate oxidation when treating grass silage; and Fedorovich et al. (2003) updated the model considering sulfate reduction.

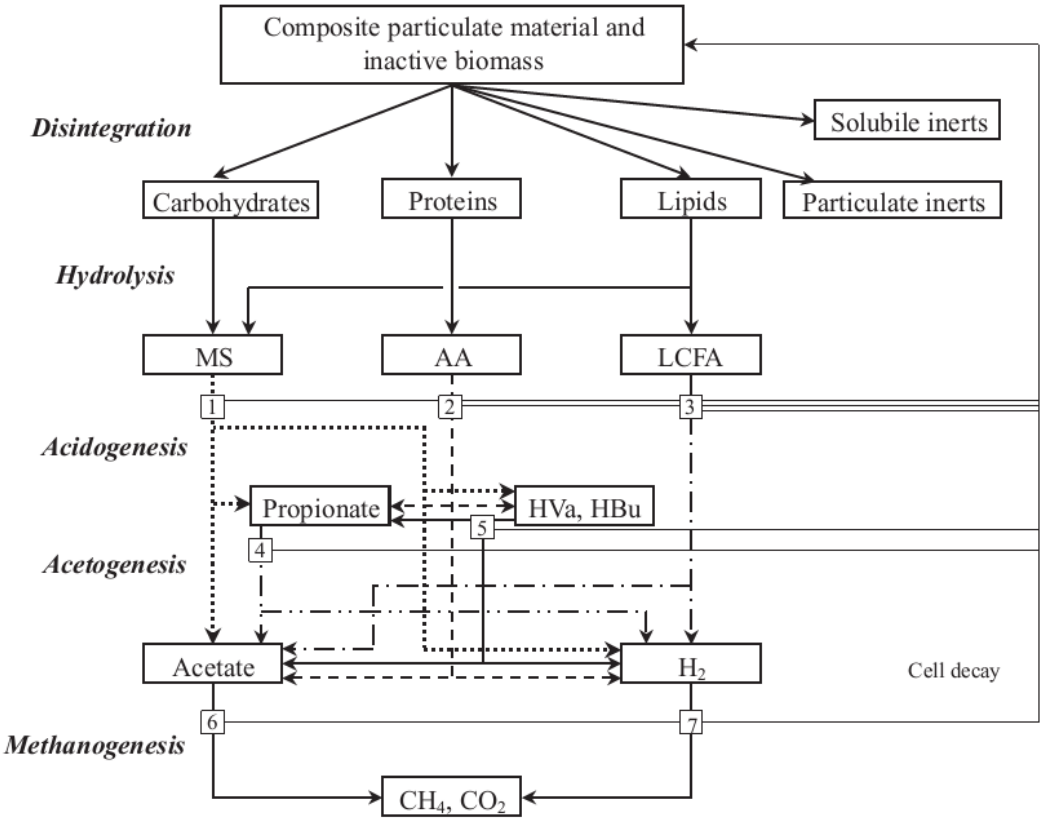

Figure 2.5. Biochemical processes as considered in ADM1 model. The biochemical processes include (1) acidogenesis from sugars, (2) acidogenesis from amino acids, (3) acetogenesis from LCFA, (4) acetogenesis from propionate, (5) acetogenesis from butyrate and valerate, (6) acetoclastic methanogenesis and (7) hydrogenotrophic methanogenesis. From Batstone et al. (2002)

2.4.1 Hydrolysis

Most organic substrate fed to an agricultural digester is usually in particulate, non-dissolved form, which cannot be assimilated directly by microorganisms. Hydrolysis is the generic term used to indicate the enzymatic extracellular solubilization of complex particulate material to monomers or small oligomers (Confer and Logan, 1998). The process is catalyzed by enzymes, which are usually produced by the organisms feeding on the solubilized substrate (Vetter et al., 1998). When considering the biodegradable fraction as being composed by carbohydrates, proteins and lipids, the hydrolysis products are monosaccharides, amino acids and long chain fatty acids, respectively.

According to Batstone et al. (2002), enzymatic hydrolysis occurs through two main pathways:

- The microorganisms secrete enzymes to the bulk liquid, where they are adsorbed onto a particle.
- The microorganisms attach to a particle and produce enzymes in the vicinity of the cell. The organism benefits from the soluble products that are released after the enzymatic reaction. This is typical of sessile microorganism organized in a biofilm structure.

The proportion between cell-free and cell-associated hydrolytic enzymes depends on the physical and chemical characteristics of the substrate, reactor hydraulics and solids concentration (Morgenroth et al., 2002, Song et al., 2005). It is possible to quantify experimentally the different proportions and activities between cell-free and cell-associated enzymes (Parawira et al., 2005, Zhang et al., 2007): however it is difficult to generalize results obtained in particular experimental conditions, and even more to make predictions based on inoculum, substrate or operation characteristics.

The complete enzymatic hydrolysis process is a complex multi-step process, which applies both to cell-free and cell-associated enzymes (Figure 2.6):

- enzyme production, at a rate which depend on environmental conditions (such as the concentration of soluble substrates);
- transport processes of enzymes from cell to bulk liquid or local cell environment, which might be limited at large particle sizes and high solids concentration;
- adsorption processes which are limited by available surface area;

- reaction rates which are limited by the surface area and enzyme concentration;
- transport of reaction products into bulk liquid or into biofilm;
- deactivation of the enzyme, which in turn depends on pH and temperature.

It is possible to model hydrolysis taking into account the influence of all these steps; however it would be very difficult to validate these models and simpler approaches are usually used.

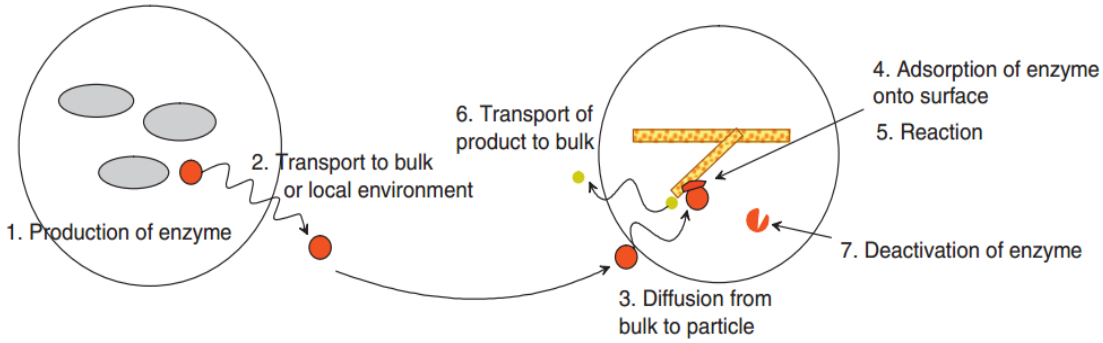

Figure 2.6. Main steps in enzymatic hydrolysis. From Batstone and Jensen (2011).

A first-order function in relation to substrate concentration is mostly used to model hydrolysis: it has been shown to be able to represent the cumulative effect of the multistep process and to return the average at which heterogeneous substrate is degraded (Eastman and Ferguson, 1981). In the ADM1 STR (Batstone et al., 2002) the first-order kinetics is recommended as the default function. In ADM1, different hydrolysis constants are attributed to different compounds (carbohydrates, protein, lipids), but in some cases the model has been modified to consider general slow and fast hydrolysable fractions (Zhao et al., 2009, Yasui et al., 2008). Hydrolysis is characterized as a first order reaction only once particulate surface is fully colonized by hydrolytic bacteria (O'Sullivan et al., 2005, Song et al., 2005). Nevertheless, there exist particular situations where predictions by first-order functions are poor and different approaches are preferred. In particular, a more complex description is necessary in certain conditions (Vavilin et al., 2008):

- The biomass to substrate ratio is low: for instance during start-up of continuous reactors, or in batch experiments (with a sigmoid curve in the experimental results indicating a colonization by the biomass). In these cases, a kinetics that shows dependency both to biomass and substrate concentration should be used. For example, Contois kinetics was used to update the standard ADM1 by Ramirez et al. (2009) when simulating the digestion of waste activated sludge in

batch reactors. The new kinetics considers new biomass groups responsible for hydrolysis, with the respective yield factors: this is just a modeling technique as no real biomass growth can happen during hydrolysis. Another more economic approach would be to consider the acidogenic biomass as the influential biomass in the Contois kinetics. This approach has been implemented by Mairet et al. (2011) when digesting microalgae.

- The influences of particle sizes and shapes on hydrolysis rates need to be investigated. It can be an interesting approach to predict how the hydrolysis constant for a certain substrate change at different levels of mechanical pre-treatment (such as in small batch in respect to full-scale continuous experiments) (South et al., 1995).
- Inhibitions by pH, or accumulation of sugars and amino acids need to be considered (He et al., 2006); functions for expressing the pH inhibition can be obtained from Veeken et al. (2000), and Sanders (2001).

Solids concentration has been shown to influence the hydrolysis rate (Pommier et al., 2007); in this regard, Koch et al. (2010a) updated the ADM1 implementation with an inhibition function in the first-order hydrolysis expression. The inhibition function introduces a new parameter (hydrolysis influence degree index) that needs to be calibrated in experiments with variable feeding solids concentration. Also Abbassi-Guendouz et al. (2012b), when calibrating the ADM1 model for batch digestion of OFMSW, found that the hydrolysis rate constants linearly decreased with increasing TS concentration for 15%<TS<30%.

The ADM1 STR considers a disintegration step prior to hydrolysis. The disintegration step was originally included for sewage sludge degradation and intended as a combination of non-biological steps such as cellular lysis, non-enzymatic decay, phase separation, and physical breakdown. However, in the case of solid wastes and agro-residues, it can be assumed that hydrolysis can occur without a disintegration step, with enzymes being able to diffuse into the substrate structure without cellular lysis: the model can be simplified by neglecting the disintegration parameters (Zaher et al., 2009). Moreover, the parameters for disintegration and hydrolysis are strongly correlated in most experimental setups. Therefore many pairs of parameters can reproduce the same experimental results with similar accuracy, as was shown numerically by Biernacki et al. (2013): this is another reason for avoiding the complication of disintegration kinetics.

2.4.2 Acidogenesis

Acidogenesis is generally defined as a microbial fermentation process in which organic compounds serve both as electron donor and as electron acceptors (Gujer and Zehnder, 1983). The substrates for fermentation are the soluble monosaccharides and amino acids produced during hydrolysis. The LCFA produced during hydrolysis of lipids are degraded through an oxidation reaction with an external electron acceptor.

Acidogenesis from monosaccharides

Fermentation from monosaccharides (sugars) is one of the most widely applied biotechnologies in the world. It is used to produce food products, renewable fuels, pharmaceuticals, and industrial chemicals. Usually it is carried over using pure or specialized microbial cultures in sterile environments, while in anaerobic digestion fermentation is realized by different microorganisms groups: the characteristics of the participating microbial groups and the composition of the fermentation products greatly depend on the process environment (Costello et al., 1991).

The ADM1 STR considers glucose as the model monomer for fermentation. Acetate, propionate and butyrate have been considered as the only fermentation products, given the possibility to analyse them simultaneously in GC analysis and their different downstream degradation paths. Other fermentation products, such as ethanol and lactate, have been omitted in the original formulation of ADM1, as their concentration as fermentation intermediates is usually low in most anaerobic digesters (Batstone et al., 2002).

Fermentation is implemented in ADM1 by considering a single group of microorganisms with lumped parameters. The value of the yields of the different fermentation products are fixed at the beginning of the simulation. A more realistic approach would include a regulation function that changes the relative yield depending on influential environmental factors (principally pH and H2 concentration), as described in detail by Mosey (1983). For instance, it is expected that a low hydrogen concentration would promote hydrogen-rich reactions, such as acetate production, and that low pH would enhance ethanol production. In this regard, Rodriguez et al. (2006) updated the ADM1 with variable stoichiometric coefficients for glucose fermentation, based on the Gibbs free energy variations of the different fermentative pathways. This approach should be applied when simulating an acidogenic reactor for biohydrogen production (Penumathsa et al.,

2008) or when a better prediction of the composition of the fermentation products (considered as fuels or chemicals) is required (Horiuchi et al., 2002); in the case of methanogenic reactors, where the rate limiting acetoclastic reaction compensates the differences in the fermentation pathways, no significant differences in the prediction of effluent quality and system robustness have been observed between the fixed and variable stoichiometry approaches (Rodriguez et al., 2006).

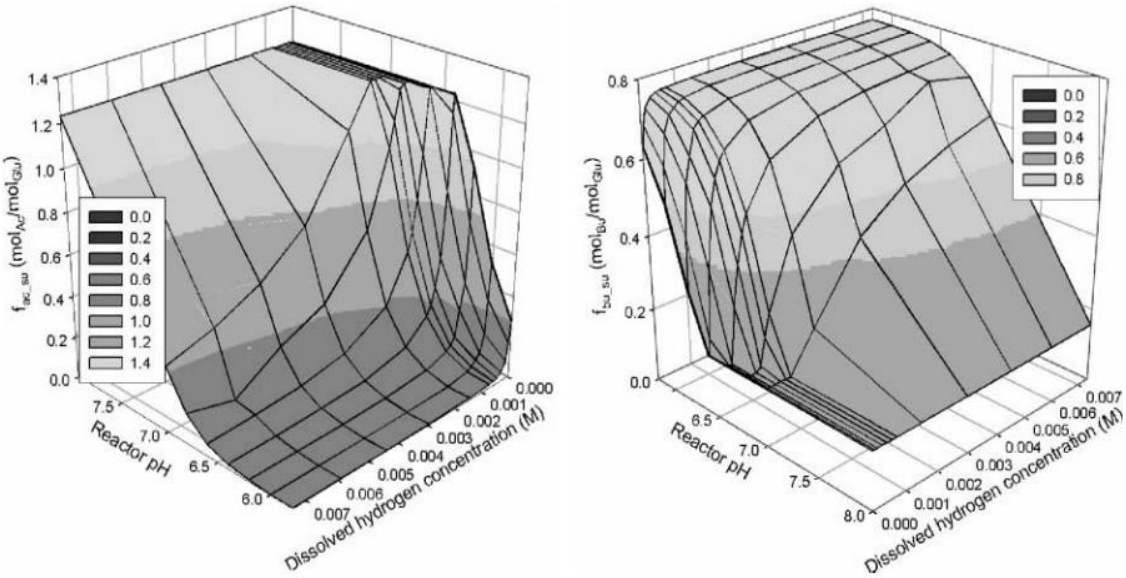

Figure 2.7. Variable stoichiometric coefficients for the fermentation of glucose as a function of pH and dissolved hydrogen concentration. From Rodriguez et al. (2006).

Acidogenesis from amino acids

Hydrolysis of proteins results in a mix of amino acids, whose relative yield depends on the protein primary structure. There are two main pathways for amino acid degradation (Batstone et al., 2002):

- Stickland oxidation-reduction paired fermentation.
- Uncoupled oxidation of single amino acids with an external electron acceptor, such as hydrogen ion or carbon dioxide.

In anaerobic digesters, with normal mixed-protein systems, it is assumed that most of the amino acid degradation occurs through Stickland fermentation, which is faster than uncoupled oxidation. Only a minor part of amino acids, typically about 10%, is degraded by uncoupled oxidation because of a shortfall of external electron acceptors, with the production of hydrogen or formate. Oxidation reaction will therefore be favoured with low hydrogen and formate concentrations or under

thermophilic conditions when oxidative reactions become more thermodynamically favourable.

The IWA task group decided to consider only Stickland reactions in the ADM1 structure (Batstone et al., 2002), thus simplifying the determination of the stoichiometric yields of the products. An estimation of the stoichiometric yields can then be obtained when knowing the following data:

- Amino acids content of a protein mix, directly from analysis or indirectly approximated from available databases (FAO/INFODOS, 2012).
- The Stickland acceptor/donor/uncoupled status of each amino acid and consequently the products of each amino acid coupled reaction. A description of the method and a spreadsheet with the Stickland products for each amino acid is available in (Ramsay and Pullammanappallil, 2001).

Most of the published applications of ADM1 have used default stoichiometric values suggested for sewage sludge in the initial STR; when the characteristic of the substrate are particular, such as high contents of proteins or specific amino acids, new stoichiometric values should be calculated.

2.4.3 Syntrophic acetogenesis and hydrogen-utilising methanogenesis

Degradation of organic acids to acetate (in the case of valerate also to propionate) is an oxidation step with hydrogen ions and carbon dioxide as external electron acceptors, which are converted to hydrogen gas and formate, respectively. The oxidation reaction becomes exergonic (thermodynamically favourable) when the concentrations of the electron carriers, hydrogen and formate, are maintained at low levels. Therefore, the acetogenesis occurs necessarily in association with hydrogenotrophic methanogenesis which is an electron consuming reaction. Close spatial relationships between oxidising *Bacteria* and methanogenic *Archaea* are usually observed in anaerobic digesters in the form of granules or biofilms: these forms of aggregation facilitate the electron transfer between species, thus increasing the global process rates. High shear stress, caused by the intense mixing, can hinder the formation of these syntrophic spatial aggregations (Stroot et al., 2001).

Three acetogenic biomass groups are implemented in ADM1, each degrading specific substrates: one for propionate, one for butyrate and valerate, and one for

LCFA (acids containing more than five carbon atoms). A single group of organisms is used to model the methanogenic removal of hydrogen.

Syntrophic reactions are thermodynamically limited in a narrow range of hydrogen concentrations. The value of these thermodynamic limitations has been used in the ADM1 to determine the kinetic parameters for (non-competitive) hydrogen inhibition, as well as the half saturation coefficients and yields. In fact, in ADM1 thermodynamic limitations are implemented through kinetic control as inhibition functions.

Methanogenesis is the major sink for electrons in an anaerobic system; other alternative, minor, sinks are nitrate reduction, sulphate reduction, iron reduction and homoacetogenic hydrogen consumption. None of them have been implemented in the ADM1 STR, as their contribution is negligible in most digesters. However, they should be considered in the modelling when the substrate contains elevated amounts of these alternative electron acceptors; or, for homoacetogenesis, in the case of digestion at low temperatures and inhibition of hydrogenotrophic methanogenesis. An update for sulphate reduction has been proposed by Fedorovich et al. (2003), while Antonopoulou et al. (2012b) have proposed an extension for homoacetogenic hydrogen consumption when modelling biohydrogen production.

2.4.4 Acetoclastic methanogenesis

In this step, acetate is cleaved to form methane and CO_2. Two genera amongst methanogenic *Archaea* have been shown to be predominant: *Methanosarcina* and *Methanosaeta*. *Methanosarcina* dominates above 10^{-3} M acetate while *Methanosaeta* dominates below this acetate level. *Methanosaeta* may have lower yields, higher k_m values, lower K_S values and be more pH-sensitive as compared to *Methanosarcina* (Palma-Behnke et al., 2011, De Vrieze et al., 2013) and therefore in flexible demand applications it is expected to have peaks in acetate concentration which would favour the growth of Methanosarcina. *Methanosaeta* is usually found in high-rate/biofilm systems, while *Methanosarcina* is more frequent in mixed digesters. In the ADM1 STR, it was recommended to implement a single group of acetoclastic methanogens, with kinetic and inhibitory parameters selected depending on the application and experimental observations.

Despite this, most ADM1 applications in the literature have made no careful selection of the parameters for acetoclastic methanogenesis; instead standard

values recommended in the STR have been used or in other cases calibrated from experiments (as can be seen in Table 2.4 in the section dedicated to model calibration).

2.4.5 Inhibition and toxicity

Inhibition can generally be understood as an adverse effect on the metabolism and function of the microorganisms. Inhibitory compounds induce a decrease in the energy available from catabolism, or an increase in the amount of energy required for biomass maintenance. Two forms of inhibition can be identified, depending on their reversibility (Batstone et al., 2002):

- Biocidal inhibition (also defined as toxicity): it is normally irreversible and it is caused by LCFA, detergents, aldehydes, nitro-compounds, antibiotics, etc.
- Biostatic inhibitions: it is normally reversible and it consists of product inhibition, weak acid/base (VFA, H_2S, NH_3) inhibition, pH inhibition, cation inhibition and other effects that can disrupt homeostasis.

While there are differences regarding the specific inhibitory mechanisms and compounds, methanogenic archaea are generally more vulnerable to inhibition and toxicity than bacteria. An order of sensitivity to inhibitions of the various biological steps, from least to most, is as follows (Batstone and Jensen, 2011): acidogenesis, hydrolysis, acetogenesis, hydrogenotrophic methanogenesis and acetoclastic methanogenesis.

A complete review of toxic and inhibitory effects on AD is available in Chen et al. (2008), and can be consulted for the thresholds of various toxic and inhibitory compounds. Most models are focused on inhibitory effects, as these usually can be reduced with an appropriate, model-based, operational strategy. Dynamic behavior of an AD systems during start-up or load changes is greatly influenced by inhibitory effects, which then should be carefully included in a dynamic model. Toxic compounds in the influent should be tackled with an appropriate pre-treatment and not allowed to influence the normal operation of an AD system.

pH inhibition is used in ADM1 to describe a combination of intracellular processes: weak acid and base inhibition, disruption of cell homeostasis and protein (enzyme) denaturation. These processes are all directly or indirectly influenced by changes in the pH environment. Various empirical forms are suggested, with different parameters for acetogenesis and acidogenesis, hydrogen-utilizing methanogens

and acetoclastic methanogens: the parameters depend on the optimal, lower and upper pH values for every microorganism group (Batstone et al., 2002). Another expression for pH inhibition implemented in ADM1 can be found in Lübken et al. (2007). Hydrolysis can be inhibited at either low or high pH values, probably by partial denaturation of enzymes: however this has not been implemented in the ADM1 STR.

In addition to pH inhibition, the ADM1 STR includes hydrogen inhibition of acetogenesis (which is a case of product inhibition) and free ammonia inhibition of acetoclastic methanogens, both implemented using non-competitive inhibition forms. Free ammonia inhibition is typical when the digester is fed with manure or with high protein content. LCFA inhibition is not included in ADM1, but should be implemented when lipid-rich substrates are fed to the reactor.

2.4.6 Influence of temperature

Microorganisms present in anaerobic systems are usually divided in three different groups, depending on their temperature range of growth: psychrophilic (10-30° C), mesophilic (20-40° C) and thermophilic (45-70° C). Every group has an optimum temperature at which the rate of growth is maximum, above which the rate decreases. Different mechanisms are used to explain the influence on biological reactions (Batstone et al., 2002):

- Increase in the reaction rate with increasing temperature.
- Decrease in the reaction rate when temperature is above the optimum (>40° C for mesophilic and >65° for thermophilic).
- At higher temperatures the microorganisms expend a higher amount of energy on maintenance, with a resulting decrease in yield and an increase in the half saturation constant (K_s).
- Higher temperatures also lead to higher decay rates.

Changes in temperature affects the available thermodynamic driving force of the reaction (von Stockar et al., 2006), with consequential changes in yield and eventually in reaction pathway. For instance, at high temperatures, acetate oxidation becomes thermodynamically favoured and its impact should be considered when modelling.

Most models are calibrated at a single temperature, and this is because active heating systems are able to maintain the process around the selected temperature

and with only a small variation. In these cases, exact relationships that model the effect of temperature are not necessary in the model. When the process temperature is expected to fluctuate with higher variations, or when the influence of the temperature on the process performance needs to be investigated, the model could be extended with relationships between kinetic constants and temperature:

- Calibrated Arrhenius equations can be used to describe the change in the kinetic constants (e.g. k_{hyd}, $k_{m,process}$) with temperature, before and above optimum (Pavlostathis and Giraldo-Gomez, 1991).
- It is more difficult to include the influence on yields and K_s, and usually the only distinction made is between mesophilic and thermophilic, for which different sets of parameters are proposed in the ADM1 STR.

2.4.7 Modelling codigestion

Anaerobic codigestion is defined as the addition of two or more sources of biomass to an AD system with complementary characteristics so that the biogas production process can be enhanced in some way such as nutrients and/or moisture balancing, thus avoiding inhibition or maximising biogas production (Mata-Alvarez et al., 2011). The nitrogen content of a feedstock is the usual reason for codigestion with optimal carbon to nitrogen (C/N) ratios quoted in the range of 12-70 being reported (Diagne et al., 2013, Hentz and Balchunas, 2000) although other reasons are still relevant, such as establishing the correct levels of micro/macro nutrients, alkalinity, potential inhibitory and/or toxic compounds, degradable matter and total solids may also be important (Flores-Alsina et al., 2016).

Recently, most modelling studies dealing with codigestion use modified versions of ADM1 (Mata-Alvarez et al., 2011), with the main differences initially focussing on the redundancy of the particulate composite component of ADM1 and instead using the three biochemical compound categories (carbohydrates, proteins and lipids) in order to describe influent organic matter (Zaher et al., 2009, Galí et al., 2009, Boubaker and Ridha, 2008, Lübken et al., 2007). On using this method, substrates of differing biochemical compositions could be fed to the system rather than using a single composite matter fraction with fixed degradation stoichiometry. Apart from this development these authors offered several enhancements or modifications to ADM1 relating to their particular modelling problem (e.g. Boubaker and Ridha (2008) modified the inhibition model for acetoclastic methanogens to better predict process failure) and were not specific to the codigestion issue.

However the work of Zaher et al. (2009) represented the largest structural modification to ADM1 in order to enhance the modelling of codigestion in that the individual biochemical components of each feedstock were allowed to degrade using different kinetics, with the flux of soluble products from each hydrolysis reaction (of each feedstock) being combined into a detailed input vector to the standard ADM1 model.

2.5 Modelling of the physicochemical processes

There are two broad types of physicochemical, non-biological mediated, processes that occur in a digester (Batstone et al., 2002):

- Ion association/dissociation: these are rapid compared to biochemical processes rates.
- Precipitation/solubilisation: these are medium/slow compared to biochemical processes rates.

The modelling of physicochemical systems is very important when building inclusive AD models:

- It allows the expression for biological inhibition factors (e.g. inhibition caused by pH, free acids and bases, etc.).
- It allows the prediction of pH and relative control strategies to maintain a certain setpoint.

2.5.1 Ion association/dissociation

In an anaerobic system there are several compounds whose pK_a values (dissociation constant) are close to the operating pH of the digester and therefore their association/dissociation processes need to be considered in the model. In particular, organic acids have a pK_a of about 4.8 and the acid-base pairs $CO_{2(aq)}/HCO_3^-$ and NH_4^+/NH_3 have a pK_a of 6.35 and 9.25, respectively.

The typical way of describing the ion behaviour is through a charge balance which considers the total cationic and anionic equivalents concentrations in the system:

$$\sum S_{cat^+} = \sum S_{an^-} \tag{2.1}$$

When applied to a digester, the balance becomes:

$$S_{cat^+} + S_{NH_4^+} + S_{H^+} = S_{an^-} + S_{OH^-} + S_{VFA^-} + S_{HCO_3^-} \quad (2.2)$$

with subscripts *VFA*$^-$ referred to dissociated volatile fatty acids and *cat*$^+$ and *an*- to cations and anions. Because association/dissociation processes are very rapid compared to biochemical processes, they can be represented as equilibrium processes with an algebraic equation for every considered species, e.g.:

$$S_{VFA^-} = \frac{K_{a,VFA} S_{VFA}}{S_{H^+}} \quad (2.3)$$

where the concentration of the undissociated species are also used in the biochemical processes equations. Finally the equation (2.2) can be solved iteratively for the unknown variable $S_{H^+}$to obtain the pH value of the system.

With systems with medium/high levels of ions (e.g. when the effluent is recycled upstream), the modelling should take into account the non-ideal behaviour and update the equilibrium equations with ion activities (Musvoto et al., 2000). This recommendation should apply to most digesters that treat high-strength substrates; however it has not been applied so far in the literature consulted.

2.5.2 Solids precipitation

Solids precipitation is the complexing of cations and anions in neutral inorganic solid form. Potentially important solid precipitates in anaerobic digesters include calcium carbonate, calcium phosphate, magnesium carbonate, metal sulphide and magnesium-phosphate complexes such as struvite. Calcium carbonate precipitation is important when wastewaters from the pulp and paper industry are treated; metal sulphide precipitation is important when iron is added to precipitate the hydrogen sulphide produced during the reduction of sulphate and sulphur rich substrates; magnesium precipitates when the influent is rich in Mg^{2+} or when $Mg(OH)_2$ is used to raise the pH (Batstone et al., 2002).

Metal-ion precipitation is generally described by equilibrium-driven dynamic relationships (similarly to acid-base description), where the anion concentration is pH dependent (Musvoto et al., 2000). In addition to equilibrium thermodynamics, the actual mechanism of crystallization is more complex and also kinetically

controlled: its kinetics depends on the influence of other factors such as the presence of seeds, promoters and inhibitors, and solution activity.

Most practical anaerobic systems do not contain a high concentrations of metal ions and therefore solid precipitations have very rarely been considered in ADM1 application in the literature. Batstone and Keller (2003) have considered and implemented calcium carbonate precipitation in the case of the digestion of the wastewater from paper industry.

In the BioCPV case, it appears that solid precipitation implementation is not necessary. When some of the selected substrates contain a high level of metal ions, the sensitivity of the model to solid precipitation could be tested. For instance, when not considering carbonates precipitations some of the following inaccuracies may arise: incorrect pH prediction; over-prediction of carbon dioxide in the gas phase; faster physicochemical dynamics in the model with respect to the system (when the precipitated carbonate have long retention times in the system).

2.5.3 Modelling the transport dynamics

Transport dynamics effects include:

- Liquid-gas mass transfer: they are normally rapid/medium compared to biochemical processes rates.
- Liquid-liquid mass transfer: they are normally rapid/medium compared to biochemical processes rates.
- Major performance variables such as gas flow are dependent on correct estimation of transport dynamics.

Liquid-gas mass transfer

During anaerobic digestion three main compounds with low solubility are produced: hydrogen, methane and carbon dioxide. It is important to determine their mass transfer to the gas phase, as it influences the amount and composition of the biogas produced, the pH of the liquid phase (CO_2) and also on the inhibition of the reaction in the liquid phase (H_2). Ammonia is not considered as its solubility is very high and thus it remains mostly in the liquid phase, and hydrogen sulphide mass transfer can be considered when its biochemical reactions are implemented.

When the gas and liquid phase reach equilibrium, the well-known Henry's law can be used to predict the equilibrium relationship for each compound between

concentration in the liquid phase and partial pressure in the gas phase. However, in dynamic AD processes the thermodynamic equilibrium is not reached and liquid effluent is significantly supersaturated. Therefore a dynamic gas transfer equation is used to describe liquid-gas transfer. Using the two film theory and neglecting the resistance to mass transfer in the gas phase, the following equation is obtained (Stumm and Morgan, 1996):

$$\rho_{T,i} = k_L a(S_{liq,i} - K_H p_{gas,i}) \quad (2.4)$$

where $\rho_{T,i}$ is the mass transfer rate of the gas *i* (mol d^{-1} l^{-1}), $k_L a$ is the mass transfer coefficient (d^{-1}), $S_{liq,i}$ is the dissolved gas concentration (M), K_H is the Henry's law coefficient (M bar^{-1}) and $p_{gas,i}$ is the partial pressure of gas *i*.

The total gas flow can be calculated from the sum of the gas transfers, after subtracting the saturated vapour pressure from the headspace total pressure; alternatively, if the headspace pressure is variable, or there is a downstream gas process, the gas flow can be calculated by a control loop in pressure (Batstone et al., 2002). The implementation of these calculation methods in the ADM1 framework presents certain computational challenges which are described in Rosen and Jeppsson (2006). An alternative calculation method for implementing the gas transfer and calculating the total gas flow in ADM1 has recently been suggested by Smith and Stöckle (2010).

Values of $k_L a$ depend on the mixing, temperature and liquid properties, and to a lesser extent also on the specific gas considered. A good overview on the mechanisms governing the value of $k_L a$, the theoretical approaches to determine it and experimental dynamic data is provided in Merkel and Krauth (1999). Interestingly, the article shows how the measured $k_L a$ values for the CO2-mass transfer differed by a factor of 2-3 from the steady-state to dynamic loading conditions. When implemented in ADM1, it has been found that the dynamics of the modelled systems are almost insensitive to changes in $k_L a$ values: Feng et al. (2006) reported that only low values of $k_L a$, smaller than 1.0 d^{-1}, affected the prediction of the model; the same result was found by Bollon et al. (2011). The relative insensitivity of the model to medium to high values of $k_L a$ might justify the adoption of default values, 200 d^{-1} (Rosen and Jeppsson, 2006), in almost all ADM1 implementations, where well mixed systems were analysed; however, care should be taken when the modelled system has low or discontinuous mixing, or with high

solids content, where low values of $k_L a$ could affect the system. For instance, Abbassi-Guendouz et al. (2012b) have shown that inhibited methane production in high solids batch reactions (higher than 30% TS) can be simulated in ADM1 using low values of $k_L a$ (0.5 d^{-1}). Accumulation of dissolved CO_2 may cause local acidification and thus inhibition of methanogenesis with further VFA accumulation and acidification. In some highly dynamic systems, such as batch reactors, the produced H_2 could be temporally removed from the liquid phase via liquid-gas transfer: in these cases a low $k_L a$ could lead as well to VFA accumulation. However it would be important to distinguish between the effect of reduced liquid-gas transfer ($k_L a$) and liquid-liquid transfer (approximated by K_S) when considering high-solid systems, while Abbassi-Guendouz et al. (2012b) only focus on the liquid-gas transfer.

A more refined analysis would consider the presence of the gas hold-up phase, and as a consequence the overall liquid-gas mass transfer occurring across the liquid phase, the gas hold-up phase and the off-gas phase (headspace). However, when the amount of gas contained in the hold-up phase is small (as in anaerobic systems), the gas hold-up phase description can be neglected in the modelling (Lizarralde et al., 2015).

Liquid-liquid mass transfer

Mass transfer of solutes, from bulk liquid to microorganisms, has not been considered in AD modelling: their influence on the overall rate of reactions is negligible in most applications when compared to rate limiting biochemical reactions. However, in certain cases the mass transfer might become influential, as in high-solid digestion or with mass transfer across granules and biofilms. When calibrating the ADM1 model, this effect is likely to be expressed by a high value of the half saturation constant K_S. Bollon et al. (2011) calibrated the model for different solid content of OFMSW and found higher K_S values at higher solids: at 35% solids content the K_S value was an order of magnitude higher than at 5%.

Hydraulic studies

ADM1 applications have been mostly focused on well mixed systems, and therefore modelled assuming CSTR or eventually CSTR in series. In this framework, the retention of solids in the reactor may be considered: the difference between HRT and SRT is described by introducing a further parameter, t_{res}, which is the difference between the mentioned retention times. It can be calculated from experimental

measurements (Antonopoulou et al., 2012a), and basically applying a mass balance around the digester (Banks et al., 2011); when sufficient measurements are not available, its value can be determined through calibration (Thamsiriroj and Murphy, 2011). In most cases, t_{res} is defined as a constant value; however, Zaher et al. (2003) introduced an update considering the solids retention time to be proportional to the hydraulic retention time, i.e. less efficient during overload conditions.

A better insight into the hydrodynamics can be obtained via tracer studies to obtain the residential time distribution of the system (RTD), and then fitting the curve with the appropriate hydraulic flow model (Bello-Mendoza and Sharratt, 1999, Capela et al., 2009): the parameters of the hydraulic flow model would then be used for the ADM1 implementation. For instance, Batstone et al. (2005) implemented ADM1 in a UASB which was modelled, after tracer studies, as plug-flow (advective-diffusive) reactor, with an internal recycle and internal bypass. The calibration of the model, with acetate pulses, included the simultaneous calibration of the kinetic ($k_{m,ac}$ and $K_{S,ac}$) and hydraulic parameters (effective sectional area). A similar modelling approach was followed by Mu et al. (2008), who also added a sludge distribution function which defines a maximal attainable biomass concentration at each reactor axial position. Fuentes et al. (2009) proposed a comprehensive modelling of an anaerobic fluidized bed reactor (AFBR), which includes (one-dimensional) differential mass and momentum balance equations for the solid-liquid-gas phases, coupled with the ADM1 framework to compute the biochemical and physicochemical processes (Figure 2.8). The growth of the biofilm is coupled to the local hydrodynamic characteristic considering a biofilm detachment rate which is a function of the specific energy dissipation rate (Paul et al., 2012).

A further step in the hydrodynamics description would be to apply a predictive CFD study of the (planned) system. Potential approaches include incorporating the biological and physico-chemical model equations in the CFD code, or selecting the outputs from the CFD analysis (mass transfer coefficients, residential time distributions, etc.) and introducing them into the biological model, keeping the two models as separate units (Glover et al., 2006).

CFD analysis of mixed anaerobic digester is currently being carried out at the Energy Research Group, Sheffield, in the framework of the BioCPV project and therefore a detailed review of the CFD analysis is outside the scope of this thesis. However it is expected that the integration of biochemical modelling (such as

ADM1, reviewed in this thesis) and the hydrodynamics analysis will assist in improving the scale up of experimental digesters and the design of full scale reactors.

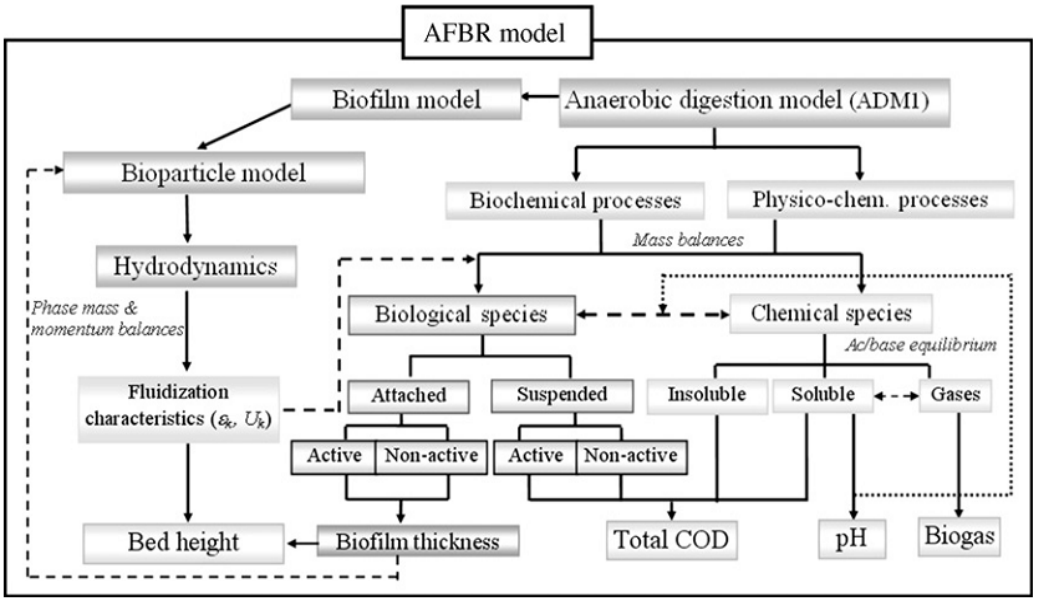

Figure 2.8. Model structure for an anaerobic fluidized bed reactor as proposed by Fuentes et al. (2009).

2.6 ADM1 – model inputs

Once the structure of the model is developed, the following input data must be provided to perform a simulation:

- Characterization of the substrate
- Initial conditions
- Value of the biochemical kinetic and stoichiometric parameters
- Physicochemical and hydrodynamics parameters
- The operation and dimensions of the reactor (feed rate, volume, pressure, etc.).

Characterization of the substrate is paramount for a successful application of the mathematical model: it directly influences the gas flow quantity and composition and possible process inhibitions. Its value has to be determined experimentally from case to case, especially in the case of complex feedstocks, as wastes, which can be considered as composed of many simpler substrates.

Initial conditions refer to the composition inside the reactor at the beginning of the simulation, and are specifically important in batch reactions which are very sensitive to the composition of the inoculum. It is less important for continuous operations (apart from start up). Inoculum composition has been addressed in different ways. In some cases, the reactor from which the inoculum is drawn has been modelled with an adequate version of ADM1: the steady state composition of the effluent has then been used as the inoculum composition. In other cases, the biomass characterisation has been calibrated using experimental results (Thamsiriroj and Murphy, 2011), but this approach appears questionable.

Stoichiometric parameters are fundamentally thermodynamically based and are usually fixed across simulations, unless a variable stoichiometric approach is taken (Rodriguez et al., 2006). The most sensitive kinetic parameters are selected and evaluated during model calibration against experimental data. Physicochemical parameters and hydrodynamics parameters show little variation and default parameters are usually used (however variations for temperature and for special process conditions, such as high solid/high strength – as was shown above - should be considered).

In the following sections the focus is on the characterization of the substrate and the calibrations techniques.

2.6.1 Characterisation of the feedstock for modelling

A key point in order to successfully apply a mathematical model to describe a bio process is to have a good influent characterisation, especially where the influent has a complex nature.

In ADM1, the substrate is characterized firstly in soluble and particulate fractions; the soluble fraction is in turn fractionated into sugars (monosaccharides), amino acids, long chain fatty acids, and VFAs (acetate, propionate, butyrate, valerate) and inerts; the particulate fraction is in turn fractionated into protein, carbohydrates, lipids and inerts. Different methods have been implemented for the experimental fractionation, simplifying: using data from the literature for similar substrate, from direct physicochemical fractionation, from elemental analysis and from the interpretation of methane production curves. Using literature data for similar substrates might be a good solution for early implementations of the model. A brief description of each technique is given below.

Using data from the existing literature

In the first stages of a process design study, data from the literature can be used to predict the main characteristics of the system behaviour. There exist many sources that can be consulted for the initial biomass characterization, such as Liao et al. (2007), Gunaseelan (1997) and the database ECN/Phyllis (n.d.).

Performing a physicochemical analysis of the substrate

In these methods the fractions required by ADM1 are directly quantified through a physicochemical analysis of the substrate. The analysis should be applied to both the soluble and particulate fraction. However, when the soluble fraction is minimal, some simplifications can be used: e.g. assuming the same fractionation in soluble and particulate fraction (equalling the proportion of amino acids to protein, LCFA to lipids, etc.), or allocating the totality of the soluble fraction to only one compound (usually monosaccharides or VFA, depending on the substrate).

Individual VFA are usually obtained from gas chromatography. The protein content is usually approximated by multiplying N_{org} by 6.25 (which is the average N-content of proteins), where N_{org} in turn is the difference between TKN and TAN determined in a standard Kjeldahl analysis (APHA, 1998). Lipids can be obtained from a Soxhlet extraction (APHA, 1998), and the total carbohydrates can be determined through the Anthrone method (Arthur Thomas, 2006). Otherwise, a fraction that includes the particulate carbohydrates and the inerts can be obtained from the VS balance (VS-protein-lipids). The inert fraction can be determined from biodegradability assays in BMP tests (Angelidaki et al., 2009). Otherwise a fibre analysis ((Van Soest and Wine, 1967) of the non-water-soluble fraction is sometimes applied as well, which consists in sequential extraction under neutral and acid detergents: it permits the determination of the hemicellulose, cellulose and lignin fraction. Then the lignin fraction can be used as proxy of the biodegradability of (lignocellulosic) substrates, thus avoiding BMP tests, as was demonstrated with good accuracy by Triolo et al. (2011) and Buffiere et al. (2006). All measurements give a fractionation in unit of mass, which must be transformed in COD using the stoichiometric formula used in ADM1 to represent the compound. Applications of direct physicochemical characterisation in ADM1 implementation can be found in Wichern et al. (2009) and Koch et al. (2010b), both treating grass silage. Important considerations regarding the possible errors and limitations of this method have been reported by Buffiere et al. (2008), in particular how the direct determination of

proteins, lipids and carbohydrates were far from being representative of the total volatile solids of the substrate.

From elemental analysis

The lumped elemental composition of the organic substrate ($CH_yO_zN_v^u$) can be calculated from analytical measurements (COD, TOC, Organic Nitrogen (N_{org}), Bicarbonate Alkalinity (Alk_{IC}), Neutralized Fatty Acids Alkalinity (Alk_{VFA})) through mass and electron balances, see Figure 2.9.

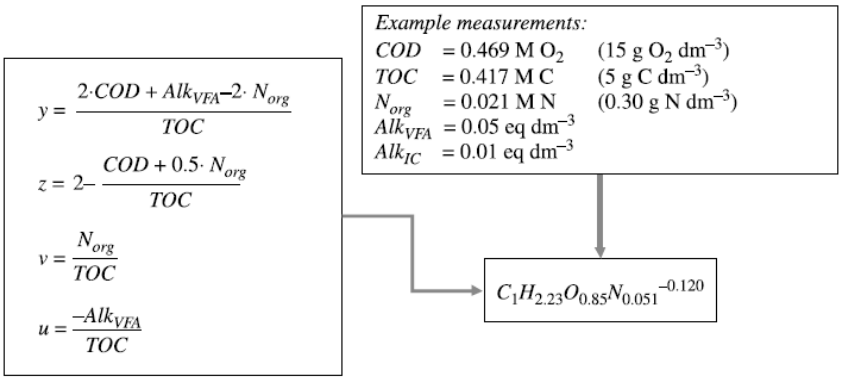

Figure 2.9. Derivation of the elemental composition of the substrate from a limited number of measurements, with an example calculation. From Kleerebezem and Van Loosdrecht (2006).

Using the elemental composition of the lumped substrate and the elemental composition of the substrates defined in the model, the required ADM1 fractions can then be calculated by solving a system of linear equations which are principally based on the balances of the moles of C, H, O and N between the fractions and on the oxidation state of the substrate (details in Kleerebezem and Van Loosdrecht (2006)). The method could be applied separately to soluble and particulate fractions. Biodegradability of the substrate must be assessed with other methods. The estimated substrate fractionation is highly sensitive to measurements (especially COD, TOC), as shown by Kleerebezem and Van Loosdrecht (2006). When an elemental analysis of the substrate is available from direct measurement, only the second step of the method could be used.

Interpretation of methane production curves

This method combines physicochemical analysis with a fractionation based on degradation kinetics in batch assays (Girault et al., 2012). From the interpretation of the methane production curve of the substrate, the biodegradable COD is described

into a slowly degradable fraction (hydrolysis is rate limiting, particulate fraction) and readily degradable (hydrolysis is not rate limiting, soluble fraction). The physicochemical analysis includes VFAs and protein, lipids, carbohydrates and total COD of the substrate. Batch assays are realized with a high biomass/substrate ratio. The composition of the biomass used (total and specific concentrations) are approximated by simulating with ADM1 the continuous reactor from which the inoculum is drawn. Blank batch assays with inoculum only are realized, from which the degradation kinetics of the pure inoculum are calculated and then considered for the interpretation of the degradation kinetics of the substrate. The methane produced in the batch assays is monitored and then a net methane production rate curve of the substrate is obtained. The particulate fraction of the substrate is assumed to be split into protein, lipids and carbohydrates according to the initial physicochemical analysis. The soluble fraction is assumed to be composed of the measured VFAs and a remaining split in amino acids, LCFA and sugars with same proportions used for the particulate. Finally, the methane production curve simulated in ADM1 is calibrated by fixing the values of the soluble and particulate fractions, and of the hydrolysis rate constant (assumed equal for proteins, lipids and carbohydrates) for the particulate fraction. Figure 2.10 shows a graphical description of the method as implemented by Girault et al. (2012).

The method is sensitive to some of its assumptions. The substrate to inoculum ratio and the origin of the inoculum should be selected carefully in order to improve the confidence in the calibrated parameters and fractionation (Girault et al., 2012). The calibration of the MPR is also sensitive to the simulated composition of the inoculum. The method is applied using a first-order hydrolysis kinetics; however different kinetics might be considered as well to describe the degradation of X-fraction. The method provides the hydrolysis rate constant for the substrate, however it has been shown that values from batch assays are usually conservative with respect to hydrolysis rates then found in scaled-up continuous reactors (Jensen et al., 2011).

In addition to these constraints, this method appears interesting because it permits the description of the substrate both in composition and kinetically. Also, a kinetic-based soluble/particulate fractionation can have advantages over a physical-based one, which is generally defined on fractionation at 0.45µm, even if this may not be the limit for physical accessibility of biomass to the substrate.

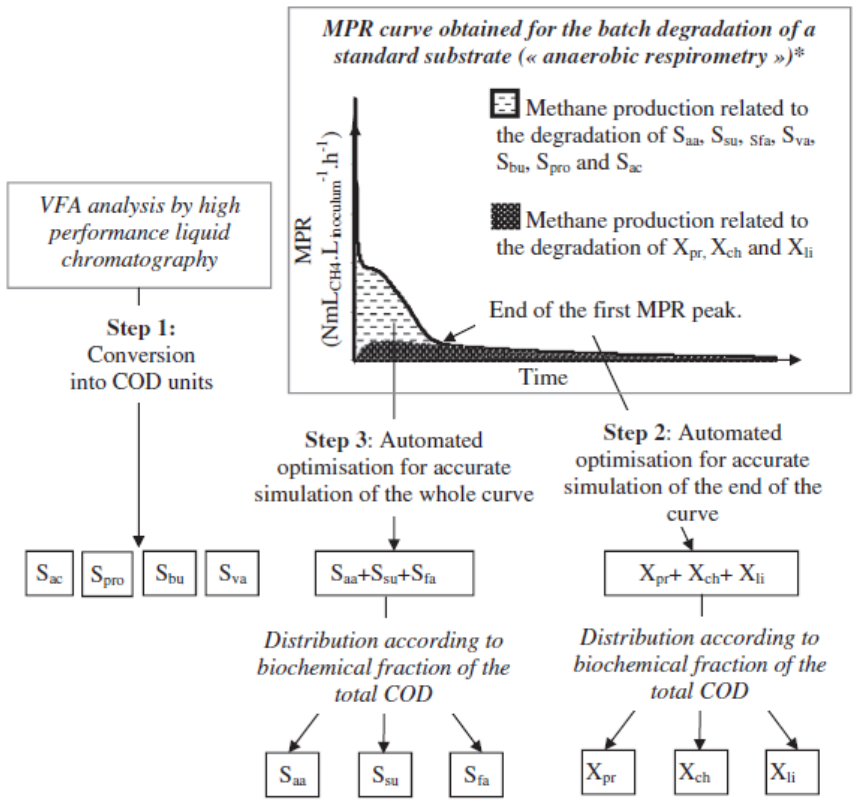

Step 4: Determination of Xi fraction according to the total COD balance (nitrogen content of Xi is adjusted to respect the total organic nitrogen balance). Other organic input state variables are considered as empty.

Figure 2.10. Framework for the fractionation of a substrate, using physicochemical and degradation kinetics. *The methane production of the inoculum is subtracted from the analysed MPR curve. Adapted from Girault et al. (2012).

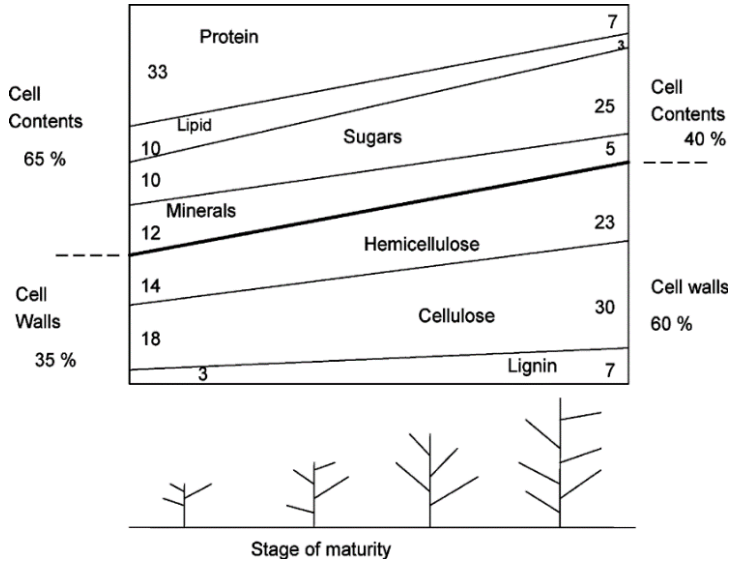

Figure 2.11. Influence of harvest time on the composition of grass (Holmes, 1980).

A final comment, that may be applied to every technique, is the intrinsic uncertainty of the input fractionation. It is important to consider that the composition of the substrate is not constant and will change across the year, depending principally on the length and conditions of storage and in the case of crops/weed on its harvest time (see for instance,

Figure 2.11). Uncertainty tools should be used as a good modelling practice (Sin et al., 2009b).

2.6.2 Model calibration

Model parameters have not universal value (otherwise they would be constant), but need an adjustment for every specific case. Calibration of complex biological models is not straightforward when considering the high number of parameters used and the difficulty in measuring state variables. Calibration of bioprocess models has been usually characterized by a wide number of approaches and procedures; a lack of common protocols for calibration hinders a comparison between different modelling experiences. In the field of activated sludge modelling, different calibration protocols have been recently proposed, so as to improve quality check and comparison (Sin et al., 2005), and the same cannot be said for the field of anaerobic digestion, particularly in ADM1 (Donoso-Bravo et al., 2011).

A commonly used protocol for parameter estimation is the following:

- Sensitivity analysis
- Estimation process
- Analysis of the results

Sensitivity analysis

Only a certain number of “meaningful” parameters should be selected for calibration: an “over calibrated” model would reproduce the experimental data but eventually would have poor predictive ability. In the original ADM1 report (Batstone et al., 2002) the following strategy for minimising the number of parameters to be optimised numerically was described:

- Taking from the literature the parameters with low variability, such as inhibition (K_I) and yield (Y) constants.
- Taking more variable parameters from studies using similar reactor design, operation and feed matrix.

- Reducing the parameters by performing a numerical analysis on identifiability, correlation and sensitivity.

Sensitivity analysis is often used to select the parameters most suitable for estimation, and reducing the size of the optimization problem. In fact, not all parameters substantially influence the output of the model, so that they do not need to be changed to fit the model to the experimental values. Generally sensitivity analyses evaluate the change in some selected outcomes of the model that result after a change in the model parameters. Most sensitivity analyses are of local nature, i.e. they explore the model around a selected state, usually steady state, and therefore only describe local model behaviour around this point. When the model is used to explore the behaviour of the process across a larger range of variation of the parameters, a global sensitivity analysis (GSA) would be a better approach (Donoso-Bravo et al., 2012).

Parameter estimation

The focus is put on the calibration of the biochemical parameters (but when the hydrodynamics of the reactor is unknown and influential, specific calibration experiments should also be realized as well for the mass transfer parameters, as it is done for example in the calibration of activated sludge models).

In general, the parameters set provided in the ADM1 STR constitute a valid starting point for the simulations and calibrations; Batstone et al. (2006), reviewed the application of ADM1 up to 2005 with different substrates, and found modifications to the kinetic parameters of the order of 20–50%.

Generally, parameter estimation should be conducted with the following recommendations (Batstone et al., 2004):

- Minimise analytical work.
- Minimise reactor operation time.
- Minimise simulation time.

Different experimental methods can be used to calibrate the kinetics parameter of the model. Table 2.4 reports the ADM1 applications, an the methods are described as follows:

Measurement from a continuous reactor

The variations in the loading rate depend on the operation of the digester: it is usually applied when calibrating full-scale reactors, where it is risky to impose pulses in the feeding. The “quality” of the results depends on the variations that occur during normal operation; if the input excitation is low, model predictions may be poor outside of the (quasi) steady state conditions used for calibration, i.e. when stronger variations occurs. This methods has been applied in ADM1 calibration by Lübken et al. (2007), Wichern et al. (2009), Batstone et al. (2009)

Measurement from a continuous reactor with imposed pulses

The input excitation is imposed with specific substrate pulses, depending on the parameters to be calibrated (e.g. using acetate pulse for acetate uptake kinetics). The response of the reactor to each pulse is monitored and used to calibrate the selected parameter. Concentration pulses allow a lower correlation between the k_m and K_S parameters in the Monod function: during a pulse, the substrate concentration increases from below to above the substrate-specific K_S value; a hydraulic pulse might cause a biomass wash-out to reach this effect. Kalfas et al. (2006b) used an interval of seven days between each pulse: the experimentation time may be longer if different parameters have to be calibrated. This method has been also used by Batstone et al. (2003).

Measurement from a batch reactor

In this case the parameters are calibrated against the measurement in batch reactors, as a predictive study for the performance of continuous reactors treating the same substrate. Galí et al. (2009) and Derbal et al. (2009) used the parameters calibrated in batch experiments to simulate continuous reactors with acceptable accuracy. In both cited cases, only disintegration and hydrolysis constants were experimentally calibrated, while default values were used for all the other parameters.

Measurement from Anaerobic Sequential Batch Reactors (ASBR)

ASBR reactors can be used for parameter estimation. This experimental mode has the following advantages (Batstone et al., 2004):

- A shorter operation time of the system is required to achieve repeatable operations and convergence with the model, in comparison to continuous reactors.

- The system is excited naturally in its operation by repeated inputs, with resulting substrate concentrations that change from well above to well below saturation concentrations in the Monod function: a proper identification of the Monod parameters is allowed.
- Repeated cycles allow an increase in the confidence of the estimated parameters.

However, attention is required in the determination of the sludge retention parameter of the system, as parameter estimation depends strongly on these values (i.e. a higher biomass concentration leads to a faster susbtrate degradation). Also, the composition of biomass might change along cycle repetitions.

Batch experiments with inoculum from a continuous reactor

Batch experiments are carried out using inoculum from the continuous reactor to be calibrated. ADM1 is used to simulate the continuous reactor and at the same time to determine the composition of the inoculum used in batch tests. Batch configuration allows for specific substrate pulses without disturbing the continuous reactor. Specific substrate pulses are selected to calibrate a specific biochemical step (e.g. using acetate if acetogenic kinetics is to be calibrated). The parameters calibrated in batch are then used to simulate the continuous reactor. Implementations of this method can be found in the works of Girault et al. (2011) and Antonopoulou et al. (2012a). A diagram explaining the process is depicted in Figure 2.12. This method was also used by Zamanzadeh et al. (2013) to calibrate kinetics of acetoclastic, propionate oxidize (with Monod), and hydrolysis (1st order)

When the parameters calibrated at lab-scale are to be used at full scale, the transportability of parameters across different systems must be considered because of the different modes of operation and enviromental conditions (Batstone et al., 2004). Differences could exist between the modes of operation, as lab-scale experiments are operated in batch or sequencing batch mode, while most full-scale systems are completely mixed continuos flow or partially plug-flow. Also, it is often not possible to replicate and maintain equal environmental factors such as nutrient, buffer, pH, and liquid-gas mass transfer conditions between the lab-scale and full-scale reactors. Finally, biomass adaptation is an important phenomenon in continuos reactors, while in batch assays the inoculum is rarely optimized for the analyzed feedstock and significant adaptation does not occur during the test (Batstone and Jensen, 2011).

For instance, Batstone et al. (2009) found that the hydrolysis constant for waste activated sludge evaluated in batch assays were an order of magnitude lower than in continuous full scale reactors; therefore they recommend using BMP testing for project feasibility analysis when the degradability of the feedstock is considered, but not for calibrating dynamic modeling.

The mathematical methods chosen in calibration (cost function and minimizations techniques) also have influence on the results (Donoso-Bravo et al., 2012), however this aspect is not covered in this thesis.

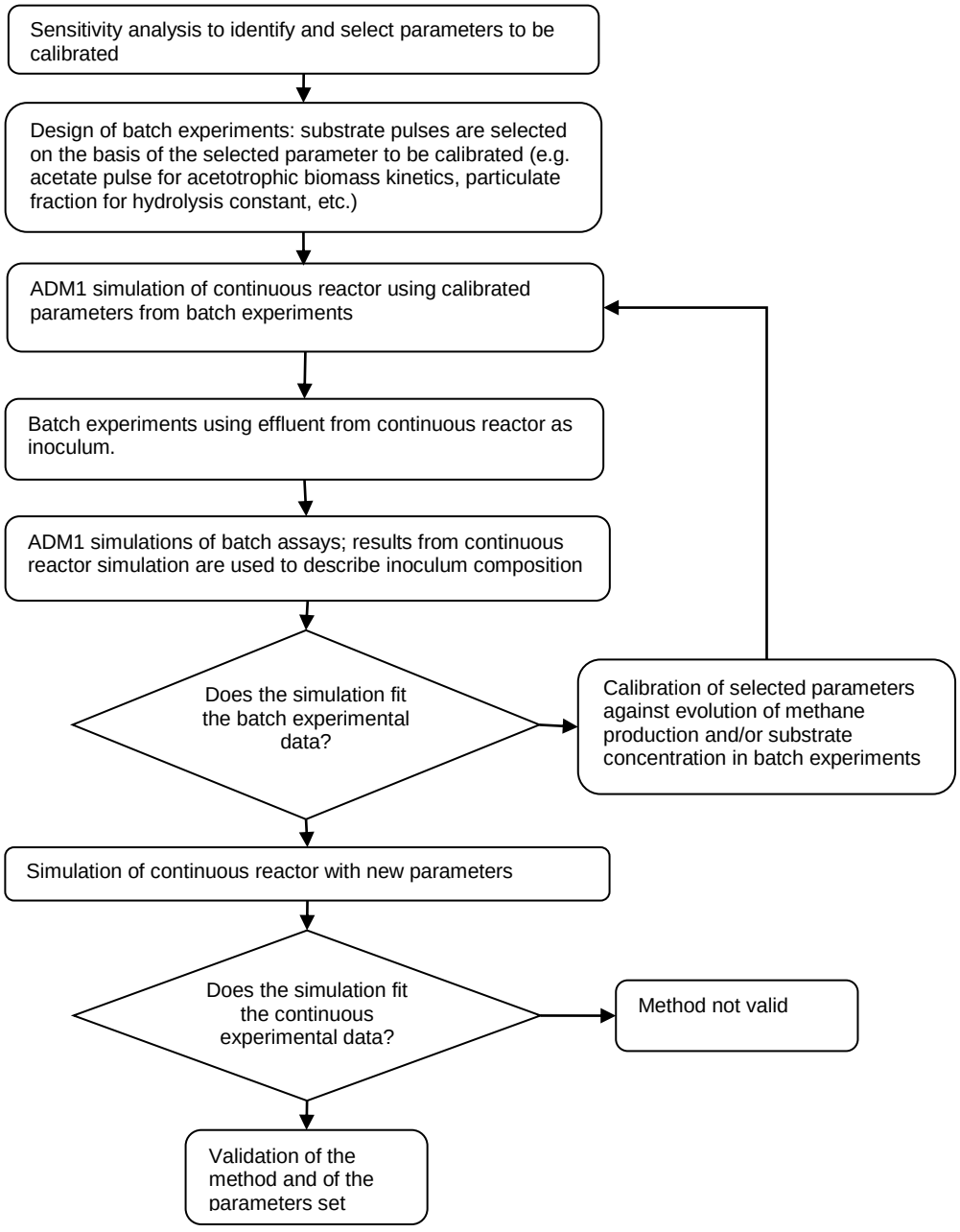

Figure 2.12. Framework for the calibration of ADM1 with batch and continuous experiments. Adapted from Girault et al. (2011).

Table 2.4. Description of the calibration protocol in some ADM1 implementations.

Method of calibration and (substrate)	Sensitivity analysis	Measurement	Parameter calibrated	Note	Reference
Continuous reactor (Grass silage)	Weighted sum of sensitivity indexes for certain objective functions (organic acids and total solid in the effluent, CH4, CO2 and H2 gas content, gas flow). Stepwise single-parameter variation (SVM) between 50%-200% of reference value.	Organic acids Total solids pH %CH4 %CO2 %H2 Gas flow	k_{dis} $k_{m,pro}$ $K_{s,h2}$ $K_{i,h2,c4}$ $K_{i,h2,pro}$ $K_{i,nh3,ac}$ $ph_{UL,acid}$ $ph_{LL,acid}$	Results of sensitivity analysis were not used for selection of parameters.	(Wichern et al., 2009)
Batch experiments with inoculum from continuous reactor. (Pig manure)	A sensitivity index was defined for certain objective functions (COD removal, methane yield, methane content, methane production after feeding). Perturbation in the parameter: ± 20% Parameters with index >30% were considered for calibration.	Biogas production in batch after specific substrate pulse.	$k_{m,su}$ $K_{s,su}$ $k_{m,pro}$ $K_{s,pro}$ $k_{m,ac}$	The method is based on the assumption that both batch and continuous operations have to be simulated using the same set of parameters. khyd appeared non sensible because of partially hydrolysed substrate	(Girault et al., 2011)
Batch experiments with inoculum from continuous reactor (acidified effluent of thefermentative hydrogen production process from sweet sorghum extract)	Only kinetic parameters of VFA and H_2 uptake are selected, because of the composition of the feed (mainly VFAs).	%CH4 VFAs and hydrogen, in batch after specific substrate pulses.	$k_{m,ac}$ $k_{m,h2}$ $k_{m,pro}$ $k_{m,bu}$	For each process, only the km,process is calibrated, while default values are used for Y, kS,process and kdec. Continuous reactor was simulated at different retention times: performance predictions were sufficiently good, and the model was used to simulate the HRT at which the process would fail.	(Antonopoulou et al., 2012a)
Continuous reactor with imposed pulses (olive pulp)	n.d.	%CH4 sCOD VFAs pH	$k_{m,ac}$ $k_{S,ac}$ $k_{m,pr}$ $k_{S,pr}$ $k_{m,bu}$ $k_{S,bu}$ $k_{hyd,ch}$ $k_{hyd,li}$ $k_{hyd,pr}$ $f_{pro,su}$ $f_{ac,su}$	The magnitude of the pulses were not justified (they might be not exciting enough)	(Kalfas et al., 2006a)

Table 2.4 (continued) Description of the calibration protocol in some ADM1 implementations.

Continuous reactor with imposed pulses (olive pulp)	n.d.	%CH4 sCOD VFAs pH	$k_{m,ac}$ $k_{S,ac}$ $k_{m,pr}$ $k_{S,pr}$ $k_{m,bu}$ $k_{S,bu}$ $k_{hyd,ch}$ $k_{hyd,li}$ $k_{hyd,pr}$ $f_{pro,su}$ $f_{ac,su}$	The magnitude of the pulses were not justified (they might be not exciting enough)	(Kalfas et al., 2006a)
Batch (agro-residues)	n.d.	Methane production in batch test.	k_{dis} (of the substrate, not of decaying biomass).	Conditions in batch reactor might be different from continuous reactor. All other kinetic parameters from (Batstone et al., 2002)	(Galí et al., 2009)
Continuous reactor (Grass silage)	n.d.	Methane production	k_{dis} and extended retention time of the solids (t_{res})	The calibrated model was unable to predict VFA accumulation in one of the reactors, probably due to the restricted set of parameter that were calibrated.	(Thamsiriroj and Murphy, 2011)
Continuous reactor (sewage sludge) Two-stage pilot scale digestion of (thermophilic/mesophilic)	Most sensitive parameters as identified in the original implementation (Batstone et al., 2002)	COD sCOD acetate propionate TKN %CO2 %CH4 pH	k_{dis} $k_{m,ac}$ $k_{m,pro}$ $k_{S,ac}$ $k_{S,h2}$ $k_{I,h2,pro}$ $k_{I,nh3}$	Most sensitive parameters were selected from literature, as the same substrate (sewage sludge) was digested.	(Blumensaat and Keller 2005)

Table 2.4 (continued) Description of the calibration protocol in some ADM1 implementations.

Continuous reactor (Dog food and flour) Two stage digestion (thermophilic/mesophilic)	A dynamic sensitivity index was defined for 7 material components: valerate, butyrate, propionate, acetate, methane, ammonia, sCOD. All 17 kinetic parameters in the implemented model were seleceted for the sensitivity analysis. Perturbation in the parameters: ± 50% with respect to their suggested values in Batstone et al. (2002). The dynamic sensitivity index was calculated averaging the differences between original and perturbed parameter across the simulated time. From the values of the calculated sensitivity index, the most sensitive parameters are selected for calibration.	COD sCOD Acetate Methane production	Thermophilic: k_{dis} k_{dec} $k_{S,su}$ $k_{S,aa}$ $k_{m,pro}$ $k_{S,pro}$ $k_{m,ac}$ $k_{S,ac}$ Mesophilic: kdis $k_{m,pro}$ $k_{S,pro}$ $k_{m,ac}$	Model implementation was simplified neglecting pH inhibition and physico-chemical processes. The perturbation range is arbitrary: some of the selected parameters have been described with smaller or larger ranges of variability (Batstone et al., 2002). Sensitivity extended to 7 components might be misleading: from a design and control point of view not all components have the same importance. A similar approach was first used by Jeong et al. (2005)	(Lee, Suh et al. 2009)
ASBR (Winery wastewater in 5L pilot scale ASBR)	n.d.	Acetate (Gas flow, pH, VFAs to validate)	$k_{m,ac}$ $k_{S,ac}$ $k_{m,ethanol}$ $k_{S,ethanol}$	ASBR are operated with the normal fill–react–settle–decant operation. Parameters are estimated using the data of four cycle of operation of the reactor, where wastewater is added. Parameters are validated with two additional cycles of operation, where only spikes of acetate and ethanol are added. Repetition of cycles increases the confidence in estimated parameters.	(Batstone et al., 2004)
Pig manure and beet energy crop in full scale mesophilic plant.	Variance-based global sensitivity analysis on a set of 21 parameters of the model, selected with prior expert knowledge. The analysis is based on a Bayesian procedure developed by Oakley and O'Hagan (2004).	n.d.	k_{dis} $f_{ch,xc}$ $f_{pr,xc}$ $f_{li,xc}$ $k_{m,ac}$ $X_{ac(}0)$	In this study SA is performed primarily to select the parameters for uncertainty analysis. The results of sensitivity analysis are dependent on the selected ratio of substrate in the feed.	(Južnič-Zonta et al., in press)

2.7 Conclusions

In this chapter the main features of anaerobic digestion modelling were reviewed. Different research and engineering problems where modelling is an essential tool were described. One main objective of this thesis is the simulation and benchmarking of operational strategies to integrate AD in a microgrid. To address this research objective, mechanistic and complex models are required, which offer extrapolation capabilities to investigate process performance under different scenarios. The ADM1 model was therefore selected as the modelling framework to use in this thesis.

This review chapter then covered the main characteristics of ADM1, including the description and limitations of the modelling of biochemical and physico-chemical reactions. A particular focus was given to two main steps for the ADM1 implementation, namely the description of the substrate characteristics as model inputs, and the calibration methods which can be employed to calibrate relevant parameters. Chapter 3 shows how the methods here reviewed are modified and improved to obtain model inputs and calibrated parameters.

3 Methodology

3.1 Model building steps

The good practice in the development and evaluation of a model should follow a number of steps, which are similar across engineering disciplines, and can be summarised as follows (Jakeman et al., 2006, Donoso-Bravo et al., 2011) (Figure 3.1):

- Definition of the modelling objectives.
- Selection of the type and structure of the model, mainly on the basis of the modelling objectives and established prior knowledge.
- Collection of experimental data.
- Model implementation, including coding and simulation software.
- Selection of the parameters to be estimated, depending on their uncertainty and sensitivity on the experimental data.
- Estimation of the parameters.
- Direct validation: goodness of fit, uncertainty, model adequacy.
- Cross validation using a different data set.
- Use of the model for process and scenario analysis.

When the direct or cross validation are not satisfactory, the modeller can return to the previous steps of model selection and parameter selection/estimation. The following sections outline how the previous steps have been implemented during this research.

3.2 Modelling objectives

In general, mathematical models are used to describe the main aspects of a system, including biological systems such as anaerobic digestion. They improve the understanding of the system, the formulation and validation of some hypotheses, the prediction of the system behaviour under different conditions, reducing the burden of experimental trials to explore all relevant possible combinations and consequently the cost and time to develop a new process.

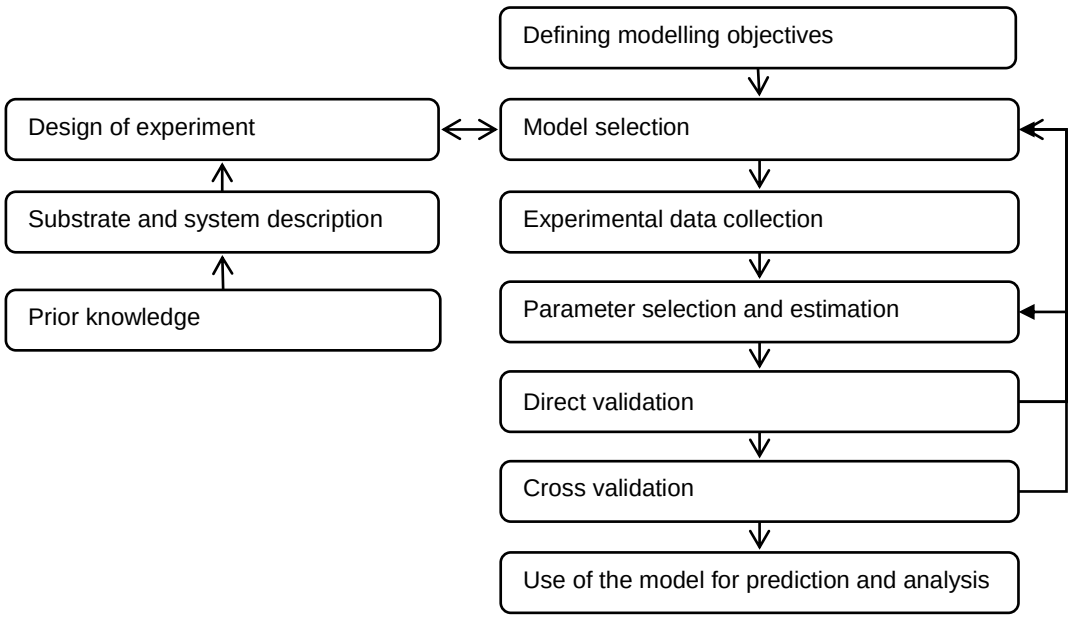

Figure 3.1 Main steps for the model building process

This research was developed following a series of objectives, which differ in terms of the systems and processes investigated but are related to each other (Figure 3.2). From wider to smaller systems:

- Development of a model of an integrated system of renewable energy technologies, including non-dispatchable systems (such as PV and wind) and anaerobic digestion, to simulate and explore different operational strategies and conditions. In particular, this research is focused on the development and validation of a complex and realistic model of AD, able to simulate the highly dynamic operation of the digester in these kind of integrated systems and the use of different substrates.
- Development and validation of a model structure that is able to describe the performance of an AD system under organic stress conditions.
- Development and validation of a model structure that is able to predict the production of biogas when substrates with different characteristics (kinetic and biochemical) are mixed.
- Development and validation of analytical and model-based tools to describe any given substrate in terms of inputs for the aforementioned models.

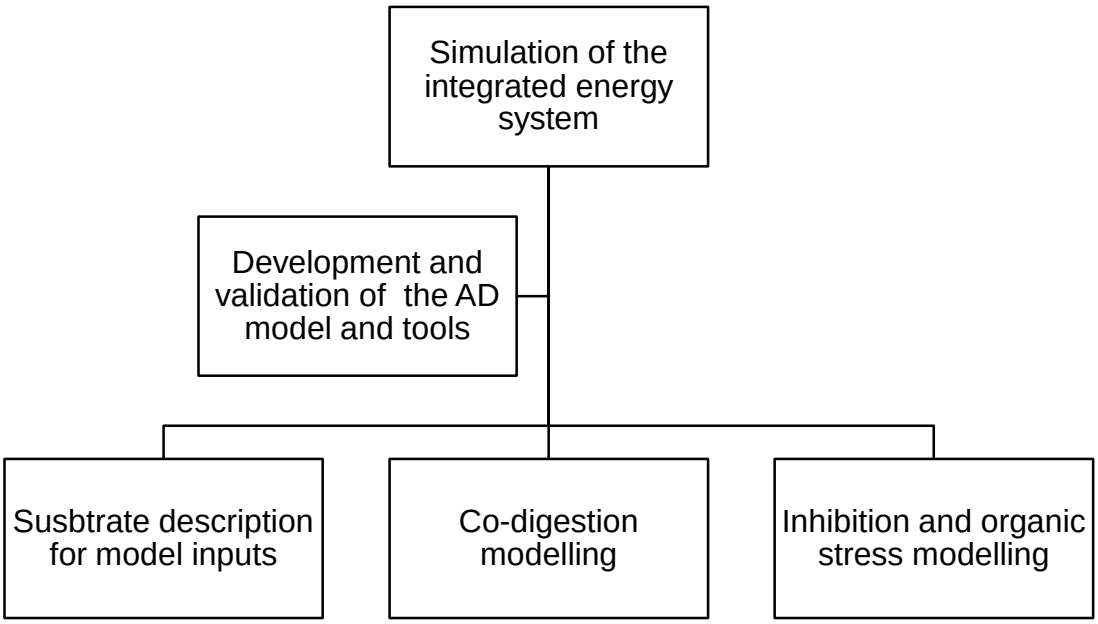

Figure 3.2 Overview of the interconnected objectives of this research.

3.3 Model selection

Different model structures for AD are available from the literature (see section 2.3.1). In theory, model structures should be chosen according to four principles (Donoso-Bravo et al., 2011): (i) simplicity, the model should be as simple as possible; (ii) causality, the model should represent the most relevant cause-effect relationships; (iii) identifiability, the values of the unknown parameters should be identifiable from the available measurements; and (iv) predictive capability, the model should remain valid under future or alternative reasonable conditions.

In this research, an explicit model selection process was not performed and instead ADM1 was chosen *a priori* as the adequate initial model structure, to be calibrated and eventually modified depending on the research objectives and available experimental data. Given the high number of parameters employed in ADM1, the model can be considered overparameterized, i.e. it is not possible to determine unique values of the parameters given plausible available experimental data. The aforementioned simplicity and identifiability principles would dictate to reduce the complexity of the model, adapting it to the observed experimental dynamics. However, overparameterized models allow for the inclusion of a more extensive prior knowledge of the system behaviour, and this is particularly useful when processes become important during the prediction period that were insignificant during the identification period (Reichert and Omlin, 1997). In this regard, ADM1 can be considered as the “state of the art” model in AD, which collects and

systematizes the current consensus of the scientific community. ADM1 in fact was developed as a common platform for anaerobic process modelling and simulations, and this thesis can be considered as an extension of this common platform to new processes and conditions.

3.4 Experimental data collection

Different experiments were performed during this research (Table 3.1), each connected to a specific research objective and also acting as an evaluation and validation of a previously defined methodology:

1. Batch tests (together with physio-chemical analysis) as a methodology to characterise four different substrates as ADM1 model inputs: green waste (GW), food waste (FW), pig manure (PM), oat residues (OAT). Tests 1a and 1b employed different inoculums.
2. Semi-continuous mono-digestion of GW and FW to validate the batch characterisation methodology, by comparing the quality of fit and the values of the parameters calibrated on the different experimental tests. Model adequacy was also investigated by evaluating the quality of fit at different OLRs.
3. Semi-continuous mono-digestion of GW and FW, at elevated OLR to select and calibrate the inhibition structure in ADM1.
4. Semi-continuous co-digestion of FW and GW to update ADM1 structure for co-digestion and evaluate co-digestion interactions.
5. Semi-continuous co-digestion of all four substrates to validate co-digestion and inhibition model structures.

3.4.1 Materials

Household segregated food waste and green waste were collected at a local recycle centre and stored at 5 C. Within 24 hours, the substrates were examined and large pieces of bone, plastic, metal, wood were removed to avoid damage to the homogenisation equipment and reduce sampling errors during later analysis. The substrates were then homogenised using a mincer to an average particle size of 1 mm, sampled for chemical analysis, and the remaining part was stored at -18 C and thawed before feeding to the digesters. Pig manure was collected at the University of Leeds Farm and stored at -18 C and thawed before feeding to the digesters. Cereal residues were collected from a muesli manufacturer and stored in

a dry environment at ambient temperature: due to the low moisture content, the substrate did not require any refrigeration.

Experiment number (Data set)	Objective	Type	Substrate	Length [days]	OLR [gCOD L^{-1} d^{-1}] Min-max
1a, 1b	Substrate characterisation	Batch - with different inoculum in 1a and 1b	GW and FW (1a) PM and OAT (1b)	60	2.5 (ISR)
R-a (2)	Validation of substrate characterisation and model adequacy	Semi-continuous mono-digestion	GW, FW	112 (GW) 144 (FW)	1-6
R-a (3)	Identify model inhibition structure	Semi-continuous mono-digestion	FW	132-204	6-10
R-a R-b R-c (4)	Co-digestion: update model structure and effect analysis	Semi-continuous co-digestion	GW, FW, PM, OAT	310	1-11
R-a R-b R-c (5)	Validation of inhibition and co-digestion model structure with different substrates	Semi-continuous co-digestion	GW, FW, PM, OAT	310	1-11

Table 3.1 Main operational details and objectives of the experiments

3.4.2 Analytical methods for substrate characterisation

Substrates, inoculum and effluent from the digesters were analysed for total solids (TS) and volatile solids (VS), volatile fatty acids (VFA), total ammonia nitrogen (TAN), intermediate and partial alkalinity (IA & PA) and pH. Elemental analysis was performed on substrates and inoculum only. VFA and TAN were measured on the supernatant obtained through centrifugation of the samples in 2.5 ml vials at 14000 rpm; in the case of the substrates, a previous dilution with two parts of water was necessary.

Total solids and volatile solids were measured according to standard methods (APHA, 2005), partial and total alkalinity were measured according to Ripley et al. (1986) through titration at pH 5.75 and 4.3 respectively, using an autotitrator. pH of digestate samples was measured with a pH meter and probe (Hach); for limited periods in experiments 3 and 5, pH was measured continuously through pH probes inserted in the reactor (Atlas Scientific) with data acquisition performed by an in-house programmed Arduino micro-controller. Volatile fatty acids were determined in a gas chromatography system (Agilent) equipped with a flame ionization detector (FID) and a DB-FFAP high polarity capillary column (30 m, 0.32 mm ID, 0.5 µm). Helium was the carrier gas and was adjusted to a flow rate of 10 mL/min. Each sample was injected automatically with a split ratio of 5:1, and the injection port

temperature was 150 °C. The detector temperature was 240 °C, while the oven temperature program was as follows: 60 °C (4 min), ramped at 10 °C min^{-1} to 140 °C, then at 40 °C min^{-1} to 200 °C, remaining at 200 °C for 5 min. Carbon (C), Hydrogen (H), Nitrogen (N) and Sulphur (S) content on TS were determined through elemental analysis in an elemental analyser (Flash EA2000, CE Instruments) equipped with a flame photometric detector (Flash EA 1112 FPD, CE Instruments), according to manufacturer's instructions. The oxygen content was then calculated by subtracting from TS the sum of C, H, N, S and ash contents, where the ash was determined by loss at ignition at 1050 C. Total ammonia nitrogen was measured using an ion chromatography (IC) system (Metrohm 940 ProfIC Vario) as per the manufacturer's instructions. The methane content was measured with an infrared sensor (Dynament Premier Series sensor), installed in the gas line, with data acquisition performed by an in-house programmed Arduino micro-controller.

3.4.3 Batch tests

Batch tests were performed in 600 ml laboratory digesters, in triplicate for both substrate and blank (inoculum only), with a working volume between 350 and 500 ml, depending on the test. Positive controls using cellulose were also performed in triplicate. The temperature of the digestion was maintained at 37 C through immersion in a water bath and agitation was supplied by a vertical stirrer operated at 60 RPM, with consecutive on/off cycles of 30 seconds each. Different inoculums were used in the tests and more details are given in Chapter 4.

The mass of the substrate added was calculated on the basis of a defined inoculum to substrate ratio. There is no accepted standardized ratio between the inoculum and substrate in the research community for batch biodegradation assays; however Raposo et al. (2012), reviewing many BMP tests, identified 2.0 $gVS_{inoculum}/gVS_{substrate}$ as a safe minimum threshold. This high ratio reduces inhibition effects and accumulation of intermediary compounds during substrate degradation, thus allowing hydrolysis rate limiting conditions for methane production from the particulate fractions. In this research, a ratio of 2.5 $gVS_{inoculum}/gCOD_{substrate}$ was finally selected, which allows to be on the conservative side of the proposed threshold, and takes into account that different substrates have different energy content and therefore COD instead of VS is used in the denominator of the ratio.

After adding the substrate in the digesters, the headspace was purged with pure nitrogen. The produced gas was scrubbed into a 3M NaOH alkaline solution, in order to remove the carbon dioxide and the hydrogen sulphide; a chemical pH indicator based on thymolphthalein was added to the solution, and the color change indicated the exhaustion of the absorbing solution and the requirement for replacement. The volume of scrubbed gas was then measured through an AMPTSII system (Bioprocess Control) (Figure 3.3), with a resolution of 10 mL methane production is reported at STP (0 C and 1 bar) and calculated assuming a scrubber efficiency of 98%, subtracting the concentration of water vapour, and taking into account the overestimation caused from the initial nitrogen content in the headspace, as detailed in Strömberg et al. (2014); for the latter an approximation of the initial biogas flow composition is required, and was approximated through the Buswell formula (Buswell and Mueller, 1952), using the elemental composition of the substrates. The experiment ended 60 days after the initial feeding.

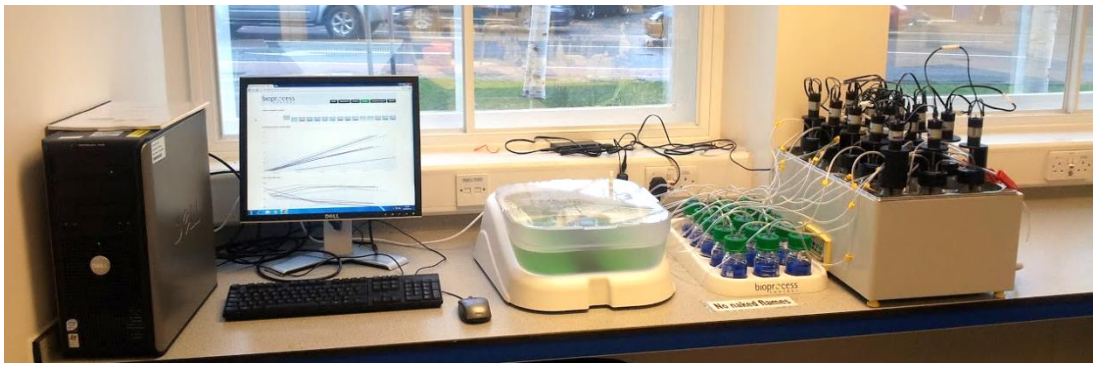

Figure 3.3 Complete setup for the batch tests, from right to left: stirred batch reactors in water bath, alkaline gas scrubbing system, multi-channel volumetric gas meter, software user interface.

3.4.4 Semi-continuous tests

Semi-continuous tests were performed in 2400 mL laboratory digesters, and in duplicate for each substrate tested. The temperature control, reactor mixing, gas scrubbing and gas volume measurement were performed as in batch tests.

Before each addition of substrate, digestate was removed and sampled for analysis. The amount of removed digestate controlled the working volume of the digester, which changed from 2100 mL to 1800 mL: smaller working volumes were maintained to reduce the risk of gas tubes becoming blocked by the foam during high organic loading rate periods. Substrates were fed through a hydraulically sealed inlet, therefore minimizing the input of air into the headspace. During

sampling and feeding, an external plastic bag with synthetic biogas (60% CH_4 and 40% CO_2) was connected to the flush gas inlet of the reactor to equilibrate the pressure in the headspace and reduce the entry of external air. The entry of air in the headspace would reduce the CO_2 concentration and therefore would then increase the first estimations of the methane flow rate after each feeding, as air would not be scrubbed by the alkaline trap and finally would "appear" as additional methane production.

Figure 3.4 The reactors used in the semi-continuous experiments.

Different semi-continuous tests were performed, each corresponding to a different objective as outlined in paragraph 3.4. The tests differed in terms of duration, the substrates fed and the OLR, as shown in Table 3.1. More details of each test are given in the respective chapters.

3.5 Model implementation

3.5.1 Aquasim implementation

ADM1 was implemented in Aquasim 2.1d (Reichert, 1998), the input file/code is supplied in Appendix 1. In short, Aquasim is a solver of systems of differential and algebraic equations, which, for the spatially homogeneous systems here investigated, can be described as follows:

$$\frac{dV_R}{dt} = Q_{in} - Q_{out} \quad \textbf{(3.1)}$$

$$\frac{dC_i}{dt} = \frac{I_{in,Ci}}{V_R} - \frac{Q_{in}}{V_R} C_i + \rho_{C_i} \quad \textbf{(3.2)}$$

where V_R is the compartment volume, Q_{in} is the volumetric inflow and Q_{out} is the volumetric outflow. The temporal change in the concentration of the substances is given in equation (3.2), where C_i is the substance concentration, $I_{in,Ci}$ is the loading of the substance described by the concentration C_i into the reactor (mass per unit of time), and ρ_{Ci} is the transformation rate of the substance described by the concentration C_i. The transformation rate describes the biological, chemical (eg. acid-base equilibria) and physical (eg. gas-liquid mass transport) reactions implemented in ADM1 (as reviewed in Chapter 2).

Each experimental test was modelled as a mixed liquid reactor with a gas diffusion link to a mixed gas headspace and a further link to a virtual gasometer (to simulate the accumulated methane volume). The complete description of the Aquasim implementation is given in the Appendix 1. It is important to model the gas headspace together with the liquid reactor, in order to take into account the following aspects:

- Although the biochemical transformation occurs only in the liquid phase, it is necessary to simulate both phases simultaneously, as the partial gas pressures of CO_2 and H_2 influence significant physicochemical and biological reactions in the liquid phase (CO_2 influencing the charge balance and H_2 inhibiting the acetogenic reaction steps).
- When the digester is operated semi-continuously, the sudden production of CO_2 (from the consumption of alkalinity) after a substrate loading will displace part of the methane content in the headspace, which will consequently be measured as a methane flow by the experimental flowmeter. The model needs to be able to reproduce this phenomenon, otherwise parameter calibration will be biased trying to reproduce the initial non-biological methane flow rate with increased hydrolysis and/or VFA uptake rates.

The temperature of the compartments is another input of the model, with the headspace temperature considered to be equal to the temperature in the reactor. Volume changes in the compartments (reactor and headspace) are due to variations in the loading and removal rates of the liquid from the reactor. The biogas

production and water evaporation are considered not to affect the reactor volume; therefore Q_{out} in equation (3.1) describes only the liquid effluent removal from the reactor. The volume of the reactor changed through the experiment (between 2100 and 1800 mL), as relatively more effluent was removed during periods of foaming in order to diminish the risk of foam reaching the gas hoses. Q_{out} was calculated in a spreadsheet so to maintain the observed volume of the reactor, and then used as input data in Aquasim.

The disintegration step was implemented for the biomass decay products, while it was omitted as the first substrate degradation step. This was to avoid an unrealistic two-step solubilisation process as also recently suggested in Batstone et al. (2015). The state variable X_c, which is used in the default ADM1 to describe both the substrate and the decayed biomass, is therefore maintained in this implementation only to describe the decayed biomass. The pulse-fed substrates were directly described in terms of their biochemical fractions. Another modification was the introduction of dedicated state variables for the products of the disintegration of X_c (e.g. $X_{ch,Bio}$ for carbohydrates). In this way it is possible to have different rate constants for the hydrolysis of compounds from substrates or from the decayed biomass. A Petersen matrix, including all the stoichiometric parameters of all the implemented reaction, the carbon (C_i) and nitrogen (N_i) content of all the compounds, was implemented in a spreadsheet (Table 3.2). With the use of the matrix, COD balances were checked to be zero. The nitrogen and carbon balances were closed in the disintegration step by changing the C_i and N_i of X_c. In the other reactions a balance different than zero shows that the reaction is a source or sink of inorganic nitrogen and carbon - and consequently the source or sinks terms are implemented in Aquasim.

Substrate loadings were implemented in Aquasim as isosceles trapezoidal pulses with a width of 90 seconds each. The duration of the experimental feeding was shorter, approximately 20 seconds to feed the whole of the substrate through the reactor inlet. However an estimated time required for the substrate to get thoroughly mixed in the reactor was also taken into account, thus justifying the slightly longer pulse duration. Also, the width of the pulses has an influence on the time required to complete the simulation, with smaller widths causing considerably higher computational time. The reasons are the following: the maximum integration step has to be maintained below the width of the pulse, otherwise some of the loadings could be missed by the solver; moreover, with shorter pulses the transients become more relevant and the number of error test failures then increases. An error test

indicates that the algorithm is trying to perform too large a time step and it has to repeat the step with a smaller step size in order to fulfil the accuracy criteria of all state and program variables. As an example, on a PC with an Intel Core2 Duo E8400 at 3.00GHz processor, the simulation of the experiment 5 (310 days with 154 feedings) took 15 minutes. Loadings included all COD-fractions and also a further ash fraction (from the substrates VS determinations) to allow the prediction of inerts accumulation in the reactor.

In some cases, simulated state variables need to be transformed into the corresponding measured outputs. In the case of VS, the state variable which are described in g COD L^{-1} need to be transformed into g L^{-1} through the known theoretical oxygen demand of the various compounds ($ThOD_x$ in g COD g^{-1}):

$$VS = \frac{X_{ac} + X_{pro} + X_{c4} + X_{aa} + X_{fa} + X_{su} + X_{h2}}{ThOD_{biomass}} + \frac{X_c}{ThOD_{Xc}} + \frac{X_{ch_{Bio}} + X_{ch} + S_{su}}{ThOD_{ch}} + \frac{X_{li_{Bio}} + X_{li} + S_{fa}}{ThOD_{li}} + \frac{X_{pr_{Bio}} + X_{pr} + S_{aa}}{ThOD_{pr}} + \frac{S_{va}}{2.04} + \frac{S_{bu}}{1.82} + \frac{S_{pro}}{1.51} + \frac{S_{ac}}{1.07} + \frac{X_I + S_I}{ThOD_I} \quad \textbf{(3.3)}$$

The $ThOD_x$ values for carbohydrates, proteins and lipids are shown in Table 3.3; inerts are considered to have the same ThOD content as the substrate from which they originate; for X_c and biomass the values from Huete et al. (2006) were used.

In the case of partial alkalinity: the measured output is transformed into bicarbonate alkalinity by a multiplication by a factor of 1.25, as empirically determined by Jenkins et al. (1983). This factor takes into account that not all the bicarbonate is being titrated at pH 5.75, and that the contribution of free ammonia and undissociated VFAs to partial alkalinity is negligible.

	Solubles										Particulates															Balances		
Process	Ssu	Saa	Sfa	Sva	Sbu	Spro	Sac	Sh2	Sch4	SI	Xc	Xch_Bio	Xch	Xpr_Bio	Xpr	Xli_Bio	Xli	Xsu	Xaa	Xfa	Xc4	Xpro	Xac	Xh2	XI	COD	SIC	SIN
Disintegration Xc										0.1	-1	0.2		0.2		0.3									0.2	0	0	0
Decay biomass Xsu											1							-1								0	3.42E-03	3.47E-03
Decay biomass Xaa											1								-1							0	3.42E-03	3.47E-03
Decay biomass Xfa											1									-1						0	3.42E-03	3.47E-03
Decay biomass Xc4											1										-1					0	3.42E-03	3.47E-03
Decay biomass Xpro											1											-1				0	3.42E-03	3.47E-03
Decay biomass Xac											1												-1			0	3.42E-03	3.47E-03
Decay biomass Xh2											1													-1		0	3.42E-03	3.47E-03
Hydrolysis Carbohydrates_Biomass	1											-1														0	0	0
Hydrolysis Carbohydrates_Substrate	1												-1													0	0	0
Hydrolysis Proteins_Biomass		1												-1												0	-4.23E-04	-1.98E-04
Hydrolysis Proteins_Substrate		1													-1											0	0	0
Hydrolysis Lipids_Biomass	0.05		0.95													-1										0	-1.95E-04	0
Hydrolysis Lipids_Substrate	0.05		0.95														-1									0	-1.95E-04	0
Uptake Sugars	-1				0.1195	0.2422	0.3668	0.1715										0.1								0	7.19E-03	-6.25E-04
Uptake Amino acids		-1		0.2443	0.2420	0.0579	0.2989	0.0770											0.08							0	5.05E-03	7.18E-03
Uptake LCFA			-1				0.6580	0.2820												0.06						0	-7.37E-04	-3.75E-04
Uptake Valerate				-1		0.5076	0.2914	0.1410													0.06					0	-5.39E-04	-3.75E-04
Uptake Butyrate					-1		0.7520	0.1880													0.06					0	-3.75E-04	-3.75E-04
Uptake Propionate						-1	0.5472	0.4128														0.04				0	8.44E-03	-2.50E-04
Upatke Acetate							-1		0.95														0.05			0	1.48E-02	-3.13E-04
Uptake Hydrogen								-1	0.94															0.06		0	-1.66E-02	-3.75E-04
Carbon content [mol C / g COD]	0.0313	0.0304	0.0217	0.0240	0.0250	0.0268	0.0313	0.0000	0.0156	0.0300	0.0278	0.0313	0.0313	0.0299	0.0304	0.0220	0.0220	0.0313	0.0313	0.0313	0.0313	0.0313	0.0313	0.0313	0.0300			
Nitrogen content [mol N / g COD]	0.0000	0.0077	0.0000	0.0000	0.0000	0.0000	0.0000	0.0000	0.0000	0.0043	0.0028	0.0000	0.0000	0.0075	0.0077	0.0000	0.0000	0.0063	0.0063	0.0063	0.0063	0.0063	0.0063	0.0063	0.0043			

Table 3.2 Stoichiometric coefficients and balances for the biochemical processes implemented

3.5.2 Hydrolysis functions

In addition to the first-order kinetics, the Contois kinetics was also implemented to determine which expression was more appropriate to describe the hydrolysis process. Contois kinetics is described by the following expression:

$$\rho_{substrate} = k_{CNT} X_{biomass} \frac{X_{substrate}/X_{biomass}}{K_{S,CNT} + X_{substrate}/X_{biomass}} \quad \textbf{(3.4)}$$

where ρ is the rate of the process for the hydrolysis of the substrate $X_{substrate}$ which is being hydrolysed by the enzyme produced by the biomass group $X_{biomass}$; $K_{S,CNT}$ is the half saturation coefficient for the ratio $X_{substrate}/X_{biomass}$ and k_{CNT} is the maximum hydrolysis parameter. It was assumed that each substrate is hydrolysed by the respective biomass group, i.e. carbohydrates by X_{su}, proteins by X_{aa}, lipids by X_{fa} - with k_{CNT} and $K_{S,CNT}$ being the same for the three processes. A similar approach was adopted by Mairet et al. (2011).

3.5.3 Charge balance

The modelling of acid-base reactions requires the solution of a charge balance, which in anaerobic systems assumes the following form (Nopens et al., 2009):

$$S_{cat} - S_{an} = S_{ac}\alpha_{ac} + S_{pro}\alpha_{pro} + S_{bu}\alpha_{bu} + S_{va}\alpha_{va} + S_{IN}\alpha_{IN} + S_{IC}\alpha_{IC} + OH^- + H^+ \quad \textbf{(3.5)}$$

where S_{IC} (inorganic carbon fraction, which in solid substrates is almost entirely in the form of hydrogen carbonate) was calculated through partial alkalinity (PA) measurements, with titration to pH 5.75 and then multiplication of the measurement by a 1.25 factor, to take into account that not all the hydrogen carbonate is titrated at pH 5.75 (Jenkins et al., 1983); S_{IN} (inorganic nitrogen) in anaerobic systems practically coincides with the measured total ammonia nitrogen; concentrations of VFAs were directly analytically determined; $H^+ = 10^{-pH}$, $OH^- = 10^{(-pK_w+pH)}$ and pK_w = 14. The specific charges α_i^{ch} for each component depend on pH and were calculated as detailed in Nopens et al. (2009). The remaining unknown variables are S_{CAT} and S_{AN} (cations and anions): to remove one degree of freedom, S_{AN} was set to zero when S_{CAT} exceeded S_{AN}, or vice versa. The charge balance is then applied for both the description of the initial conditions and substrate loadings.

3.5.4 Initial conditions

Initial conditions have to be defined for both compartments, for each state variable of the model, prior to any simulation. For the initial conditions in the headspace, the same gas composition used for the calculation of gas flow (as described in Section 3.4.3) was employed.

For the initial conditions in the liquid phase, two qualitatively different sets of variables can be identified: physico-chemical and microbial biomass state variables. The physico-chemical variables can be, for most of the cases, analytically measured or otherwise approximated with negligible effect on model outputs. Microbial biomass initial conditions are more complicated to determine experimentally. Two cases can arise, depending on whether the inoculum is sourced from a digester which can be adequately modelled or is from an external digester whose operation cannot be described in enough detail. The first case is the preferred option: sourcing the inoculum from a digester for which operational conditions and substrate characteristics are known, and using the simulated state variables as initial conditions for the experiment. Examples of this approach may be found in Batstone et al. (2004) and Girault et al. (2012).

In the second case, analytical measurements of the biomass need to be transformed into the relevant model state variables. A traditional method used for the determination of the quantity of microorganisms is the measurement of the volatile suspended solids (VSS). However the VSS values can't be accurately transformed into the mass of the microorganisms, as other non-degraded organic particulates are usually present in the inoculum which are measured by VSS analysis, especially when the source digester is fed on solid wastes. Additionally, the overall microbial mass needs to be allocated into the various microbial groups simulated in ADM1, an allocation that would need further assumptions. Other techniques have been suggested and implemented, such as the in-situ hybridization and microscope counting (Lübken et al., 2007), coenzyme M quantitation (Page et al., 2008) and bicinchoninic acid (BCA) protein assays (Jensen et al., 2008). In general, novel molecular techniques have been increasingly developed in recent years (Pobeheim et al., 2010) which can give a more accurate description of the microbial community. However these techniques are rather complex and specialized, their connection with dynamic modelling is far from being standardized and therefore their use was not considered in this research. Biomass concentrations can also be treated as parameters to be

calibrated, however this method usually leads to high correlation and identifiability problems when also the uptake rate parameters need to be calibrated. The initial rate technique, which involve simultaneous batch experiments at different substrate/biomass ratio has been used to improve the parameters identifiability (Flotats et al., 2006) and to explicitly estimate biomass concentration for ADM1 applications (Jabłoński and Łukaszewicz, 2014). These techniques are promising and design of experiment methods can be applied to optimize the parameter identification (Franceschini and Macchietto, 2008) - however a higher number of reactors is needed.

The experimental mode, batch or (semi)continuous, finally influences the required accuracy of the initial conditions estimation. In batch experiments, the initial conditions are the sole inputs of the system (in addition to the substrate loading) and therefore they will exert a significant influence on the model outputs. On the other hand, in (semi)continuous systems the influence of the initial condition will decrease with each loading event, becoming negligible in the case of long term operations.

In this research, both approaches of the model based and analytical determination have been used. In the batch test 1b the inoculum was sourced from the semi-continuous test 2, and simulated state variables were evaluated as initial conditions for the batch test, taking into account the degassing period.

In the case of external unknown inoculum the following method was designed and employed:

1. Charge balance in the liquid phase, using the required physico-chemical measurements: pH, TAN, VFA, alkalinity.
2. Dissolved methane and carbon dioxide in liquid phase are calculated by being in equilibrium with the headspace conditions.
3. Total biomass concentration is calibrated from the gas production in the control batch test (only inoculum). This calibration is conditional on the decay rate parameter value.
4. Allocation of the total biomass to different trophic groups based on literature values or known composition of feedstock in the source digester.

3.6 Parameter selection

As was reviewed in Chapter 2, ADM1 includes a large number of parameters, which can be divided into different classes:

- Physio-chemical parameters, which define acid-base equilibria and liquid-gas mass transfer. Acid-base equilibria are described by accurate first-principle formulae and therefore they must not be included in the calibration. The liquid-mass transfer rate depends on the value of the gas-liquid transfer coefficient k_La, which in turn depends on the rheology and mixing in the reactor. Although formulae exist to calculate k_La from wastewater engineering principles (Tchobanoglous and Burton, 1991), these are deemed to be not accurate in describing anaerobic laboratory scale systems. Therefore literature data was used in the initial model implementation
- Biological parameters:
    - Stoichiometric yields, which describe the transformation of substrates into products and biomass, depends on the microbial metabolism (network of catabolic and anabolic reactions), and methods are available for deriving the value of the parameters from a thermodynamic analysis of the system (Kleerebezem and Van Loosdrecht, 2010).
    - Kinetic uptake and decay rates, which describe the empirically accepted reaction scheme implemented in the model. In ADM1, the uptake rates are described by the Monod kinetics expressions, which include a maximum uptake rate and half saturation coefficients.

As it has been reviewed in section 0, the common practice in ADM1 implementations has been to focus on the calibration of the biological kinetic parameters, leaving the other parameters at their default values indicated in the original ADM1 STR. In this thesis a similar approach was followed, and for each experiment a set of sensitive parameters was selected for calibration and practically identifiable subsets were calibrated:

- Batch tests. Souza et al. (2013) performed a sensitivity analysis on the methane volume from batch tests, evaluating most of the ADM1 parameters, and showed how the hydrolysis constants had highest values of sensitivity indexes. Previous studies have satisfactorily used ADM1 default uptake kinetic parameters to

simulate batch tests (Souza et al., 2013, García-Gen et al., 2015). Therefore only the hydrolysis and degradability parameters were selected for calibration, based on the assumption that methane production (calibration target) occurred mostly under hydrolysis limited conditions: therefore only hydrolysis and degradability parameters were calibrated.

- In the semi-continuous test 2, the same parameters calibrated in batch tests were evaluated.
- In the semi-continuous test 3, parameters describing different inhibition functions were calibrated.

All parameters estimated have to be considered as conditional on the other parameters left at fixed values. The other stoichiometric and kinetic parameters were taken from Rosen and Jeppsson (Rosen and Jeppsson, 2006), with the exception of the stoichiometric parameters for proteins which were modified to reflect the protein molecular formula adopted (see Section 3.8.3) and k_La from Siegrist et al. (2002)

3.7 Parameter estimation method

Parameters were estimated by a weighted least square method, minimizing the following function (Gujer, 2008):

$$\chi^2 = \sum_{i=1}^{n} \left(\frac{y_{m,i} - y_i(p)}{\sigma_{m,i}} \right)^2 \quad \textbf{(3.6)}$$

where $y_{m,i}$ is the i^{th} measured value of the accumulated methane, assumed to be a normally distributed random variable; $y_i(p)$ is the model prediction at the i^{th} time instance, which is function of the set of parameters p to be estimated; $\sigma_{m,i}$ is the standard error of the measurement $y_{m,i}$ and weights each term of the sum. The same cost function is implemented in Aquasim as the parameter estimation routine. A residual analysis was performed to identify and remove outliers, and eventually parameter estimation was performed on the new processed data set.

In the case of batch tests, the only target measurement is the accumulated volume (calculated as the sum of consecutive volume measurements). The standard error of each measurement was calculated by the uncertainty propagation as the quadratic sum of all previous errors (Taylor, 1996):

$$\sigma_{m,k} = \sqrt{\sum_{i=1}^{k-1} {\sigma_{m,i}}^2} \quad \textbf{(3.7)}$$

As a consequence, the initial volume measurement in batch tests are considered more accurate and have more weight than latter measurements. Using data from the equipment manufacturer and a conservative approach, each measurement was characterised by a standard error of 0.5 mL.

Every batch replicate was treated as a separate data point set for the estimation algorithm, rather than fitting the average of the data points. The Secant Algorithm (Ralston and Jennrich, 1978) implemented in Aquasim was used as the minimization technique, with a tolerance for convergence of 4E-3 in the objective function. Different initial guesses of the target parameters were used in the estimation process to check the convergence of the algorithm towards the same optimum parameters values.

In the case of semi-continuous tests, the methane flow rate was used as the target measurement. Flow rates were calculated from measured volume data points through backward differences. The standard error of each measurement was calculated by uncertainty propagation for the case of quotients (flow rate as the quotient of volume and time interval), which results in the weights in equation (3.6) being proportional to the experimental flow rate:

$$\sigma_{m,i} = \sigma_{rel} y_{m,i} \quad \textbf{(3.8)}$$

For the estimated 0.5 mL uncertainty in volume measurement, a relative standard error σ_{rel} of 7% results for the flow rate. As a consequence, the cost function will “give” similar importance to the experimental periods with low flow rate and high flow rate.

Different fit targets (gas volume in the batch tests, flow in the semi-continuous tests), can be explained as follows: although the volume is the measured quantity by the measuring device, and therefore more accurate than the derived quantity gas flow, the accumulated volume accumulates as well as the uncertainty of each measure; this would lead to a highly imprecise measurement in the semi-continuous experiments, where thousands of data points are collected, with respect to hundreds in batch experiments.

3.7.1 Multivariate estimation

In the case of semi-continuous experiments, the analysis of the effluent provided more experimental data for parameter calibration; the cost function was updated as follows:

$$\chi^2 = \sum_{j=1}^{k} \sum_{i=1}^{n} \left(\frac{y_{m,k,i} - y_{k,i}(p)}{sc_{k,i}} \right)^2 \quad \textbf{(3.9)}$$

where $y_{m,k,i}$ is the i^{th} measurement of the k^{th} variable, $y_{k,i}(p)$ is the model prediction at the i^{th} time instance, function of the set of parameters p to be estimated; and $sc_{k,i}$ is a scaling factor to make the sum term non-dimensional and to standardize the different value ranges and number of measurements n_k of the k variables:

$$sc_{k,i} = \sqrt{n_k} \sigma_{rel,k} y_{m,k,i} \quad \textbf{(3.10)}$$

The relative standard error of the VFA measurement was fixed at 25%, so to maintain more weight on the gas flow measurements, which were deemed more accurate (and also because the gas flow was considered more important to predict than VFAs level).

3.7.2 Quality of fit and parameter uncertainty

Uncorrelated confidence intervals of the parameters are then obtained as follows (Dochain and Vanrolleghem, 2001):

$$p_i \pm t_{\alpha;n-p} \sigma(p_i) \quad \textbf{(3.11)}$$

where $\sigma(p_i)$ is the standard error for the estimated parameter, as calculated by the secant algorithm in Aquasim, and the t-values are obtained from the Student-*t* distribution, for a confidence level specified at 100(1-α)% and n-p (data points - number of parameters) degree of freedom.

3.8 Substrate characterization

A combined biochemical and kinetic fractionation methodology is used to describe the substrate composition in terms rate of degradation and of the various ADM1 state variables (X_{ch}, X_{pr}, X_{fa}, X_I, S_{su}, S_{aa}, S_{fa}, S_{ac}, S_{pr}, S_{bu}, S_{va}, S_I). The methodology is described in the following paragraphs.

3.8.1 Theoretical oxygen demand

In ADM1, organic matter transformations are described on a COD basis; therefore substrate loadings need to be analysed for their COD content. The COD of wastewaters can be determined with high accuracy and with standardized methods; however the application of standard methods to the analysis of solid or semisolid heterogeneous wastes usually produces results with low precision and large confidence intervals, this is because of the non-representative sampling and incomplete COD recovery (Raposo et al., 2008). Optimized methods for the characterization of solid wastes have been recently proposed, based on “solid dilution” (Noguerol-Arias et al., 2012), but their adoption by the research community has been very limited so far.

In this study an alternative approach was employed and the COD of the substrates was approximated by their calculated Theoretical Oxygen Demand (ThOD), using the measured elemental composition of the substrate. The substrate is considered to be fully oxidised to carbon dioxide and water, with nitrogen reduced to ammonia (as it occurs in anaerobic systems) (Baker et al., 1999):

$$C_nH_aO_bN_c + \left(n + \frac{a}{4} - \frac{b}{2} - \frac{3}{4}c\right)O_2 \rightarrow nCO_2 + \left(\frac{a}{2} - \frac{3}{2}c\right)H_2O + cNH_3 \qquad \textbf{(3.12)}$$

and therefore:

$$ThOD\ [gCOD\ gVS^{-1}] = 32 \times \left(n + \frac{a}{4} - \frac{b}{2} - \frac{3}{4}c\right) \qquad \textbf{(3.13)}$$

Molecular formulae ($C_nH_aO_bN_c$) of the tested substrates were calculated from the measured elemental composition (Rittmann and McCarty, 2001) neglecting the sulphur content as sulphur transformations were not implemented in the model.

The method depends on the correct use of the results from the elemental analyser. In elemental analysis, a sample is burned in an excess of oxygen, with the combustion products then being further converted in a series of gas traps, separated in a chromatography column and quantified by a thermal conductivity detector. Combustion occurs in a dedicated reactor maintained at temperatures between 900-1050 °C, reaching temperatures up to 1800 °C during the reaction (Thermo Fisher Scientific Inc., 2008). The equipment used in this research could measure the C, H, N and S content, while the O content had to be determined by difference using the sample ash content. The ash content is known to be dependent

on the ignition temperature used in its determination: lower ash contents are obtained at higher temperature, mainly due to dehydration of structural hydroxyl groups of minerals and thermal decomposition (especially of carbonates) (Matthiessen et al., 2005). The usual ash determination is by ignition to a constant weight at 550 °C (APHA, 2005), which is considerably lower than the temperature reached in the elemental analysis. For this reason, the ash content was also determined by the loss on ignition in a furnace maintained at 1050 °C, and the influence of the temperature of ignition on ThOD and the biochemical fractionation was evaluated.

3.8.2 Biochemical fractionation

Biochemical fractionation allocates ThOD of the substrate to the three biochemical compound groups defined in ADM1: carbohydrates/sugars, proteins/amino acids and lipids/fatty acids. It is assumed that different kinetic fractions have the same biochemical fractionation, and only three parameters are defined: f_{ch}, $f_{pr,}$ and f_{li}. These parameters are treated as unknown and calculated through the biochemical fractionation.

The fractionation is based on the following assumptions:

- All VFA is lost during sample preparation (drying) for elemental analysis, therefore all ThOD is allocated to the sum of the particulate and non-volatile soluble fractions (X_{ch}, X_{pr}, X_{li} and S_{su}, S_{aa}, S_{fa}).
- All ammonical nitrogen (S_{IN}) is lost during sample preparation (drying) for elemental analysis, therefore all nitrogen measured in elemental analysis is of organic character and allocated to proteins (X_{pr}) and amino acids (S_{aa}).

The following system of 3 equations with 3 unknowns allows the calculation of the biochemical fractions, by maintaining a nitrogen, COD and mass balance between the measured substrate and the fractionation of the ThOD.

Nitrogen balance

$$f_{pr} = \frac{g\ N_{substrate}}{gCOD_{\ substrate}} \cdot \frac{gCOD_{pr}}{g_{pr}} \cdot \frac{g_{pr}}{g\ N_{pr}} \quad \textbf{(3.14)}$$

COD balance

$$f_{ch} + f_{pr} + f_{li} = 1 \quad \textbf{(3.15)}$$

Mass balance

$$\left(f_{ch}\frac{g_{ch}}{gCOD_{ch}}+f_{pr}\frac{g_{pr}}{gCOD_{pr}}+f_{li}\frac{g_{li}}{gCOD_{li}}\right)\frac{gCOD_{substrate}}{gVS_{substrate}}=1 \quad \textbf{(3.16)}$$

The required values for the COD contents (g COD g^{-1} for carbohydrate/sugar, protein/amino acid and lipid/fatty acids) were calculated assigning to each biochemical fraction an ideal molecular formula and deriving the relative ThOD (in g COD g^{-1}). Carbohydrates were described as polyhexoses with infinite linear chains and lipids as palmitic triglycerides, thus maintaining the original ADM1 STR description. In the case of proteins, a different molecular formula was used for each substrate, in order to account for possible differences in COD and nitrogen content - this approach is explained in Section 3.8.3. Table 3.3 reports the formula and significant ratios used for the biochemical fractionation. The resulting system of equations was then solved in Excel.

Biochemical compound	**Molecular formula**	**ThOD [gCOD g^{-1}]**	**Nitrogen content [gN gVS^{-1}]**	**C_i in ADM1 [mol-C $gCOD^{-1}$]**	**N_i in ADM1 [mol-N $gCOD^{-1}$]**
Carbohydrates	$C_6H_{10}O_5$	1.184	0	0.031	0
Lipids	$C_{51}H_{98}O_6$	2.874	0	0.022	0
Proteins - GW	$C_{3.95}H_{7.74}NO_{2.06}$	1.285	0.137	0.030	0.0076
Proteins - FW	$C_{3.85}H_{7.64}NO_{2.17}$	1.221	0.136	0.031	0.0079
Proteins - PM	$C_{3.96}H_{7.66}NO_{1.98}$	1.313	0.139	0.029	0.0075
Proteins - OAT	$C_{4.04}H_{7.72}NO_{2.25}$	1.234	0.132	0.031	0.0076

Table 3.3 Formulae and significant ratios used for the biochemical fractionation of the substrate and model implementation.

3.8.3 Determination of the protein formulae and degradation stoichiometry

The ADM1 STR reports the stoichiometric coefficients for protein degradation in the case of sewage sludge, and recommends to derive new parameters for different substrates. This recommendation has usually not been followed in other ADM1 implementations in the literature, with most of researchers using the default values.

Exceptions are the works of Flotats et al. (2006) and Yuan et al. (2014), which use a similar methodology to the one described below.

The procedure outlined by Ramsay and Pullammanappallil (2001) was employed for the determination of proteins degradation stoichiometry, which mainly depends on the protein primary structure. The procedure consists of the following steps.

Assumptions. It was assumed that the amino acid fermentation pathway remains constant during the experiment, regardless of the changing organic loading conditions. Therefore for each substrate, the stoichiometric coefficients are fixed and remain constant.

Determination of the protein amino acid content and molecular formula of the protein fraction in the substrate. The amino acid composition of the substrate can be measured through an amino acid analysis (usually by the hydrolysis of the purified protein, and quantification of the amino acids by liquid chromatography). In this research, literature data were used, assuming that they would still give a valuable description of the amino acid profile of each feedstock and highlighting possible relative differences between them. The following sources were used (Table 3.5): food waste from Myer et al. (2000); green waste from Gerloff et al. (1965); pig manure from Low (1979); cereal residues from Pomeranz et al. (1973). From the relative amino acid composition and the exact molecular formula of each amino acid, the protein molecular formula is obtained for each substrate. From the molecular formula, the ThOD, C and N contents in proteins are calculated. Table 3.3 reports all the calculated values.

Selection of the dominant amino acid fermentation reactions. For each amino acid, the stoichiometric yields of products compiled by Ramsay and Pullammanappallil (2001) were used, which in turn were based on the assumption that the Stickland reactions are dominant reactions.

Determination of the overall stoichiometry for protein degradation to acids. The amino acid composition of the substrate protein, and the stoichiometric yields for each amino acid are multiplied and then summed to obtain the overall stoichiometric yields of amino acid fermentation (Table 3.6). With respect to the default values in ADM1, the acetate production is reduced in favour of the other products (VFAs and H_2). However, the difference in the stoichiometric values is relatively small.

3.9 Kinetic fractionation

Every substrate was considered as composed of fractions which degrade at different rates. Particulate fractions (X) have, by definition, hydrolysis as the limiting rate and therefore their rate of degradation was described by a first-order hydrolysis kinetics (Vavilin et al., 2008). Soluble fractions (S) are directly assimilated by microorganism and therefore their rate of degradation depends on the biomass concentration and their respective uptake rates. In the case of particulate fractions a further distinction was made between readily (X_r) and slowly (X_s) degradable fractions, which can be physically explained by different particle sizes, bioavailability to microorganism colonization, association with recalcitrant polymers (e.g. lignin) or a combination thereof. The hydrolysis rate constants for the particulate fractions were assumed to be identical for proteins, carbohydrates and lipids, as the available experimental measurements would not have allowed distinguishing their rate of degradation. The fractionation between soluble, readily and slowly degradable particulates can be modelled by introducing appropriate parameters which map the initial degradable COD of the substrate into the respective fractions. The degradable COD is described by a degradable extent parameter f_d which defines the fraction of the ThOD of the substrate that is degradable; the not degradable fraction ($1-f_d$) is allocated entirely to the inert fraction X_I. The degradable fraction is then considered to be made of a soluble fraction f_s and a particulate fraction ($1-f_s$). The particulate fraction in turn is allocated into fractions which degrades at different rates, which in the simplest case are two readily and slowly fractions according to another "split" constant (fX_r). Figure 3.5 is an overview of the whole substrate fractionation method, from biochemical to kinetic.

For each substrate different fractionation combinations were tested (Table 3.4) and the respective quality of fit to the experimental data and uncertainty in parameter estimation evaluated.

Model name	**Fractionation**	**Parameters estimated**
X	1 particulate (X)	f_d, k_{hyd}
XS	1 particulate (X) and 1 soluble (S)	f_d, f_S, k_{hyd}
XX	2 particulates (X_r and X_s)	f_d, f_{Xr}, $k_{hyd,r}$, $k_{hyd,s}$
XXS	2 particulates (X_r and X_s) and 1 soluble (S)	f_d, f_S, f_{Xr}, $k_{hyd,r}$, $k_{hyd,s}$

Table 3.4 Model descriptions and parameters estimated.

Amino Acid	[mol amino acid / mol protein]			
	FW	GW	PM	OAT
Arginine	0.032	0.047	0.031	0.048
Histidine	0.029	0.018	0.037	0.018
Lysine	0.061	0.055	0.061	0.033
Tyrosine	0.004	0.029	0.041	0.023
Tryptophan	0.006	0.010	0.023	0.019
Phenylalanine	0.034	0.046	0.043	0.039
Cysteine	0.014	0.007	0.043	0.024
Methionine	0.018	0.018	0.041	0.026
Threonine	0.051	0.055	0.080	0.033
Serine	0.066	0.058	0.067	0.062
Leucine / Isoleucine	0.122	0.146	0.117	0.105
Valine	0.058	0.068	0.071	0.058
Glutamate	0.170	0.101	0.033	0.218
Aspartate	0.091	0.094	0.077	0.077
Glycine	0.096	0.096	0.085	0.083
Alanine	0.079	0.094	0.108	0.064
Proline	0.070	0.056	0.044	0.070

Table 3.5 Amino acid composition for each analysed substrate. Data from literature: food waste (FW) from Myer et al. (2000); green waste (GW) from Gerloff et al. (1965); pig manure (PM) from Low (1979); cereal residues (OAT) from Pomeranz et al. (1973).

Coefficient	FW	GW	PM	OAT	ADM1
fac,aa	0.330	0.308	0.330	0.332	0.4
fpro,aa	0.056	0.057	0.068	0.071	0.05
fbu,aa	0.282	0.245	0.255	0.270	0.26
fva,aa	0.260	0.300	0.248	0.254	0.23
fH2,aa	0.072	0.090	0.099	0.073	0.06

Table 3.6 Stoichiometric coefficients for amino acids fermentation, for analysed substrates and using default values in ADM1.

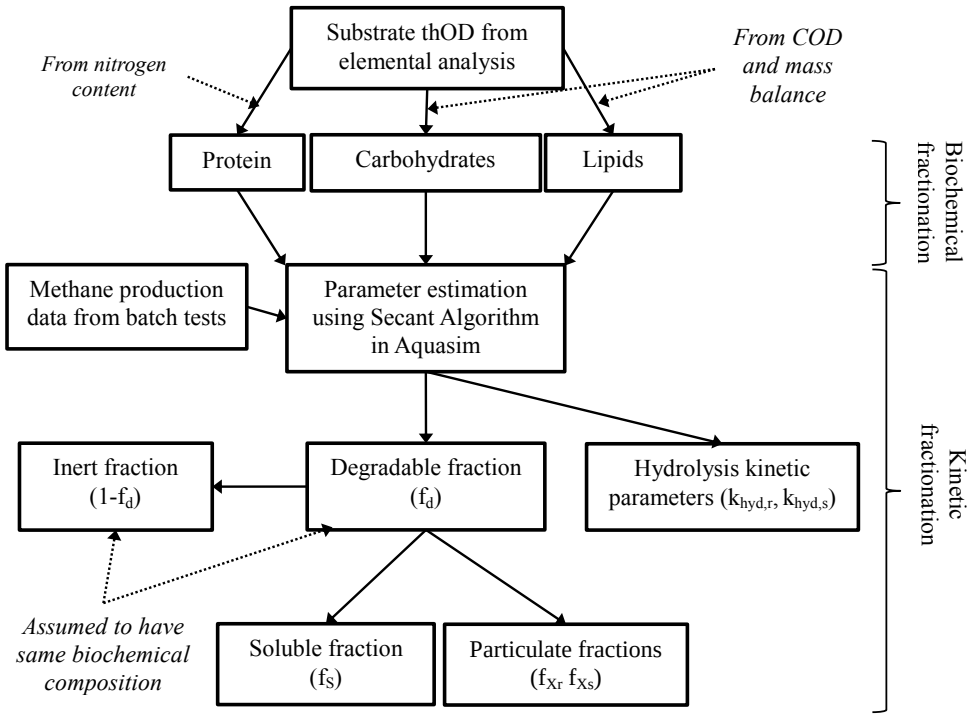

Figure 3.5 Overview of the substrate fractionations method: biochemical and kinetic (not shown: charge balance).

Table 3.7 shows a complete list of the state variables which are needed by ADM1 to describe any given feedstock. For each variable the experimental method or the expression from the kinetic fractionation is shown. In practice, in Aquasim, the XXS model is implemented as the most general fractionation. It is then possible to change the fractionation model by changing the values of the soluble fraction or particulate readily fraction to zero.

3.10 Co-digestion approach

In the case of co-digestion, the charge balance and the biochemical and kinetic fractionations are applied to each substrate, so that each substrate is described by an appropriate vector as given in Table 3.7. With this information, it is then possible to implement the loadings of the COD fractions and of the charge bearer elements in Aquasim, for all substrates considered. New state variables are implemented in Aquasim for each particulate fraction of each substrate. In this way it is possible to simulate the degradation in parallel of different particulates, degrading at different rates and producing the same soluble compounds whose transformations are then modelled by the same ADM1 structure as in the case of mono-digestion.

Variable	XXS model
S_{su}	*ThOD* $f_d f_{ch} f_s$
S_{aa}	*ThOD* $f_d f_{pr} f_s$
S_{fa}	*ThOD* $f_d f_{li} f_s$
S_{ac}	measured (GC)
S_{pro}	measured (GC)
S_{bu}	measured (GC)
S_{va}	measured (GC)
S_{h2}	0
S_{ch4}	0
S_{IC}	measured (titration)
S_{IN}	measured (IC)
S_I	0
X_c	0
X_{ch}	*0*
X_{pr}	*0*
X_{li}	*0*
$X_{ch,r}$	*ThOD* $f_d f_{ch} (1\text{-}f_s) f_{Xr}$
$X_{pr,r}$	*ThOD* $f_d f_{pr} (1\text{-}f_s) f_{Xr}$
$X_{li,r}$	*ThOD* $f_d f_{li} (1\text{-}f_s) f_{Xr}$
$X_{ch,s}$	*ThOD* $f_d f_{ch} (1\text{-}f_s)(1\text{-}f_{Xr})$
$X_{pr,s}$	*ThOD* $f_d f_{pr} (1\text{-}f_s)(1\text{-}f_{Xr})$
$X_{li,s}$	*ThOD* $f_d f_{li} (1\text{-}f_s)(1\text{-}f_{Xr})$
X_{su}	0
X_{aa}	0
X_{fa}	0
X_{c4}	0
X_{pro}	0
X_{ac}	0
X_{h2}	0
X_I	*ThOD* $(1\text{-}f_d)$
S_{H+}	measured (pH)
S_{OH-}	measured (pH)
S_{cat}	charge balance
S_{an}	charge balance

X model: $f_s = 0$, $f_{Xr} = 0$
XS model: f_s = *calibrated* , $f_{Xr} = 0$
XX model: $f_s = 0$, f_{Xr} = *calibrated*
XXS model: f_s = *calibrated* , f_{Xr} = *calibrated*

Table 3.7 ADM1 state variables used to describe substrate and their definition in the fractionation model XXS.

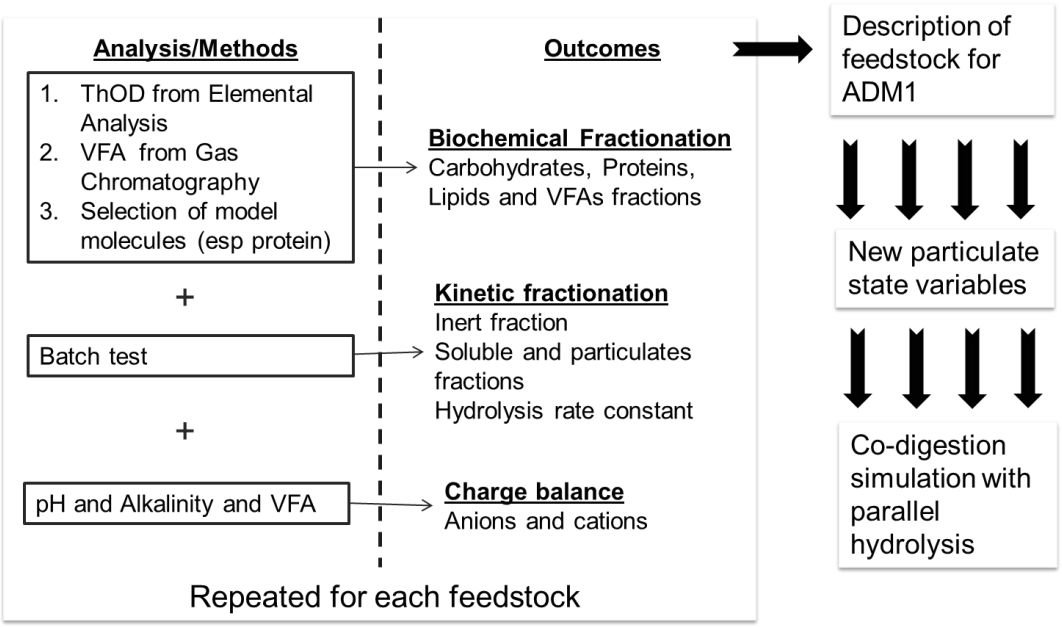

Table 3.8 Overview of the approach to the modelling of the co-digestion experiments.

3.11 Model validation

Direct validation consists in evaluating the ability of the model in reproducing the experimental data that has been used for estimating the parameters. When the fitting is considered by the modeller not to be adequate, then previous model building steps should be checked and potentially modified, especially to model selection and parameter selection and estimation.

Different methods can be employed in direct validation. The simplest is visual inspection: the model has to follow well the data evolution while smoothing out the noise (a model that tends to reproduce noise is over-parameterized and will fail later cross-validation tests) (Donoso-Bravo et al., 2012).

A more rigorous approach was used in this thesis and this is based on residual analysis and derivation of mathematical indicators. Each calibration was evaluated on the basis of their weighted sum of square χ^2, the coefficient of determination R^2, the relative absolute error rAE, and the confidence interval of the estimated parameters. R^2 was calculated as follows:

$$R^2 = 1 - \frac{\sum_{i=1}^{n}\left(y_{m,i} - y_i(p)\right)^2}{\sum_{i=1}^{n}\left(y_{m,i} - \overline{y_m}\right)^2} \quad \textbf{(3.17)}$$

where $\overline{y_m}$ is the average of experimental data points. The rAE was calculated as follows:

$$rAE = \frac{\sum_{i=1}^{n}\left(\frac{\left|y_{m,i} - y_i(p)\right|}{y_{m,i}}\right)}{n} \quad \textbf{(3.18)}$$

Direct validation is a necessary condition, but not a sufficient condition, to accept the model as able to reproduce the behaviour of the system under consideration. It is in fact possible that the model fits well the data that has been used for parameter estimation, while showing inadequate performance when new data is used. In this thesis, the fractionation models estimated with the batch tests 1a and 1b are cross-validated with semi-continuous tests 2 and 5; and the inhibition model estimated in test 3 are cross-validated in test 5.

The identification of the model parameters through the method of weighted sum of least squares is based on certain assumptions on the residuals (Gujer, 2008), namely:

a) normally distributed with an average value of zero and a standard deviation equal to the standard error of the measurement processes.
b) having constant variance.
c) being independent, i.e. not autocorrelated.

Assumption a) was visually verified by plotting a residual histogram; assumption b) and c) were verified by the visual inspection of a scatter plot of the residuals against time or the experimental data. Autocorrelation of the residuals is an indication of the structural inadequacy of the model, which is unable to describe all the dynamics of the process.

Models selection

Different fractionation and inhibition models are compared in this thesis. These models contain a different number of calibrated parameters and therefore a procedure to compare and select an appropriate one is needed. This is a situation which is often encountered when modelling biotechnological processes. Mathematical models for biotechnological processes in fact include many parameters of uncertain value and relatively few measured outputs, which in turn makes them difficult to calibrate due to structural/practical identifiability issues (Dochain and Vanrolleghem, 2001). Attempts to fit all the parameters

simultaneously usually result in very low confidence in the estimated parameters. As a consequence, two conflicting objectives characterise the calibration of biotechnological models: the goodness of fit and the estimated parameter confidence. Increasing the number of parameters leads to a closer fit between model predictions and experimental data; at the same time, additional parameters will lead to increased uncertainty, because of the correlation between the parameters and experimental data being not sufficiently informative (both low quality and quantity of data).

A parameter identification procedure has been employed in this thesis for the systematic comparison of parameter combinations (which in turn correspond also to different model structures of substrate fractionation and reaction inhibition). The procedure starts with the simplest combination and then adding one parameter at a time, until some threshold on estimated parameter error is reached, or otherwise until the procedure is computationally and timewise tractable. Finally the selection is based on two criteria: (1) Is maximum relative standard error of the estimated parameters above a certain user-specified threshold? (2) How good is the fit? The former is used to detect and eliminate those parameter combinations which yield low confidence estimates and the latter is used to rank the parameter combination tested.

3.12 Conclusion

In this chapter, the methods employed in this thesis were described. The methods include the tools required to build a calibrated and validated model, which can be used to investigate the operation of an AD system in a microgrid (investigation which is described in Chapter 6). Therefore both experimental and modelling aspects were covered.

Experimental tools included the laboratory scale digesters, needed to investigate the kinetics of degradation of different substrates, and the analytical methods used to characterise the substrate at a physico-chemical level. Modelling tools included a detailed description of the ADM1 implementation in the simulating software Aquasim, the derivation of initial conditions, and the parameter estimation methods employed in this thesis. Experimental data and parameter estimation techniques were combined in order to achieve a description of the biochemical and kinetic characteristics of any given substrate This allows the modelling of the mono-

digestion and co-digestion of different substrates, which is the subject of Chapters 4 and 5, respectively.

4 Substrate fractionation

4.1 Introduction

This chapter presents the experimental details and results of the biochemical and kinetic fractionation of four different substrates, with the objective of identifying and evaluating a methodology which can be used to characterize any given substrate and produce accurate inputs for the ADM1 model. Elemental analysis of the substrates was used to derive the biochemical fractionation of the substrates, and the influence of the ash determination on the results is discussed. The kinetic fractionation method, based on the calibration of the methane production curve from a batch test, was used to characterise the substrate in terms of fractions having different rates of degradation. The method updates the approach introduced by Girault et al. (2012) by using parameter estimation and model selection; relative differences and improvements between the methods are discussed. As single step models are usually used by other researchers for modelling batch tests, calibrated parameters using ADM1 and single step models are compared.

Semi-continuous tests on two of the four substrates were performed to validate the fractionation method. The kinetic fractionation parameters were determined also on the semi-continuous data sets and compared with the batch calibration. The apparent temporal variation of the parameters across the experiment was also evaluated. The ability of the model in reproducing other measured outputs in addition to gas flow rate were evaluated. Contois kinetics was compared with first-order kinetics as an alternative option for hydrolysis.

4.2 Materials and methods

Materials and analytical methods employed in this thesis are described in Chapter 3.

4.2.1 Batch test conditions

Two different batch tests were performed, with different substrates and inoculum employed. Table 4.1 shows how the substrate, inoculum, volume and ratio between the inoculum and substrate (ISR) changed in the two tests.

Test	Substrate	Inoculum	Volume	ISR (COD basis)	ISR (VS basis)
1a	GW	External digester	0.35	2.5	3.6
	FW		0.35	2.5	4
1b	PM	Lab digester-modelled	0.5	2.5	3.3
	OAT		0.5	2.5	3.1

Table 4.1 Experimental conditions for the batch tests

Inoculum for test 1a was taken from an external digester, with limited information about its operation, and the respective method described in Chapter 3 Section 3.5.4 was used. Inoculum for test 1b was a mixture of the effluents withdrawn from the digesters used in semi-continuous test 2, therefore simulations of the source digesters were used to estimate the initial conditions for microbial biomass. In both cases the inoculum was filtered through a 0.5 mm sieve and then incubated for 4 days in the reactors, in order to allow the degradation of most of the residual easily degradable matter.

4.3 Substrate characterisation and biochemical fractionation

Measured composition of the four substrates is shown in Table 4.2. All substrates have high solids content above 25% based on weight basis, reaching 93% in the case of the oat residues. The addition of water would be therefore an important design parameter in the case of these substrates. Ash content is highest in GW, at 31% on total solids, due to soil and grit contamination, while it is lowest in OAT at 3%. Nitrogen content determines the protein content in the substrates: it is highest in OAT at 4.3% on TS, and then lower in FW (3.3%), PM (2.9%) and GW (2.0%). The relative content of C, H, O and N describes the state of oxidation of the substrate and determines the value of the calculated ThOD. The highest value for ThOD (on a VS basis) is for FW with 1.61 g COD g^{-1} VS and this is followed by GW with 1.42 g COD g^{-1} VS), PM with 1.31 g COD g^{-1} VS and OAT with 1.23 g COD g^{-1} VS. The ThOD of the whole substrate (on a wet basis) it is clearly highest for OAT, given its very low moisture content.

The pH and alkalinity values are related to the type of substrate and its previous storage conditions. Food waste, green waste and pig manure were collected and analysed after being stored for a period of 3-4 days at the recycling site and farm. During this period the waste underwent a fermentation process, which increased the volatile fatty acids and alcohols content and decreased the pH. The low moisture content of the oat residues prevented any biological fermentation from

occurring. The results obtained confirm this aspect, with pig manure showing the highest amount of fermentation products. The pH is about 5 for food waste and green waste, while the high content of ammonia in pig manure maintains the pH at 6.3. Therefore partial alkalinity is absent in the case of food waste and green waste, while is still present in PM and OAT. In the case of food waste, Aichinger et al. (2015) found lactic acid being the most abundant product from the fermentation of stored biowaste (up to 25 g/L after 3 days storage). In this research, gas chromatography analysis was not calibrated for lactic acid and therefore it is possible that the reported total VFAs underestimates the fermentation products from waste storage.

Table 4.3 shows the biochemical fractionation for all substrates, on a VS and COD basis. Carbohydrates are the main compounds in all the substrates (on a VS basis), about 65% in the case of GW, PM and OAT and 48% in the case of FW. The protein content is between 20 and 33% across the substrates, with the highest prevalence in OAT and FW. The lipid content shows the highest variation between the substrates, with minimum content in OAT (1.9%) and increasing in PM (5.7%), GW (12.8%) and highest in FW (23.6%) due to the occurrence of various fatty residues in this waste (cheese, meat parts, discarded oils etc.). Lipids content in GW appears to be higher than the reported amounts from other databases or publications; e.g. from consulted entries in a comprehensive biomass database (ECN/Phyllis), averages values about 5% are found. Two reasons for this result may be:

- The potential contamination with cooking oil (household collections make part of the green waste).
- The influence of lignin content, which has COD:mass ratio of 1.56; considering a ratio of 1.18 for carbohydrates and 2.87 for lipids, it is evident how the presence of lignin would shift the biochemical fractionation towards a higher content of lipid (while proteins are directly determined by the N content).

Notwithstanding the possible influence of contamination, the aforementioned influence of lignin is theoretically valid and shows a limit of the proposed method: in the case of substrates which have a relatively high content of lignin, the results will have an artificially higher content of lipids. While the COD balance and C/N ratio are still correctly maintained, an artificially higher concentration of lipids will affect some metabolic interactions in ADM1, such as: higher content of slowly consumed

fatty acids, amount of H2 produced from fatty acid oxidation, biased parameter values when fatty acid inhibition is implemented and calibrated. An alternative is to directly measure the lignin content and allocate it fully to the inert fraction, as done by Koch et al. (2010a). However the procedure would become more time-consuming.

		Substrates			
Analysis	Units	FW	GW	PM	OAT
TS	g/kg	296.5	401.7	272.2	930.5
VS (at 550 C)	g/kg	260.3	259.7	241.9	897.6
Ash	% TS	11.2	34.8	11.0	3.6
C	% TS	48.8	34.7	44.1	44.8
H	% TS	7.2	4.5	5.2	6.1
N	% TS	3.3	2.0	2.9	4.3
S	% TS	0.10	0.03	0.10	0.08
O	% TS	33.1	27.2	36.7	41.3
ThOD of VS	g ThOD/g VS	1.61	1.42	1.31	1.23
ThOD of substrate	g ThOD/g substrate	0.44	0.39	0.31	1.11
pH		4.74	5.02	6.30	6.88
Partial Alkalinity	mg CaCO3/kg	nd	nd	5798	3946
Intermediate Alkalinity	mg CaCO3/kg	3443	3181	16168	7536
Total Ammonia Nitrogen	mg N-NH4/kg	528	630	2178	nd
VFA and alcohols					
methanol	mg/kg	348	102	nd	nd
ethanol	mg/kg	4185	218	48	nd
acetic	mg/kg	3029	4173	9195	nd
propanoic	mg/kg	27	223	2834	nd
i-butyric	mg/kg	19	12	503	nd
n-butyric	mg/kg	53	136	2831	nd
i-valeric	mg/kg	0	25	762	nd
n-valeric	mg/kg	2	8	668	nd

Table 4.2 Physicochemical analysis of the substrates.

Results of the application of charge balance to the four substrates are shown in Table 4.4, and indicated as state variables employed in ADM1 in the description of the substrate loadings: overall, each substrate loading is finally described through COD, ash and charge loadings. Charge loadings directly influence the changes in the pH of the system: all substrates present an acidic character which will tend to reduce the pH of the system after the feeding. At the same time the ammonia loadings (S_{in} in ADM1) and hydrogen carbonate (S_{ic}) will increase the buffering capacity of the system. OAT is the only substrate which has an hydrogen carbonate content.

		Substrates			
	Units	**FW**	**GW**	**PM**	**OAT**
ThOD from elemental analysis	$gO_2\ g^{-1}_{substrate}$	0.440	0.391	0.311	1.107
ThOD from VFA and alcohols	$gO_2\ g^{-1}_{substrate}$	0.013	0.006	0.027	0
Total ThOD	$gO_2\ g^{-1}_{substrate}$	0.453	0.397	0.338	1.107
fractionation on COD					
Carbohydrates	% ThOD	35.3%	53.9%	58.0%	62.0%
Proteins	% ThOD	19.6%	18.8%	21.9%	33.5%
Lipids	% ThOD	42.3%	25.9%	12.3%	4.5%
VFA and alcohols	% ThOD	2.8%	1.4%	8.1%	0.0%
fractionation on VS					
Carbohydrates	% VS	47.8%	64.6%	65.6%	64.5%
Proteins	% VS	25.7%	20.7%	22.4%	33.5%
Lipids	% VS	23.6%	12.8%	5.7%	1.9%
VFA and alcohols	% VS	2.9%	1.9%	6.7%	0.0%

Table 4.3 Biochemical fractionation of the substrates.

		Substrates			
ADM1 variables	Units	FW	GW	PM	OAT
S_{ac}	g COD L^{-1}	3.241	4.465	10.680	0
S_{pro}	g COD L^{-1}	0.040	0.337	4.782	0
S_{bu}	g COD L^{-1}	9.369	0.878	8.423	0
S_{va}	g COD L^{-1}	0.004	0.068	3.427	0
S_{in}	M	0.038	0.045	0.156	0
S_{ic}	M	0	0	0	0.098
OH^-	M	4.42E-10	5.69E-10	1.60E-08	6.10E-08
H^+	M	1.82E-05	1.41E-05	5.01E-07	1.32E-07
S_{cat}	M	0.013	0	0.182	0.076
S_{an}	M	0	0.002	0	0

Table 4.4 Substrate description based on charge balance.

4.3.1 Influence of ash determination on substrate fractionation

Table 4.5 shows the results obtained for solids and ash determinations at two different temperatures of the elemental analysis, and how different ash contents influences the calculated ThOD values. With lower ash content, the calculated oxygen content results higher, which in turn increases the oxidation state of the substrate, finally driving down the ThOD. Using ash values determined at 550 °C, the ThODs are relatively overestimated by 7% in FW, 8% in GW, 5% in PM, 4% in OAT, respect to the (hypothetically more correct) values obtained at 1050 °C. The biochemical fractionation is also affected by the temperature dependent ash determination (Table 4.6): overestimated ThOD will result in overestimated lipid and reduced carbohydrate fractions (while proteins remain approximately constant as

related to N content). Using ash values determined at 550 °C, the calculated lipid content is relatively overestimated by 18% in FW, 41% in GW, 50% in PM and 89% in OAT. It is evident how the lipid fraction is sensitive on the ash determination, especially for substrates which have a low ThOD/gVS. Ash loadings, which are required to predict the solids content in the reactor, are instead described by the ash content as determined at 550 °C.

		Temperature of loss-on-ignition	
	Units	**550 °C**	**1050 °C**
Food waste			
volatile solids on wet weight	%	26.0%	27.4%
ash on volatile solids	%	11.2%	7.5%
ThOD of VS	g COD g^{-1} VS	1.71	1.60
ThOD of substrate	g COD $g^{-1}_{substrate}$	0.45	0.44
Green Waste			
volatile solids on wet weight	%	26.0%	27.5%
ash on volatile solids	%	34.8%	31.6%
ThOD of VS	g COD g^{-1} VS	1.54	1.43
ThOD of substrate	g COD $g^{-1}_{substrate}$	0.40	0.39
Pig Manure			
volatile solids on wet weight	%	23.6%	24.2%
ash on volatile solids	%	13.4%	11.0%
ThOD of VS	g COD g^{-1} VS	1.38	1.31
ThOD of substrate	g COD $g^{-1}_{substrate}$	0.33	0.31
Oat Residues			
volatile solids on wet weight	%	88.1%	89.8%
ash on volatile solids	%	4.8%	3.6%
ThOD of VS	g COD g^{-1} VS	1.27	1.23
ThOD of substrate	g COD $g^{-1}_{substrate}$	1.11	1.11

Table 4.5 Influence of the temperature of ignition on the ash content and calculated ThOD.

		Temperature of loss-on-ignition	
		1050 °C	**550 °C**
Food waste			
Carbohydrates	% ThOD	36.3%	28.7%
Proteins	% ThOD	20.2%	19.7%
Lipids	% ThOD	43.5%	51.6%
Green waste			
Carbohydrates	% ThOD	54.7%	44.5%
Proteins	% ThOD	19.0%	18.5%
Lipids	% ThOD	26.2%	37.0%
Pig manure			
Carbohydrates	% ThOD	63.1%	56.6%
Proteins	% ThOD	23.8%	23.4%
Lipids	% ThOD	13.4%	20.1%
Oat residues			
Carbohydrates	% ThOD	62.0%	58.4%
Proteins	% ThOD	33.5%	33.2%
Lipids	% ThOD	4.5%	8.5%

Table 4.6 Influence of temperature of ignition on the biochemical fractionation

4.4 Kinetic fractionation from batch tests

4.4.1 Estimation of initial conditions

Table 4.7 shows the estimated parameters for the description of the two inoculum, and Figure 4.1 the experimental and calibrated methane volume production curves from the control reactors in the batch tests 1a and 1b. The parameter values are comparable, with inoculum 1a having a slightly higher concentration of biomass and a higher degradation rate; also from Figure 4.1, it is evident how the inoculum 1a degrades faster than inoculum 1b.

Estimated parameters have very high standard errors, especially in the case of total particulate and decayed biomass X_c (>50% for X_c), due to their almost complete correlation (>0.99, results not shown), while errors in biomass concentrations are lower (<5% in both cases). In both cases the goodness of fit was very high (R^2 = 0.99). Alternative tests were performed by calibrating less parameters (e.g. with X_c at a fixed value), but achieving lower goodness of fit. In the simulation of substrate batch tests, the methane production is the result of the degradation of the substrate together with the inoculum: therefore an accurate kinetic characterisation of the substrate is dependent on an accurate description of the degradation of the inoculum. For this reason, although poorly identifiable, the estimated parameters were accepted as the initial conditions of the tests.

In the case of inoculum 1b, the model based total biomass concentration was initially calculated from simulations of the semi-continuous reactors in test 2, from which the inoculum was sourced, together with four days of degassing period in the batch reactor. This value was compared with the value obtained from the calibration of the methane production curve of the control batch reactor, similar to test 1a. The total biomass concentration estimated from model simulations resulted in a value around twice as high, compared to the experimentally calibrated value. The difference can be explained by considering that the inoculum was previously filtered before starting the batch experiments. In fact, part of the biomass is in a sessile form, attached to particles as biofilms (Jensen et al., 2008), and therefore removed during filtration. Finally, it was decided to use the experimentally calibrated value, since it was considered a more accurate estimation of the total initial biomass. Model based characterisation of the inoculum still was used to split the total initial biomass into the respective trophic groups (which in turn are dependent on the composition of the substrates fed in the source digester).

	Estimated parameters	units	value	standard error
Inoculum 1a	Initial total biomass	gCOD/L	3.12	4%
	Initial decayed biomass (X_c)	gCOD/L	0.89	57%
	Initial total degradable particulate	gCOD/L	0.42	26%
	Hydrolysis rate of initial particulate (khyd,ino)	d-1	0.39	15%
Inoculum 1b	Initial total biomass	gCOD/L	2.14	2%
	Initial decayed biomass (X_c)	gCOD/L	0.31	58%
	Initial total degradable particulate	gCOD/L	0.85	17%
	Hydrolysis rate of initial particulate (khyd,ino)	d-1	0.20	9%

Table 4.7 Estimated inoculum parameters for batch tests 1a and 1b.

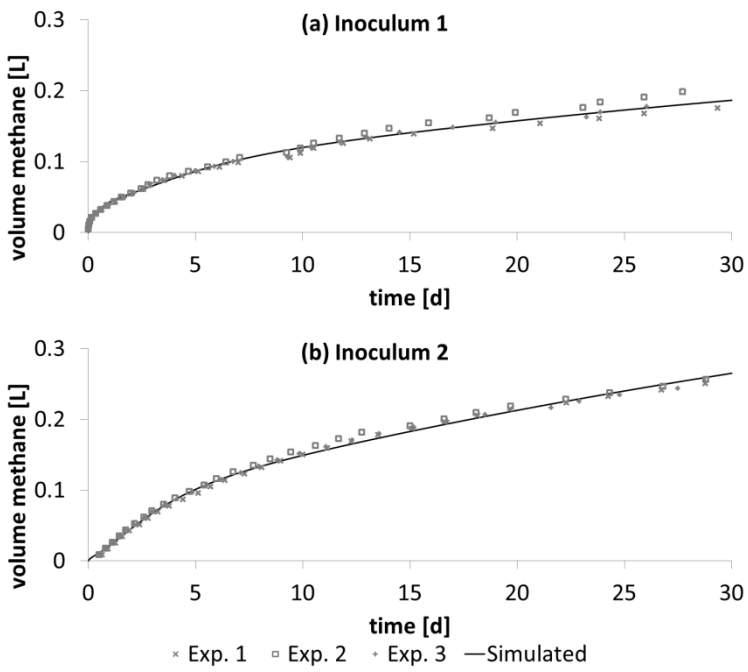

Figure 4.1 Experimental and simulated methane production for inoculum. (a) batch test, (b) batch test 2.

4.4.2 Parameter estimation of the kinetic fractionation

Table 4.8 shows the parameters estimated for the kinetic fractionation of the four substrates, while the experimental data and the simulated calibrated curve for the accumulated methane in batch tests are shown in Figure 4.2 for food waste, Figure 4.3 for green waste, Figure 4.4 for pig manure, and Figure 4.5 for oat residues. In general, an increase in the complexity of the model, given by the numbers of parameters calibrated, corresponded to a better fit to the experimental data, as visually represented in the graphs and quantified by a higher R^2 and lower rAE. This is to be expected in the case of nested models, where the model with more

parameters can better adapts to the experimental data. Especially in the case of food waste and pig manure, it is graphically evident that in order to achieve a good fit with the experimental data at least two fractions are needed. The case of oat residues is different, as the different fractionation models show almost identical goodness of fit, without improvement with more complex models.

However, the increase of complexity also corresponded to an increase in the uncertainty of the estimation of the parameters, as given by their calculated confidence interval. Especially the XX and XXS fractionations led to high standard errors in the estimated parameters (highest for GW, above 20%), and therefore wide confidence intervals. High values of standard errors are related to the experimental data not being rich enough and to a low sensitivity of the selected parameter to the modelled output. In the case of OAT, standard errors could not be computed as the calibrated parameter f_{Xr} were on the inferior bound of the *a priori* parameter range (0.05-0.95 for f_{Xr}), in which case the secant algorithm of Aquasim fails to give an estimation of the errors.

In all fractionations, there is an increase in the value of f_d with complexity. In fact, with more complex models the calibration is able to take into account also the less precise volume measurements towards the end of the experimental period, while with simpler models the calibrated parameters is mainly determined by the more precise initial data.

Feed	Model	Parameter values					Standard errors (%)					rAE	R^2
		f_d	f_S	f_{Xr}	k_{hyd_r}	k_{hyd_s}	f_d	f_S	f_{Xr}	k_{hyd_r}	k_{hyd_s}	(%)	(%)
GW	X	0.3				0.682	1.5				4.7	7.4	98
	XS	0.327	0.255			0.296	0.9	3.3			4.3	4.3	99.1
	XX	0.326		0.451	1.57	0.192	2.2		8.1	13.4	14.3	4.3	99.1
	XXS	0.344	0.212	0.44	0.68	0.136	1.8	5.3	26.4	25.9	25.9	3.9	99.2
FW	X	0.747				1.09	0.8				3.1	5.1	97.4
	XS	0.811	0.332			0.37	0.8	3.2			4.5	4.5	98.8
	XX	0.897		0.541	2.54	0.13	1.7		2.4	6.4	10.2	3.5	99.5
	XXS	0.905	0.156	0.499	1.48	0.12	1.6	7.6	3.3	8.5	11.8	3.0	99.4
PM	X	0.625				0.275	1				2	7.3	98.0
	XS	0.663	0.125			0.178	0.5	3.0			1.7	3.0	99.6
	XX	0.682		0.245	2.085	0.130	0		1	2	1	0.8	99.9
	XXS	0.683	0.010	0.241	1.894	0.129	0.1	15.7	0.9	2.4	0.7	0.8	99.9
OAT	X	1.006				0.731	0.3				0.9	3.6	99.4
	XS	1.006	0.008			0.714	0.3	50.6			1.7	3.6	99.4
	XX	1.006		0.050	0.900	0.724	not available					3.6	99.4
	XXS	1.006	0.008	0.050	0.900	0.707	not available					3.6	99.4

Table 4.8 Results of the model parameter estimation from the batch test data, including the parameter values, standard errors and quality of fit.

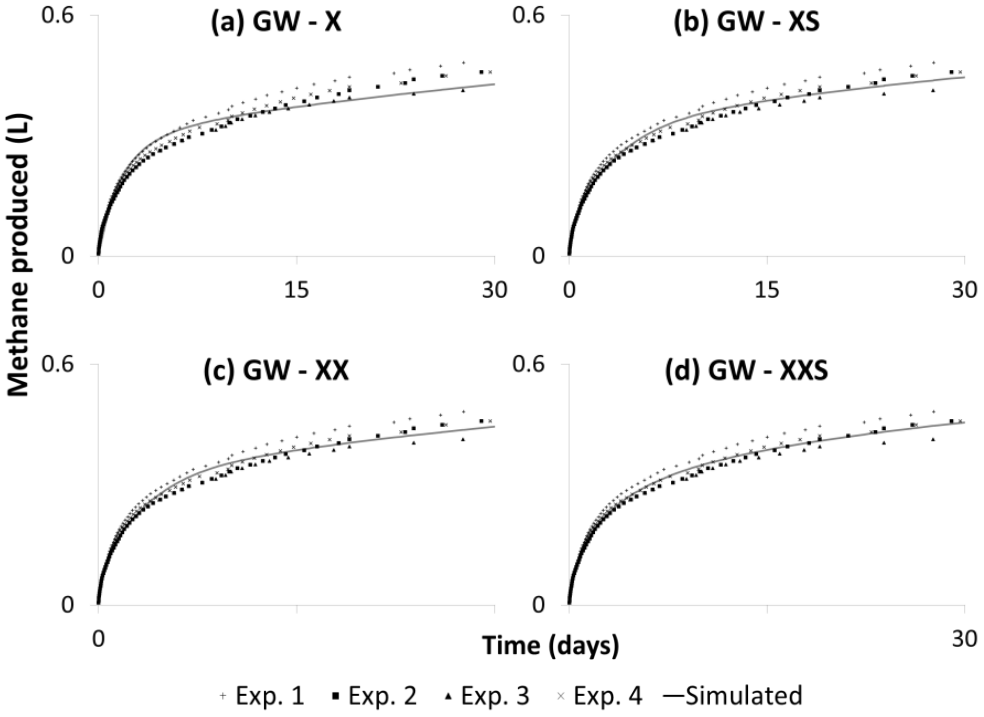

Figure 4.2 Experimental batch data for GW and the simulated volume obtained with X, XS, XX and XXS calibrated fractionations (only the first 30 days are shown).

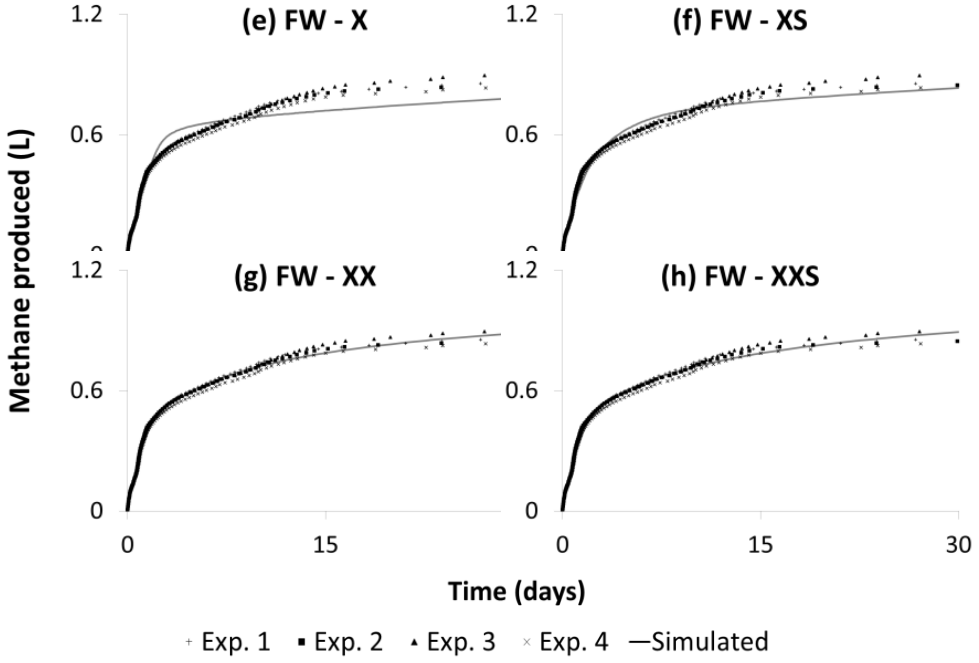

Figure 4.3 Experimental batch data for FW and the simulated volume obtained with X, XS, XX and XXS calibrated fractionations (only the first 30 days are shown).

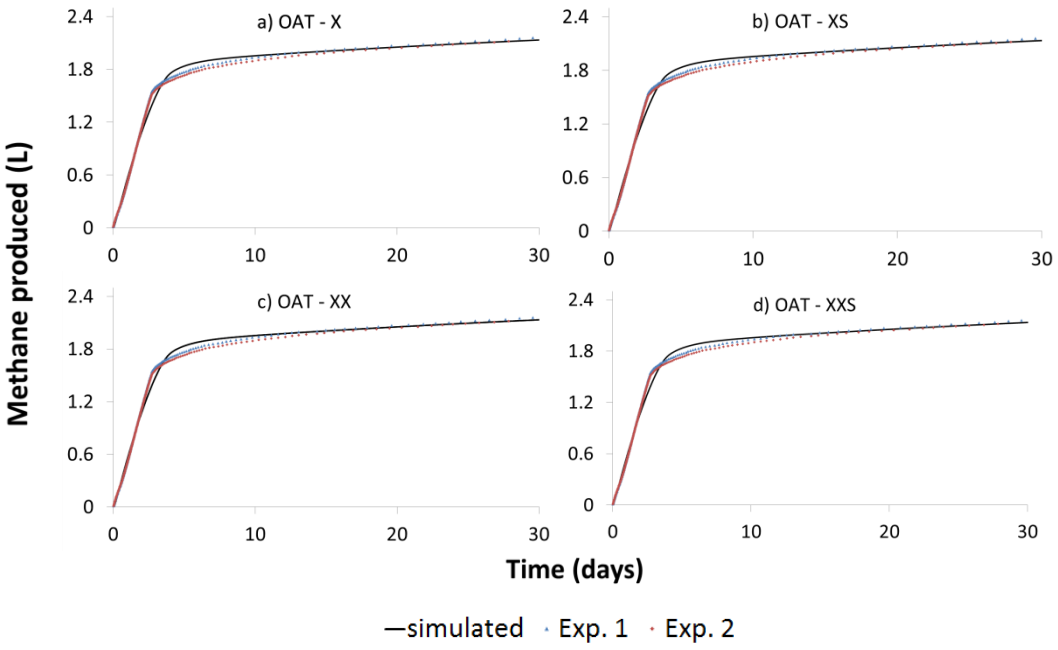

Figure 4.4 Experimental batch data for OAT and the simulated volume obtained with X, XS, XX and XXS calibrated fractionations (only the first 30 days are shown).

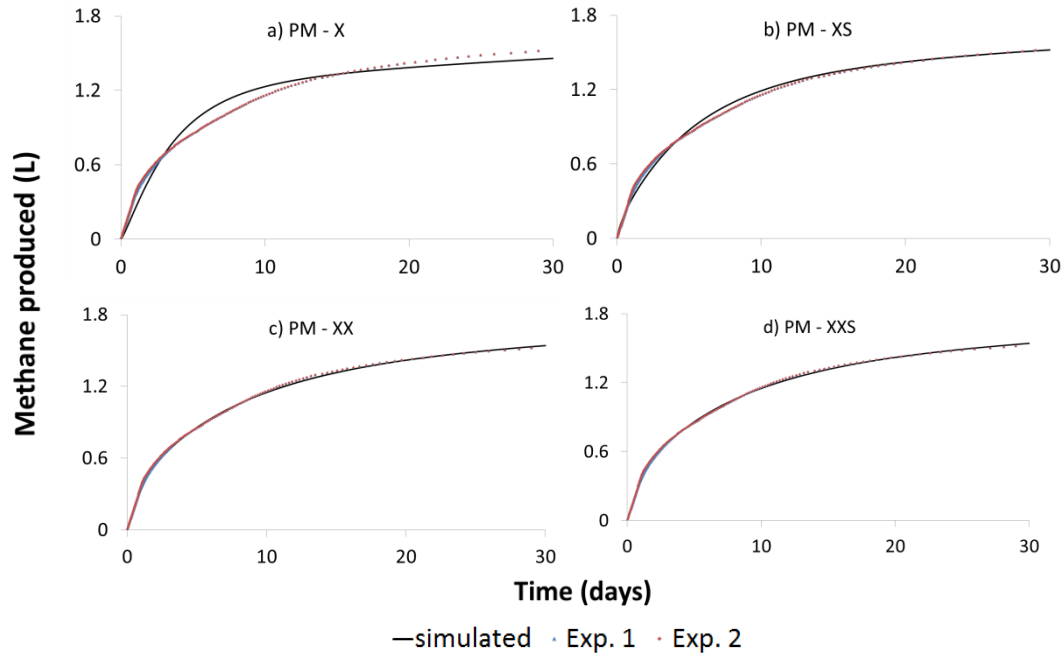

Figure 4.5 Experimental batch data for PM and the simulated volume obtained with X, XS, XX and XXS calibrated fractionations (only the first 30 days are shown).

As discussed in Section 3.11, model selection is based on the goodness of fit and a maximum acceptable uncertainty in the parameters. In the case of GW, model XXS is discarded due to the excessive uncertainty; XS and XX fractionations resulted in similar goodness of fit and uncertainty: it cannot be concluded from a batch test which fractionation to select to adequately describe the substrate degradation. In the case of FW, the model XXS or model XX could be selected, as well as in the case of PM. In the case of OAT, the simplest model X would be selected.

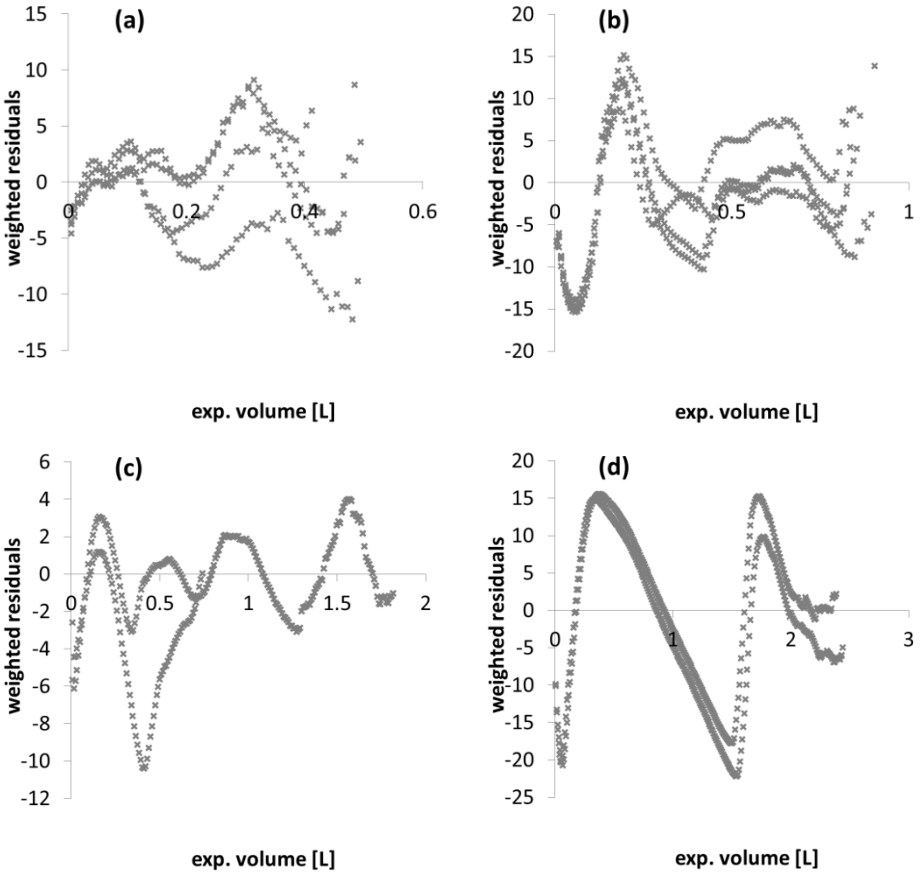

Figure 4.6 Residual plots for (a) GW, (b) FW, (c) PM, (d) OAT batch tests.

The residual plots for the four batch tests are shown in Figure 4.6. Each plot shows the weighted residuals (used in eq. (3.5)) against the fitted experimental value (volume). Residual plots were used to check the presence of outliers from the experimental data and to evaluate the residual distribution characteristics. In fact, application of least square regression requires for the residuals to be independent and normally distributed with zero mean and constant variance (as discussed in Section 3.11). Two main aspects can be discussed:

- There is no unique indication regarding the stabilization of variance of the residuals, with plot (d) being closer to constant variance (homoscedasticity),

plot (b) and (c) having slightly higher variance at low experimental volume values and plot (a) with increasing variance with increasing volumes. It cannot be concluded if the weights used in eq. (3.5) are effectively stabilising the residuals variance.

- The residuals are evidently autocorrelated, and not randomly distributed: this can be interpreted as a structural deficiency in the model, which is not able to account for all dynamic characteristics of the process (Gujer, 2008).

4.4.3 One-step model

A one-step model was also implemented to compare the values of estimated parameters between simpler and more complex models. In the one-step model, a single lumped reaction is defined, which directly converts the substrate to methane. This is a common approach used to describe methane production in batch tests (Angelidaki and Sanders, 2004, Jensen et al., 2011). The following equation was implemented in Aquasim:

$$\frac{\mathrm{d}P}{\mathrm{d}t} = P_0 V\left(k_{hyd,r} X_{ini} f_d f_{Xr} + k_{hyd,s} X_{ini} f_d (1 - f_{Xr})\right) \qquad \textbf{(4.1)}$$

where P is the methane volume, P_0 the conversion factor between degraded substrate and methane produced (0.354 L CH_4/g COD), V the reactor volume, X_{ini} the concentration of the substrate batch-fed, f_d the extent of degradation constant, $k_{hyd,r}$ and $k_{hyd,s}$ are the hydrolysis rate constants for readily and slowly degradable fraction, and f_{Xr} the fraction of the substrate which is readily degradable. The equation therefore allows to kinetically fractionate the substrate in the same way as was done with the ADM1 implementation; however only the X and XX fractionations can be calibrated in a simple 1-step model, as the soluble fraction S would need a more complex model with also a lumped biomass state variable implemented.

Table 4.9 reports the calibrated values and goodness of fit indicators. On comparing with the ADM1 calibrated values, two main aspects can be emphasized. The extent of degradation in the 1-step model is 5 to 10% lower than the ADM1 values, as the simpler model can't take into account the substrate that gets transformed into biomass (beside methane); the difference agrees well with the values of the biomass yields implemented in ADM1, which are as well in the range of 0.04-0.1 gCOD $gCOD^{-1}$. While the split fraction f_{Xr} has similar values in both models, the hydrolysis rate constants for the 1-step model are lower than the ADM1-calibrated. This aspect can be seen for all substrates, but it is especially

noticeable for FW and OAT with ADM1 values being 2 to 3 times higher. In fact, in the ADM1 model it is possible to take into account the accumulation of the intermediates, which introduces a lag between the hydrolysis and the methane production.

As an example to illustrate this aspect, Figure 4.7 shows the simulated profiles for all soluble variables in ADM1: it is evident how after the feeding of the substrate there is an accumulation of intermediates, with both acidogenic and acetogenic steps introducing a delay between solubilization of particulates and methane production. In particular, the sum of all soluble intermediates reach a peak after approximately 12 hours, at 1.6 gCOD L^{-1}, with LCFA, acetate and propionate being the species which reach higher concentrations.

A higher goodness of fit is achieved with the ADM1 implementation, as more phenomena can be taken into account, especially the accumulation of intermediates and the interaction with the gas headspace.

	calibrated values				goodness of fit indicators	
fractionations	**f_d**	**f_{Xr}**	**$k_{hyd,r}$**	**$k_{hyd,s}$**	**R^2**	**rAE %**
FW X	0.732			0.533	0.976	7%
FW XX	0.859	0.607	0.765	0.095	0.991	5%
GW X	0.308			0.497	0.952	11%
GW XX	0.364	0.504	1.019	0.107	0.981	6%
PM X	0.569			0.266	0.966	9%
PM XX	0.649	0.363	0.666	0.088	0.998	2%
OAT X	0.907			0.356	0.968	8%
OAT XX	0.907	0.897	0.370	0.257	0.968	8%

Table 4.9 Calibrated values and goodness of fit indicators for the 1-step degradation model.

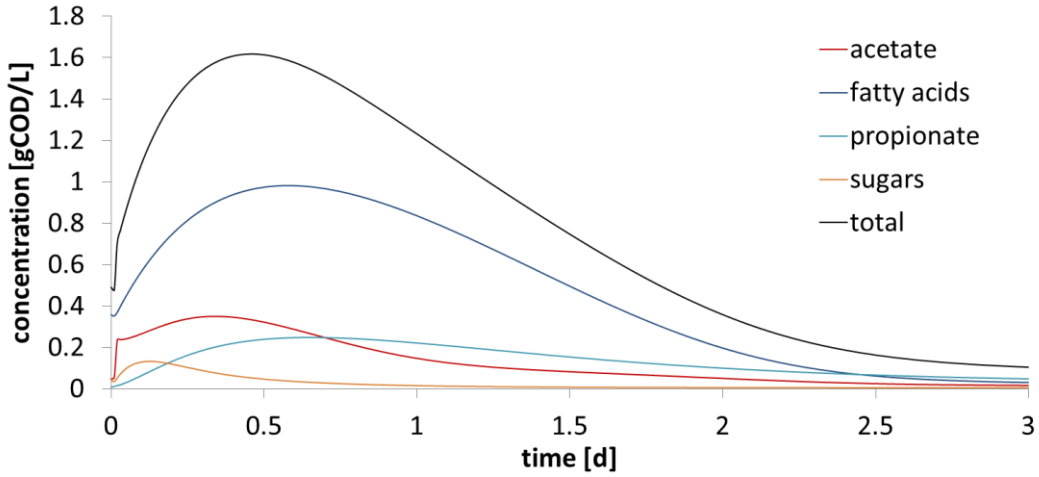

Figure 4.7 Simulation of selected ADM1 soluble state variables, for the FW batch test (XX model): the variables with negligible concentration are not shown.

4.5 Semi-continuous experiments

Two experiments with digestion of single substrates, GW and FW, were performed in order to validate the kinetic fractionation obtained with the batch test. The experiments also allowed the evaluation of the effect of increasing the loading rates on the process performance and on the values of the calibrated parameters. The experiments were performed in duplicate using the methods and performing the analysis described in Chapter 3.

Substrate loadings were identical for both substrates GW and FW, and ranged from approximately 1 to 12 gCOD/L (Figure 4.8). The digesters were fed three times a week during the first 80 days, and then the frequency increased up to 5 times a week until the end of the experiment. Average organic loading rates (OLRs) were calculated taking into account the amount of substrate fed across six consecutive feedings, and the associated time interval: this average value therefore indicates how the feedings changed across the experiment, but taking into account that organic stress on the digester gradually builds up after repeated high loadings. Figure 4.8 shows the temporal variations of the organic loadings and of the averaged OLRs across the whole semi-continuous test, with OLRs starting at 0.5 and reaching a maximum of 4 and 10 gCOD L^{-1} d^{-1} for GW and FW experiments, respectively.

The durations of the experiments were different, with the GW experiment lasting 112 days and the FW 166 days. The GW experiment was terminated earlier due to repeated foaming events occurring after each feeding, at an OLR between 3 and 4

gCOD $L^{-1}day^{-1}$, which greatly complicated the monitoring of the experiment. In particular, the gas volume measurements became unreliable, due to the sequence of: obstruction of the gas hose by foam, gas pressure build up in the headspace, displacement of foam in the gas hose and sudden release of the accumulated gas, very high gas flow through the measuring device (above its working ranges) with a partial loss of the recorded volume and inaccurate determination of the gas flow rate.

The FW experiment lasted longer and allowed to reach higher OLRs, at which organic stress and inhibition mechanisms became evident in the methane flow profile. The experiment was then terminated when high VFAs concentrations (above 20 g COD L^{-1}) were reached, with reduced methane specific yields and first phenomena of foaming.

Figure 4.9 shows the measured methane flow rate for both substrates. FW has higher flow rates than GW, mainly due to higher degradability and rapidity of degradation (as already calculated in the batch experiment). Figure 4.10 shows the temporal variation of the specific yields for both experiments. Again the specific yields were calculated in a similar fashion as the OLRs, taking into account the amount of gas produced and the amount of substrate fed across 6 consecutive feedings, therefore giving an indicative representation of the changing performance of the digester. The length of the averaging period is arbitrary, however very short periods would depend disproportionally on the interval between feedings (with longer intervals giving higher specific yields as the substrate has more time to be fully degraded, and shorter intervals artificially low, not taking into account accumulated intermediates not yet degraded); on the other hand, long averaging periods would excessively smooth the variations originated by changes of the organic stress, which gradually builds up during overloading periods.

In the case of GW, the specific yields remained fairly constant around its overall average of 0.19 LCH_4 $g^{-1}VS$. A slight decrease can be observed after about 90 days of the experiment, which corresponded to an increase (almost doubling) of OLR. However no significant moments of organic stress could be observed, also confirmed by the low level of accumulation of VFAs in the digester effluent. In the case of FW, the overall average specific yield was 0.42 LCH_4 $g^{-1}VS$. It can be noticed an increase during the first period of the experiment, up to 0.5 LCH_4 $g^{-1}VS$, which can be related to an adaptation of the microbial biomass to the substrate; also it is noticeable the same drop as in the case of GW after about 90 days. The

main variation occurred with the further increase in the OLR around 140 days, from about 5 to 10 gCOD L^{-1} day^{-1}, where the specific yields dropped from 0.5 to less than 0.1 LCH_4 $g^{-1}VS$. This variation is interpreted as being caused by a strong inhibition in some of the metabolic steps conducing to methane production; VFAs accumulation confirms the organic stress on the process (Ahring et al., 1995), with acetoclastic and acetogenic steps being more affected. Chapter 5 will further investigate and quantify the whole inhibition process.

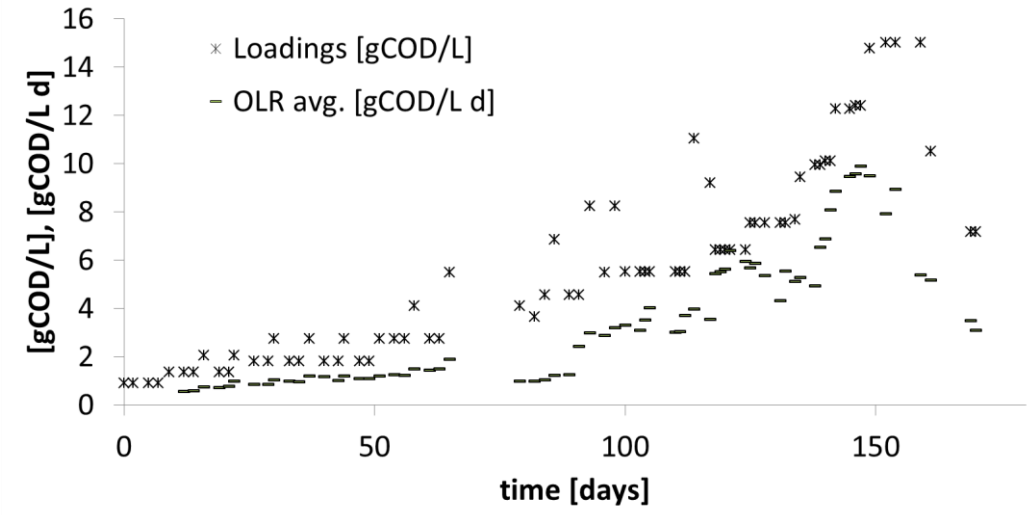

Figure 4.8 Substrate loadings and OLR (averaged to 6 consecutive feedings) in semi-continuous experiments for FW and GW.

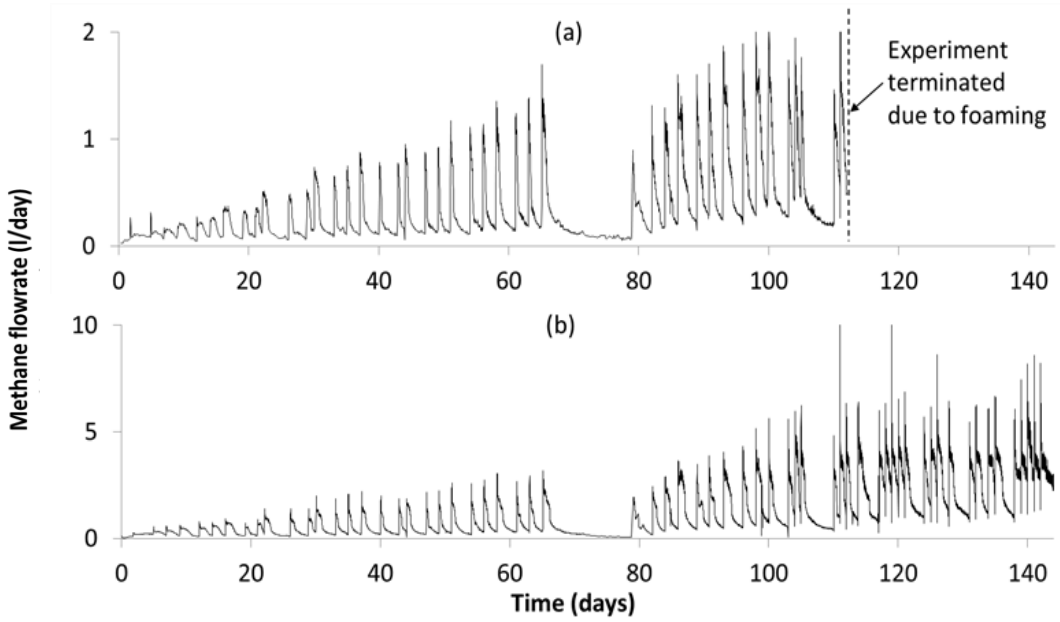

Figure 4.9 Experimental methane flow rate from (a) GW and (b) FW semi-continuous experiments (note different scale on ordinates).

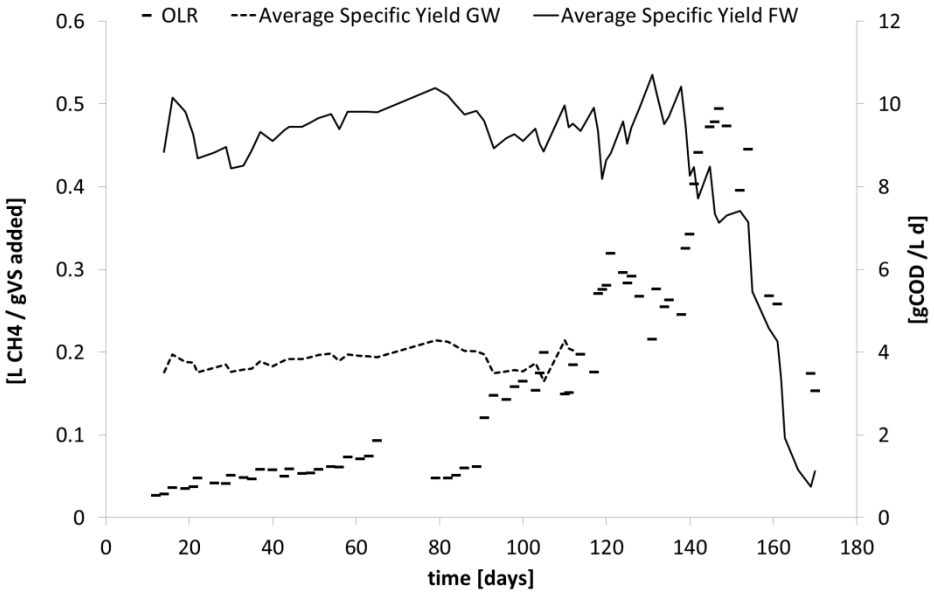

Figure 4.10 Specific yields for GW and FW, calculated from the volume of gas and amount of fed substrate in 6 consecutive feedings.

4.5.1 Kinetic fractionation

The same approach as employed in the batch experiments has been employed in semi-continuous experiments to calibrate the kinetic fractionation parameters and identify the most appropriate fractionation model. The parameters were calibrated against the calculated methane flow rates, with the cost function, weights and minimization technique as explained in section 3.11 . The number of data points was 4073 and 23644 for GW and FW respectively; FW data points extended up to 144 days, excluding the last three weeks characterised by dominant (and evident) inhibition conditions (which will be instead analysed in chapter 5). The alkalinity, ammonia, pH, TS, VS, VFAs measurements were also collected and used to evaluate the model predictions.

Calibrated kinetic parameters are shown in Table 4.10, together with standard errors and goodness of fit indicators. Similarly to batch tests, more complex models resulted in a better fit. In the GW fractionation, the coefficient of determination R^2 increased from 79.8% for model X, to 93.3 % for model XXS; in the FW fractionation R^2 increased from 74.0% for model X to 90.0% for model XXS.

Standard errors of calibrated parameters were lower than in batch tests, and therefore the parameters have a better identifiability: average standard error in of all GW fractionations is approximately 2%, with maximum of 9.7% (respect to an average of 10% and maximum of 26.4% in batch tests); in FW fractionation,

average is approximately 1%, with maximum of 3.5% (respect to an average of 5% and maximum of 11.8% in batch tests). The difference is due to the much higher number of data points and feeding events in the semi-continuous experiments, which overall produced a more informative data set.

Semi-continuous estimation also increases the differences in goodness of fit between alternative fractionations: in the case of GW, XX fractionation now also appears better suited than XS, while they appeared equivalent from batch estimation.

Absolute values of goodness of fit are however higher in semi-continuous estimation than in batch: in GW fractionation, the average R^2 is 88.2%, with respect to 98.8% in batch tests; in FW fractionation, the average R^2 is 82.5%, with respect to 98.7% in batch. Differences in fit targets (volume in batch, flow rate in semi-continuous) and experimental conditions (higher loadings in semi-continuous) explain the differences in goodness of fit. A further note can be made regarding the cost function: in semi-continuous tests the cost function gives less weight to higher flows, as they are less precise. However, the goodness of fit indicators consider equally all data points and therefore the lack of fit in the high flow sections of the experiments disproportionally increases the error values.

Regarding the values of the calibrated parameters, different observations can be made. The extent of degradation f_d remained similar in batch and semi-continuous tests, with a slight increase for the GW semi-continuous test, with an average increase of 11% across the various fractionations. Similarly, the parameter f_{Xr} showed small variations between the tests, and remained within the range 0.44-0.54 for GW, and 0.49-0.54 for FW. The parameter f_S showed larger variations, especially in the case of GW with higher values obtained in batch tests (ranges 0.21-0.25 in batch and 0.05-0.16 in semi-continuous). The hydrolysis rate constants displayed noticeable variations: much higher values in the semi-continuous tests, with a marked increase in GW (2 to 5 times higher depending on the fractionation, respect to batch tests) and twice as high in FW (with only X fractionation maintaining similar values). The main reason for this difference appears to reside in the adaptation of the microbial biomass to the substrate, as will be further supported by analysing the variation of the parameters across the experiment (see section 4.5.2).

Feed	Model	Parameter values					Standard errors (%)					rAE	R^2
		f_d	f_S	f_{Xr}	k_{hyd_r}	k_{hyd_s}	f_d	f_S	f_{Xr}	k_{hyd_r}	k_{hyd_s}	(%)	(%)
GW	X	0.330				1.42	0.6				1.3	24.5	79.8
	XS	0.350	0.167			0.97	0.6	3.1			1.6	21.8	86.7
	XX	0.380		0.514	4.75	0.19	0.4		0.7	1.6	2.8	13.1	93.1
	XXS	0.383	0.049	0.495	5.62	0.19	0.3	9.7	0.8	2.0	2.4	13.0	93.3
FW	X	0.766				1.16	0.2				0.6	50.8	74.0
	XS	0.783	0.197			0.77	0.2	1.2			0.8	44.7	81.0
	XX	0.846		0.492	5.98	0.24	0.2		0.4	1.0	1.3	35.1	85.0
	XXS	0.848	0.152	0.484	3.22	0.21	0.1	3.5	0.6	1.4	1.4	30.0	90.0

Table 4.10 Calibrated parameters for different kinetic fractionation models, for the two semi-continuous experiments with GW and FW.

The experimental and simulated flow rates for the GW tests are shown in Figure 4.11 (for X and XX fractionations) and Figure 4.12 (for XS and XXS fractionation); for the FW tests are shown in Figure 4.13 (X fractionation), Figure 4.14 (XS fractionation), Figure 4.15 (XX fractionation), Figure 4.16 (XXS fractionation). Experimental loadings are also shown on the figures, as flow rate profiles (shape and height) also depends on the loading magnitude.

In general, for both tests and in all fractionations, a better fit is achieved in the sections with low flow, and this is for the following reasons:

- The calibration method favours fitting with the low flow rate data points, as considered more precise (experimental error described as proportional to flow).
- System dynamics that occurs after each feeding are more complex to model, with accumulations of intermediates and inhibitions that influence the simulated flow rate. Instead, the low flow conditions are more clearly hydrolysis limited and therefore easier to simulate and calibrate.

Regarding the GW fractionations, the following observations can be made. X fractionation tends to underestimate both the high flow and low flow data points. The introduction of a further particulate fraction in XX model substantially improves the fitting. The introduction of the soluble fraction in XS model improves the fitting of the high flow data points respect to X model, while the fitting at the end of the feeding period remains less accurate. XXS model is practically identical to XX model, as also indicated by the equal goodness of fit indicators.

Some preliminary conclusions can be drawn: green waste is better described by two different particulate fractions which degrades at different rates (XX model); the

soluble fraction in green waste is negligible; semi-continuous tests distinguished between the XS and the XX models, which were practically identical in batch tests.

Regarding the FW fractionations, the following observations can be made. Small spikes in the gas flow rate, coincident with each feeding, are reproduced by the model. These spikes are originated by the acidic character of the substrate which rapidly reacts with the alkalinity available in the reactor, thus producing a spike of carbon dioxide, which in turn displaces part of the methane contained in the headspace. This spike is especially evident in the X fractionation, while it merges with the faster biochemical methane production in the other fractionations models. In the case of GW, this spike was less evident as the concentration of VFAs in the substrate was smaller than in FW.

The X fractionation, similarly to GW, tends to underestimate both the high flow and low flow rate data points. The introduction of a soluble fraction in the model XS allows to better reproduce the high flows after the feedings, although the fitting in the remaining part of the profile is less accurate. In the XX model, the profile is better simulated, but the high flows after the feedings are underestimated. XXS model is finally able to give the best fit both in the high and low flow rate sections. It can be concluded that food waste is better described through a fractionation that includes a soluble fraction (15% of the degradable COD) and two particulates having a similar share of degradable COD and different rates of degradation (differing by one order of magnitude).

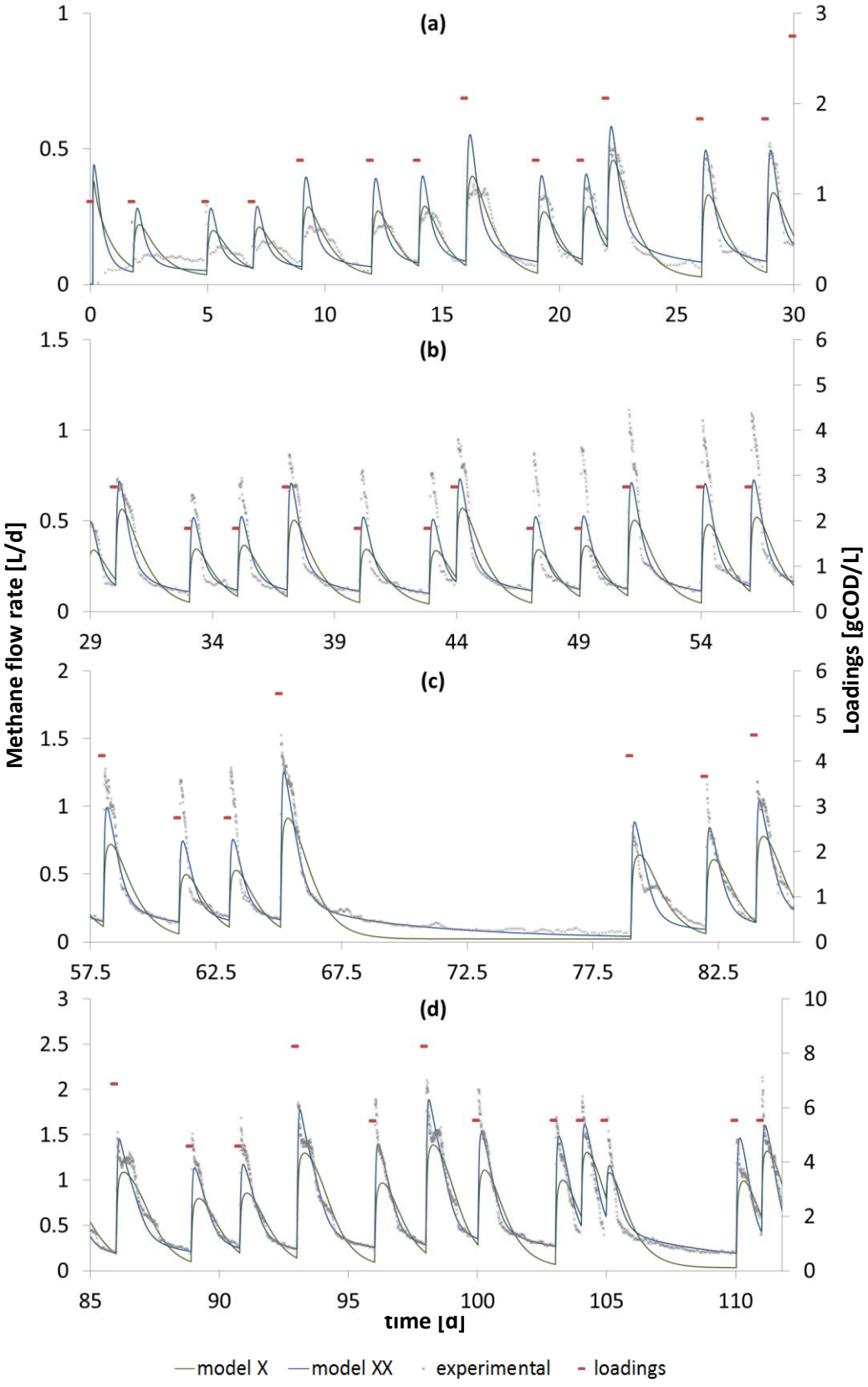

Figure 4.11 Experimental and simulated gas flow rates for calibrated fractionation models X and XX, for GW substrate, on 4 different time intervals.

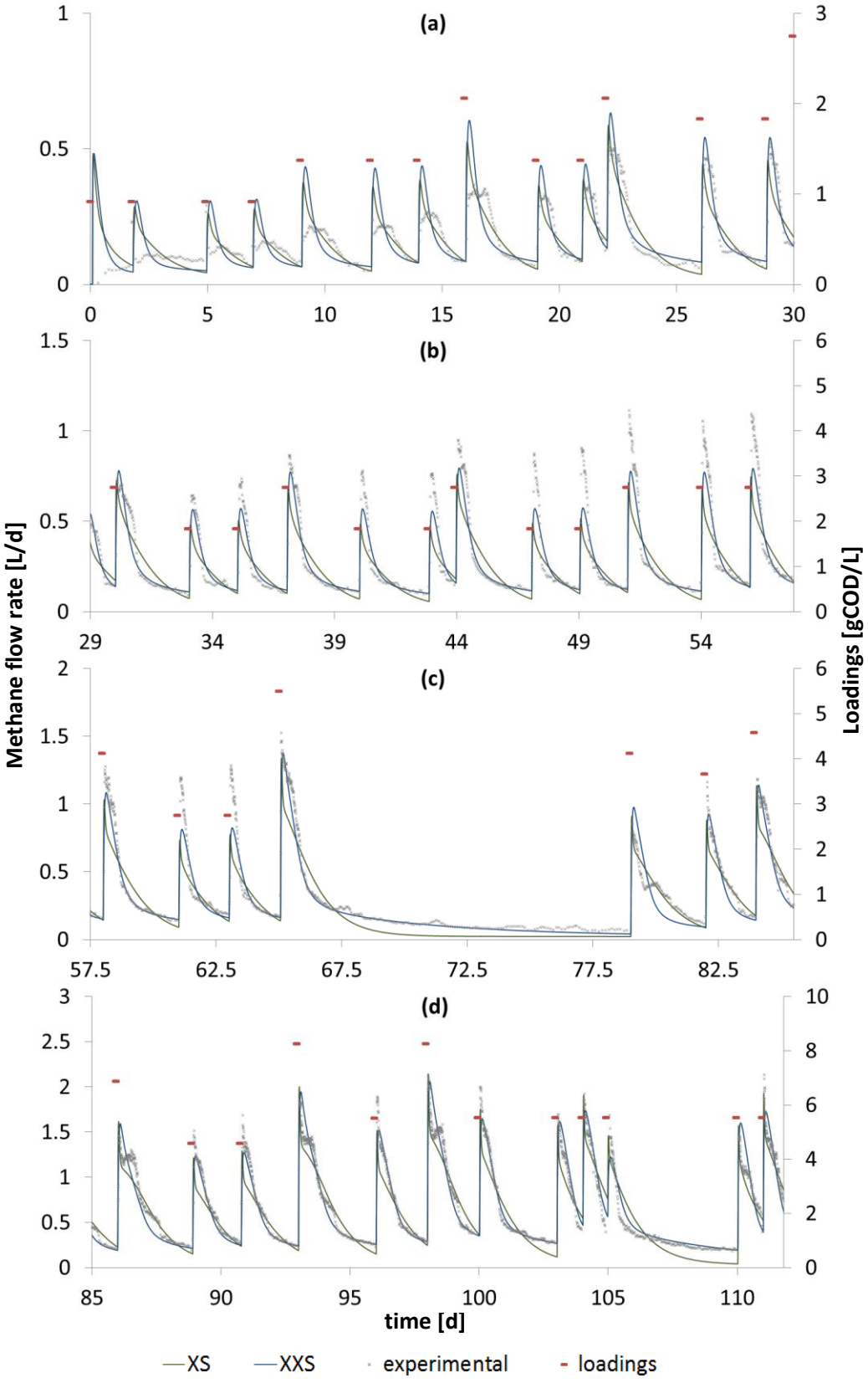

Figure 4.12 Experimental and simulated gas flow rates for calibrated fractionation models XS and XXS, for GW substrate, on 4 different time intervals.

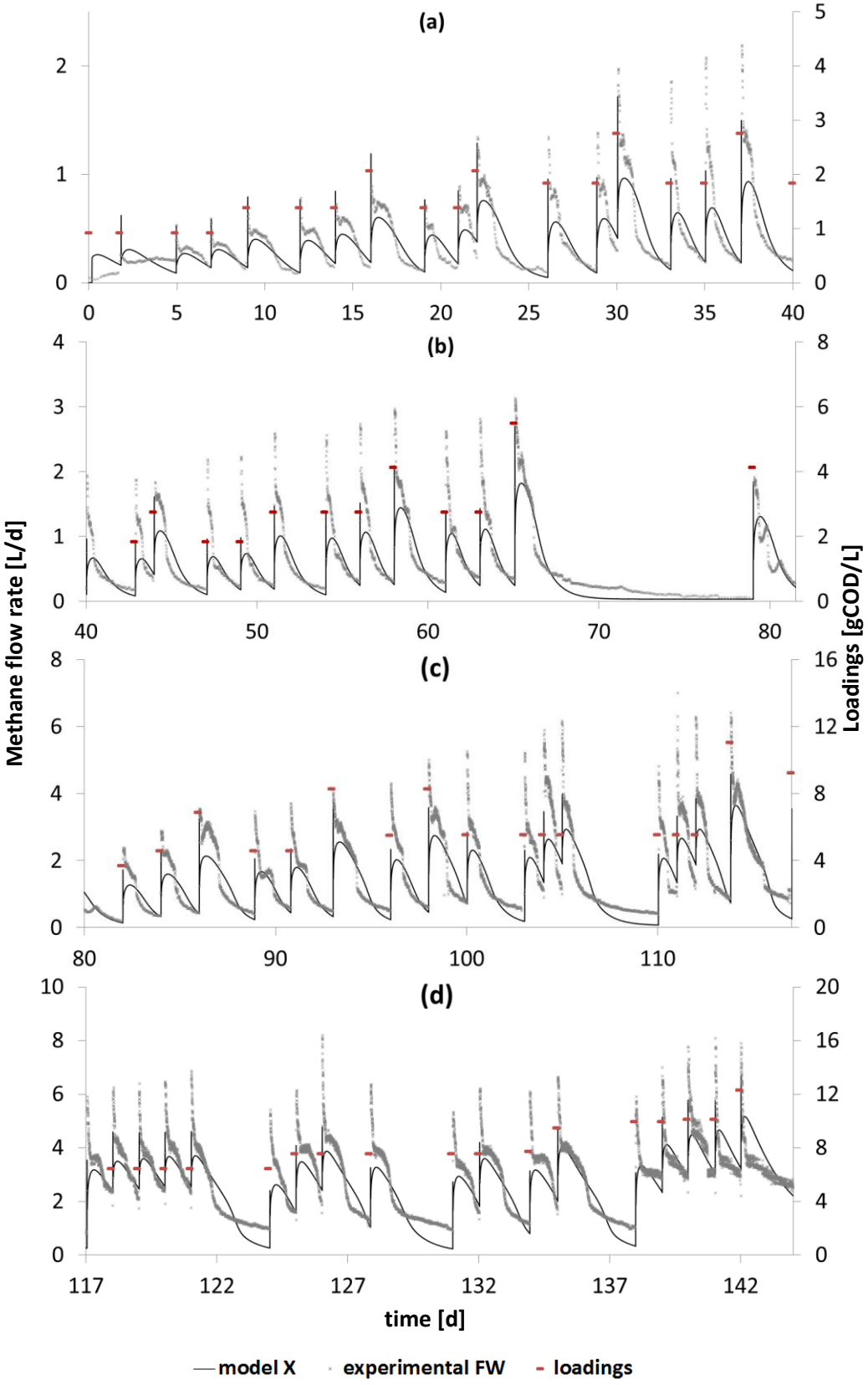

Figure 4.13 Experimental and simulated gas flow rates for calibrated fractionation model X, for FW substrate, on 4 different time intervals.

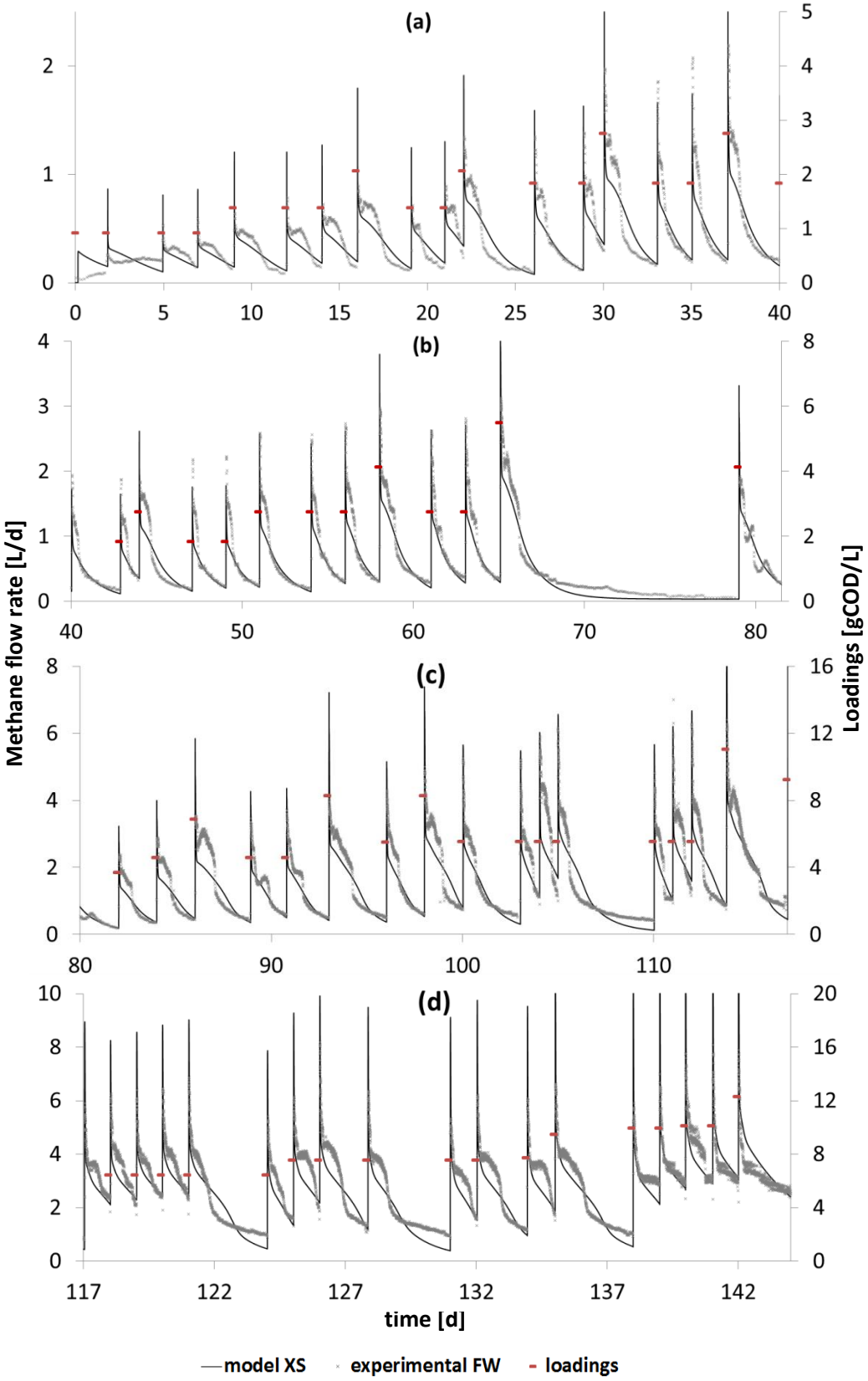

Figure 4.14 Experimental and simulated gas flow rates for calibrated fractionation model XS, for FW substrate, on 4 different time intervals.

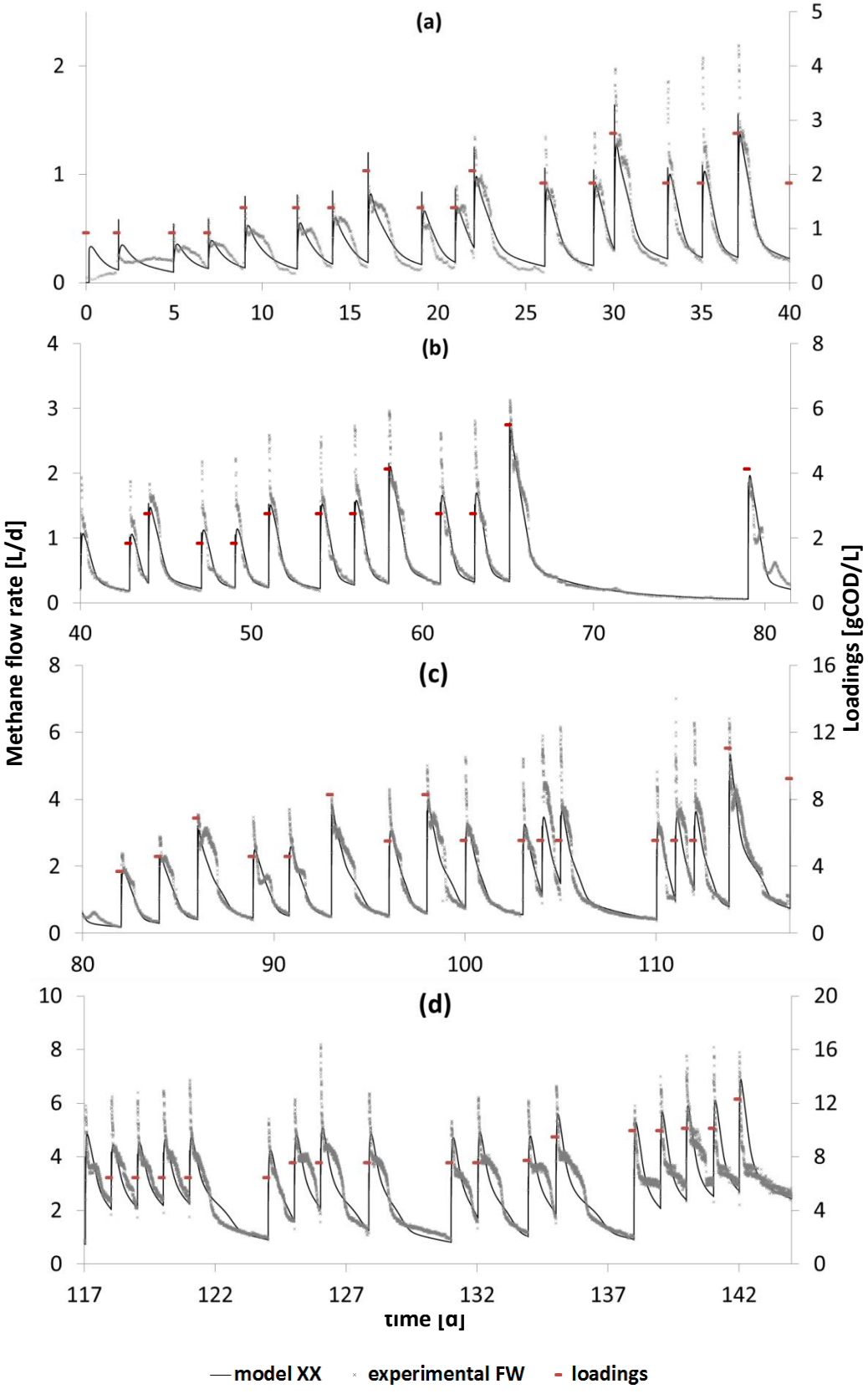

Figure 4.15 Experimental and simulated gas flow rates for calibrated fractionation model XX, for FW substrate, on 4 different time intervals.

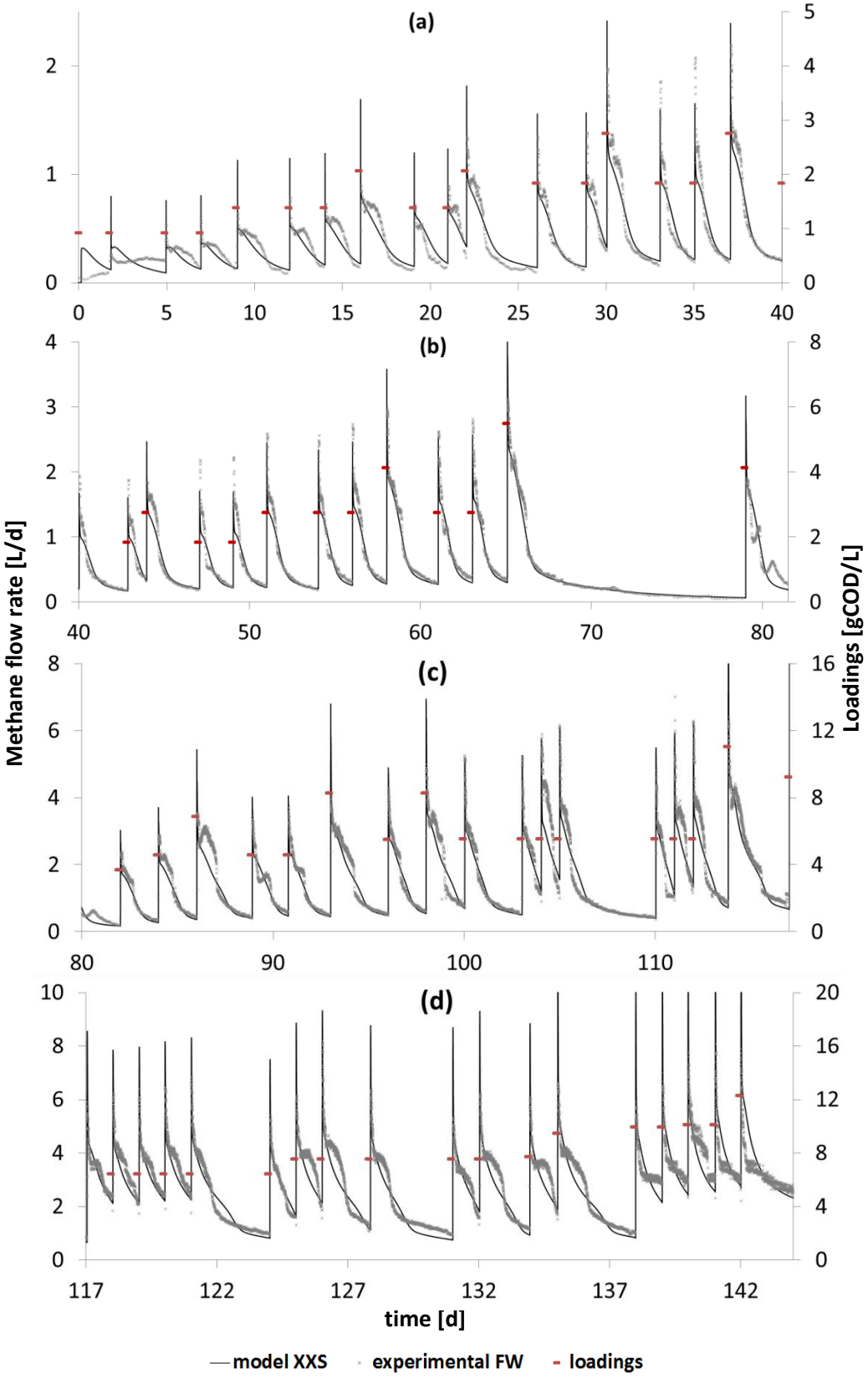

Figure 4.16 Experimental and simulated gas flow rates for calibrated fractionation model XXS, for FW substrate, on 4 different time intervals.

4.5.2 Temporal variation of the parameters and adequacy of the model

The previous section has made it clear how each substrate has an appropriate fractionation model which can be estimated from the methane flow rates. In addition, a further qualitative analysis of the experimental and simulated methane flow rates (for appropriate fractionations as the XX models), reveals how the goodness of fit changes along the experiment. Some qualitative distinctions can be made:

- The shape of the experimental flow curve, between each feeding event, is rather flattened during the initial part (approximately first 15 days): the model is hardly able to reproduce these shape characteristics.
- The fitting of the model improves in the following part, with the experimental flow showing a peak more defined and a monotonic shape between the feeding events, especially in the range 25-80 days in both tests.
- The fitting quality decreases again in the remaining period, with many curves showing a non-monotonic shape between the feeding events, which are not reproduced by the model.

Therefore a further calibration study was completed in order to assess if a possible variation of the fractionation parameters along the experiment could explain the aforementioned qualitative observations. Previous research has also analysed and identified temporal variations of the parameters during long term experiments (Batstone et al., 2009). For GW and FW, the whole collected data was split into smaller intervals, each containing 5 feeding events. On each interval the same calibration method as used previously was applied. For both GW and FW the XX fractionation was analysed, with the split fraction f_{Xr} fixed at the previously calibrated value using the whole data set: in this way the focus is on the variation of the constant of hydrolysis rates, extent of degradation and goodness of fit.

Figure 4.17 and Figure 4.18 shows the calibrated values for each data set interval, together with values previously estimated for the whole semi-continuous and batch data sets, for easier comparison. Figure 4.26 and Figure 4.27 show the calibrated curves, for GW and FW respectively, on different time intervals. Two trends appear for both substrates. The hydrolysis rate constant for the readily degradable fraction $k_{hyd,r}$ increases during the experiment, to then peak after 15 feedings for FW and 20 feedings for GW; the calibrated values then tend to decrease during the remaining

part of the experiment. A similar trend can also be identified for $k_{hyd,s}$ and for the extent of degradation f_d, with minimum values occurring at the beginning of the experiment, then reaching the highest values with increasing number of feedings. The goodness of fit R^2 as well exhibits a similar trend, especially in the case of FW, with a noticeable drop in the last of the data set intervals. For all the parameters, the value estimated using the whole data set is effectively an average value with respect to the interval calibrated ones. Especially in the case of $k_{hyd,r}$ and $k_{hyd,s}$ the variation is noticeable, up to four times between minimum and maximum values, while the variation is more limited in the case of f_d. The initial increase in the hydrolysis parameters can be explained by two phenomena:

- A gradual adaptation in the microbial biomass responsible for the hydrolysis with the production of adapted enzymes for the substrates.
- An increase in the microbial biomass concentration, with resulting change in the biomass/substrate ratio. It has been shown how the concentration of biomass influences the hydrolysis rate (Jensen et al., 2009) and the first-order hydrolysis is an adequate description only when the substrate is fully colonized by the bacteria.

On the other hand, the final decrease in the hydrolysis parameters is the result of slower methane production, which in turn can be explained by the development of inhibitive conditions in the last part of the experiment. Various phenomena can explain the increase in the inhibition (e.g. ammonia, weak acid inhibition) and this will be further explored in Chapter 5. The decreased value of the hydrolysis rate constant has therefore to be interpreted as an apparent decrease, as the slower methane production could be instead the result of a decrease in the uptake of soluble compounds. The lower R^2 values at the end of the experiment shows the structural inadequacy of the model in describing the inhibition phenomena; while sections with higher R^2 are an indication that the model is more adequate to describe the phenomena, and in turn the calibrated parameters are realistic. While the inhibition phenomena will be further explored in Chapter 5, the next section will examine the possible influence of the biomass/substrate ratio on the hydrolysis, with the use of Contois kinetics.

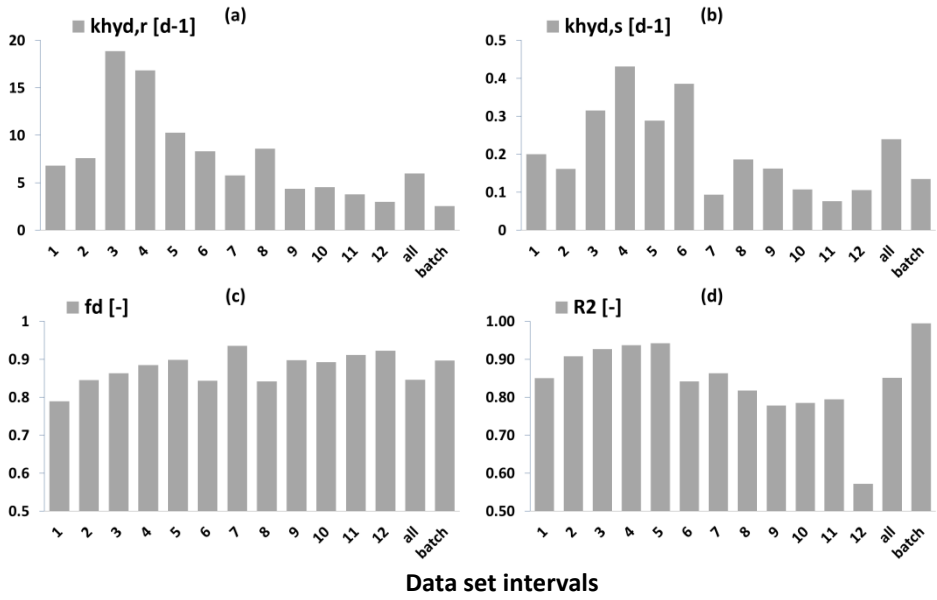

Figure 4.17 Temporal variation of the kinetic fractionation parameters (a) khyd,r, (b) khyd,s, (c) fd and (d) R2 goodness of fit for the FW semi-continuous experiment. Parameters are estimated on 12 consecutive intervals with 5 feeding each; parameters estimated with the whole data set and in batch experiment are also reported for comparison.

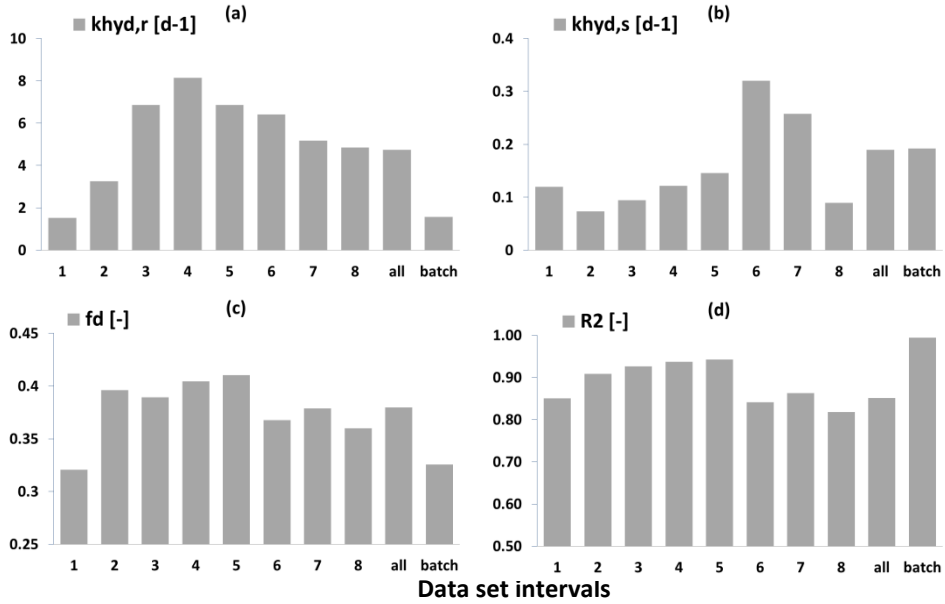

Figure 4.18 Temporal variation of kinetic fractionation parameters (a) khyd,r, (b) khyd,s, (c) fd and (d) R2 goodness of fit for the GW semi-continuous experiment. Parameters are estimated on 8 consecutive intervals with 5 feeding each; parameters estimated with the whole data set and in batch experiment are also reported for comparison.

4.5.3 Prediction of the other measured outputs

Figure 4.19 and Figure 4.20 shows how calibrated model simulations compare with the other experimental measurements, in addition to the methane flow rate, for FW and GW tests respectively. Table 4.11 shows the relative absolute errors (rAE) between the measured and simulated values. In the following paragraphs the trends in the experimental values and the goodness of fit from the simulations are discussed.

The total and volatile solids are important variables to predict, as they have a direct influence on a series of aspects, namely:

- They are proxies for unconverted degradable matter still available in the effluent.
- They influence engineering aspects, such as reactor mixing and digestate pumping.
- They influence the performance of downstream equipment, such as solid/liquid separators.
- They influence mass transfer processes in the reactor (Abbassi-Guendouz et al., 2012b).

In both experiments, total and volatile solids increased during the test, and this is as a consequence of no water being used for dilution and the accumulation of inerts and the slowly degradable particles. For total solids, measured concentrations of 65 and 78 gTS/L were reached towards the end of the experiment for FW and GW tests respectively, starting from a concentration in the inoculum of 16 gTS/L. For volatile solids, the increasing trend is similar, reaching a concentration of 43 and 55 gVS/L, starting from a concentration in the inoculum of 8 gVS/L. FW simulations achieve a significant goodness of fit (rAE 7%) for the TS, while the VS is underestimated in the first part of the experiment, resulting in a higher error (rAE 18%). In the case of GW, it is noticeable that there is an increasing error in the prediction of TS, indicated by a relatively high rAE of 19%. The errors in the predictions can be caused by a series of reasons:

- Sampling from the reactor and analytical errors: although the reactor are stirred almost on a continuous basis, sedimentation of heavier fractions are likely to have occurred and therefore excluded from sampling (which was from the mid height of the reactor). This can explain the trend in the underestimation of TS in GW test, as the high content of ash (grit) in GW is likely to have settled.

- Conversions factors: as was seen in eq. (3.3), the ADM1 state variables in gCOD/L are transformed into solids concentrations using some conversion factors which are necessarily an approximation.

Total ammonia nitrogen has a direct influence on the inhibition of many microbial processes, and therefore it is important for the model to be able to reproduce the experimental data. The experimental trend is again of a constant increase in concentration: from an initial 1.4 g $N\text{-}NH_4$/L to a final value of 3.5 and 1.7 g $N\text{-}NH_4$/L in FW and GW tests, respectively - after 112 days (length of GW test), the TAN content in FW was 2.3 g $N\text{-}NH_4$/L. The higher increase of TAN in FW is due to a higher nitrogen content together with a higher degradability of the substrate. The goodness of fit was very good for FW (rAE 5%), which validates the value of the calibrated extent of degradation for the protein content in FW. In the case of GW the simulation slightly overestimates the experimental values (rAE 12%) at the end of the experiment.

Bicarbonate alkalinity (BA) is the main buffer in anaerobic systems, reducing the change in pH following VFAs production: its measure indicates resistance to organic overload and together with VFA is the main indicator of process stability (Steyer et al., 2006). A BA accurate prediction is therefore important as it is related to the overall prediction accuracy of pH changes and process stability. Experimental values show an initial trend of increasing BA, especially for FW tests. The increase can be explained by analysing the charge balance of the anaerobic system (eq. (3.4)): the above-mentioned increase in TAN corresponds to an increase in positive charges (inorganic nitrogen mostly in the form of ion ammonium NH_4^+, with pK_a = 9.25) which in turn allows a higher amount of the negatively charged bicarbonate ion HCO_3^- to remain in solution (and not being transformed into gaseous CO_2). In the case of FW test, it is noticeable how there is a decrease in BA towards the end of the experiment, which is due to the accumulation of VFA, in turn related to higher loading rates. In fact, VFA are almost completely in dissociated form (pK_a 4.76-4.88) and therefore the increased amount of H^+ ions drives the transformation of part of the BA into CO_2. In the case of GW, there is a less defined increasing trend, and this can be related to the lower TAN content in the GW system. Similar to FW, also in GW higher loading rates correspond to a decrease, or at least a stabilization, in the BA content. BA simulations capture in both cases the experimental trends, with acceptable rAE of 10% and 5% for FW and GW, respectively. In the case of FW, the simulation predicts the initial increase and the final decrease. There is a noticeable underestimation in the final experimental values, and for which it is

difficult to identify a single cause. One possible explanation could be the inaccuracy in the experimental determination of BA. This was in fact approximated by titration to pH 5.75 and using an empirical factor to convert the measurement (partial alkalinity) to bicarbonate alkalinity (Jenkins et al., 1983). However, in systems with a high concentration of TAN and VFA, the empirical factor is less accurate and BA could be overestimated: the titration in fact also converts the free ammonia to ion ammonium and part of the available VFA into the undissociated form. Different empirical factors could be used depending on the state of the system, but this goes beyond the scope of this thesis.

VFAs are the main products of the fermentative and acetogenic steps; accumulation of VFAs in the liquid phase are indicators that the reaction rates of consumption of VFAs (namely methanogenic reaction for acetic acid, and acetogenic reaction for propionate, butyrate and valerate) are slower than the production rates. If this imbalance is protracted in time, it will eventually lead to a failure of the whole anaerobic process, due to an excessive inhibitory acidity in the system. In fact, VFAs have been since long accepted as the main indicators of process stability (Ahring et al., 1995, Boe et al., 2010). Single VFAs species were measured and simulated, however the sum of all single species is here reported - as the focus is more on the process imbalance between acid production and consumption rates. Excluding the end period of the FW test, the VFA content in the effluents remained at very low levels, with an average concentration of 0.05 gCOD L^{-1} in GW test and 0.1 gCOD L^{-1} in the FW test, sign that the applied loading rates did not imbalance the system. Highest peak in the GW test was 0.13 gCOD L^{-1} at 100 days, while in the case of FW a peak of 3 gCOD L^{-1} was registered. Simulations show how the spikes in VFA concentration, after each feeding, are reduced to low levels before the following feeding. Also the final accumulation of VFAs in FW test is well predicted. However, the error is very high at 159% and 173% for FW and GW, respectively, as the simulations tend to overestimate the residual VFA. Most of the error is caused by an overestimation of the very low levels of VFA, which from an engineering and control point of view are less important to predict. A calibration of the half saturation constants in the VFA uptake rates would have reduced the error, but this was beyond the scope of the chapter.

pH is the result of the interaction of all charge bearing species in the system. In both the FW and GW cases, the pH is quite stable between 7.5 and 7.75, with increasing values during the first 50 days of the experiment and then a decline and stabilization. The initial increase can be related with an increase of TAN in the

system, with higher VFA concentrations reducing the pH in the second part of the experiment. The simulations tends to underestimate the pH during the initial period of the experiment, while the fit improves after about 70 days in both experiments. It is difficult to identify a reason for the initial lack of fit, although it can be observed how the implemented ADM1 cannot take into account some important influencing pH phenomena, including: phosphate buffer, sulphate-sulphide system, precipitation of carbonates (e.g. calcite $CaCO_3$), formation and precipitation of struvite. The simulations also show how the pH drops after each feeding, with the drops being proportional to the size of the feeding and related to the VFA and CO_2 production, which in turn increase the amount of H^+ ions in the liquid.

Methane content in the produced gas was only measured in the FW experiment, and for a limited period of time. Methane content is directly related to the biochemical composition of the substrate and in particular with the oxidation state of carbon, e.g. lipids degradation will produce a methane-richer gas than carbohydrates. At the same time, in highly dynamic systems, the gas composition also depends on the relative rates of the various processes. Simulated CH_4 and CO_2 flows and their ratio are shown in Figure 4.21b: it is evident how the ratio decreases abruptly after each feeding, as the degradation of the fresh substrate produces initially a relatively high amount of CO_2 through fermentation and fatty acids oxidation. The ratio then increases again and peak, through the reduction of CO_2 to methane in hydrogenotrophic methanogenesis and the gradual conversion of the accumulated acetate to methane. The experimental methane content (Figure 4.21a) follows exactly the same pattern, as obviously is the result of the combination of the different gas flows. The simulated methane content follows remarkably well the experimental values (rAE 5%).

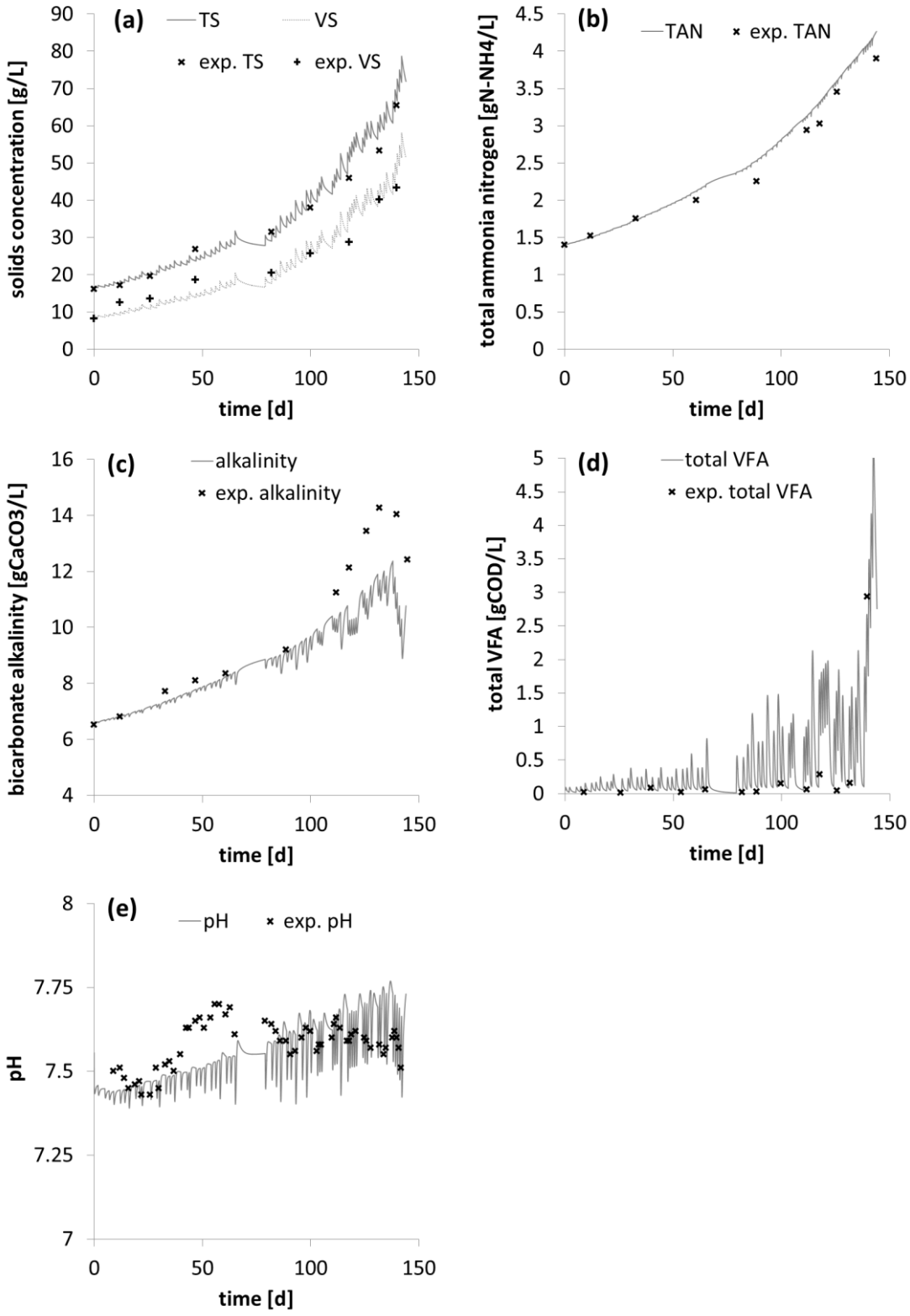

Figure 4.19 Simulated (calibrated XX model) and experimental measured outputs in the FW semi-continuous experiment: (a) total and volatile solids, (b) total ammonia nitrogen, (c) bicarbonate alkalinity, (d) total VFA (sum of all species) and (e) pH.

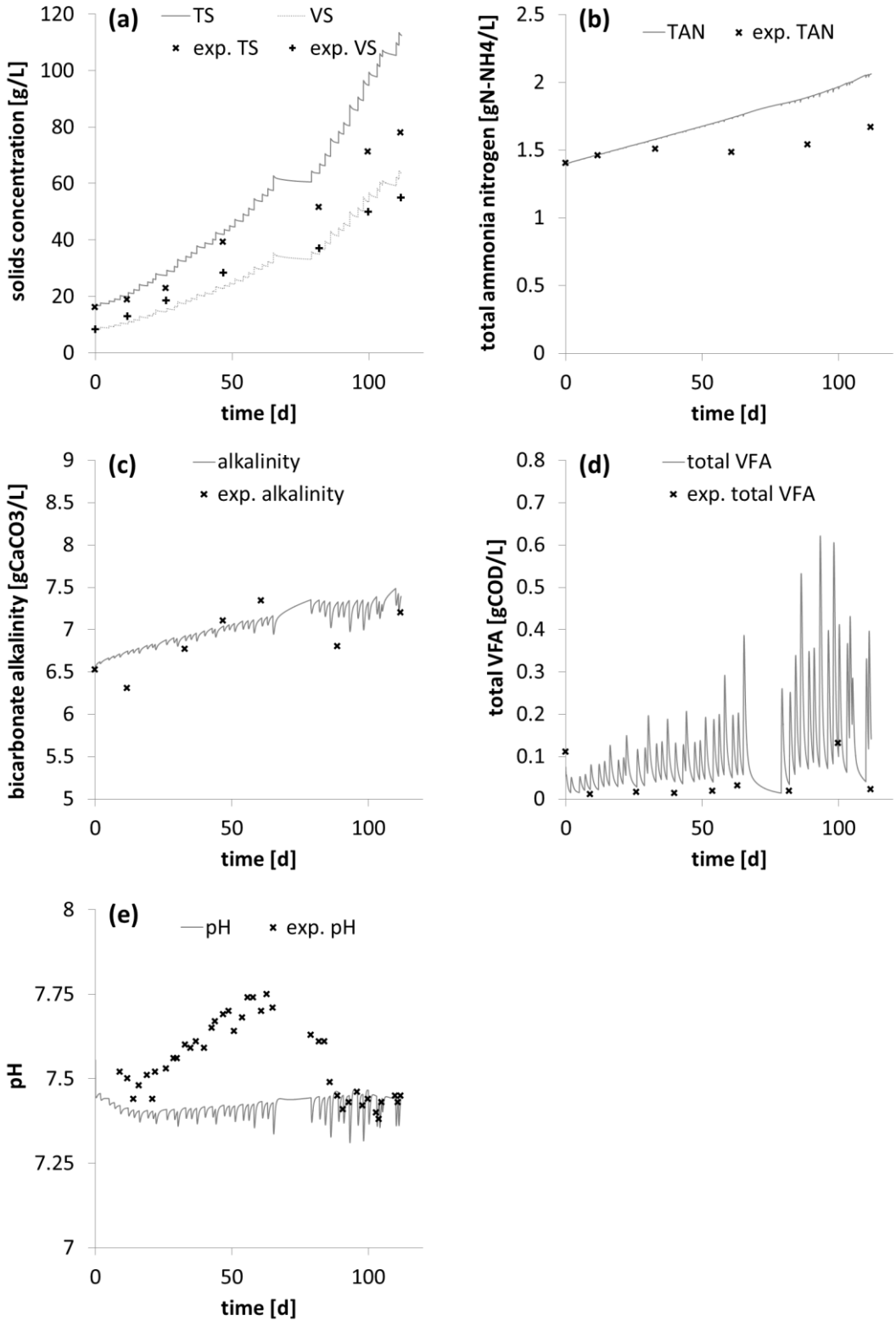

Figure 4.20 Simulated (calibrated XX model) and experimental measured outputs in the GW semi-continuous experiment: (a) total and volatile solids, (b) total ammonia nitrogen, (c) bicarbonate alkalinity, (d) total VFA (sum of all species) and (e) pH.

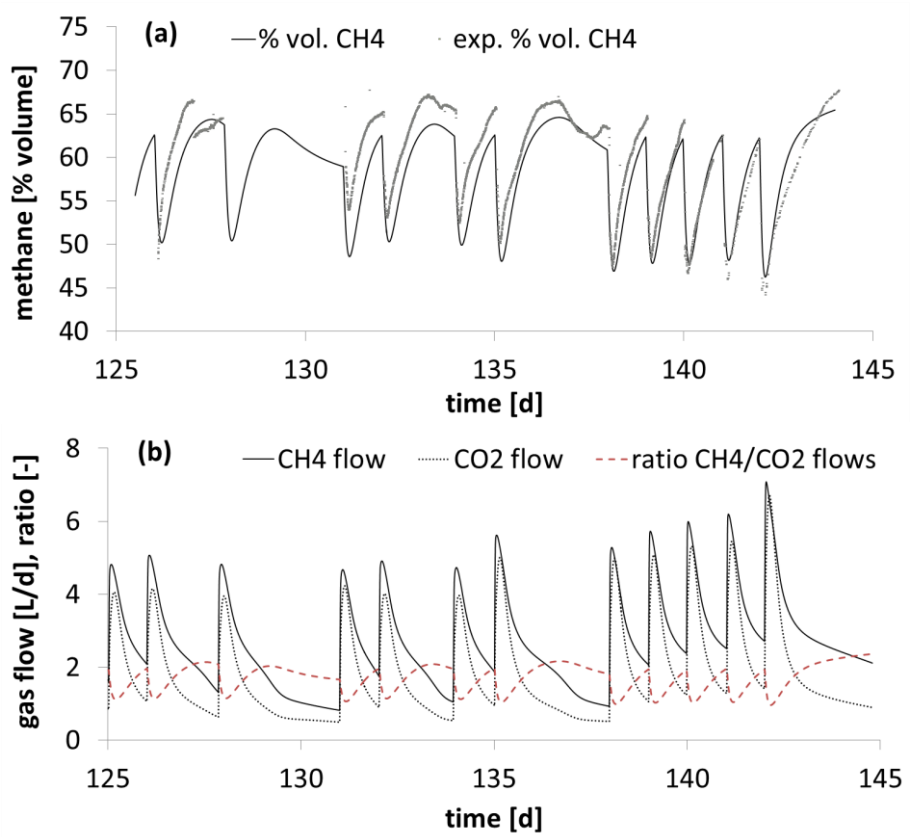

Figure 4.21 (a) Simulated and experimental CH4 content in the produced gas in the FW test; (b) simulated CH_4 and CO_2 gas flow rate in the FW semi-continuous test.

	rAE %	
	FW	**GW**
TS	7%	19%
VS	18%	13%
TAN	6%	12%
Alkalinity	10%	5%
VFA	159%	173%
pH	1%	2%
CH4 %vol.	5%	n.d.

Table 4.11 Goodness of fit indicated by relative absolute errors in the measured outputs in the GW and FW semi-continuous tests.

4.5.4 Residual analysis

A residual analysis was performed to check the assumptions on the least square method. Residual plots as a function of time show how the residuals are homoscedastic for FW (Figure 4.22(a)) and partially for GW (Figure 4.23(a)); autocorrelation is evident in both cases. Histograms plots (Figure 4.22(b) and Figure 4.23(b)) show how in both cases the residuals follow a normal distribution,

although skewed negatively (average of the residuals: -0.68 for FW and -0.49 for GW).

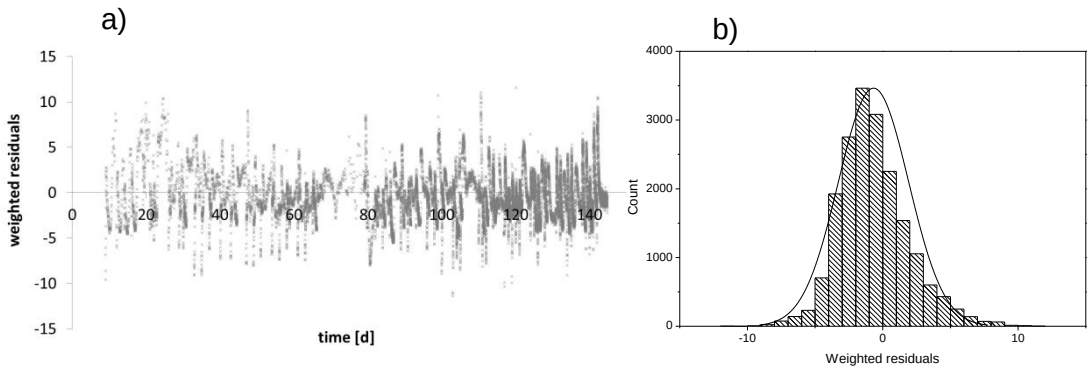

Figure 4.22 (a) Residual plot and (b) histogram distribution for calibrated XX model for test 2 and FW substrate.

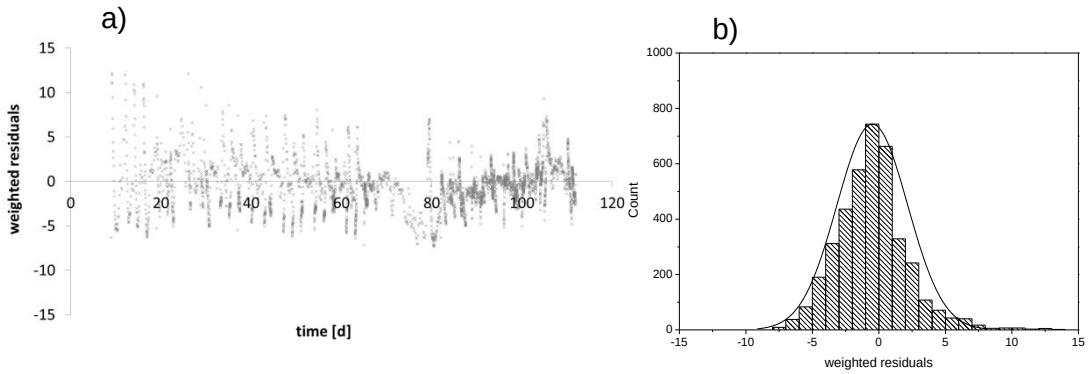

Figure 4.23 (a) Residual plot and (b) histogram distribution for calibrated XX model for test 2 and GW substrate.

4.5.5 Hydrolysis described by Contois kinetics

Contois kinetics (eq. (3.4)) is a more comprehensive kinetic description of hydrolysis, and it describes the saturation effects for both the substrate and biomass (Vavilin et al., 2008), with two limiting cases:

- When the substrate is abundant and biomass limiting, i.e. the ratio substrate/biomass >> half saturation coefficient $K_{S,CNT}$: the substrate

degradation rate only depends on the biomass concentration (first-order hydrolysis in the biomass).

- When the biomass is abundant and the substrate limiting, i.e. the ratio substrate/biomass << $K_{S,CNT}$: the substrate can be considered always to be fully colonized by the biomass, and its rate of degradation only depends on the substrate concentration (first-order hydrolysis in the substrate).

Semi-continuous digester operations are characterised by rapid changes in substrate concentration. Simulations with the previously calibrated models XX were realized to quantify these changes, and compare them with the variations in the acidogenic biomass, which is producing the exo-enzymes which hydrolyse the particulate. Figure 4.24 shows the concentrations of the lumped acidogenic biomass (i.e. in ADM1: X_{su} + X_{pr} + X_{fa}) and of the readily ($X_{ch,r}$+$X_{pr,r}$+$X_{li,r}$) and the slowly degradable particulates ($X_{ch,s}$+$X_{pr,s}$+$X_{li,s}$), for both GW and FW tests. In both these tests there is an accumulation of the slowly degradable particulate, while fast particulate is completely degraded during each feeding period. Also the biomass concentration tends to increase during the experiment, especially in FW test due to the higher degradability of the substrate. Figure 4.25 shows the ratio of the substrate on the lumped biomass: in both tests there is a slightly increasing trend for the slowly degradable particulate ratio, while the trend is more constant for the fast particulates. A much higher variation in these ratios occurs between each feeding, and this could lead to situations of substrate saturation (biomass limiting) after each feeding. To explore the possible influence of this phenomena, the ADM1 model was updated with the Contois kinetics, the parameters of the Contois calibrated and the goodness of fit evaluated. Similar to the model with first-order kinetics, various fractionation models have been also implemented and calibrated. In the fractionation model with two particulates (XX and XXS), the kinetics was implemented with two half saturation coefficients $K_{S,CNT,r}$ and $K_{S,CNT,s}$ for the respective particulates.

In all the calibrations, the estimated values of $K_{S,CNT}$ coincided with the superior bound of the defined parameter range in Aquasim (fixed at 100). This value is much higher than the substrate/biomass ratio shown in Figure 4.25 (in all cases below 2): this indicates that the Contois kinetics described a situation of substrate limitation and practically coincides with first-order kinetics. Moreover, the half saturation coefficients were fully correlated with the hydrolysis rate constants, thus resulting in very elevated standard errors.

To further analyse the Contois kinetics, calibrations on feeding intervals were realized, similarly to first-order kinetics. To reduce the correlation and uncertainty, a single half saturation coefficient was implemented for all the particulates. To force the calibration algorithm to find “interesting” solutions (i.e. not coincident with first-order hydrolysis), the possible values of $K_{s,hyd}$ were bounded to a maximum value of 0.5. In all calibration results (not shown) again $K_{s,hyd}$ coincided with the maximum value and the goodness of fit was lower than with the models implementing first order hydrolysis. The only case where the Contois kinetics performed better than the first-order was when the first interval data set was considered. Figure 4.26(a) and Figure 4.27(a) show the simulated curves obtained in these cases: it can be observed how the Contois kinetics better represents the flat profile of the methane flow rate. An interpretation could be as follows: the inoculum was not adapted to the new substrates fed, and the Contois kinetics describes this situation as a biomass limiting condition, with a very low half saturation constant (Ks=0.01). The simulated curves obtained in the other intervals, although having a lower goodness of fit than the first-order hydrolysis models, show interesting characteristics. In particular, the Contois kinetics, with the XXS fractionation model, is able to partly reproduce the non-monotonic characteristic of the flow rate curves (Figure 4.26(b)(c) and Figure 4.27(b)(c)). The peak in flow rate is given by the fast uptake of the soluble S fraction, while the hydrolysis of the particulates causes the flat section (or second peak) in the curve. An interpretation could be as follows: after each feeding there is an excess of substrate with respect to the biomass, further the substrate/biomass ratio is higher than the half saturation constant (Ks=0.5) and therefore the hydrolysis rate is in the saturation zone of the kinetic curve, i.e. the rate of hydrolysis is almost constant and not changing with the substrate concentration. In the case of the first-order hydrolysis model, the initial peak can be also simulated by a very fast hydrolysis of the particulate and then the rate of hydrolysis monotonically decreases with the decrease of the substrate.

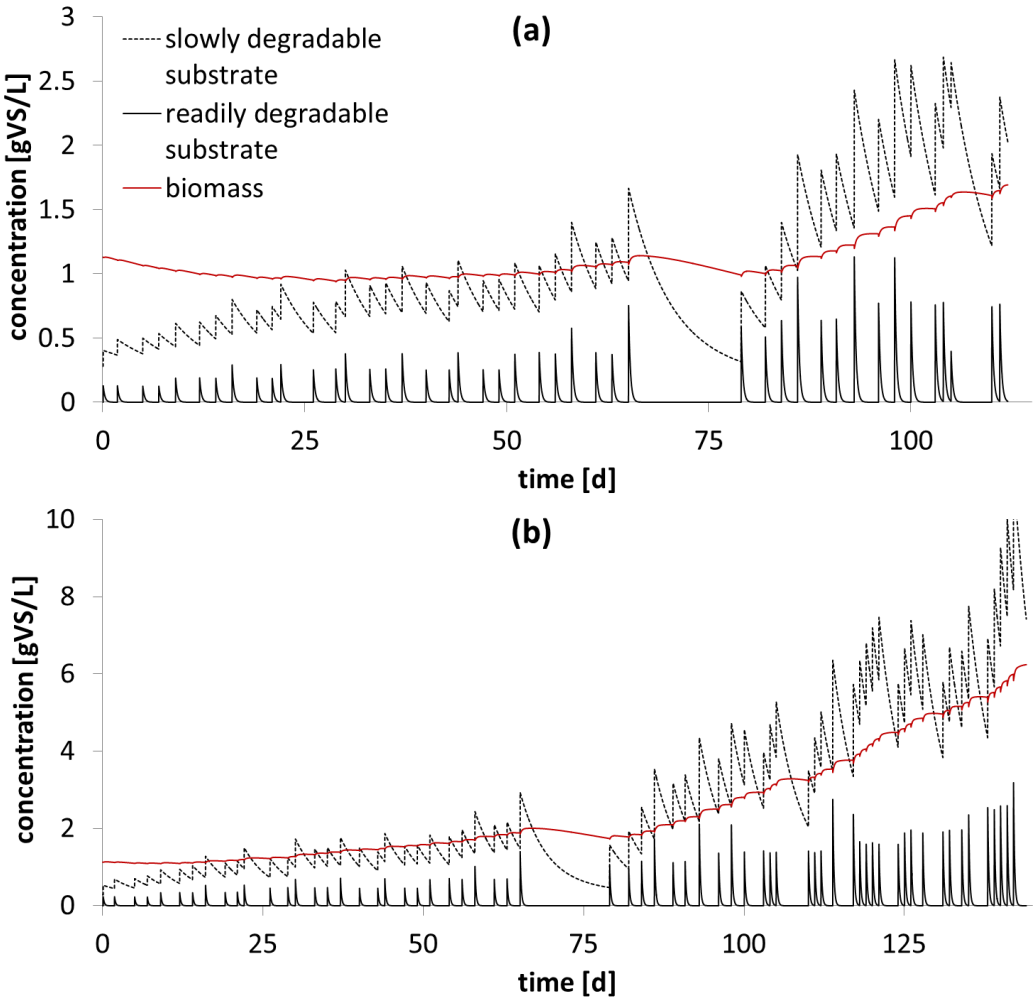

Figure 4.24 Simulated lumped acidogenic biomass and degradable substrate fractions for the (a) GW and (b) FW experiments (calibrated XX fractionation).

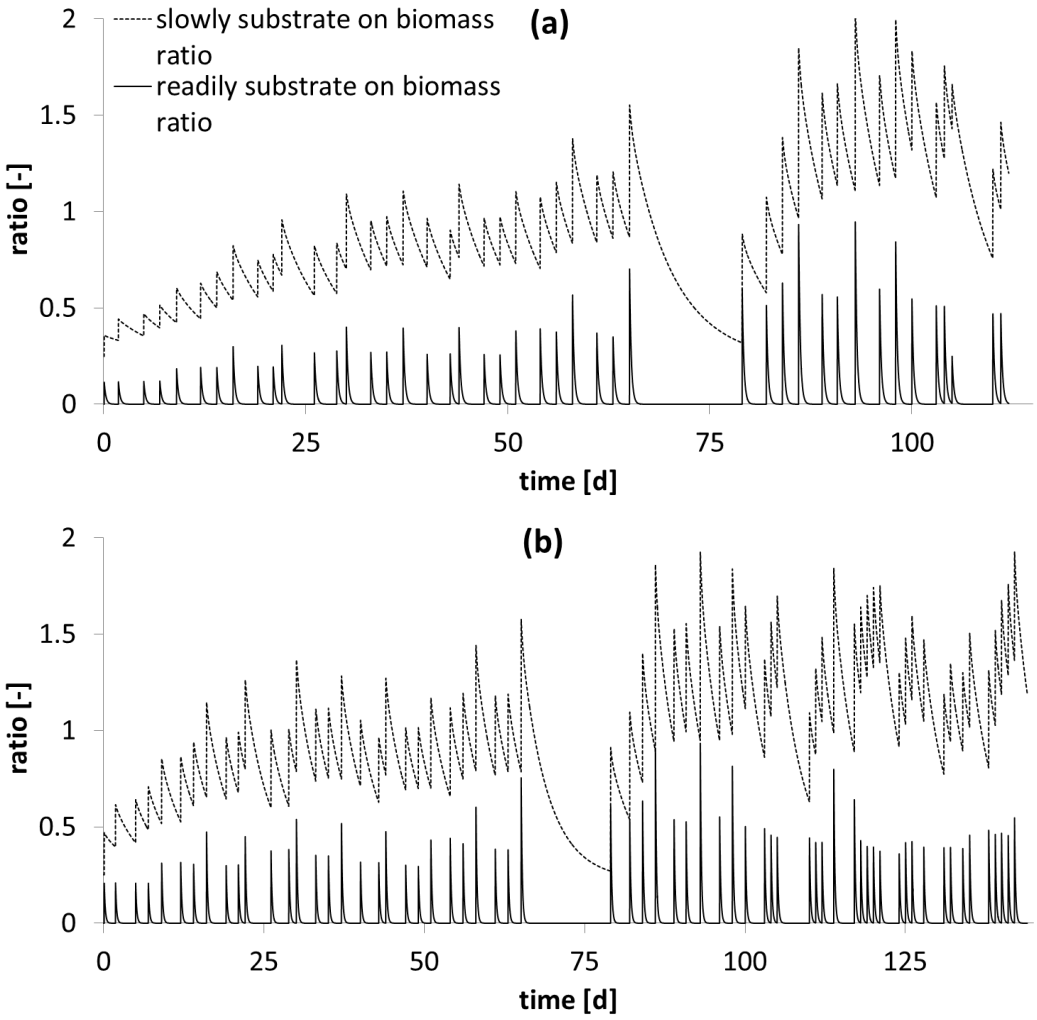

Figure 4.25 Simulated ratios of the slowly and degradable substrate to the lumped acidogenic biomass, for the (a) GW and (b) FW experiments (calibrated XX fractionation).

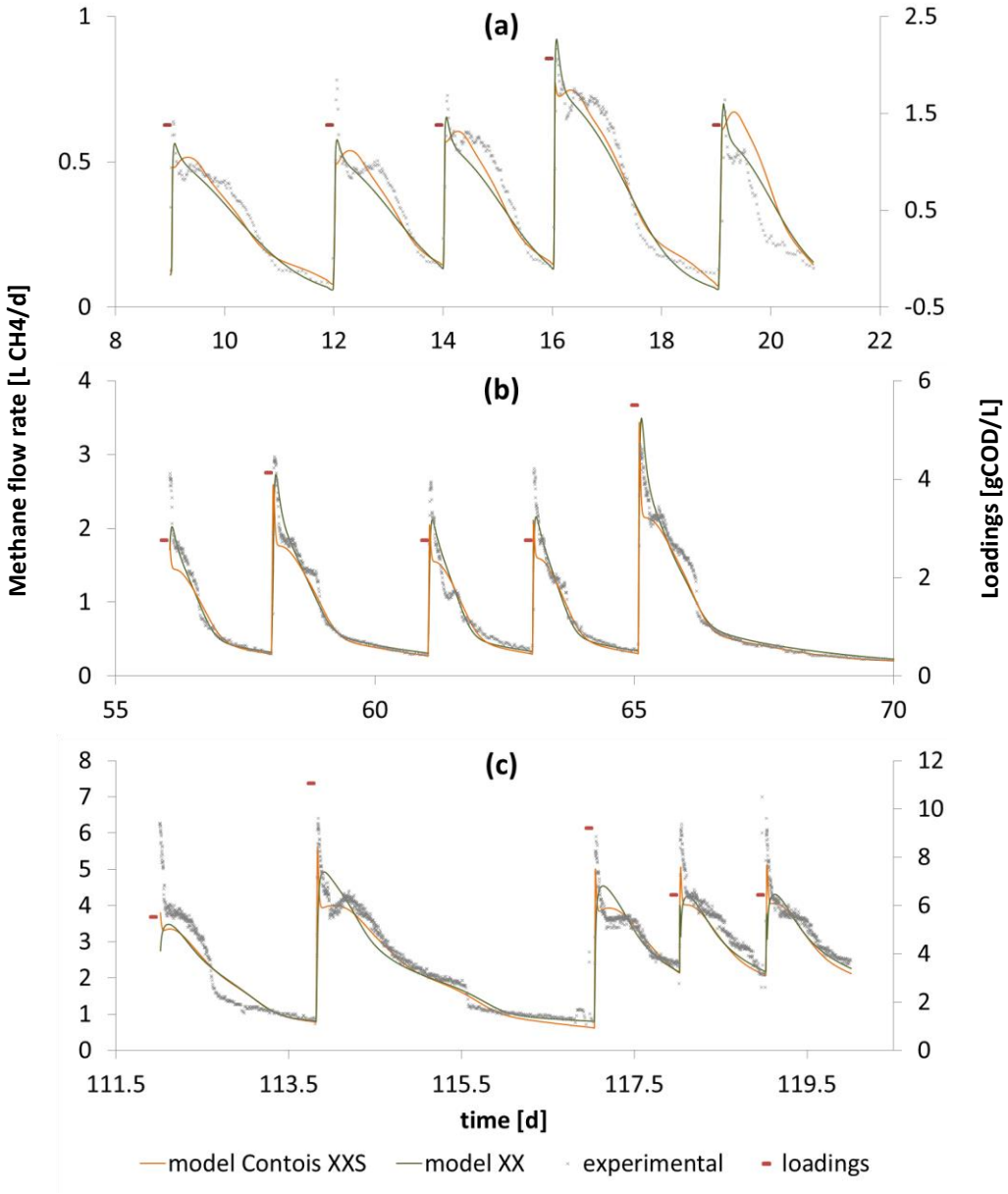

Figure 4.26 Calibrated XX model and XXS Contois model on three different intervals, with 5 feedings each, for the FW test: (a) 9-21 days, (b) 56-70 days, (c) 112-120 days.

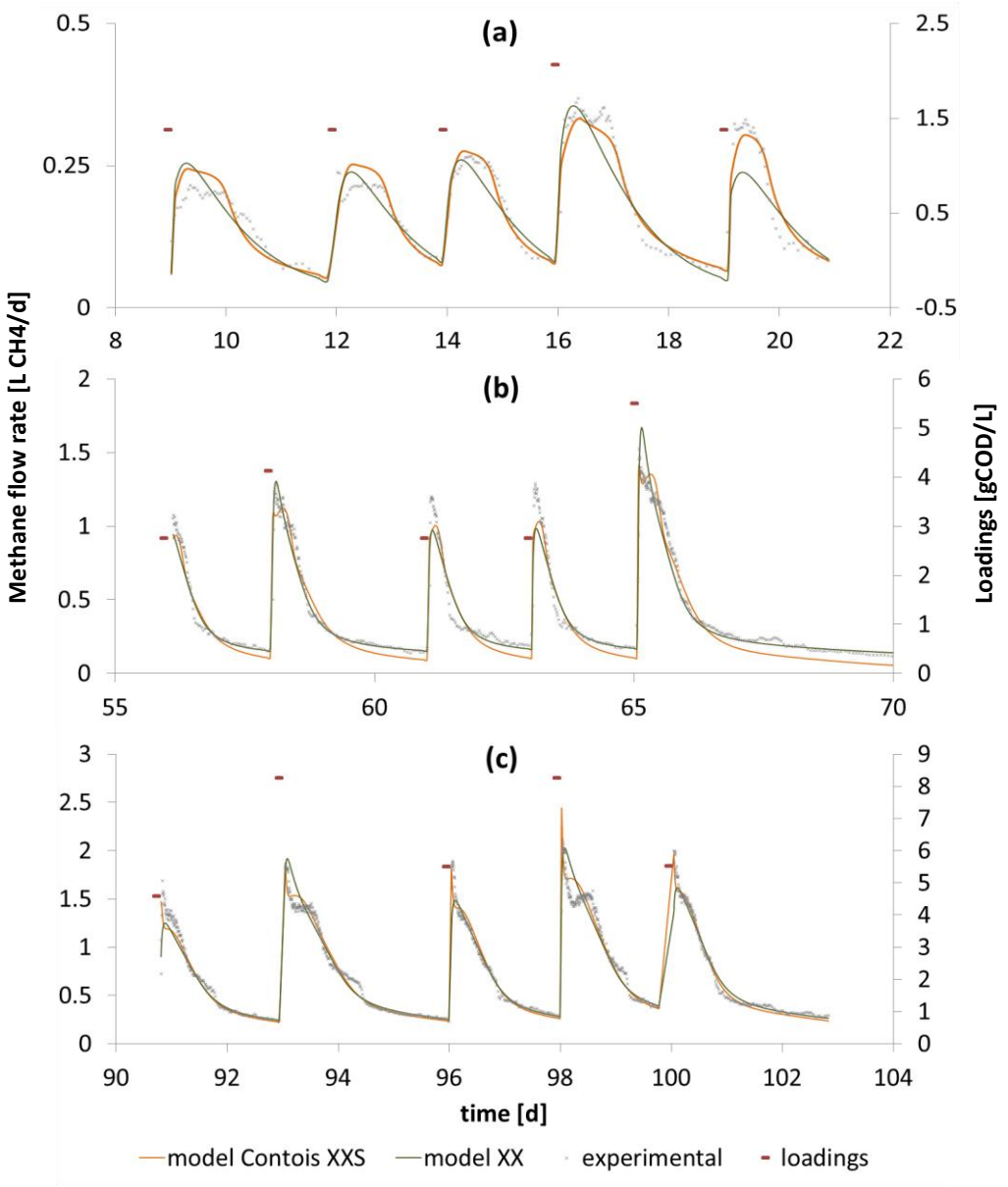

Figure 4.27 Calibrated XX model and XXS Contois model on three different intervals, with 5 feedings each, for the GW test: (a) 9-21 days, (b) 56-70 days, (c) 91-103 days.

4.5.6 Maximum rate analysis

Figure 4.28 shows the ratio between the maximum methane flow rate and substrate loading for each feeding event, for the GW and FW tests. In both tests the ratio is not constant. Some correlations and trends can be identified from the figure as follows:

- Abrupt increases in the loadings (e.g. at days 15.9, 36.9, 43.9, 65.0, 85.9, 92.9, 113.7) correspond to a decrease in the ratio.
- A trend of increasing ratio at the beginning of the experiment; a defined decrease after the 13 days period of no feeding; a further increase in the ratio, almost to levels preceding the interruption in the feeding; in FW test, a final decrease corresponding to the highest loadings.

In the case of the hydrolysis being the limiting reaction, the ratio would be constant when the hydrolysis is described as first-order reaction (rate of degradation proportional to substrate concentration). The identified non-constancy of the ratio can be explained as follows:

- After feedings, hydrolysis is not the limiting reaction, and instead accumulation of intermediates occurs (mainly acetate, propionate and fatty acids) as also shown in the case of batch tests (see Figure 4.7). The decrease in the ratio after the period of no feeding can be interpreted as a decline in the biomass responsible for the uptake of the intermediates.
- The hydrolysis is not described by a first-order reaction, and there is a saturation effect in the substrate.
- The final decline in the ratio may again be explained by the arising of inhibiting conditions.

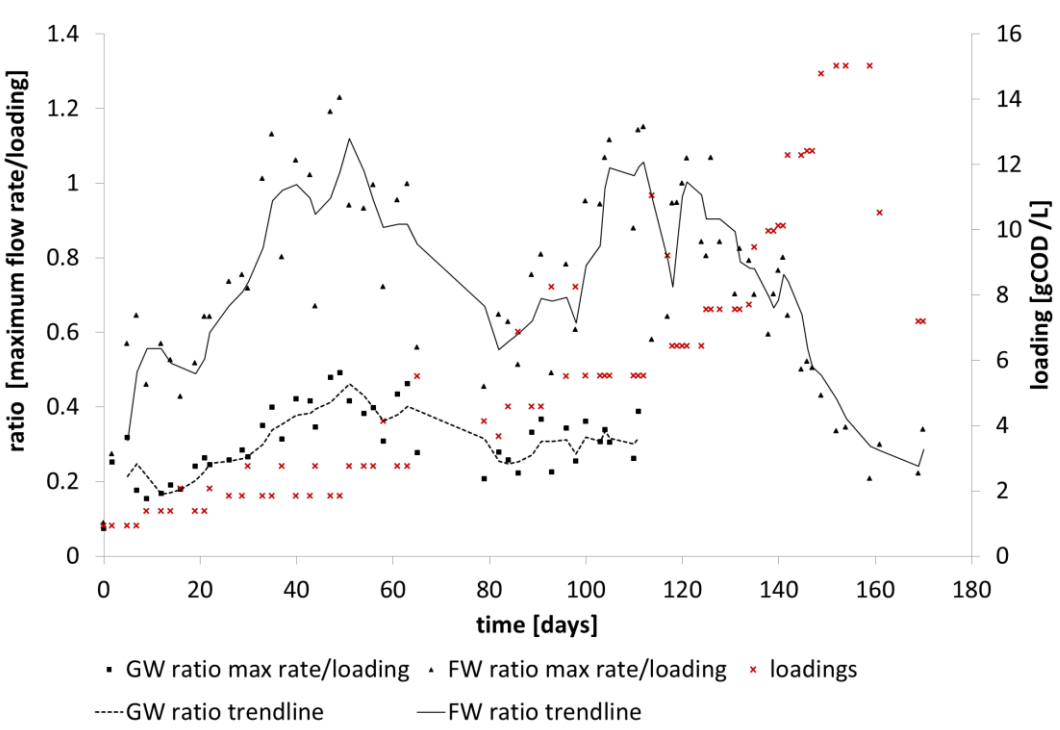

Figure 4.28 Ratio between the experimental maximum methane flow rate and the loading for each feeding event, for the FW and GW tests. Trendline as moving average, calculated over a period of three feedings.

4.6 Conclusions

Several conclusions can be drawn from the analysis carried out in this chapter, regarding the methods and processes explored.

4.6.1 Biochemical fractionation

The proposed method has the main advantage of using a single, fast and accurate analytical technique (elemental analysis). This is an advantage compared to the alternative approach of direct analysis of the biochemical compounds, which requires longer and less accurate analytical method. Direct analysis in fact could lead to an underestimation of the total COD of the substrate. Buffiere et al. (2006) found how the direct determination of proteins, lipids and carbohydrates were far from being representative of the total volatile solids. They put forward some explanations regarding the accuracy of the methods used: some carbohydrates may not be measured by the anthrone reagent method; protein and sugar measurements are colorimetric methods calibrated on a single type of component (bovine serum albumin for proteins, and glucose for sugars). Therefore the use of the direct method could lead to an inaccuracy in the biochemical fractions used in

ADM1. On the other hand, it has been shown how a high quantity of lignin could lead to overestimation of lipids with the proposed method. More research is needed to evaluate the impact of this error and when a direct measure of lignin is required. It has been also shown how the method is sensitive on the ash determination temperature: it is recommended that a higher temperature than the usual 550 °C employed in the VS determination is used, although a further understanding of elemental analysis is needed to determine the optimal temperature.

4.6.2 Kinetic fractionation

It has been shown that substrates need to be described in terms of the fractions degrading at different rates, and that the common description of substrate as degrading at a single rate might lead to important inaccuracies in the prediction of the methane production rate. These inaccuracies may be negligible when digesters are operated in continuous mode with steady supply of substrate; however, in the case of demand-driven, dynamic operations, an accurate prediction of gas production is necessary in order to predict the energy demand satisfaction and possible overloading inhibitions.

This research has also highlighted how the required fractionation complexity is a reflection of the substrate complexity. In the case of oat residues, the substrate is quite homogeneous in its composition and particle size, and therefore a single fraction is sufficient for the description of its degradation; on the other hand, food waste, green waste and pig manure are intrinsically a mixture of substances of different composition and size, and this is reflected in the degradation kinetics complexity requiring at least two kinetic fractions.

The proposed method of estimating the kinetic parameters, using explicit numerical calibration and uncertainty estimation, constitutes an improvement on the fractionation methods employed by Girault et al. (2012) and García-Gen et al. (2015), which were based on ambiguous visual interpretations of the methane flow rate (as described in chapter 2). More research is required to better understand how to select the most appropriate fractionation based on the goodness of fit and uncertainty in the estimated parameters, e.g. through uncertainty analysis (Sin et al., 2009a). A further improvement could be gained by the implementation of intelligent algorithms that are able to identify, in real time, the influence of the batch test duration on the prediction of the kinetic parameters, with the objective of

shortening the length of the test (as was done by Strömberg et al. (2015), but only focusing on the determination of the extent of degradation).

Comparison of batch and semi-continuous tests for fractionation. The use of two different testing platforms (batch and semi-continuous) allows a comparison of the values of the estimated fractionation parameters.

- The extent of degradation is rather independent of the testing platform. Therefore estimation from batch tests can be safely used when planning and designing and AD system.
- Hydrolysis parameters estimated from batch tests should be used as conservative values. Semi-continuous tests have shown the influence of biomass adaptation on the hydrolysis parameters, with maximum values obtained in semi-continuous tests being as 7 times higher than in batch tests. A similar conclusion was reached by Batstone et al. (2009): when comparing the digestion of hydrolyzed activated sludge in batch and full-scale digesters, they found parameters estimated in batch tests being an order of magnitude smaller than continuous digesters.
- Additional care should be taken when parameters are estimated in batch tests through the use of simplified mechanistic models, e.g. with one step methanisation models. This is especially relevant when testing quickly degradable substrates (such as food waste), as in these cases the uptake of soluble products become the limiting condition. A similar conclusion was reached by Jensen et al. (2011) and he advised to maintain a very high inoculum/substrate ratio to reduce the biomass limiting condition in the soluble uptake. However, here it is recommended to also use more complex models, such as ADM1, to estimate the parameters.

4.6.3 Model implementation

A method for determining the initial conditions have been outlined. However more research is required to evaluate the impact of inaccurate initial conditions, especially the biomass concentration, on the simulation results. Biomass concentration estimated through control batch tests is conditional on the accuracy of the biomass decay rate parameter, which is in turn dependent on the kind of reactor and system condition: there is no consensus in literature about which value should be used (Batstone et al., 2006). Biomass concentration estimated from a modelled and calibrated reactor is in theory a more robust method, however the

method couldn't be properly applied in this research as the inoculum was filtered before being used. It is therefore recommended to avoid filtration when model based estimation of biomass is applied.

Model calibration

Weights proportional to flow rate allow to maintain a constant variance in the residuals. However, as a result, the fit to the low flow experimental data is unnecessarily accurate, while the more interesting dynamics occurring after the feeding are given less importance during the estimation. Another approach would have been the use of weights composed of a part proportional to the flow rate and a part which is constant for all data points: this approach needs to be further investigated.

Model predictions

The calibrated model on the gas flow was able to reproduce, with good accuracy the evolution of other variables of engineering interest (Solids, TAN, alkalinity). A further validation of the model will be done in chapter 5, including an updated inhibition structural model.

Semi-continuous operation

This research was conducted with semi-continuous operation of the digesters. This kind of operation allows a richer kinetic data and therefore better identifiability of the governing parameters. However, from an engineering point of view, semi-continuous operation leads to a lower maximum methane volumetric productivity with respect to the continuous operation, as was demonstrated by Bensmann et al. (2013), especially when the feeding period increases (e.g. > 1 day). The reason for this being that larger amounts of substrate need to be fed to the reactor to increase the productivity, thus inducing larger overloadings which are not recovered before the following feeding. Another drawback of a semi-continuous operation is the important variation in the gas composition that occurs after each feeding, with the experimental data showing a decreases from 65 down to 40% by volume. This variation can adversely influence the performance of downstream processes (e.g. combustion, gas scrubbing), and would require increased gas buffer storages or more complex control systems.

On the other hand, semi-continuous feedings can be proposed as a way to cope with the changes in biogas demand, and quick degradable substrates (similar to the

food waste analysed in this thesis) could be fed semi-continuously to match the gas production with the demand.

4.6.4 Control

An analysis of the experimental data could be used to derive some simple indicators about the state of the system. In particular it has been shown how the analysis of the shape of the flow rate variation with time, i.e. its monotonicity, could allow the identification of biomass limiting situations. However, it has also been shown how alternative interpretations are possible: the interruption of the monotonicity, in fact could be the result of a limit in the hydrolysing biomass (exo-enzymes), as described by the Contois kinetics, or an inhibition in the methanisation of soluble compounds (as will be discussed in chapter 5). The two interpretations would bring about different control actions: while the former is not a risk of process imbalance (and growth in time of the biomass would reduce the limiting condition), the latter if prolonged would reinforce the inhibiting conditions up to a complete rupture of the methanogenic process. An analogue indicator is the ratio of the maximum flow rate to the loading, with the added characteristics that it can be easily quantified and trended. Further research could identify better ways of analysing and combining these indicators.

4.6.5 Microbial biomass adaptation

The initial improvement in the kinetic parameters, was interpreted as an adaptation of the inoculum to the different substrates. The adaptation process can be understood as the induction of metabolic pathways for biodegradation, an increase of microorganism affinity for the compound and also an increase in the number of specific degraders (Raposo et al., 2012). A similar conclusion was reached by Girault et al. (2012), who reported how the use of adapted and non-adapted inoculum produced significant differences in the estimated kinetic parameters. On a similar note, De Vrieze et al. (2013) reports an interesting experiment comparing two reactors fed with different feeding patterns, with the same amount of substrate being fed every one or two days. They demonstrated how the more dynamic reactor (fed every two days) developed through the experiment a higher degree of bacterial community dynamics. The reactor appeared also to be more tolerant to organic shocks up to 8 g COD L^{-1} and ammonium levels up to 8000 mg L^{-1}. They concluded that the regular application of a limited pulse of organic material and/or a

variation in the substrate composition may promote higher functional stability in anaerobic digestion.

5 Codigestion and inhibition modelling

5.1 Introduction

This chapter presents the whole result data sets obtained through the semi-continuous tests R-a, R-b, R-c.

The chapter is structured as follows:

- Description of the experimental conditions for the tests R-a, R-b, R-c.
- Analysis of the codigestion data over the whole period of operation in order to validate the ADM1 implementation for modelling co-digestion and the substrate fractionation described in Chapter 4.
- Analysis of the data for the test R-b over the period 0-144 days in order to assess any synergistic effects of codigestion.
- Data from the test R-a over the period 132-204 days is used to update and calibrate the inhibition structure of ADM1.
- Whole period dataset for R-a, R-b and R-c is used to validate the identified inhibition structure.

5.2 Methodology

The three semi-continuous experiments were realized using the apparatus and analytical methods described in Chapter 3, in duplicate for each combination of substrate. The complete series of substrate loadings are shown in Figure 5.1, while Figure 5.2 shows the water loadings and the calculated HRT for each experiment: R-a, R-b, R-c. The HRT for a semi-continuous experiment is calculated considering the interval that occurs between each consecutive feeding, as follows:

$$HRT(t_i) = \frac{reactor\ volume(t_i)}{volume\ of\ material\ added(t_i) \Big/ (t_{i+1} - t_i)}$$

The values of substrate and water added at each feeding, together with the variations in the reactor volume, are detailed in Table 5.1, Table 5.2 and Table 5.3. The initial part of R-a (days 0-144) and R-c (days 0-112) have already been presented in Chapter 4 for the kinetic fractionation of GW and FW; the information is here maintained to give a better overlook of the whole semi-continuous experiment and for comparison with R-b.

Substrate loadings were designed in order to explore certain phenomena:

- Different co-digestion combinations of substrates, as would occur in a real AD application treating a variety of urban or rural solid wastes. Starting from day 193 until the end of the experiment, all four substrates were co-digested in different proportions.
- Different levels of substrate loadings (indicated as gCOD L^{-1}), as would occur with demand driven applications of AD, with the biogas demand changing temporally.
- The temporal variation of the loadings (Figure 5.1) was approximately similar for all reactors, with a gradual increase up to a peak of 15 gCOD L^{-1} after 150 days, followed by a decline and another peak of 13.5 gCOD L^{-1} at the end of the experiments.

In all the three tests, water was not added during the first part of the experiment. As a consequence, in the first part of the tests the HRT was very high (between 1000 and 200 days, in the first 100 days of the experiments). Water was first added in the test R-a in the period 155-170 days, to facilitate the recover from organic stress by dilution of the inhibiting VFA accumulation; it was then added to all tests starting from day 193 in order to maintain a similar HRT in all three tests, and in turn reduce the increase of solid concentration in the reactor. With water addition, for all tests the HRT diminished and stabilised within a range of 150-30 days.

5.3 Validation of the ADM1 co-digestion modelling and substrate fractionation method

The substrate fractionations (kinetic, charge and biochemical) obtained in Chapter 4 were used to model the complete experiment R-a, R-b and R-c. In the cases of FW and GW, the kinetic fractionation parameters estimated from the semi-continuous data set 2 were used (values in Table 4.10). In the case of PM and OAT, the kinetic fractionation parameters estimated from the batch test 1b were used (values in Table 4.8). The other stoichiometric and kinetic parameters, and model structure, were as in Rosen and Jeppsson (2006). For each experiment, model prediction and experimental values were compared. Figure 5.3, Figure 5.4 and Figure 5.5 show experimental and simulated methane volumetric productivity, methane specific yield, OLR, total VFA, acetate and propionate and pH for experiments R-a, R-b and R-c, respectively. Figure 5.6, Figure 5.7 and Figure 5.8 show experimental and simulated results for bicarbonate alkalinity, TAN, TS and VS for experiments R-a,

R-b and R-c, respectively. The rAE for each measurement and simulated quantity is shown in Table 5.4.

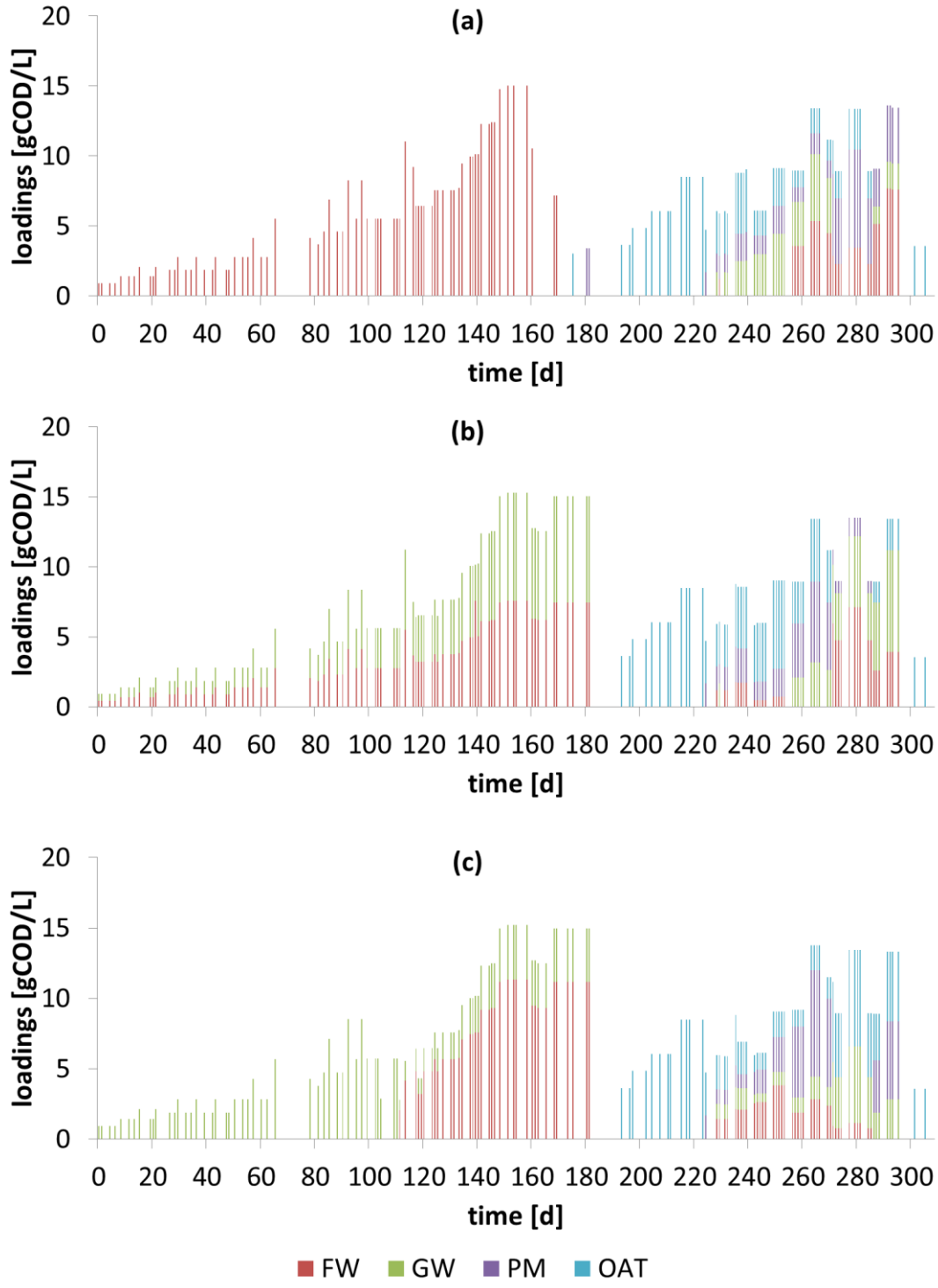

Figure 5.1 Substrate loadings for the complete semi-continuous experiments: (a) R-a, (b) R-b, (c) R-c.

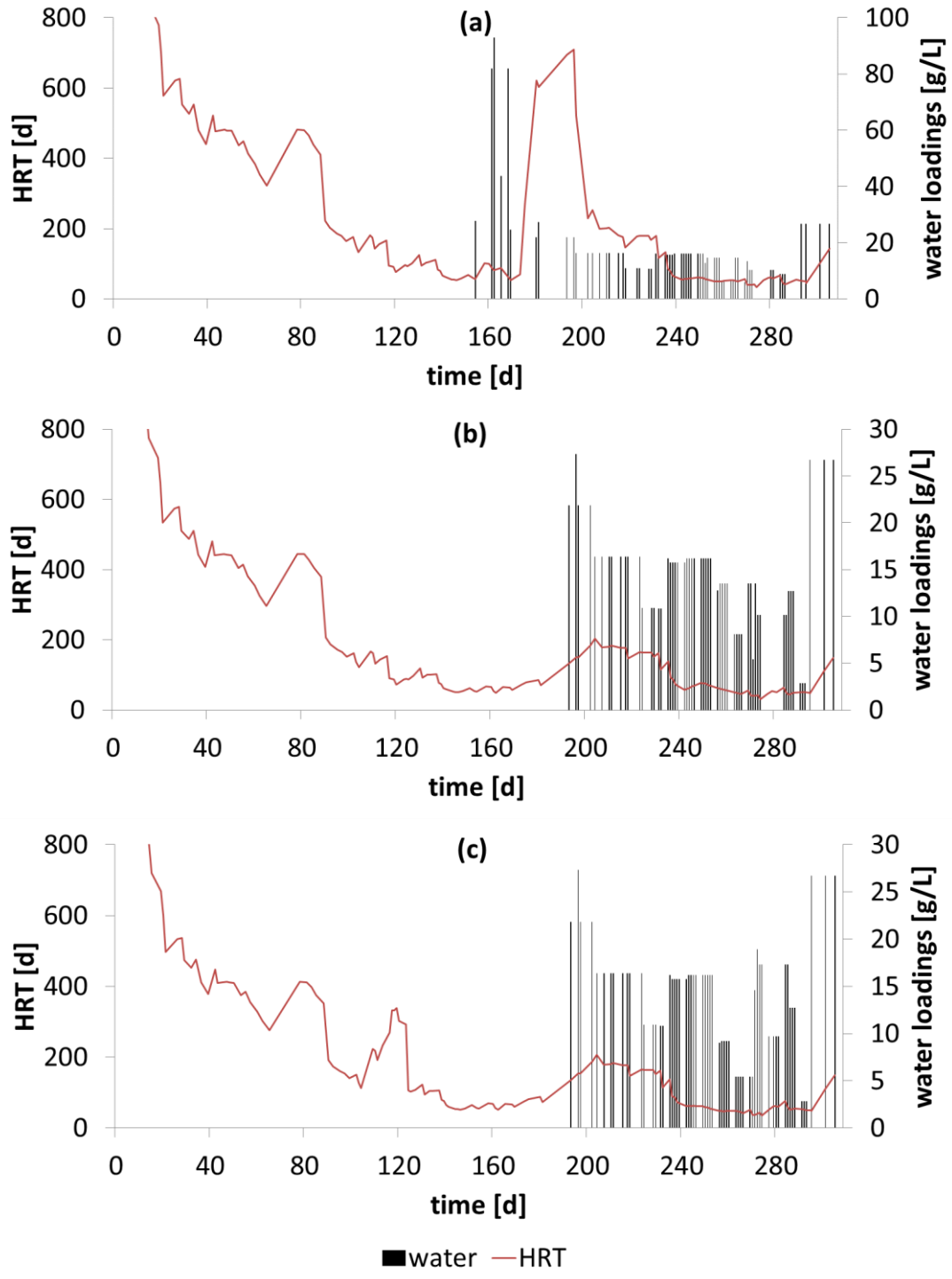

Figure 5.2 Water loadings and calculated Hydraulic Retention Time (HRT) (averaged across five consecutive feedings) for the complete semi-continuous experiments: (a) R-a, (b) R-b, (c) R-c.

	Substrate added [grams]							Substrate added [grams]							Substrate added [grams]						
days	FW	GW	PM	ALA	Water	Volume reactor [L]	days	FW	GW	PM	ALA	Water	Volume reactor [L]	days	FW	GW	PM	ALA	Water	Volume reactor [L]
0	4.27					2.05	119.96	29.85					2.04	232.99		8.00	8.00	5.00	30.00	1.9
1.76	4.27					2.05	120.97	29.85					2.04	235.98		12.00	12.00	7.50	30.00	1.9
4.90	4.27					2.05	123.97	29.85					2.04	236.98		12.00	12.00	7.50	30.00	1.9
6.88	4.27					2.05	124.97	35.00					2.04	237.95		12.00	12.00	7.50	30.00	1.9
8.95	6.40					2.05	125.97	35.00					2.04	238.97		12.00	12.00	7.50	30.00	1.9
11.93	6.40					2.05	127.81	35.00					2.04	239.99		12.00	12.00	7.50	30.00	1.85
13.93	6.40					2.05	130.95	35.00					2.04	242.98		14.00	8.00	3.00	30.00	1.85
15.95	9.60					2.05	131.97	35.00					2.04	243.98		14.00	8.00	3.00	30.00	1.85
19.01	6.40					2.05	133.89	35.00					2	244.84		14.00	8.00	3.00	30.00	1.85
20.91	6.40					2.05	134.96	43.00					2	245.94		14.00	8.00	3.00	30.00	1.85
21.98	9.60					2.05	137.93	43.00					1.9	246.93		14.00	8.00	3.00	30.00	1.85
26.01	8.53					2.05	138.95	43.00					1.9	249.87		21.00	12.00	4.50	30.00	1.85
28.78	8.53					2.05	139.93	43.00					1.87	250.92		21.00	12.00	4.50	30.00	1.85
29.97	12.80					2.05	140.98	43.00					1.87	252.00		21.00	12.00	4.50	30.00	1.85
32.99	8.53					2.05	141.96	51.60					1.85	252.95		21.00	12.00	4.50	23.60	1.85
34.96	8.53					2.05	144.77	51.60					1.85	253.97		21.00	12.00	4.50	27.00	1.85
36.99	12.80					2.05	145.96	51.60					1.83	256.97	15.00	15.00	6.00	2.00	27.00	1.85
39.95	8.53					2.05	146.97	51.60					1.83	257.99	15.00	15.00	6.00	2.00	27.00	1.85
42.81	8.53					2.05	148.82	61.44					1.83	258.98	15.00	15.00	6.00	2.00	27.00	1.85
43.91	12.80					2.05	151.97	61.44					1.8	259.99	15.00	15.00	6.00	2.00	12.00	1.85
47.01	8.53					2.05	153.97	61.44					1.8	260.99	15.00	15.00	6.00	2.00	12.00	1.85
48.98	8.53					2.05	154.95					50.00	1.8	263.93	22.50	22.50	9.00	3.00	12.00	1.85
50.93	12.80					2.05	158.97	61.44					1.8	265.00	22.50	22.50	9.00	3.00	12.00	1.85
53.95	12.80					2.05	160.97	43.00					1.8	265.98	22.50	22.50	9.00	3.00	27.00	1.85
55.95	12.80					2.05	161.93					150.00	1.83	266.96	22.50	22.50	9.00	3.00	27.00	1.85
57.95	19.20					2.05	162.76					170.00	1.83	270.00	18.75	18.75	7.50	2.50	11.00	1.85
60.97	12.80					2.05	165.96					80.00	1.83	270.98	18.75	18.75	7.50	2.50	25.00	1.85
62.97	12.80					2.05	168.98	29.85				150.00	1.83	271.97	12.00		35.00	4.00	19.20	1.85
65.01	25.60					2.05	169.99	29.85				45.00	1.83	272.96	9.60		28.00	3.20	19.20	1.85
78.96	19.20					2.05	173.79						1.83	273.97	9.60		28.00	3.20		1.85
81.94	17.07					2.05	175.82				5.00		1.83	274.84	9.60		28.00	3.20		1.85
83.93	21.33					2.05	180.83			20.00		40.00	1.83	277.72	14.40		42.00	4.80		1.85
85.94	32.00					2.05	181.72			20.00		50.00	1.83	279.94	14.40		42.00	4.80		1.85
88.84	21.33					2.05	193.93				6.00	40.00	1.83	280.95	14.40		42.00	4.80	19.20	1.85
90.73	21.33					2.05	196.95				6.00	40.00	1.83	281.80	14.40		42.00	4.80	19.20	1.85
92.94	38.40					2.05	197.91				8.00	30.00	1.83	284.99	9.60		28.00	3.20	16.50	1.85
95.96	25.60					2.05	202.92				8.00	30.00	1.83	285.98	9.60		28.00	3.20	16.50	1.85
97.94	38.40					2.05	204.95				10.00	30.00	1.83	286.98	21.50	6.00	16.00		16.50	1.85
99.96	25.60					2.04	207.96				10.00	30.00	1.83	287.98	21.50	6.00	16.00			1.85
102.96	25.60					2.04	210.96				10.00	30.00	1.83	288.98	21.50	6.00	16.00			1.85
103.97	25.60					2.04	211.96				10.00	30.00	1.83	291.88	32.25	9.00	24.00			1.85
104.93	25.60					2.04	215.88				14.00	30.00	1.83	292.97	32.25	9.00	24.00			1.85
109.97	25.60					2.04	217.94				14.00	30.00	1.83	293.93	32.25	9.00	24.00		50.00	1.87
110.95	25.60					2.04	218.97				14.00	20.00	1.83	295.00	32.25	9.00	24.00		50.00	1.87
111.94	25.60					2.04	223.95				14.00	20.00	1.83	295.97					50.00	1.87
113.76	51.20					2.04	224.97			10.00	5.00	20.00	1.83	301.97				6.00	50.00	1.87
116.98	42.66					2.04	228.84		8.00	8.00	5.00	20.00	1.85	305.97				6.00	50.00	1.87
117.96	29.85					2.04	229.98	5.00		10.00	5.00	20.00	1.85							
118.97	29.85					2.04	231.89		8.00	8.00	5.00	30.00	1.85							

Table 5.1 Amounts of substrate added and volume of the reactor at each feeding for the whole semi-continuous test R-a.

	Substrate added [grams]							Substrate added [grams]							Substrate added [grams]						
days	FW	GW	PM	ALA	Water	Volume reactor [L]	days	FW	GW	PM	ALA	Water	Volume reactor [L]	days	FW	GW	PM	ALA	Water	Volume reactor [L]
0	2.13	2.49				2.05	119.96	14.93	17.29				2.04	232.99	5.00		10.00	5.00	20.00	1.85
1.76	2.13	2.49				2.05	120.97	14.93	17.29				2.04	235.98	7.50		15.00	7.50	30.00	1.85
4.90	2.13	2.49				2.05	123.97	14.93	17.29				2.04	236.98	7.50		15.00	7.50	30.00	1.90
6.88	2.13	2.49				2.05	124.97	17.50	20.28				2.04	237.95	7.50		15.00	7.50	30.00	1.90
8.95	3.20	3.73				2.05	125.97	14.93	17.25				2.04	238.97	7.50		15.00	7.50	30.00	1.90
11.93	3.20	3.73				2.05	127.81	17.50	20.28				2.04	239.99	7.50		15.00	7.50	30.00	1.90
13.93	3.20	3.73				2.05	130.95	17.50	20.28				2.04	242.98	2.00		8.00	7.00	30.00	1.90
15.95	4.80	5.60				2.05	131.97	17.50	20.28				2.04	243.98	2.00		8.00	7.00	30.00	1.85
19.01	3.20	3.73				2.05	133.89	17.50	20.28				2.00	244.84	2.00		8.00	7.00	30.00	1.85
20.91	3.20	3.73				2.05	134.96	21.50	24.80				2.00	245.94	2.00		8.00	7.00	30.00	1.85
21.98	4.80	5.60				2.05	137.93	21.50	24.80				1.90	246.93	2.00		8.00	7.00	30.00	1.85
26.01	4.27	4.98				2.05	138.95	21.50	24.80				1.90	249.87	3.00		12.00	10.50	30.00	1.85
28.78	4.27	4.98				2.05	139.93	32.25	12.40				1.87	250.92	3.00		12.00	10.50	30.00	1.85
29.97	6.40	7.46				2.05	140.98	21.50	24.80				1.87	252.00	3.00		12.00	10.50	30.00	1.85
32.99	4.27	4.98				2.05	141.96	25.80	29.76				1.85	252.95	3.00		12.00	10.50	30.00	1.85
34.96	4.27	4.98				2.05	144.77	25.80	29.76				1.85	253.97	3.00		12.00	10.50	30.00	1.85
36.99	6.40	7.46				2.05	145.96	25.80	29.76				1.83	256.97		10.00	23.00	5.00	23.60	1.85
39.95	4.27	4.98				2.05	146.97	25.80	29.76				1.83	257.99		10.00	23.00	5.00	25.00	1.85
42.81	4.27	4.98				2.05	148.82	30.96	35.71				1.83	258.98		10.00	23.00	5.00	25.00	1.85
43.91	6.40	7.46				2.05	151.97	30.96	35.71				1.80	259.99		10.00	23.00	5.00	25.00	1.85
47.01	4.27	4.98				2.05	153.97	30.96	35.71				1.80	260.99		10.00	23.00	5.00	25.00	1.85
48.98	4.27	4.98				2.05	154.95	30.96	35.71				1.80	263.93		15.00	34.50	7.50	15.00	1.85
50.93	6.40	7.46				2.05	158.97	30.96	35.71				1.80	265.00		15.00	34.50	7.50	15.00	1.85
53.95	6.40	7.46				2.05	160.97	25.80	29.76				1.80	265.98		15.00	34.50	7.50	15.00	1.85
55.95	6.40	7.46				2.05	161.93	25.80	29.76				1.80	266.96		15.00	34.50	7.50	15.00	1.85
57.95	9.60	11.20				2.05	162.76	25.80	29.76				1.83	270.00		12.50	28.75	6.25	25.00	1.85
60.97	6.40	7.48				2.05	165.96	25.80	29.76				1.83	270.98		12.50	28.75	6.25	25.00	1.85
62.97	6.40	7.48				2.05	168.98	30.96	35.71				1.83	271.97	25.00	20.00	6.50		10.00	1.85
65.01	12.80	14.96				2.05	169.99	30.96	35.71				1.83	272.96	20.00	16.00	5.20		25.00	1.85
78.96	9.60	11.20				2.05	173.79	30.96	35.71				1.83	273.97	20.00	16.00	5.20		18.80	1.85
81.94	8.54	9.97				2.05	175.82	30.96	35.71				1.83	274.84	20.00	16.00	5.20		18.80	1.85
83.93	10.67	12.46				2.05	180.83	30.96	35.71				1.83	277.72	30.00	24.00	7.80			1.85
85.94	16.00	18.69				2.05	181.72	30.96	35.71				1.83	279.94	30.00	24.00	7.80			1.85
88.84	10.67	12.46				2.05	193.93				6.00	40.00	1.83	280.95	30.00	24.00	7.80			1.85
90.73	10.67	12.46				2.05	196.95				6.00	50.00	1.83	281.80	30.00	24.00	7.80			1.85
92.94	19.20	22.43				2.05	197.91				8.00	40.00	1.83	284.99	20.00	16.00	5.20		18.80	1.85
95.96	12.80	14.95				2.05	202.92				8.00	40.00	1.83	285.98	20.00	16.00	5.20		18.80	1.85
97.94	19.20	22.43				2.05	204.95				10.00	30.00	1.83	286.98	11.00	23.00		2.50	23.50	1.85
99.96	12.80	14.95				2.04	207.96				10.00	30.00	1.83	287.98	11.00	23.00		2.50	23.50	1.85
102.96	12.80	14.95				2.04	210.96				10.00	30.00	1.83	288.98	11.00	23.00		2.50	23.50	1.85
103.97	12.80	14.95				2.04	211.96				10.00	30.00	1.83	291.88	16.50	34.50		3.75	5.25	1.85
104.93	12.80	14.95				2.04	215.88				14.00	30.00	1.83	292.97	16.50	34.50		3.75	5.25	1.85
109.97	12.80	14.95				2.04	217.94				14.00	30.00	1.83	293.93	16.50	34.50		3.75	5.25	1.85
110.95	12.80	14.95				2.04	218.97				14.00	30.00	1.83	295.00	16.50	34.50		3.75	5.25	1.85
111.94	12.80	14.95				2.04	223.95				14.00	30.00	1.83	295.97					50.00	1.87
113.76	25.60	29.91				2.04	224.97			10.00	5.00	20.00	1.83	301.97				6.00	50.00	1.87
116.98	17.06	19.94				2.04	228.84	5.00		10.00	5.00	20.00	1.83	305.97				6.00	50.00	1.87
117.96	14.93	16.79				2.04	229.98		8.00	8.00	5.00	20.00	1.83							
118.97	14.93	17.29				2.04	231.89	5.00		10.00	5.00	20.00	1.85							

Table 5.2 Amounts of substrate added and volume of the reactor at each feeding for the whole semi-continuous test R-b.

	Substrate added [grams]					
days	FW	GW	PM	ALA	Water	Volume reactor [L]
0		4.97				2.05
1.76		4.97				2.05
4.90		4.97				2.05
6.88		4.97				2.05
8.95		7.46				2.05
11.93		7.46				2.05
13.93		7.46				2.05
15.95		11.19				2.05
19.01		7.46				2.05
20.91		7.46				2.05
21.98		11.19				2.05
26.01		9.95				2.05
28.78		9.95				2.05
29.97		14.92				2.05
32.99		9.95				2.05
34.96		9.95				2.05
36.99		14.92				2.05
39.95		9.95				2.05
42.81		9.95				2.05
43.91		14.92				2.05
47.01		9.95				2.05
48.98		9.95				2.05
50.93		14.92				2.05
53.95		14.92				2.05
55.95		14.92				2.05
57.95		22.40				2.05
60.97		14.96				2.05
62.97		14.96				2.05
65.01		29.91				2.05
78.96		22.40				2.05
81.94		19.94				2.05
83.93		24.92				2.05
85.94		37.38				2.05
88.84		24.92				2.05
90.73		24.92				2.05
92.94		44.86				2.05
95.96		29.90				2.05
97.94		44.86				2.05
99.96		29.91				2.04
102.96		29.91				2.04
103.97		29.91				2.04
104.93		14.95				2.04
109.97		29.91				2.04
110.95		29.91				2.04
111.94	9.60	3.74				2.04
113.76	19.20	7.48				2.04
116.98						2.04
117.96	22.39	8.40				2.04
118.97	14.92	5.76				2.04

	Substrate added [grams]					
days	FW	GW	PM	ALA	Water	Volume reactor [L]
119.96	14.92	5.76				2.04
120.97	22.38	8.64				2.04
123.97	22.38	8.64				2.04
124.97	26.25	10.14				2.04
125.97	22.38	8.64				2.04
127.81	26.25	10.14				2.04
130.95	26.25	10.14				2.04
131.97	26.25	10.14				2.04
133.89	26.25	10.14				2.00
134.96	32.25	12.40				2.00
137.93	32.25	12.40				1.90
138.95	32.25	12.40				1.90
139.93	32.25	12.40				1.87
140.98	32.25	12.40				1.87
141.96	38.70	14.88				1.85
144.77	38.70	14.88				1.85
145.96	38.70	14.88				1.83
146.97	38.70	14.88				1.83
148.82	46.44	17.85				1.83
151.97	46.44	17.85				1.80
153.97	46.44	17.85				1.80
154.95	46.44	17.85				1.80
158.97	46.44	17.85				1.80
160.97	38.70	14.88				1.80
161.93	38.70	14.88				1.80
162.76	38.70	14.88				1.83
165.96	38.70	14.88				1.83
168.98	46.44	17.85				1.83
169.99	46.44	17.85				1.83
173.79	46.44	17.85				1.83
175.82	46.44	17.85				1.83
180.83	46.44	17.85				1.83
181.72	46.44	17.85				1.83
193.93				6.00	40.00	1.83
196.95				6.00	50.00	1.83
197.91				8.00	40.00	1.83
202.92				8.00	40.00	1.83
204.95				10.00	30.00	1.83
207.96				10.00	30.00	1.83
210.96				10.00	30.00	1.83
211.96				10.00	30.00	1.83
215.88				14.00	30.00	1.83
217.94				14.00	30.00	1.83
218.97				14.00	30.00	1.83
223.95				14.00	30.00	1.83
224.97			10.00	5.00	20.00	1.83
228.84	6.00	5.00	6.00	4.00	20.00	1.83
229.98	6.00	5.00	6.00	4.00	20.00	1.83
231.89	6.00	5.00	6.00	4.00	20.00	1.85

	Substrate added [grams]					
days	FW	GW	PM	ALA	Water	Volume reactor [L]
232.99	6.00	5.00	6.00	4.00	20.00	1.85
235.98	9.00	7.50	9.00	6.00	30.00	1.85
236.98	9.00	7.50	6.00	4.00	30.00	1.90
237.95	9.00	7.50	6.00	4.00	30.00	1.90
238.97	9.00	7.50	6.00	4.00	30.00	1.90
239.99	9.00	7.50	6.00	4.00	30.00	1.90
242.98	11.00	3.00	10.00	2.00	30.00	1.90
243.98	11.00	3.00	10.00	2.00	30.00	1.85
244.84	11.00	3.00	10.00	2.00	30.00	1.85
245.94	11.00	3.00	10.00	2.00	30.00	1.85
246.93	11.00	3.00	10.00	2.00	30.00	1.85
249.87	16.00	4.50	15.00	3.00	30.00	1.85
250.92	16.00	4.50	15.00	3.00	30.00	1.85
252.00	16.00	4.50	15.00	3.00	30.00	1.85
252.95	16.00	4.50	15.00	3.00	30.00	1.85
253.97	16.00	4.50	15.00	3.00	30.00	1.85
256.97	8.00	5.00	30.00	2.00	16.70	1.85
257.99	8.00	5.00	30.00	2.00	17.00	1.85
258.98	8.00	5.00	30.00	2.00	17.00	1.85
259.99	8.00	5.00	30.00	2.00	17.00	1.85
260.99	8.00	5.00	30.00	2.00	17.00	1.85
263.93	12.00	7.50	45.00	3.00	10.00	1.85
265.00	12.00	7.50	45.00	3.00	10.00	1.85
265.98	12.00	7.50	45.00	3.00	10.00	1.85
266.96	12.00	7.50	45.00	3.00	10.00	1.85
270.00	10.00	6.25	37.50	2.50	10.00	1.85
270.98	10.00	6.25	37.50	2.50	10.00	1.85
271.97	4.00	21.50		9.50	27.00	1.85
272.96	3.20	17.20		7.60	35.00	1.85
273.97	3.20	17.20		7.60	32.00	1.85
274.84	3.20	17.20		7.60	32.00	1.85
277.72	4.80	25.80		11.40	18.00	1.85
279.94	4.80	25.80		11.40	18.00	1.85
280.95	4.80	25.80		11.40	18.00	1.85
281.80	4.80	25.80		11.40	18.00	1.85
284.99	3.20	17.20		7.60	32.00	1.85
285.98	3.20	17.20		7.60	32.00	1.85
286.98		9.00	22.00	5.50	23.50	1.85
287.98		9.00	22.00	5.50	23.50	1.85
288.98		9.00	22.00	5.50	23.50	1.85
291.88		13.50	33.00	8.25	5.25	1.85
292.97		13.50	33.00	8.25	5.25	1.85
293.93		13.50	33.00	8.25	5.25	1.85
295.00		13.50	33.00	8.25	5.25	1.85
295.97					50.00	1.87
301.97				6.00	50.00	1.87
305.97				6.00	50.00	1.87

Table 5.3 Amounts of substrate added and volume of the reactor at each feeding for the whole semi-continuous test R-c.

In general the model shows a good fit for all measured outputs, including the volumetric and specific methane yield, pH, alkalinity, TAN, TS and VS with rAE values in the range of 1.1-28%. The exception to this is the VFA predictions, which are less good with rAE values of 64-81%. The general trend is that the model does not predict well for periods of organic overload which generally coincide with the two large peaks in OLR occurring around days 140 and 280 of the experiments. Organic overload is indicated in all cases by the increase in VFA concentration which is generally not predicted by the model. This poor prediction of VFA also has the effect of increasing the divergence of the methane production values somewhat, which can be related to the VFA (represent potential methane) being removed in the effluent from the experimental system but since the model does not predict the VFA there is no such effect in the model output. This is especially notable in the later periods of the experiment when the HRT is shorter.

The specific methane yield follows well the experimentally data (except during overload) and the value is a direct consequence of the feed mixture which validates the substrate fractionation method. Oats achieve the highest specific methane yield approaching 0.35 (the theoretical limit of COD conversion), owing to their high degradability.

The model is able to predict the effect of water additions as shown in the alkalinity, TAN and TS/VS changes that occur around day 155 in experiment R-a (Figure 5.6).

The accumulation of VFA predicted by the model is in most cases much lower than the experimental values, but also of note is that the experimental results show accumulations of acetate follow after a period by propionate, whereas accumulations in the simulations consisted of only acetate. It is thought that this is because the ADM1 model has fixed stoichiometry for acetogenesis but in a real system the products of acidogenesis/fermentation can change depending on the environmental conditions and accumulation of acetate would favour the formation of other longer chain VFAs (propionate, butyrate, etc.).

The pH measurements came from two different sources: offline during the period 0-140 days, and online during the period 130-300 days. From the online data we can compare: the trend which the simulations match well; the changes during overload conditions which the simulations match badly; the absolute values which show good agreement in R-b and R-c but not with R-a, again supporting that organic overload leads to bad model predictions; and the amplitude of pH variations after each

feeding which correlates well with the organic stress, i.e. much larger in R-a than R-b or R-c.

In general, the results from the validation of the codigestion modelling and substrate fractionation show that the model and substrate descriptions are correct and can be used to predict the behaviour of the real system well, except for VFA and during periods of organic stress. This indicates that the model components relating to organic stress are poorly calibrated, this is addressed in the section 5.5.

	rAE [%]		
	R-a	**R-b**	**R-c**
Specific Yield	27%	19%	11%
Volumetric Productivity	28%	19%	12%
VFA	78%	64%	81%
pH	3.5%	1.1%	1.5%
Alkalinity	9%	17%	13%
TAN	11%	9%	10%
TS	13%	9%	17%
VS	22%	13%	15%

Table 5.4 Goodness of fit indicated by relative absolute errors in the measured outputs in the R-a, R-b and R-c semi-continuous tests. ADM1 simulation using the substrates fractionation parameters from Chapter 4.

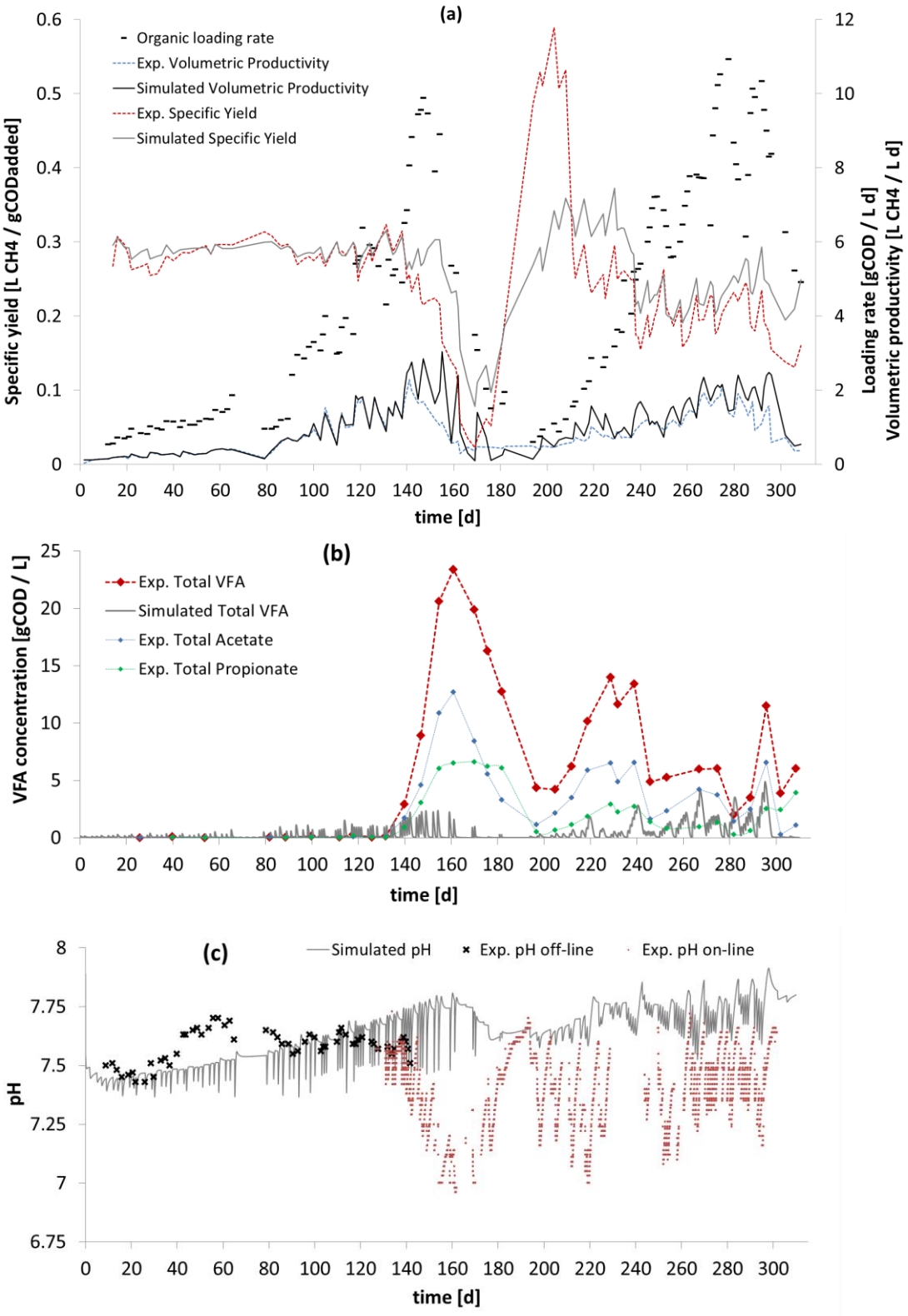

Figure 5.3 Experimental and simulated results for experiment R-a: (a) volumetric productivity, specific yield (averaged across 6 feeding) and OLR (averaged across 6 feedings); (b) Total VFA, acetate and propionate; (c) pH.

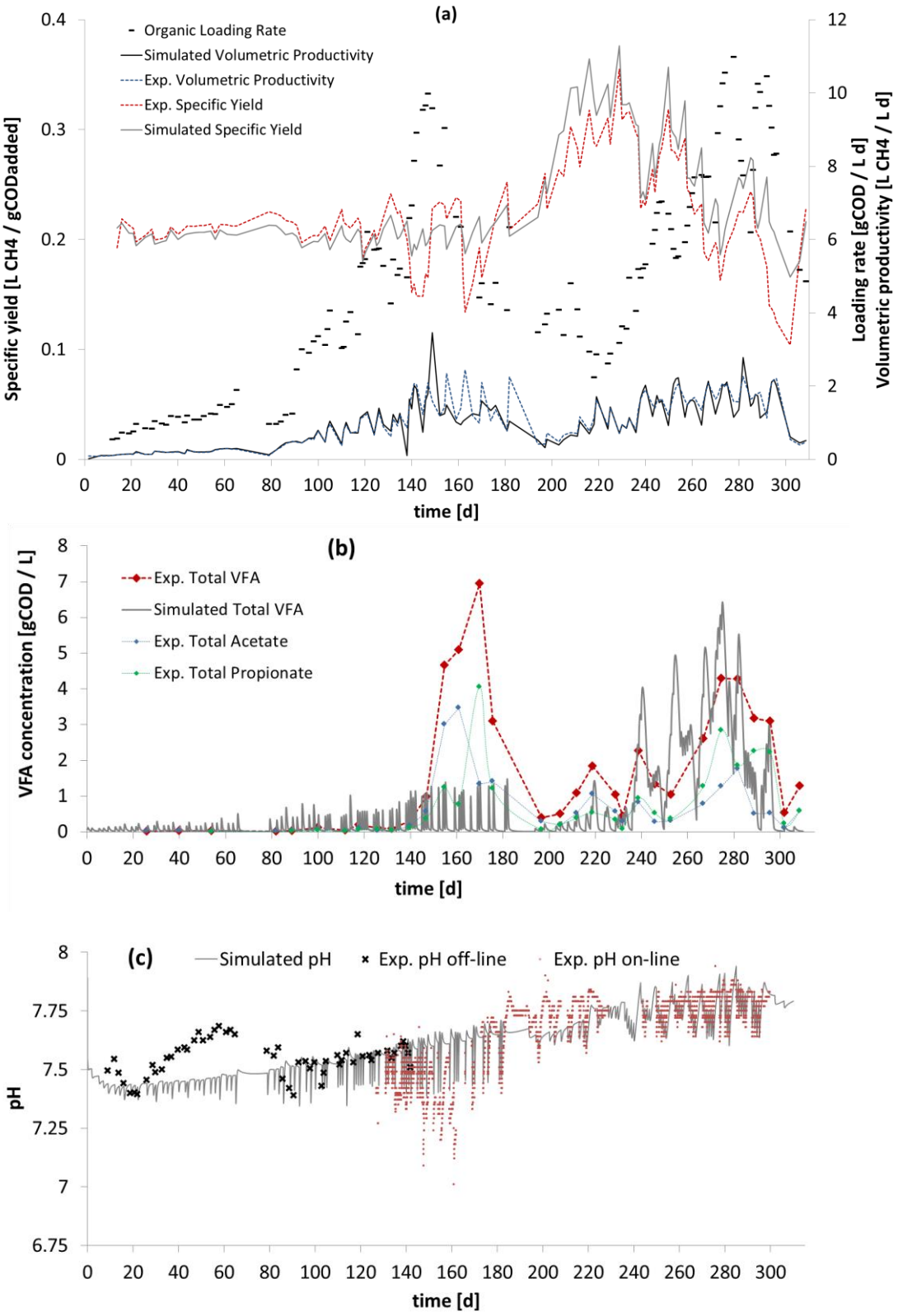

Figure 5.4 Experimental and simulated results for experiment R-b: (a) volumetric productivity, specific yield (averaged across 6 feeding) and OLR (averaged across 6 feedings); (b) Total VFA, acetate and propionate; (c) pH.

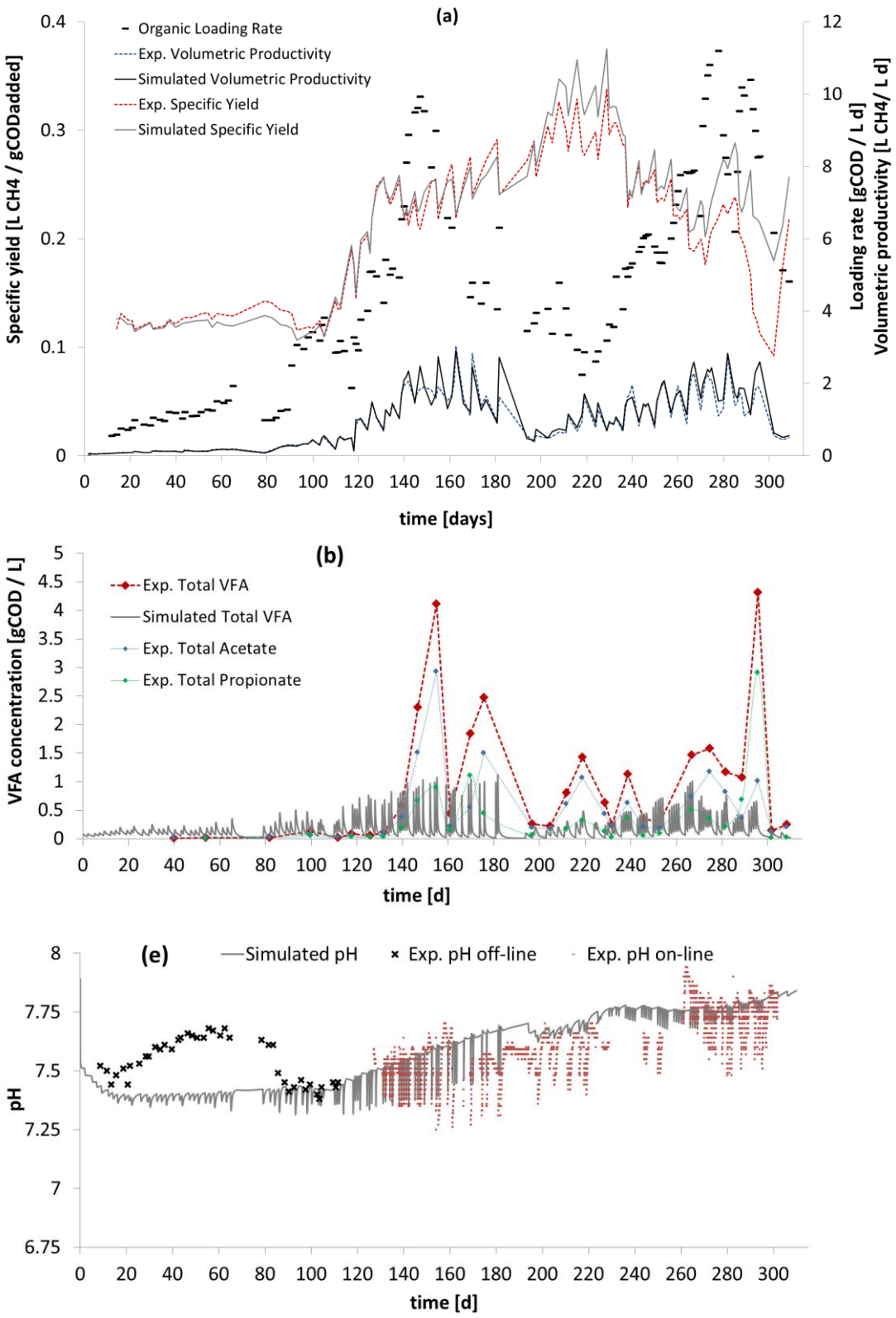

Figure 5.5 Experimental and simulated results for experiment R-c: (a) volumetric productivity, specific yield (averaged across 6 feeding) and OLR (averaged across 6 feedings); (b) Total VFA, acetate and propionate; (c) pH.

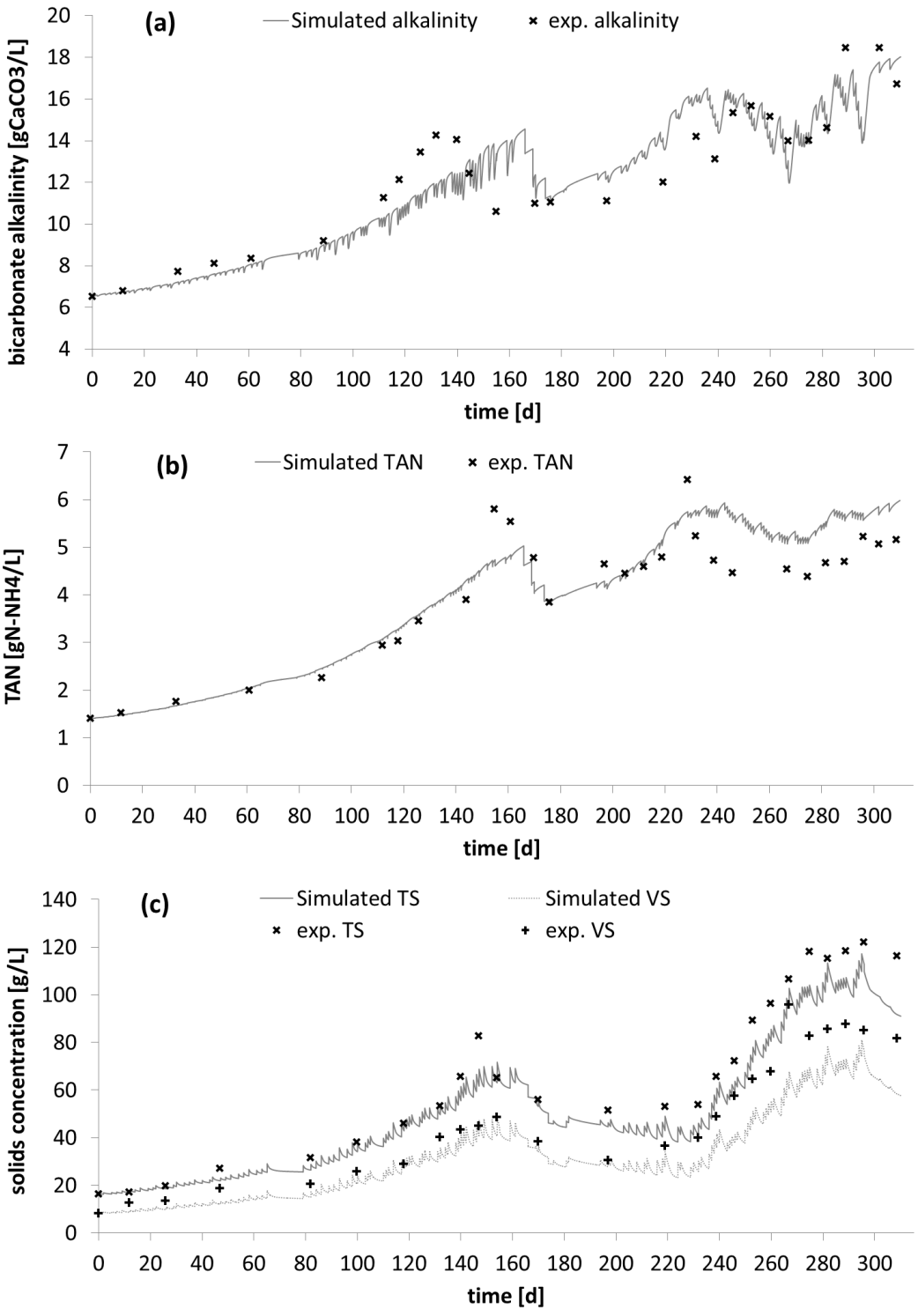

Figure 5.6 Experimental and simulated results for experiment R-a: (a) bicarbonate alkalinity; (b) Total Ammonia Nitrogen (TAN); (c) Total Solids and Volatile Solids concentration.

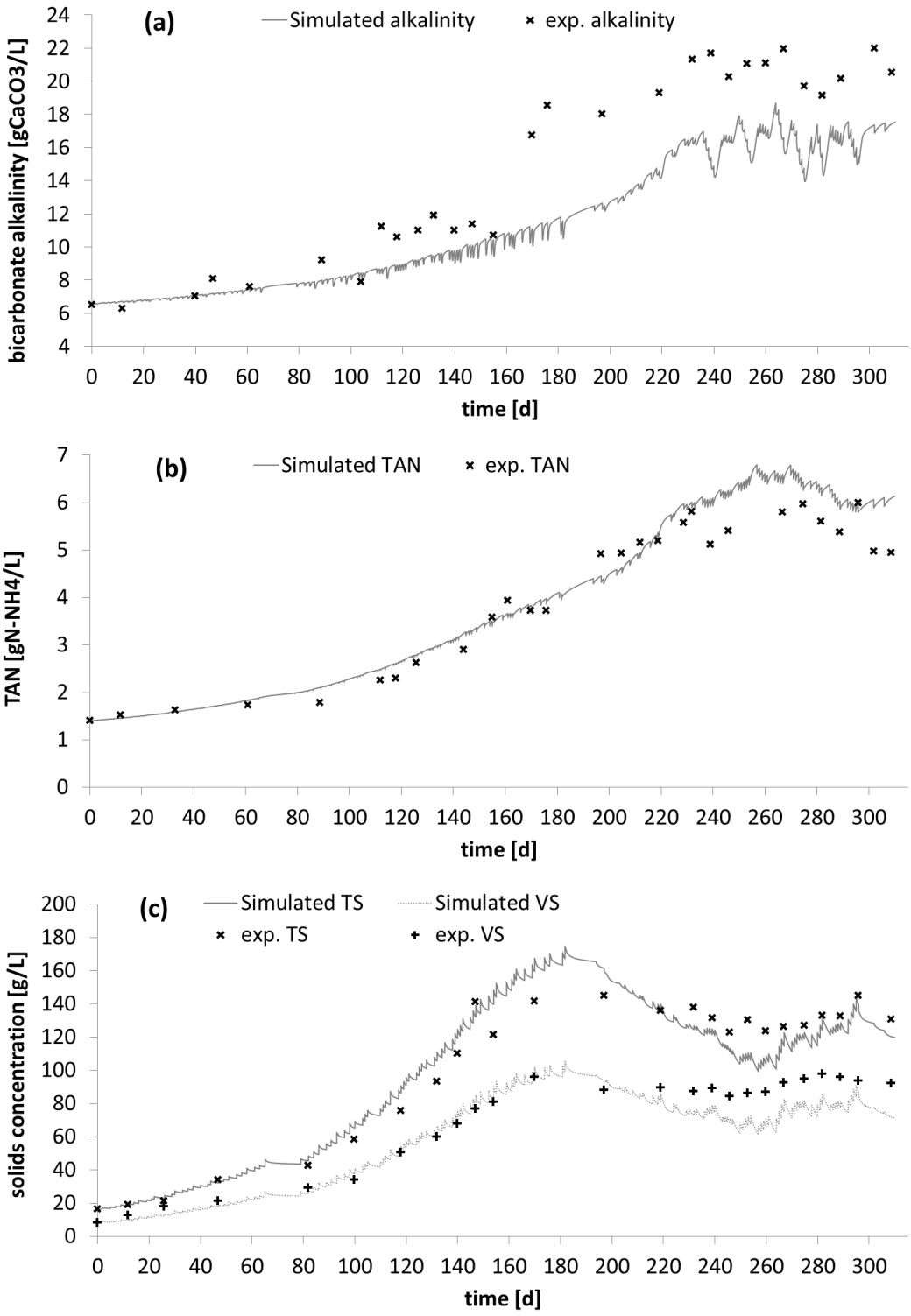

Figure 5.7 Experimental and simulated results for experiment R-b: (a) bicarbonate alkalinity; (b) Total Ammonia Nitrogen (TAN); (c) Total Solids and Volatile Solids concentrations.

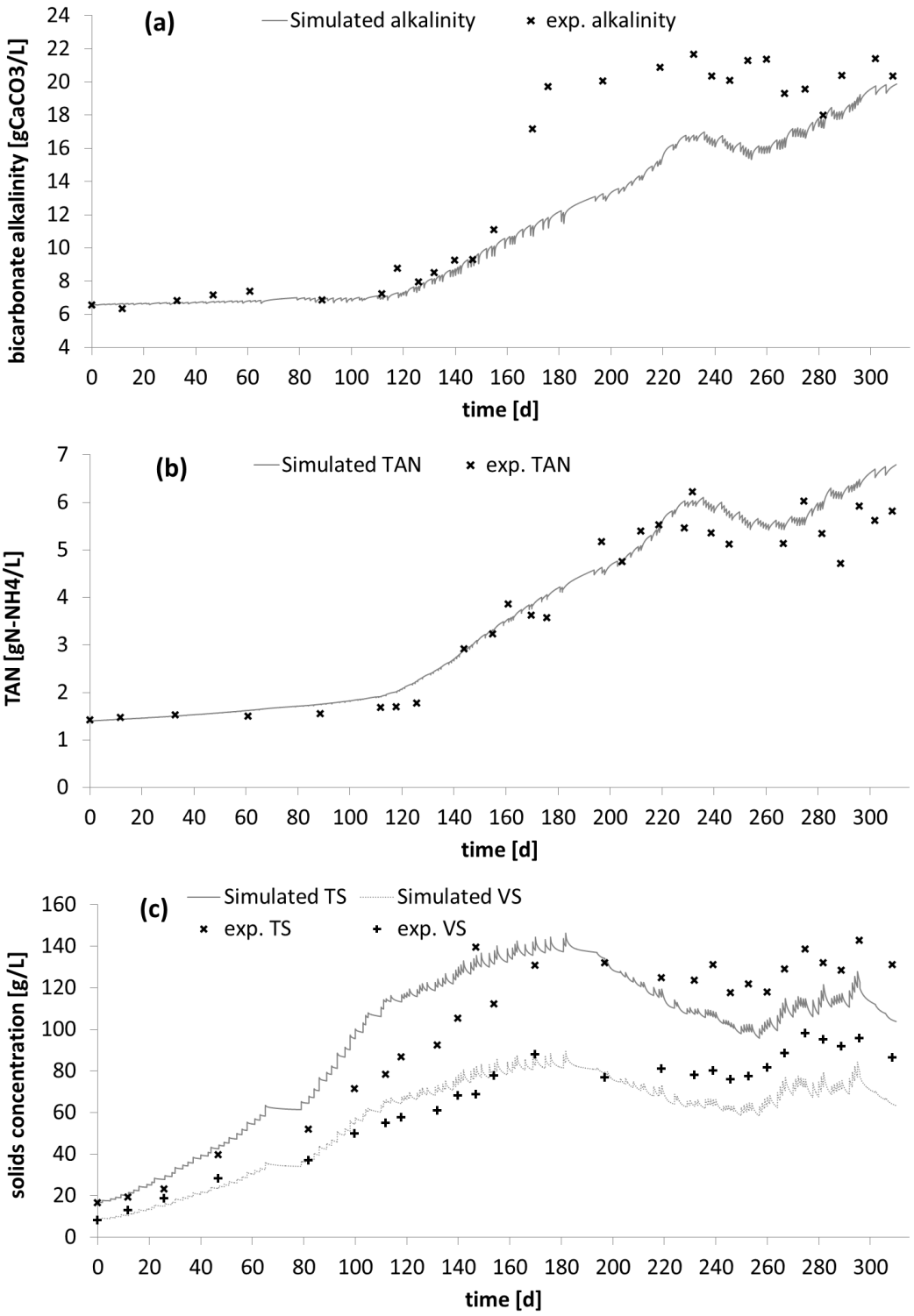

Figure 5.8 Experimental and simulated results for experiment R-c: (a) bicarbonate alkalinity; (b) Total Ammonia Nitrogen (TAN); (c) Total Solids and Volatile Solids concentrations.

5.4 Synergistic effects of codigestion

The substrate characterisation for FW and GW were performed using experimental data R-a and R-b, respectively, for periods 0-144 and 0-112 days respectively. Using these values the data comparison between experimental and simulated specific methane yield can be made for experiment R-b for the period 0-144 days in order to assess directly any synergistic effects of codigestion. This can be performed visually by observing this period in Figure 5.4 and there does appear to be a slight increase in the experimental methane production relative to the simulation, which would indicate some synergy occurring. However analysis of this data shows that the difference is about 5% and it is doubtful that this is statistically significant.

To cross check this result, a calibration was performed using the experimental data from R-b for the period 0-144 days in order to assess the degradability of FW and GW. The f_d values for FW and GW were 0.38 and 0.89, respectively (c.f. 0.38 and 0.85 from the mono-digestion trials) which is an increase of only 3.3%. As may be expected the values for f_d were highly correlated in the calibration algorithm, which means that although the result shows an improvement in food waste degradability, the same result could have been achieved by an equivalent change in the degradability of green waste.

Several other calibrations were performed using increasing parameter sets (to include the other hydrolysis kinetic parameters) and in all cases complete correlation between the parameters was reported. As an example, an equivalent methane production increase could have been the result of an increase in the degradation rate of the slowly degrading fraction.

The results of this study indicate that while there may be a small synergistic effects of the codigestion of FW and GW, it is probably too small to be found using the current method.

5.5 Inhibition

As was shown in Chapter 4, in the decreasing values of the apparent degradation kinetics and goodness of fit especially in FW with increasing loading rate, and in Section 5.3 in the VFA, pH and methane production divergence during overload conditions, both indicate a deficiency in the inhibition mechanism in ADM1. The analysis performed Chapter 4 with mono digestion of FW and GW (Figure 4.19 and

Figure 4.20) showed that the prediction of VFA by the model was overestimated compared with the experimental data, whereas in this chapter the model was an underestimation relative to the experimental data; therefore it is assumed that the reason for the accumulation of VFA shown is due to some transient variation in some inhibiting compounds, rather than incorrect values of the Monod kinetics for uptake of VFA.

Therefore it was decided to investigate the most likely inhibition mechanisms caused by transient conditions of which undissociated VFA and LCFA were the most promising. Inhibition by VFA is deemed relevant since it shows a relationship with both pH and total VFA concentration (weak acid inhibition) and inhibition by LCFA due to high lipid content of FW. The effect of TS was not considered.

5.5.1 Analysis of different inhibition mechanisms on the methane production rate

A reduced data set from experiment 2 FW (days 120-127.8, comprising 5 feeding was used to explore the effect of different inhibition structures and parameter values on the methane flow rate.

All inhibitions were described as non-competitive inhibitions, calculating an inhibition function I which multiplies the non-inhibited uptake rate:

$$I = \frac{1}{1 + \frac{S_I}{K_I}}$$

where S_I is the concentration of the inhibiting compound and K_I is the inhibition constant (concentration of the inhibiting compound at which the uptake rate is reduced by 50%)

The following combinations were tested one at a time:

i. Default ADM1 parameters and inhibition structures.
ii. Calibration of the uptake parameters of acetate (km_ac and Ks_ac).
iii. Fatty acid inhibition on acetate uptake (fa_ac).
iv. Undissociated VFA inhibition on methanogenic hydrogen uptake (HVFA_H_2).
v. Undissociated VFA inhibition on methanogenic acetate uptake (HVFA_ac).

vi. Undissociated volatile fatty acid inhibition on all bacterial processes (acidogenesis and acetogenesis) (HVFA_bac).

vii. Undissociated volatile fatty acid inhibition on all hydrolysis processes (HVFA_hyd).

For all combinations, hydrolysis was described as a first-order reaction: as shown in Chapter 4, overall this kinetics obtained a better goodness of fit in describing the dynamics of test 2 compared to Contois. Parameters from kinetic fractionation were left at a fixed value during the inhibition calibration, in order to avoid correlations with inhibition parameters. The parameters calibrated on interval 5 for the XX model (see paragraph 4.5.2) were used, as on this interval the non-modified ADM1 achieved the highest goodness of fit. The parameters used are as follows: $f_d = 0.90$, $f_{Xr} = 0.48$, $k_{hyd,r} = 10.28$, $k_{hyd,s} = 0.29$.

Results from simulations are shown in Figure 5.9 and Figure 5.10, with ADM1 default results compared with 4 different combinations in each figure. The goodness of fit of all combinations is shown in Table 5.5. Some qualitative considerations can be made, considering the combinations in order of increasing goodness of fit:

- ADM1 with default parameters and inhibition structures, and first order hydrolysis, achieves the worst fitting. From Figure 5.9c it is visually evident how the simulation overestimates the methane flow rate after the feeding; acetate and hydrogen uptake rates are also the highest between all combinations (Figure 5.9a and Figure 5.9b).
- The calibration of combination (ii) produced a lower maximum uptake rate km_ac and a higher half saturation coefficient Ks_ac than those using the ADM1 default values. As a consequence, the uptake rate of acetate is decreased and a higher accumulation of acetate (result not shown) occur, which result in a smaller uptake rate after the feeding (due to the reduced maximum uptake rate) together with a higher uptake rate at the end of the feeding (due to the accumulation of acetate and higher half saturation coefficient).
- Inhibition of hydrolysis by HVFA results in an overall slower solubilization of the substrate, with a reduced peak and delayed methane production. Both acetate and hydrogen uptake rates are affected.
- Inhibition of acetate uptake by HVFA results in a reduced acetate uptake rate, with a more flattened profile, due to the persistence of HVFA after the feeding - a similar profile is observed in the methane flow rate, qualitatively similar to the experimental data. The hydrogen uptake rate is not affected and coincide with ADM1 default.

- ADM1 with Contois hydrolysis (as calibrated in Chapter 4) is included for comparison. The methane flow and acetate uptake rate have a more flattened profile with respect to ADM1 with first-order hydrolysis. The initial peak is given by the uptake of the soluble fraction which was included in the Contois implementation; it is evident how the soluble fraction does not sufficiently reproduce the initial methane peak.
- Inhibition of acidogenesis and acetogenesis by HVFA (HVFA_bac) overall influence both the production of hydrogen and acetate. The initial peak in the simulated methane flow rate is stretched compared to ADM1 default and it is more similar to the experimental data. The effect of reduced CO_2 from acidogenesis is also influential on the methane flow rate (as less methane in the headspace is displaced).
- Inhibition of hydrogen uptake by HVFA influences directly the hydrogen uptake rate and indirectly the acetate uptake rate, by increasing the hydrogen inhibition on the acetogenic processes. As a result the simulated methane profile rate becomes closer to the experimental data.
- Inhibition of acetate uptake by fatty acids results in the best fit of all the combinations. The acetate uptake rate curve displays an interesting profile: the acetate uptake becomes progressively more inhibited with more fatty acids being produced by hydrolysis, reaches a minimum and then progressively increases again along with the fatty acids degradation.

• **Parameter**	**rAE (%)**
fa_ac	7.9%
HVFA_h2	8.5%
HVFA_bac	9.5%
ADM1 Contois	12.1%
HVFA_ac	12.6%
HVFA_hyd	13.2%
km_ac ks_ac	13.6%
ADM1 First Order	15.4%

Table 5.5 Goodness of fit of various inhibitions structures, calibrated on the interval 120-127.8 days for the FW test 2.

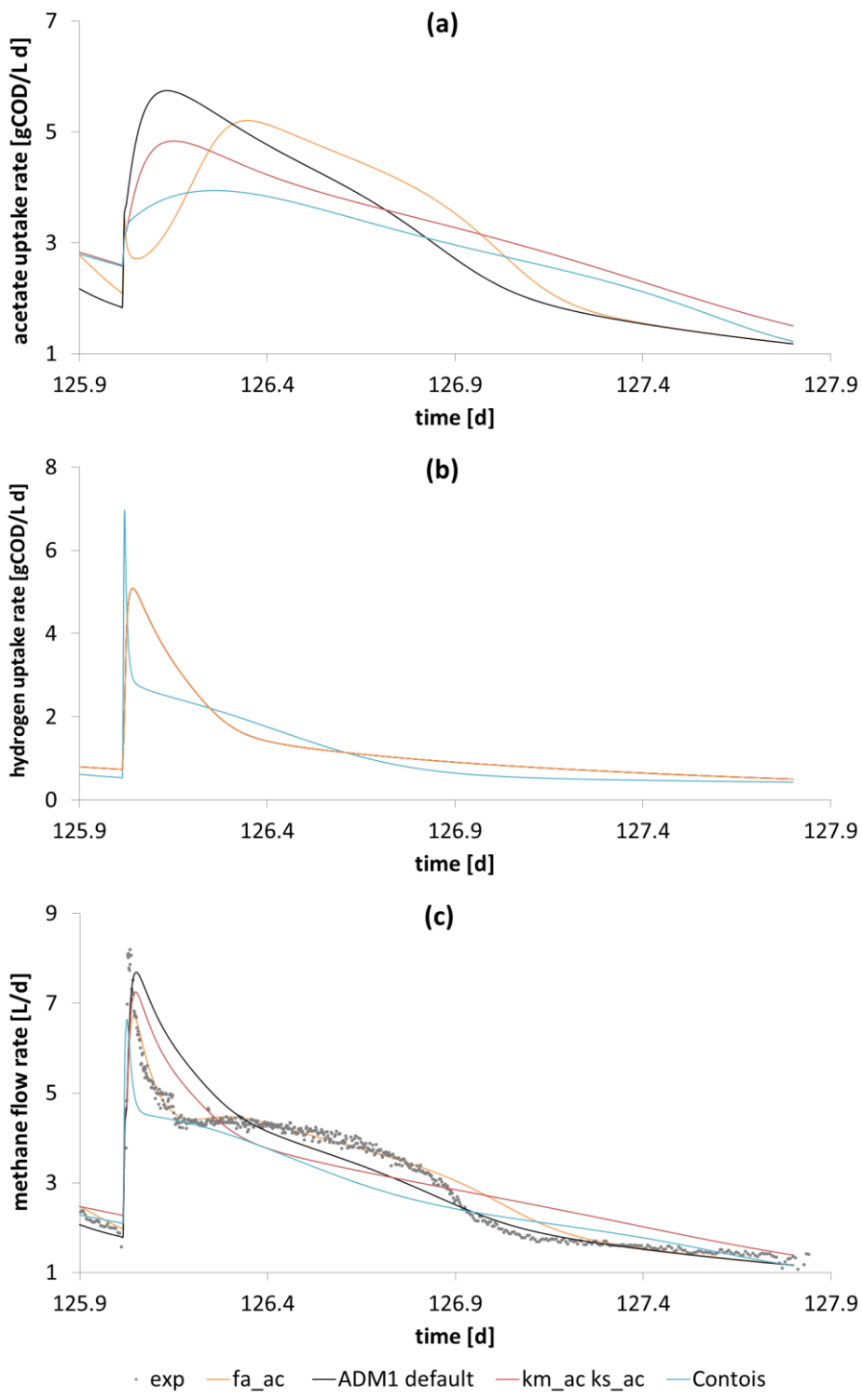

Figure 5.9 Comparison of (a) simulated acetate uptake rate, (b) hydrogen uptake rate, (c) experimental and simulated methane flow rate for default ADM1, ADM1 with Contois hydrolysis and LCFA inhibition on acetate uptake, updated Monod parameters for acetate uptake.

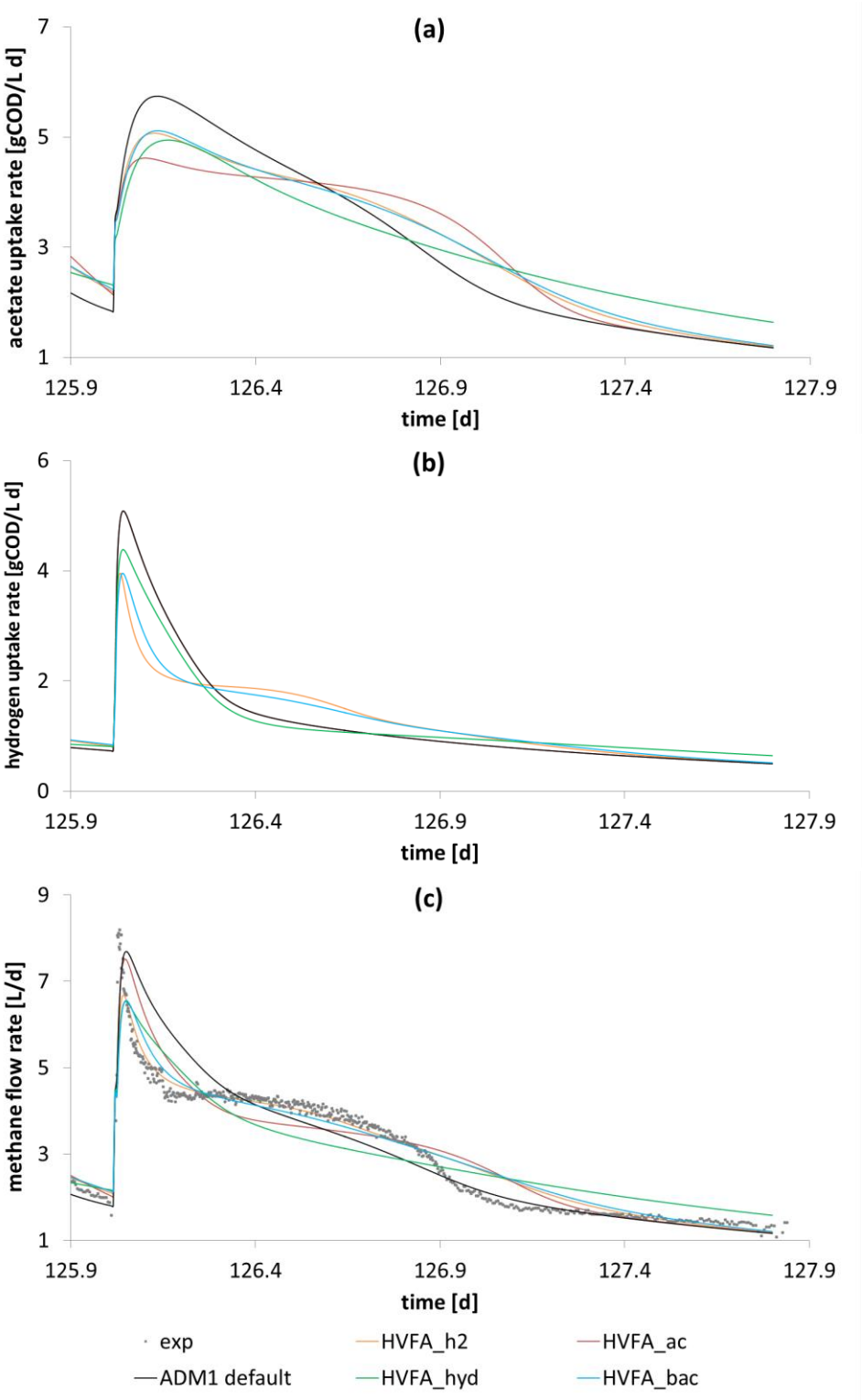

Figure 5.10 Comparison of (a) simulated acetate uptake rate, (b) hydrogen uptake rate, (c) experimental and simulated methane flow rate for default ADM1, HVFA inhibition on hydrogen uptake, acetate uptake, fermentation/acetogenic and hydrolysis processes.

5.5.2 Comparison of inhibition combinations

Based on the results shown in Table 5.5 3 inhibition combinations were developed using the best fitting individual mechanisms; HVFA-bac was split into the separate inhibitions of fermentation (HVFA_fer) and acetogenesis (HVFA_VFA):

- (I-1) Fa_ac + HVFA_ac + HVFA_h2
- (I-2) Fa_ac + HVFA_ac + HVFA_h2 + HVFA_VFA
- (I-3) Fa_ac + HVFA_ac + HVFA_h2 + HVFA_VFA + HVFA_fer

These results are shown in Figure 5.11-Figure 5.14.

Experimental methane production in Figure 5.11 shows decreases larger than the decrease in loadings and further produces no peak during the feedings at days around 174, both indicating the presence of inhibition in the process. There is accumulation of VFA as shown in Figure 5.12 including propionate, butyrate and valerate.

Comparison of the three inhibition combinations for reproduction of methane production shows a general trend of improvement from ADM1→ I1 → I2 →I3. As shown in Figure 5.11a, ADM1 default values overproduces methane production peaks after feeding and the characteristic shape of the kinetic is different from the experimental data. Sustained methane production and noticeable peaks at each feeding event can be observed throughout the period. On the other hand, I1-3 all reproduce the reduction in peak methane production rate over the calibration period shown in Figure 5.11b-d. I3 accurately reproduces the peaks and the complete lack of response to the feedings around day 174 in agreement with the experimental data.

While the ADM1 simulation shows no VFA accumulation over the calibration period (results not shown) all three of the inhibition combinations reproduce to a varying degree the VFA peak shown in the experimental data (Figure 5.12) but again I3 shows the best fit since it includes the accumulation of the longer chain VFA rather than just acetate. Again, the pH data shown in Figure 5.13 show that I3 can best represent the experimental data.

Figure 5.14 shows that accumulation of fermentable species are being used by inhibition combination I3 as the mechanism to allow VFA accumulation and reduction in methane production.

However I3 is still unable to reproduce the longer term effects of inhibition, such as the significant VFA concentration, at about 5 gCOD/L, seen in the period after 192 days – with the model on the other hand predicting a complete recover of the system, with negligible VFA concentration. This suggests that further mechanisms of inhibition are still not included.

In summary, the simpler inhibition models, including all single species mechanisms (section 5.5.1) and inhibition combinations I1 and I2 fail to reproduce:

- VFAs speciation (rather than just accumulation of acetate)
- Cessation of methane production under inhibition conditions
- Peak methane production
- Characteristic methane production kinetic

The I3 inhibition combination can produce all of the phenomena seen in the experimental data and therefore is likely to be a better mechanistic representation of the actual inhibition taking place in the biological process.

Inhibition combination	Inhibition parameter				
	fa_ac	HVFA_ac	HVFA_fer	HVFA_h2	HVFA_VFAs
	[gCOD/L]	[mM]	[mM]	[mM]	[mM]
I-1	1.905	0.126		0.026	
I-2	1.920	0.120		0.091	0.217
I-3	0.906	0.133	0.008	0.118	0.018

5.6 Calibrated parameter values for inhibition combinations I-1, I-2 and I-3.

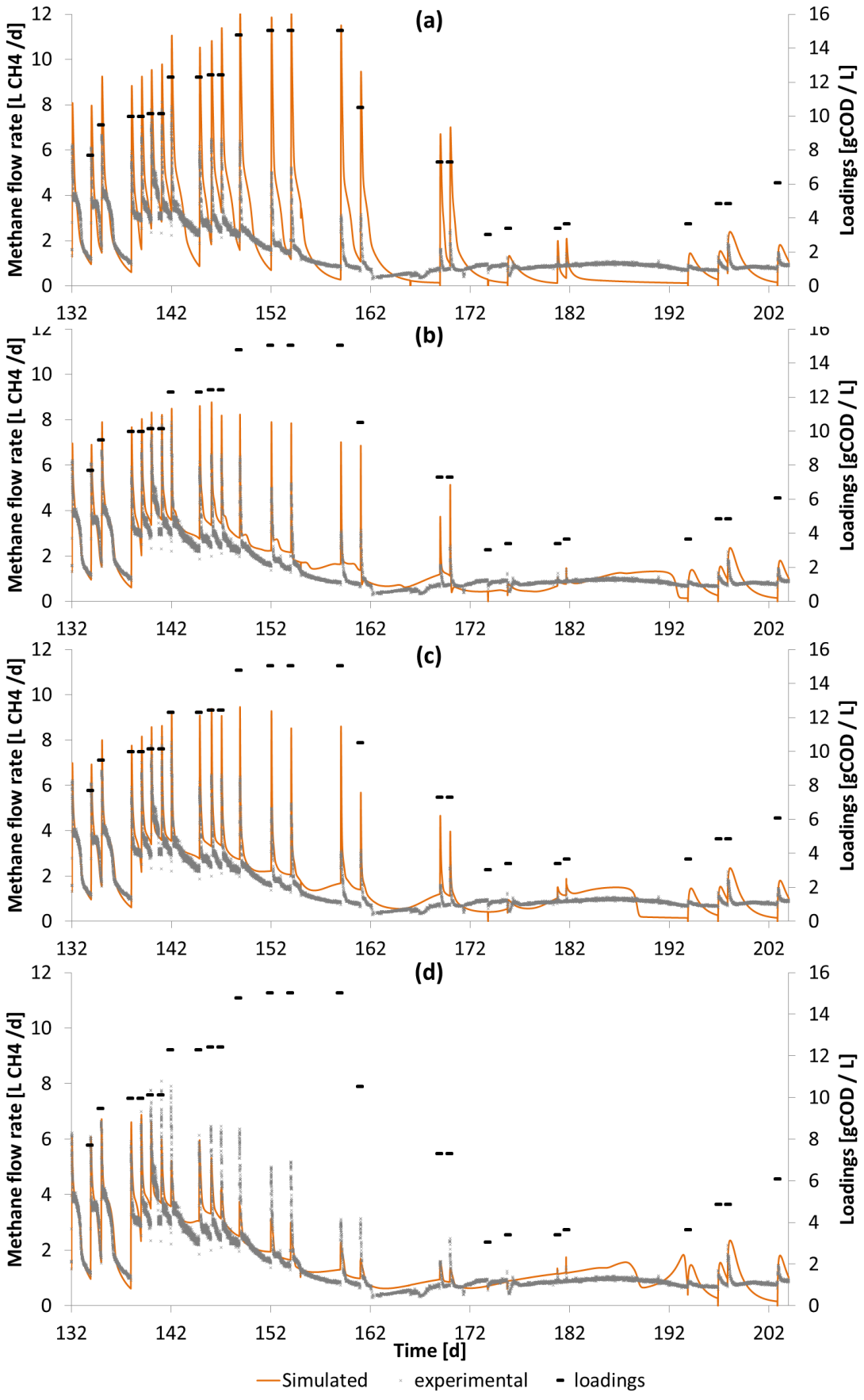

Figure 5.11 Simulated and experimental results for methane flow rate for model inhibition structures: (a) default ADM1, (b) I-1, (c) I-2, (d) I-3.

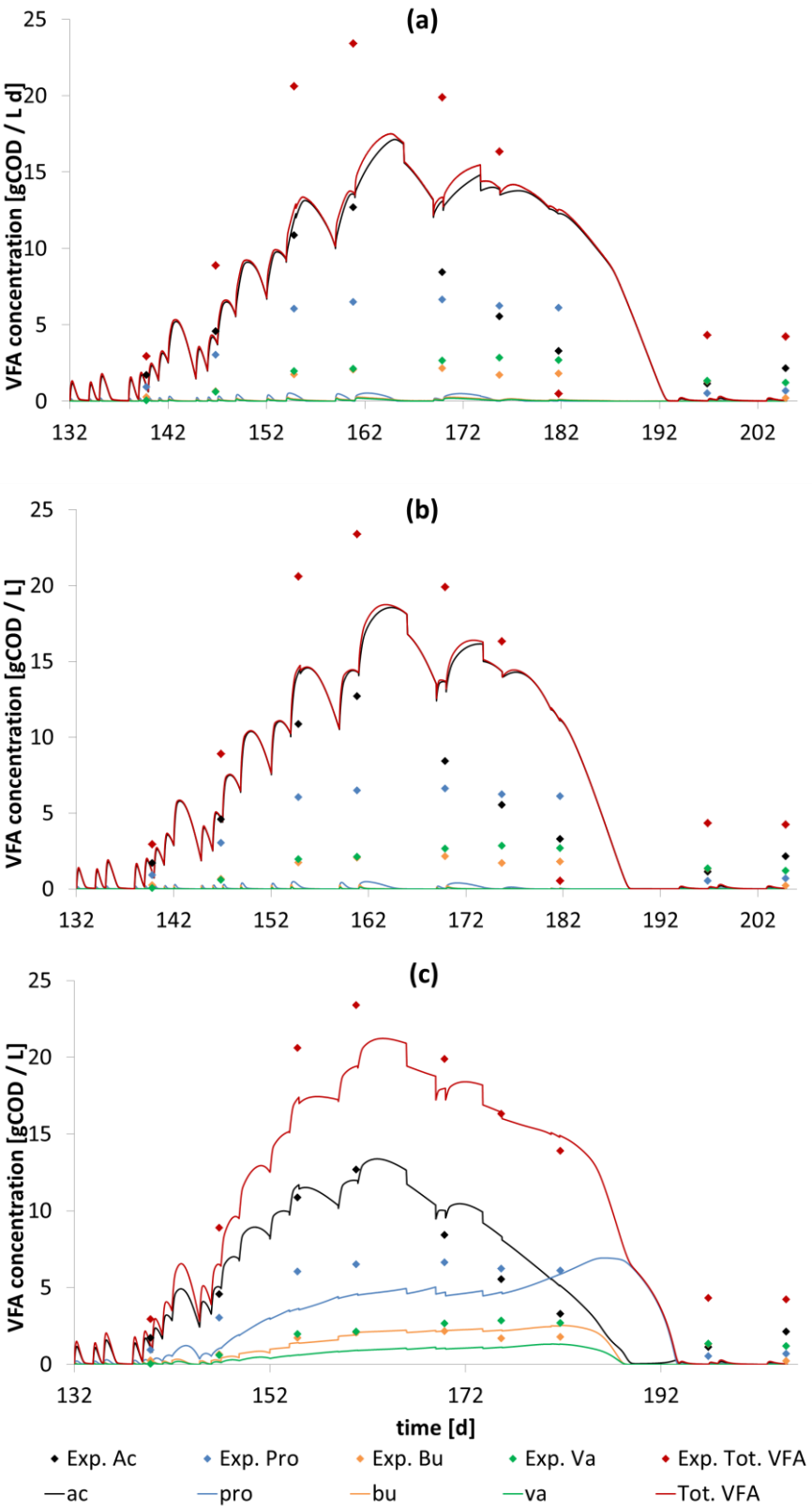

Figure 5.12 Experimental and simulated values for the total and single VFAs, for the three different inhibition structures (a) I-1, (b) I-2 and (c) I-3.

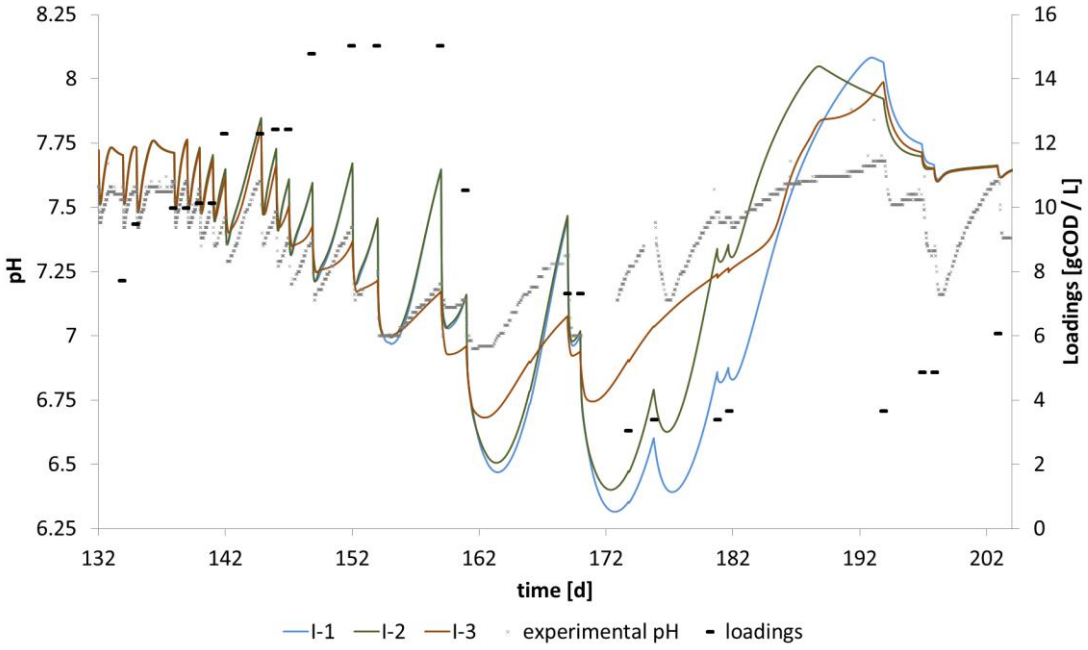

Figure 5.13 Experimental and simulated pH for the three different model inhibition structure I-1, I-2, I-3.

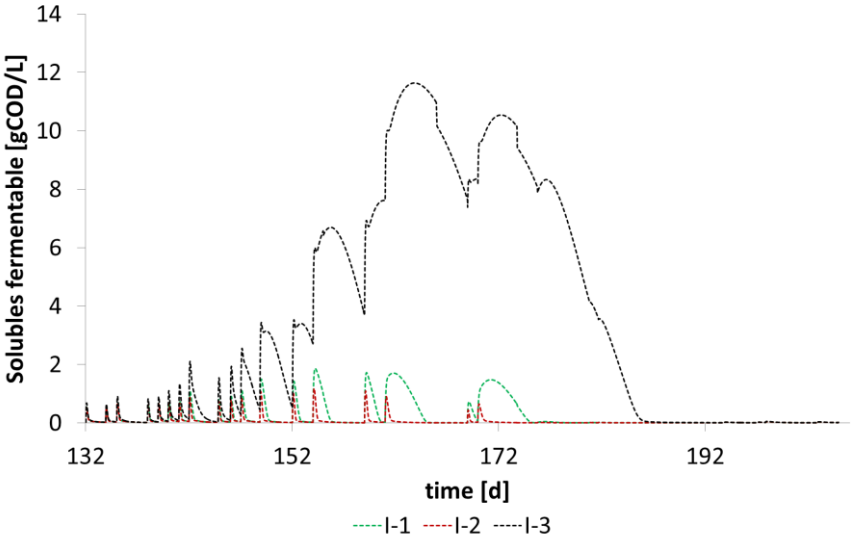

Figure 5.14 Simulated concentration for the total solubles fermentable, for the three different inhibition structures (a) I-1, (b) I-2 and (c) I-3.

5.5.3 Validation of inhibition parameters

In order to validate the inhibition structure calibrated in section 5.5.2, a different experimental data set was used, with respect to the data used for the calibration. The inhibition structure I-3 was used to simulate the whole experimental period of R-a, R-b and R-c. Results are shown in Figure 5.15. The issue is that in all cases, the methane production decreased and finally a process failure occurred, and this is

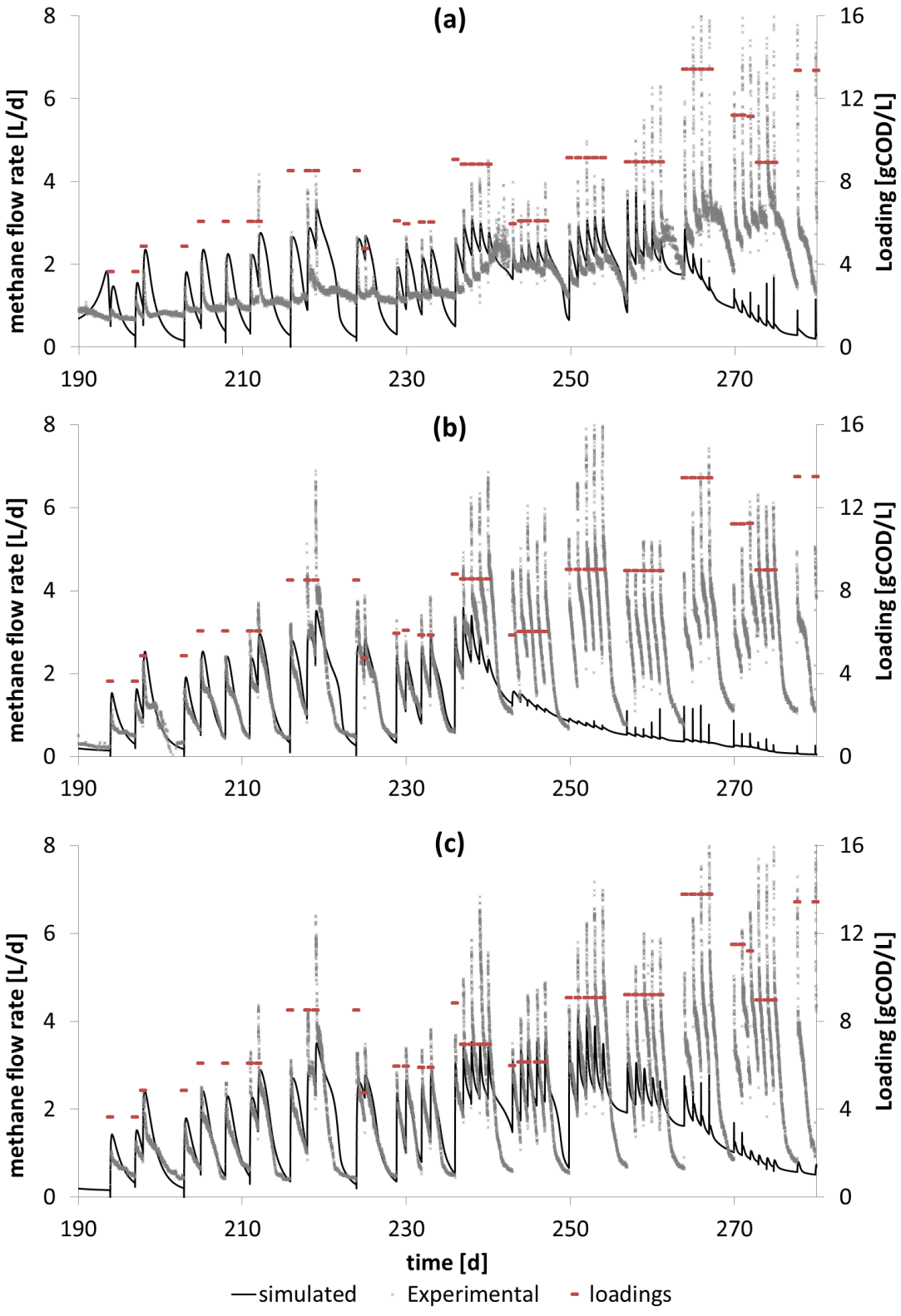

Figure 5.15 Experimental and simulated methane flow rate for the (a) experiment R-a. (b) experiment R-b, (c) experiment R-c for the inhibition structure I-3 calibrated on the data set 3; showing the occurrence of process collapse.

in contrast to the experimental data, which showed sustained methane production. This indicates that the chosen inhibition structure appears to be too sensitive to a high organic loading rate and therefore introduces too much inhibition into the process. This demonstrates how the calibration of the bioprocess model depends strongly on the calibration dataset and therefore cannot always be generalised to all process conditions.

5.6 Conclusions

Data from experiments R-a, R-b and R-c were used to successfully validate both the codigestion modelling methodology and the substrate fractionation method presented in Chapters 3 and 4. The model (with default inhibition parameters) was able to predict the behaviour of the experimental system, except in the periods of organic overload. The worst predicted measured output was in all cases VFA with rAE of 64-81% over the 310 day experimental period.

Also, the tests explored different experimental conditions in terms of HRT and solids content, mainly driven by the addition of water. The digestion of pure substrates without water addition corresponded to higher levels of solids in the reactor, especially for test R-b fed mostly with GW. The addition of water is not a preferred option when operating a digester, since it uses a valuable resource, increases the volume of digestate to be treated/distributed, and diminishes the process HRT. However it can become necessary when feeding poorly degradable substrate, as in the case of GW, to avoid mass-transfer inhibiting conditions caused by an excessive solid concentration (Abbassi-Guendouz et al., 2012a). Also it was shown how the addition of water potentially helped the recovery from process imbalances in test R-a, with water diluting the inhibiting substances (ammonia and VFA). A properly calibrated model could be used to estimate the optimal level of water addition, taking into account the changes in the reactor process kinetics and potentially also the characteristics of the downstream digestate usages.

Using data from the same three experiments allowed an assessment of the synergistic effects of codigestion of FW and GW. The results were inconclusive since although a small increase in the specific methane yield was shown in the codigestion experiment relative the mono-digestion cases (+3.3%) it was postulated that this is within the experimental error.

The investigation into the important inhibition mechanisms found that the best model fit of the experimental data R-a, during the organic overload event, fed on

only FW, included inhibition by LCFA on acetoclastic methanogens, and of undissociated VFA on fermentation, acetogenesis and both types of methanogens. Using this combination of inhibition mechanisms, the important phenomena of the experiment could be replicated by the model.

When validated against the whole R-a, R-b and R-c datasets, the model with the selected inhibition parameter set showed poor agreement and predicted an inaccurate process collapse: the system showed higher resistance to organic stress in the later co-digestion part of the experiment, compared to the mono-digestion of food waste which was used to calibrate the inhibition parameters. One possible influence on this different system behaviour, during those different organic overload periods, is the bioavailability of the trace elements. It has been shown how the concentration of trace elements, such as Co, Mo, Ni, Se, and W, have a significant influence on the performance of food waste digestion (Facchin et al., 2013). Of particular relevance to this thesis is the work by Banks et al. (2012) who have investigated the influence of trace elements in the semi-continuous digestion of food waste. They demonstrated how the addition of Se and Co allowed the stable semi-digestion of food waste, at organic loading rates as high as 5 gVS L^{-1} day^{-1}, while the digester showed VFA accumulation at 2 gVS L^{-1} day^{-1} and collapsed at 3 gVS L^{-1} day^{-1}, the latter after just 100 days of operation. It is difficult to make quantitative comparisons between these works, especially since no trace element analyses were performed in this thesis on the inoculum and substrate. However, one possible explanation of the higher resilience to overload shown by the investigated system during the co-digestion period could be the increased nutrient availability brought about by the different co-digested substrate. Pig manure, green wastes and oat residues may have a trace nutrient profile that complement the deficiencies in food waste. ADM1 could be supplemented with additional state variable, describing the availability in the system of the required trace elements, and introducing inhibition functions which are dependent on threshold concentrations. However, the nutrients bioavailability is a function of the physico-chemical conditions (such as pH, and other elements concentration, which influence nutrients precipitation, complexation etc.), thus making the modelling more difficult.

6 Modelling microgrid energy systems containing anaerobic digesters

The integration of anaerobic digestion (AD) in a microgrid is a novel concept that has been poorly covered by previous research. In this configuration, the AD system (digester and gas storage) can be used to compensate energy supply fluctuations from intermittent renewable sources, or to compensate seasonal changes in energy demand. The AD system can compensate microgrid energy fluctuations in two ways. In the short term (hours), using the biogas that has been stored in the external storage. In the long term (days), a change in the loading rate of the digester is required in order to increase the biogas produced and restoring the biogas reserve in the external storage. Therefore in this concept the operation of the AD system is driven by the dynamics of the microgrid. Changes in the loading rate can be realized by an increase in the mass loading rate, or by a higher ratio of degradable and energy-rich substrates. AD processes are affected by changes in loading rate and substrate composition, with the effect dependent on the state of the process and on the type, duration and frequency of the change (Leitao et al., 2006). An inappropriate operation can result in a collapse of the process. Given this inherent risk in dynamic operation, a decision support system is necessary for the operator to select on a daily basis the amount and composition of the feeding which can satisfy the required energy demand. This chapter aims to explore the role of AD in a microgrid system, and follows the following steps:

- In Section 6.1 the work of Castellanos et al. (2014) is introduced and summarised. This section focuses on the use of the modelling software HOMER which is used to optimise microgrid designs based on economic analysis. Note that this chapter is based upon the published journal article above.
- Section 6.26.3 focuses on some minor modifications to the microgrid system proposed by Castellanos et al. (2014) and develops some additional biogas demand profiles with varying levels .
- Section 6.3 is dedicated to modelling the AD component of the microgrid system using ADM1, with a focus on how a digester can meet the biogas demands of the system.

A schematic of the overall concept of the role that AD can play in a microgrid system is shown in Figure 6.1, resuming the concepts already introduced in Chapter 1 (Section 1.1) and which will be analysed in this Chapter.

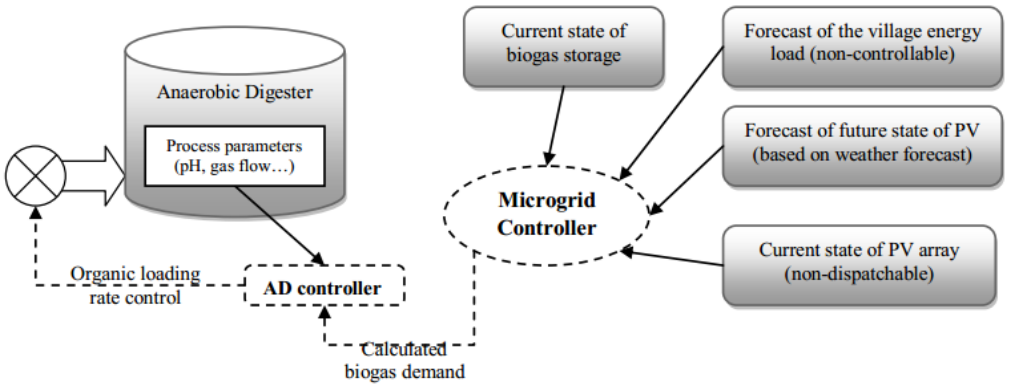

Figure 6.1 Schematic of concept of use of AD in a micro-grid incorporating demand predictions and AD controller (from Poggio et al. (2013)).

6.1 Modelling an off-grid energy system for rural electrification in India using photovoltaics and anaerobic digestion – a HOMER optimisation study

This work surrounds the design optimisation of an off-grid energy system for use in rural electrification in India. India has shown an accelerated economic growth, however like other developing countries most of its population (~70%) live in remote rural areas which are not connected to the national electrical grid and small scale power plants that can satisfy the electrical demands of a local area can prove an attractive alternative to extension of the national grid.

Given the abundance of sunlight and biomass available in the research area (India), the chosen energy conversion technologies were PV and anaerobic digestion (AD), with a Combine Heat and Power (CHP) generator fuelled by biogas. CHP systems based on both reciprocating engines and microturbines (MT) were considered and scenarios were based on combinations of these along with two storage technologies: vanadium redox batteries (VRB), and the combination of a water electrolyser and hydrogen storage with fuel cell for electricity production. A third storage option, zinc bromide batteries, was also briefly assessed. In order to determine a final optimal IRES configuration, the various technologies mentioned above were combined with each other. Figure 6.2 portrays the general concept of the IRES proposal for a typical rural village.

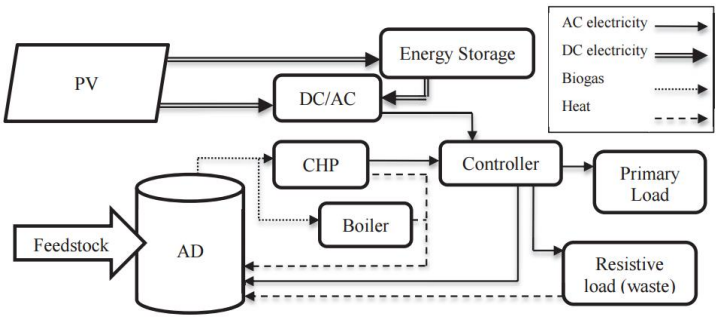

Figure 6.2 Integrated renewable energy system general configuration used in the HOMER optimisation study (from Castellanos et al. (2014)).

6.1.1 Load profile

This research forms part of the Bridging the Urban-Rural Divide (BURD) joint India/UK project and as part of this work a load profile was created that represents the electrical demand of a village in West Bengal containing around 1000 residents who currently have no direct access to electricity. This is shown in Figure 6.3. The demand is split into various categories and includes economic activity i.e. grinding spices, water pumping, the operation of a medical centre, adult and child education facilities, lighting and entertainment. The demand increase around noon was justified based on the predicted commercial and productive activities, while the demand increase at night was justified based on the predicted lighting and entertainment activities. The overall electrical load is equivalent to 22 MWh/year.

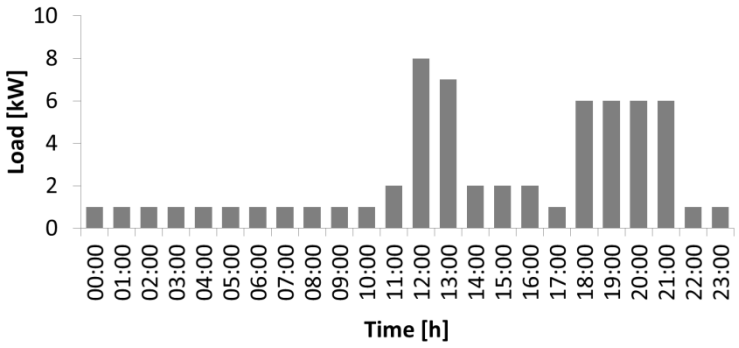

Figure 6.3 Total electrical demand for rural Indian village, used in the HOMER optimization study (from Castellanos et al. (2014)).

6.1.2 Micro-grid system modelling - HOMER

Micro-grid modelling was performed using HOMER. This software allows simulation of the performance of an energy system with uncertain operational conditions, allowing robust design with reduced project capital risk. A large number of

permutations of the overall system were created with varying capacity (storage, power output) of each component. Each of these permutations was tested to assess whether it could meet the load requirement. The HOMER package was then used to list the permutations of the systems that can meet the demand and reports various economic indicators upon which the optimal scenario could be chosen.

Scenarios considered

The scenarios that were explored are shown in Table 6.1. Scenarios A and B use PV as the primary energy generator with differing storage technologies. Scenarios C-F use AD and a biogas CHP as the primary energy generation, with differing generation technologies and capacities of the CHP used. For each CHP technology two scenarios were explored; one with a high and low capacity engine and one with two similarly sized engines. Note that this approach was chosen since initial results with only a single CHP showed large amounts of wasted energy since the CHP needed to be scaled according to the peak demand which is much higher than the base load. Finally, scenario G, the fully integrated energy system, was designed based on the better ranked technologies from the previous modelling.

For detailed descriptions of the components (PV, vanadium redox batteries (VRB), CHP based on both reciprocating engines and microturbines (MT) and AD) and financial variables used in the HOMER modelling the reader should refer to Castellanos et al. (2014), however the input solar data used for the site (latitude 23 160 north and longitude 87 150 east) which was used in all HOMER simulations is shown in Table 6.2.

Scenario	Technologies involved
A	PV + VRB + DC–AC
B	PV + Fuel Cell + Electrolyser + H_2 tank + DC–AC
C	AD + 2 CHP (Microturbine); high and low capacity
D	AD + 2 CHP (Microturbine); similar capacity
E	AD + 2 CHP (Reciprocating Engine); high and low capacity
F	AD + 2 CHP (Reciprocating Engine); similar capacity
G	PV + VRB + DC–AC + AD + 1 CHP (Microturbine)

Table 6.1 Scenarios investigated in the HOMER optimization study (from Castellanos et al. (2014)).

Month	Clearness index	Daily radiation [kWh m^{-2} day^{-1}]	Ambiant temperature[a] [°C] max, min, average
January	0.6	4.195	31, 9, 19
February	0.59	4.757	34, 12, 22
March	0.593	5.568	40, 13, 27
April	0.588	6.148	40, 17, 30
May	0.542	5.968	40, 18, 30
June	0.466	5.198	40, 21, 30
July	0.382	4.22	36, 22, 29
August	0.419	4.445	38, 18, 28
September	0.449	4.358	36, 18, 28
October	0.579	4.882	35, 16, 27
November	0.592	4.268	31, 16, 24
December	0.596	3.956	30, 9, 20
Average	0.533	4.829	36, 16, 26

Scaled annual average 4.829 kWh m^{-2} day^{-1}.

Table 6.2 Monthly average solar radiation and temperatures for the micro-grid location, used in the HOMER optimization study (from Castellanos et al. (2014)).

6.1.3 Summary of results and discussion of the HOMER optimisation study

Since the study was based on a financial optimization the main results are summarised in Figure 6.4. It is clear that the fully integrated scenario (G) was the most promising relative to the other scenarios which were based on fewer elements. The capital, and O&M results follow a similar trend with the scenario B (with H_2 tank, electrolyser and fuel cell) being by far the most expensive, with scenario G, incorporating PV, AD, MT and VRB being the cheapest, and therefore most attractive. A full description of the system components and their characteristics is shown in Table 6.3.

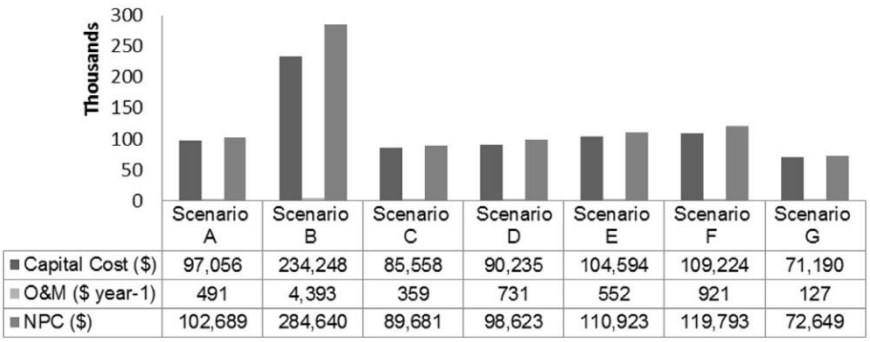

Figure 6.4 Financial requirements of the different scenarios investigated in the HOMER optimization study (from Castellanos et al. (2014)).

Scenario G	PV + VRB + DC–AC + AD + CHP Microturbine		
PV [kW]	Battery rated power [kW]	Battery storage capacity [kWh]	Converter [kW]
7	3	45	3
AD volume [m^3]	CHP Microturbine [kW]	Excess electricity generated per year [%]	
62	8	4.50	

Table 6.3 Scenario G optimal system configuration (from Castellanos et al. (2014)).

HOMER ranks the different systems according to its NPC, taking into account that this research targeted, low income, rural location within developing countries, the cost of energy (COE) was determined as the most important economic feasibility indicator of the project, the results of which are shown in Figure 6.5. The capital cost of each of the scenarios has the largest impact on the effective COE but is also influenced by the total electrical supplied in each case.

Figure 6.5 COE ($/kWhr) results of the different scenarios investigated in the HOMER optimization study (from Castellanos et al. (2014)).

Further to the financial recommendation for scenario G, due to the fact that it does not simply depend on one technology but on two energy generation technologies such as PV and AD, the system could also have increased reliability. The reduction in capital cost is due to the synergy between the schedulable, non-schedulable and storage elements in this integrated system. It is worth stressing that the scaling of the components in each scenario can be sensitive to the selected loss of load probability (LOLP). The LOLP represents the probability that the energy demand will exceed capacity during a given period (one year in this case). The 1% LOLP which has been used here represents a relatively high quality of supply in rural India and before embarking on such a project it would be worth considering the required or acceptable quality of supply since economic savings could be made in the case of a higher LOLP. To attempt to quantify this, scenario G was simulated at additional LOLP values of 2, 5, 10 and 20%, with the results shown in Table 6.4 and whilst it is true that reducing the desired quality of supply to a LOLP of 20% results

in a reduction in the capital cost and the installed generation capacity by 15% and 27%, respectively, this benefit is not carried forward to the cost of the electricity over the life of the project. The COE is only reduced by 2.1% for a LOLP of 20% due to less electricity being supplied by the system despite a huge decrease in the supply quality. It is worth mentioning that a benefit of increasing the allowed LOLP is that less excess electricity is generated and therefore wasted, mainly because the PV system is not over-dimensioned to meet unusual peaks in demand.

LOLP [%]	Total generation capacity [kW]	Capital cost [$]	NPC [$]	COE [$ kWh^{-1}]	Excess electricity generated per year [%]
1	15	71,190	72,649	0.289	4.50
2	14	69,433	70,855	0.284	1.64
5	13	67,371	68,814	0.282	0.42
10	12	65,332	66,690	0.285	0.10
20	11	60,341	61,103	0.283	0.20

Table 6.4 Scenario G sensitivity to LOLP (from Castellanos et al. (2014)).

The electricity cost of the system proposed in this work of $ 0.289 kWh^{-1} is comparable with other works in rural India e.g. 0.258 for a PV and battery system (Suganthi and Samuel, 2012), 0.24-0.47 for different configurations of PV, wind and batteries (Mellit and Pavan, 2010) and 0.216 for a PV, diesel and battery system (Soman et al., 2010) (all in $ kWh^{-1}). Furthermore a Greenpeace study (Martensen et al., 2012) found that the cost of electricity of microgrid systems based on biomass (thermal) and PV in India was 0.304-0.384 $ kWh^{-1} , and that this can be reduced to 0.176-0.208 $ kWh^{-1} if a local hydro power source is available. The report goes on to explore the comparison between the cost of electricity from these isolated systems to the extension of the electricity grid. While the cost of electricity for grid connected customers is reported to be as low as 0.08 $ kWh $^{-1}$, clearly much cheaper than the cost from the IRES reported, once the costs of extending the grid are taken into account the total cost can become greater for a distance as little as 5-13 km.

A broader discussion of the benefits of the IRES would include the fact that AD offers liquid and fibrous by-products which act as soil fertilisers and can improve crop yields and soil conditions. This is a particular benefit to rural communities that otherwise may not have the financial resources to add nutrients to their cultivated fields. Therefore, they would improve the productivity within agriculture and livestock sectors, or could even commercialise the fertilisers to neighbouring villages, thus, increase their economic revenues. Nonetheless, any scenario

involving AD represents a commitment to a work load demand from the community and there may be local resistance to this aspect of the technology. AD not only provides biogas to the microturbine, but this purpose is achieved by treating waste, and hence AD is also a waste remediation alternative. Therefore, in addition to the scenario G system being low COE, this scenario may represent a better option due to the other benefits from AD.

6.2 Development of biogas demand profiles from microgrid modelling

The hybrid energy system modelling using HOMER mainly focused on modelling the whole hybrid energy system with only simple treatment of the AD component: in fact it was assumed that biogas would be available to the micro turbine under any condition of demand and across the whole simulation period. Digester operation was assumed to be at steady state conditions during all the year, at a conservative constant loading rate of 2 kg VS m^{-3} day^{-1} (corresponding to 3.25 kg COD m^{-3} day^{-1} in the case of 50% FW and 50% GW on a weight basis). As a consequence, it was implicitly assumed that a biogas storage were available to buffer any difference between biogas production and demand. However the dimensioning of the storage was not addressed in that study, and as will be demonstrated in the following sections it is an important design variable which could influence the techno-economic viability of the hybrid energy system.

As reviewed in Chapter 1, the operation of a digester could be approached in a more complex way than constant loading, and it is interesting to investigate the possibility of adapting the loading rate to the demand of biogas and the state of the AD system. Therefore modelling will be employed in this chapter to systematically investigate the relations between:

- Different biogas demand profiles, being characterised by different oscillation amplitudes.
- Different forecasting ability of the biogas demand, i.e. knowledge of the amount of biogas required with different forecasting windows lengths.
- Different knowledge of the AD system: pH, gas flow, storage level.
- Effect of loading strategies on storage requirements.
- Effect of loading strategies on stress indicators of the AD system (e.g. VFA content).

6.2.1 Development of biogas demand profiles using HOMER

As a first step of this benchmark study, different biogas demand profiles were created in order to explore the aforementioned system interactions under different conditions. The starting point was the previously described HOMER study. The economically optimal Scenario G was selected as the baseline scenario, and five further scenarios were developed by changing the ability of the microturbine (MT) at lower loading, by allowing flexible scheduling of the MT and by imposing a greater daily and hourly variability to the overall design energy demand of the micro grid (previously depicted in Figure 6.1); the six cases are listed in Table 6.5. PV and MT sizes (kW) remained as per Scenario G, while size (kWh) and power (kW) of the batteries were allowed to change during HOMER optimization; reduction of minimum loading and flexible scheduling of the MT allowed the MT to be operated for longer periods during the day with respect to the baseline scenario.

Case #	Description
1	Base case as per Castellanos et al. (2014)
2	As case 1 with reduction in micro turbine minimum loading to 10% of capacity
3	As case 2 with no scheduling of the micro turbine
4	As case 3 with +/- 25% deviation from design demand profile (daily and hourly)
5	As case 3 with +/- 50% demand variation (daily and hourly)
6	As case 3 with +/- 75% demand variation (daily and hourly)

Table 6.5 Scenarios for hybrid energy system modelling in Homer Energy Pro with reference to the base case as per Castellanos et al. (2014).

The results of the HOMER optimization are shown in Table 6.6. Modifications across the 6 cases did not show a large change in the NPC ($72,600-$74,600) or COE (0.289-0.315 $/kWh) for the system but there were significant changes in terms of the system overall performance in Cases 5-6 in the form of a reduction in LOLP (5 and 9%, respectively). This was caused by the large variation in the electrical demand profile (+/- 50% and 75% for Cases 5 and 6, respectively) which effectively increased the peak demand of the system leading to an inability to meet the electrical demand. This could have been solved by allowing HOMER to change the size of the MT and PV elements but the focus of this study was to investigate the behaviour of the system when faced with unexpected variations in the design demand profile and the ability of the AD system to provide the necessary supply of gas. Further case by case results can be commented as follows:

1. Case 2 – changing the minimum operating load of the microturbine made only a small change to biogas demand characteristics.

2. Case 3 – removal of MT scheduling had the effect of replacing battery capacity and power with a greater biogas demand (24.6 cf. 22.2 m^3 day^{-1}) and daily variability (standard deviation 6.1 cf. 2.2 m^3 day^{-1}). As can be seen in Figure 6.6, there is more variability in the on/off cycle of the MT although there is still a daily pattern due to the low variability of the electrical demand (+/- 15%) relative to Cases 4-6.
3. Cases 4-6 – increasing the variation in electrical demand had major effects on the required biogas demand and the daily variation. Figure 6.6 shows a larger variation in the on/off cycling of the MT. Shorter cycles of the MT could induce higher O&M requirements of the MT, and introduce efficiency losses due to repeated warm-ups of the MT: both effects were not considered in the analysis.

From the optimized scenarios, the calculated overall biogas demand was exported to then be used as input into the ADM1 based simulations of the AD system: the demand comprises both the biogas used by the MT to supply the required electricity and the biogas required for an external boiler to heat the digester. Each case produced a biogas demand characterized by incrementally greater temporal variations and therefore it is more challenging for the AD system to satisfy. This can be seen in Table 6.6, where the magnitude and variability of each biogas demand are shown: the biogas demand increases in its average value across the six cases (from 22.2 m^3 day^{-1} in Case 1 to 28.4 m^3 day^{-1} in Case 5); it increases in the maximum daily demand (from 27.2 to 72.3 m^3 day^{-1}) and in its variability (standard deviation from 2.2 to 15.1 m^3 day^{-1}). Biogas demand profiles are shown in Figure 6.6-Figure 6.8 on 3 different timescales: the hour to hour demand as shown in Figure 6.6, the day to day demand as shown in Figure 6.7 (160 days excerpt) and the month to month demand as shown in Figure 6.8 (monthly variation with respect to yearly average). From the hour to hour profile, it is evident how the biogas demand is composed of a smaller cyclic demand for the boiler and superimposed larger peaks coincident with the MT operation. The daily timescale makes it evident how the daily biogas demands are affected by the imposed random variations, which are superimposed on a more similar long term trend. The monthly timescale makes evident how the biogas demand changes also according to the environmental conditions, with peaks corresponding to months of lower solar irradiation and lower temperature: it is the case of August which falls in the monsoon period with lower solar irradiation, and December and January which have both low solar irradiation and temperature (Table 6.2). Random variations in the demand (Cases 4,5,6) also play a role in determining the monthly variations.

Case #		1	2	3	4	5	6
Battery power	kW	3	3	2	3	4	4
Battery capacity	kWh	45	45	20	30	25	30
AC/DC	kW	3	3	3	3	4	4
COE	$ kWh^{-1}	0.289	0.289	0.282	0.289	0.303	0.315
NPC	k$	72.6	72.6	71.1	72.6	74.5	74.6
Biogas demand	m^3 yr^{-1}	8103	7994	8979	8651	8842	9928
	m^3 day^{-1}	22.2	21.9	24.6	23.7	24.3	27.2
Largest daily demand	m^3 day^{-1}	27.2	27.2	46.6	48.3	57.9	67.1
Std. dev. of daily biogas demand	m^3 day^{-1}	2.2	2.5	6.1	7.5	15.1	13.6
LOLP requirement	%	1	1	1	1	5	9

Table 6.6 Modified system design, performance indicators and biogas demand of hybrid energy systems with modifications from base case as per Castellanos et al. (2014).

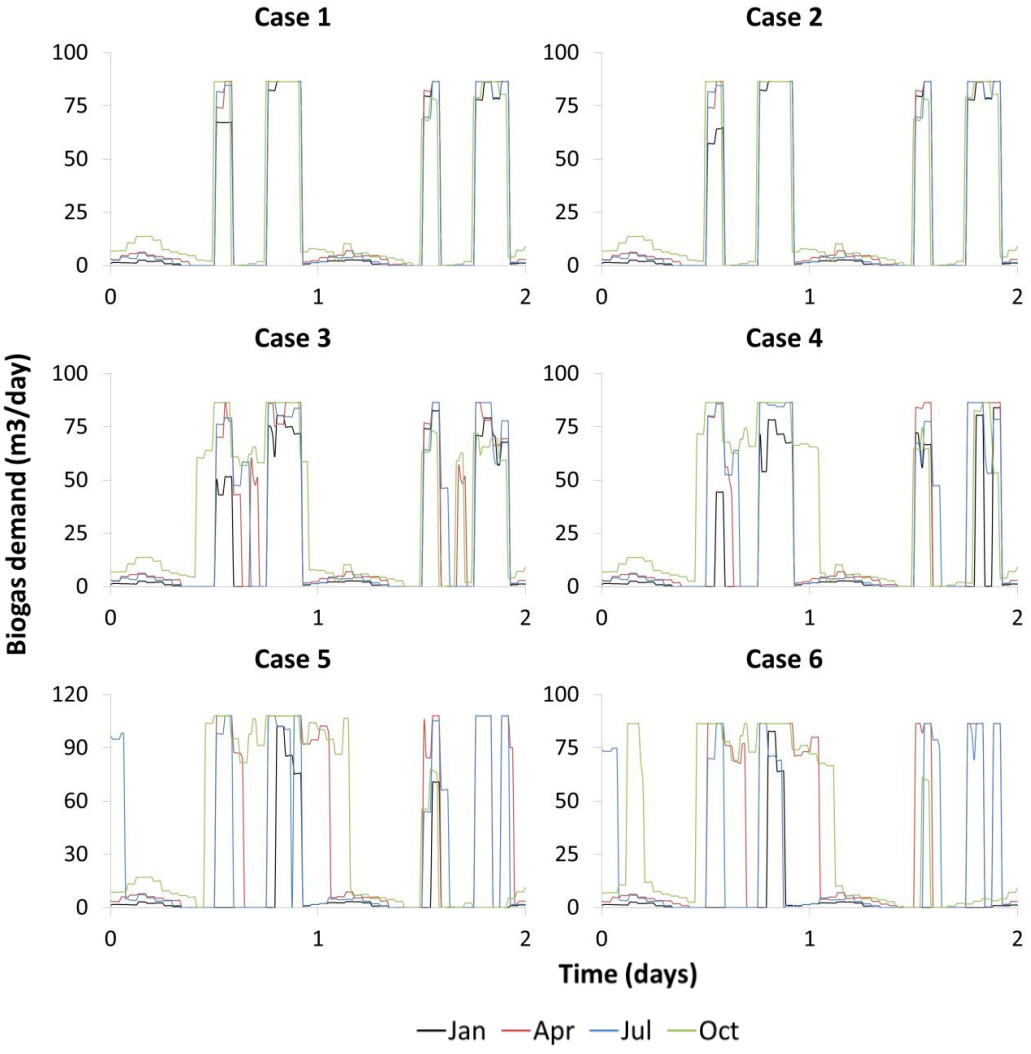

Figure 6.6 Example daily methane demand profiles for the hybrid energy systems in Cases 1-6 for January, April, July and October.

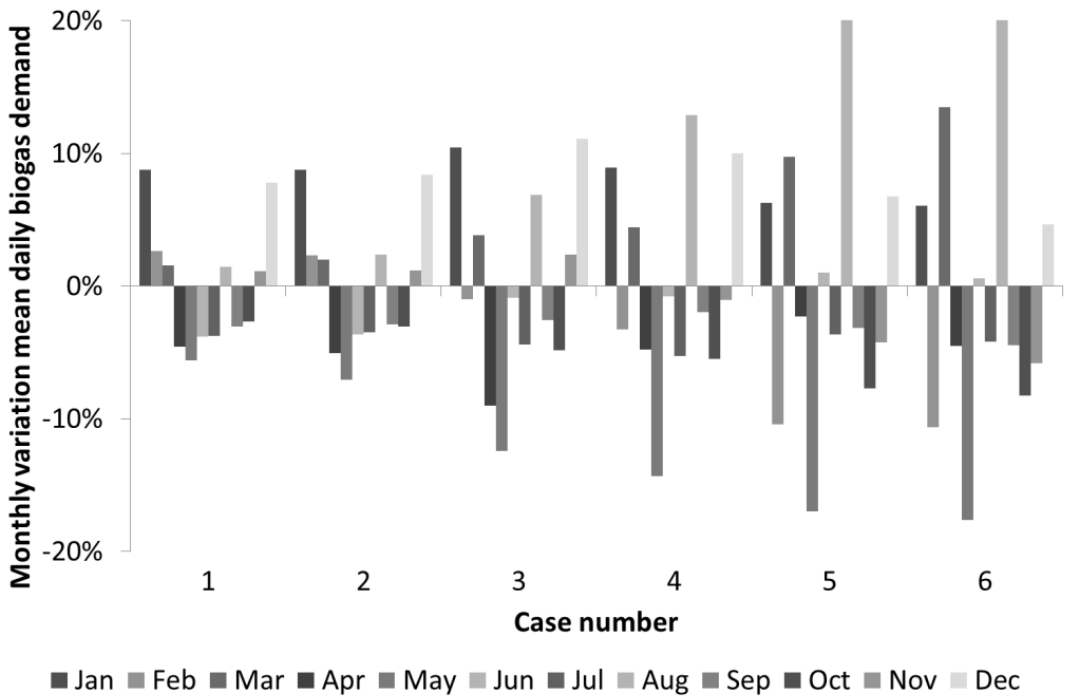

Figure 6.7 Variation in monthly biogas demand for the hybrid energy systems in Cases 1-6.

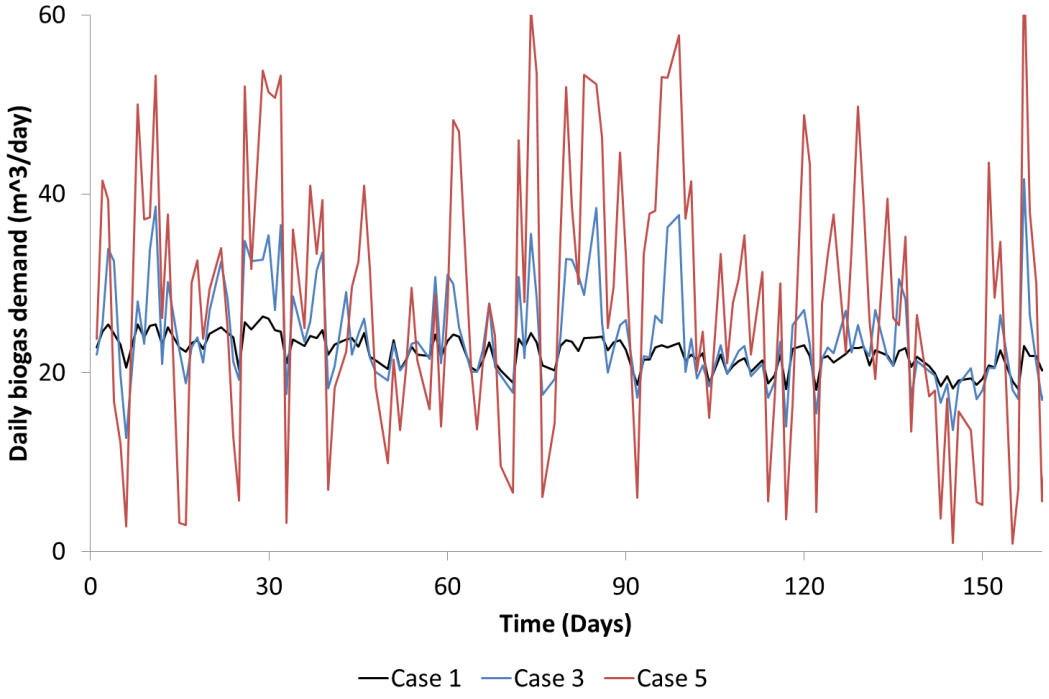

Figure 6.8 150 day excerpt of the daily total biogas demand in cases 1, 3 and 5 (Cases 2, 4 and 6 omitted for visual clarity).

6.3 Modelling of the AD process to meet the demand of an island mode hybrid energy system

In this section the AD model developed in chapters 4 and 5 is used to investigate the ability of an AD system to satisfy the biogas demand profiles developed in the previous section 6.2. Three different operational strategies were developed and *in silico* assessed through a simulation of a year-long operation of the digester:

- Simple operation strategies such as: constant loading rate based on yearly and monthly biogas demand average; and basic feedback control which changes the loading rate depending on the state of the biogas storage (gasometer). These strategies are described in Section 6.3.1.
- Variation of the loading rate of the digester based on a prediction of the biogas demand of the hybrid system. The study is based on the assumption of having accurate 1, 2 and 7 day predictions and how these predictions can influence the AD dynamics and the biogas storage requirements. No detailed investigations are developed regarding the methods available to predict the demand. These strategies are described in Section 6.3.2.
- Expert feedback control which complements the future prediction of the demand of the energy system together with information about of the state of the AD system. In this way the control strategy calculate a loading rate of the digester to satisfy the required loading, provided the conditions of the AD system are within established measured indicators of AD process stability.

The operational strategies are benchmarked against a common set of key performance indicators; biogas storage requirement of the system, expressed as the volume of gas at STP conditions, and maximum and average the total VFAs concentration in the digester. The biogas storage was calculated as the difference between the maximum and minimum volume of the stored biogas over the whole year of simulation. As will be shown, the requirement for storage of biogas in a hybrid energy system with an unsteady biogas demand could become very large relative to the size of the digester and therefore could represent a large cost (and land use) relative to the other system components: hence its importance as an indicator of the suitability of the operational strategy. The VFA concentration, both maximum and average, are used as an indicator of the stress on the AD system. In fact, different operational strategies may be equally able to match the biogas demand, but causing different levels of organic stress and process inhibition. An

operational strategy which satisfies the biogas demand set point while reducing the stress on the system, is therefore preferred and deemed more robust.

For this benchmark study, the ADM1 model was implemented in MATLAB/Simulink (Mathworks, USA). Green waste and food waste were selected as substrate and described with the biochemical and kinetic fractionation parameters estimated in Chapter 4. The model was also updated with inhibition structure and parameters identified in Chapter 5. Despite the lack of validation of this parameter set its use can be justified as a conservative approach since it is more sensitive to organic overload conditions. All other model parameters and structures are as per the default values listed in Rosen and Jeppsson (2006). Finally the model is structurally identical in the Aquasim and Simulink implementations. The Simulink implementation allows rapid testing of a variety of operation strategies, subject to differing demand profiles, due to the user friendly graphical interface and is more suitable than Aquasim for this kind of system based *in silico* testing. The ODE15s solver was used in MATLAB/Simulink, which uses a fourth-order Runga-Kutta method with a maximum step size of 0.002 days

The feedstock for all simulations was a co-substrate of 50% FW and 50% GW by volume. Initial conditions for all studies were determined from a year-long simulation of a digester fed at a steady state loading rate of 3 gCOD L^{-1} day^{-1} .

The biogas demand profiles for Cases 1, 3 and 5 have been chosen for further analysis throughout this section due to their variation temporal biogas demand as shown in Figure 6.8. An increase in the variability in the biogas demand profile is expected to put additional requirements on the AD component of the hybrid system using either increased storage of biogas or a variable loading rate. Biogas demand profiles from cases 2, 4 and 6 have been omitted from this section since they are quantitatively similar to those from Cases 1, 3 and 5 respectively. In order to compare the response of an AD system to the different demand profiles a linear scaling to the digester volume has been made to the average daily biogas demand in each of the three cases using an assumed volumetric biogas production of 2 m^3_{biogas} $m^{-3}_{digester}$ day^{-1} giving digester volumes of 11.0, 12.0 and 14.1 m^3 for Cases 1, 3 and 5 respectively. The assumed volumetric production of 2 m^3_{biogas} $m^{-3}_{digester}$ day^{-1} is in line with the average values achieved during the experimental data in Chapter 5.

6.3.1 Demand matching using simple operational strategies and biogas storage

Given that the focus of the work on hybrid energy systems is on rural electrification in India there is an argument for the operational strategy to be simple and low cost. In this section three simple strategies are proposed to allow the AD system to meet the biogas demand in the three selected cases. These are as follows:

- 'Constant' – The digester is operated at constant loading rate to meet the annual demand, with variations in biogas demand being completely absorbed by the biogas storage.
- 'Monthly' – The loading rate to the AD system is varied proportionately with the forecasted monthly demand of the system as predicted by the modelling in HOMER, with the loading rate step-changed at the beginning of each monthly period. This leads to the loading profiles as shown in Figure 6.9 for Cases 1, 3 and 5.
- 'Feedback' – A simple device for measuring the volume of gas stored in the gasometer is installed in the system and a proportional feedback is applied between the stored volume and the digester loading rate. The controller schematic is shown in Figure 6.10. Since this controller is based on a single sensor (e.g. a proximity infrared or ultrasonic sensor) it is expected to be cost effective.

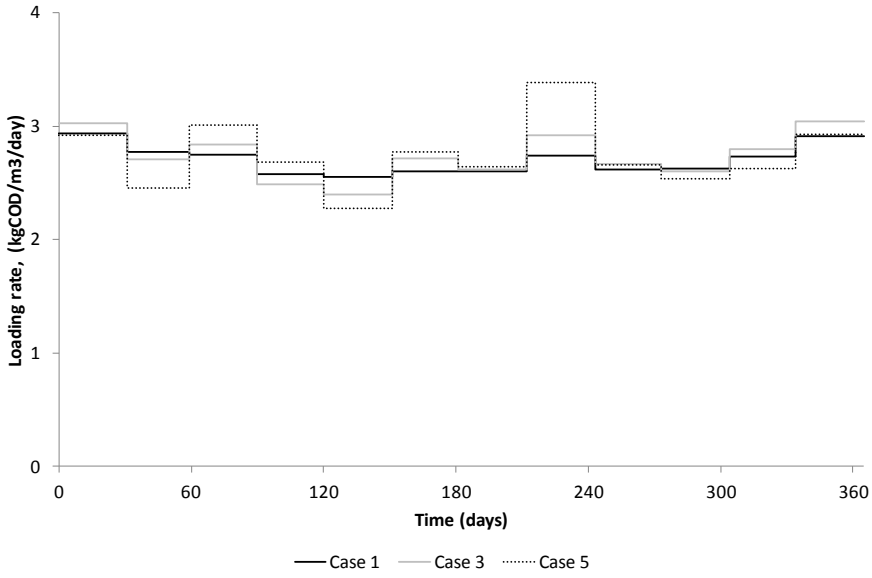

Figure 6.9 Loading rate variations for the 'monthly' strategy for Cases 1, 3, and 5.

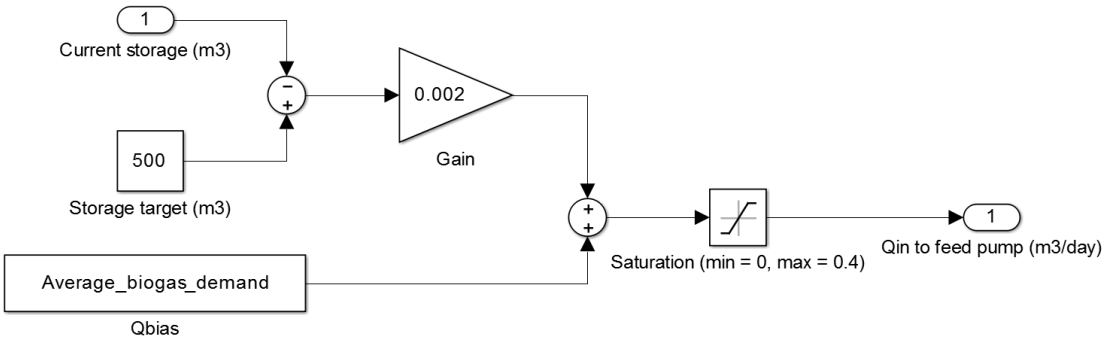

Figure 6.10 Description of simple feedback controller based on stored biogas volume and a bias of average yearly biogas demand.

Results from the benchmark simulations are shown in Table 6.7, which summarises the proposed three operational strategies performances in response to the demand profile of the three energy systems considered (Cases 1, 3 and 5). Figure 6.11-Figure 6.13 show the biogas storage and VFA concentrations over the simulated period of 1 year for the Cases 1, 3 and 5, respectively.

Some comments can be made regarding the performance of the operational strategies but in general all three operational strategies can meet the energy demand for Cases 1 and 2, but process failure occurs when using feedback control to meet the demand in Case 3.

Case 1 demand profile

Constant loading is the worst case scenario, where there is no adaptation of the loading during the year. This results in a large requirement of 150 m^3 (670% of daily demand) for the biogas storage, which is used to cover the higher biogas requirements in monsoon and winter periods. The reactor is operated at a constant loading rate of 5.4 gCOD L^{-1} d^{-1} which results in a HRT of 77 days.

Monthly adapted loading and feedback strategies result in similar important reductions in the required biogas storage, to 38 and 34 m^3 or 170% and 151% of the average daily demand, respectively. These two strategies are able to change the loading rate of the digester, as indicated by the minimum and maximum range of the imposed loadings: between 5.1 and 5.8 gCOD L^{-1} d^{-1} in the case of monthly adaptive strategy and between 5.8 and 6.2 gCOD L^{-1} d^{-1} in the case of feedback strategy. Higher loading rates leads also to higher organic stress, as indicated by the maximum concentration of VFA reached in the digester: 0.56 gCOD L^{-1} for both the adaptive and feedback strategy, compared to a lower level of 0.38 gCOD L^{-1}

which was achieved in the case of constant loading. The maximum VFA level is reached across December-January when is higher the biogas demand.

Case 3 demand profile

Constant loading is again characterised by a very large storage requirement of 236 m^3 (959% of daily demand). This is even greater than case 1 due to increased quantity and variability in demand.

Monthly adapted loading and feedback strategies allow again a reduction in the required biogas storage to 84 and 76 m^3, respectively, compared to constant loading. However they show differences in the process stability, with feedback strategies producing higher concentration of VFA at 1.39 gCOD L^{-1} compared to 0.59 gCOD L^{-1} of the monthly adapted. In fact the feedback strategy impose a wider range of loading rates between 3.7 and 7.3 gCOD L^{-1} d^{-1} compared to 4.8 and 6.1 gCOD L^{-1} d^{-1} of the monthly adapted. Figure 6.7 shows how the energy demand peak for case 3 occurs in December, while from Figure 6.12 it is evident how the VFA peak occurs for both strategies during the month of August. The difference can be explained by a more abrupt change in energy demand occurring in August relatively to previous months, while a more gradual increase leads to the peak in energy demand in December. It can be concluded how both the relative change and absolute values of loading rates are both influencing the process stability.

Case 5 demand profile

The constant and monthly operational strategies were both able to meet the demand whereas the simple feedback controller caused several process instabilities and eventually a failure of the process indicated by an increased VFA concentration (>20 gCOD L^{-1}), decrease in pH and large decrease in methane content of the biogas.

Despite being able to meet the demand, the constant and monthly operational strategies still require a very large storage of biogas, 372 and 254 m^3 respectively (1368% and 933% of daily demand respectively). This could significantly affect the system cost, and it is not taken into account in the original HOMER economic optimisation.

The monthly adapted strategy involves a large change in loading rate in August (Figure 6.9) which leads to an accumulation of VFA in the digester to 2.67 gCOD L^{-1}

(Figure 6.13), part of which is converted to biogas in the following month when the biogas demand is lower.

The failure of the system using the feedback strategy occurs during March when there is an increase in the biogas demand and therefore the controller attempts to compensate for this. However, the fast nature of the feedback controller imposes a too high loading rate to the digester (up to 8.1 gCOD L^{-1} d^{-1}), which imbalance the process stability through VFA accumulation, inhibition on the methanogenic step and finally further VFA accumulation and consequent process collapse.

Some conclusions can be drawn from the previous analysis, regarding the characteristics of the proposed operational strategies.

- Constant feeding results unfeasible in all cases, as would lead to excessive storage requirements to satisfy the year-round energy demand.
- Monthly adapted feeding performs well in Cases 1 and 3, while with the most demanding gas profile of Case 5 storage requirements become hardly sustainable. Variations in loading rates are more limited than in feedback strategy, and process stability is maintained in all cases.
- Feedback strategy gives the lowest storage requirements, as it is able to follow more closely the biogas demand profile. However this rapidity of action, which neglects the knowledge of the state of AD system, introduces additional stress into the AD system, and can lead to process failure as it was shown in the Case 5.
- Feedback control does not require any knowledge of future energy demand, and is based on cost-effective measurements of the gas storage: this could be considered an advantage in terms of simplicity of the controller implementation. To reduce the risk of process imbalance, the digester could be slightly over-dimensioned with respect to the yearly energy demand, i.e. a lower value of the volumetric productivity could be used in the design phase. The relations between storage and additional digester capacity on an economic bases could further be analysed in future studies. Feedback control which incorporates also the knowledge of the state of the AD process is considered in Section 6.3.3.
- Process imbalances occur at loading rates above 8 gCOD L^{-1} d^{-1} which are similar to the values which caused imbalance in the experimental trials in chapter 5. An absolute threshold value however cannot be determined *a priori*, as process imbalances are also the result of the duration of the high-loading periods together with the previous history of the digester; abrupt changes in

loading rates are in fact more destabilising than gradual increases, as a larger microbial community for VFAs uptake can be developed in the latter case.

Demand profile	Loading strategy	Biogas storage	VFA (max)	VFA (average)	Demand met	HRT (max)	HRT (min)	Process failure
#		m^3	kg m^{-3}	kg m^{-3}	Yes/No	days	days	#
1	Constant	150	0.38	0.38	Yes	77	77	NA
	Monthly	38	0.56	0.38	Yes	81	71	NA
	Feedback	34	0.56	0.39	Yes	91	67	NA
3	Constant	236	0.56	0.38	Yes	77	77	NA
	Monthly	84	0.59	0.40	Yes	87	68	NA
	Feedback	76	1.39	0.43	Yes	112	57	NA
5	Constant	372	0.38	0.38	Yes	77	77	NA
	Monthly	254	2.67	0.52	Yes	91	61	NA
	Feedback	NA	20.45	11.60	No	166	51	March

Table 6.7 Summary of AD system performance characteristics using simple operational strategies for biogas demand matching in cases 1, 3 and 5.

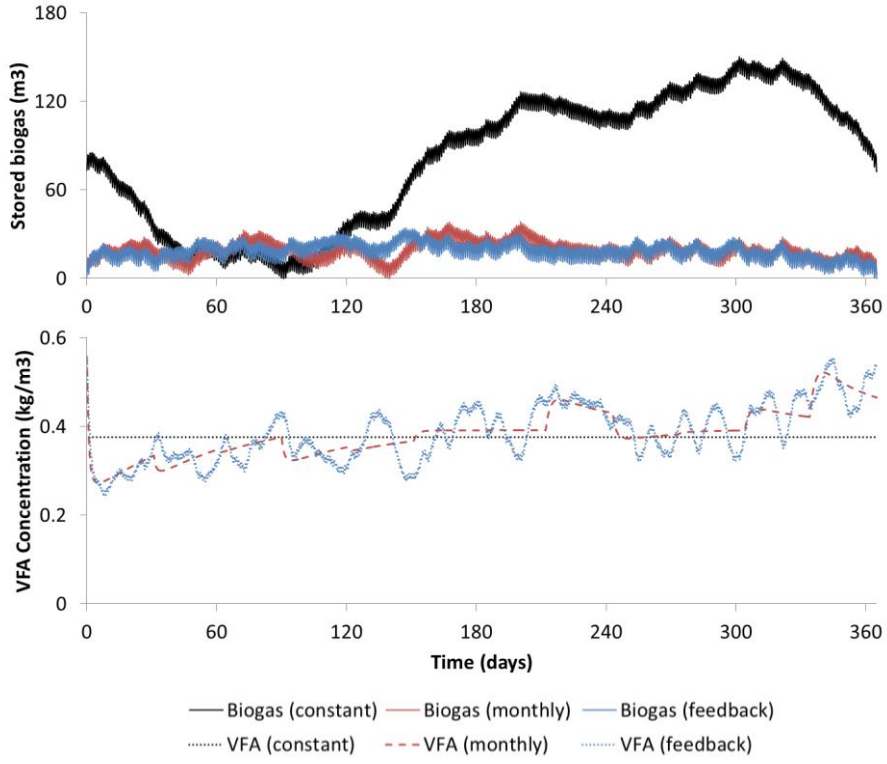

Figure 6.11 Biogas storage requirement and VFA concentration for biogas demand from Case 1 using simple operating strategies.

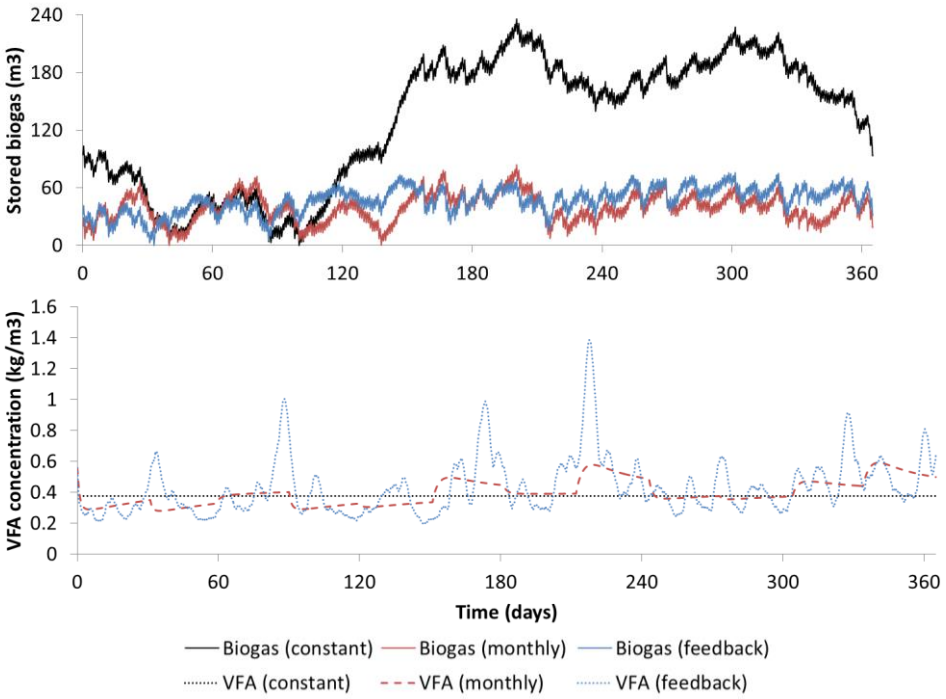

Figure 6.12 Biogas storage requirement and VFA concentration for biogas demand from Case 3 using simple operating strategies.

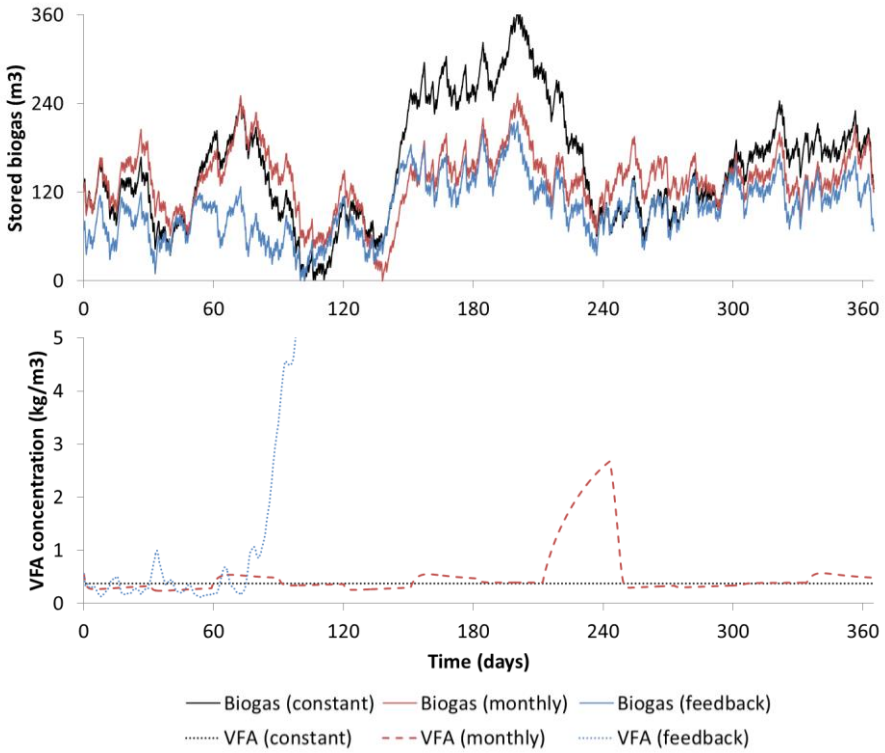

Figure 6.13 Biogas storage requirement and VFA concentration for biogas demand from Case 5 using simple operating strategies.

6.3.2 Demand matching using prediction of biogas demand

The previously explored monthly adaptive control strategy could be further refined by considering different lengths of the biogas demand forecasting. Recent research has been very active both in investigating methods for forecasting the demand side (as reviewed by Suganthi and Samuel (2012)) and methods for the forecast of intermittent energy supplies, such as PV (as reviewed by (Diagne et al. (2013)) and wind (as reviewed by Soman et al. (2010)). Based on the availability of this information, control strategies for the integrated energy system have been developed to optimally manage the controllable elements of the system (Palma-Behnke et al., 2013, Chen et al., 2011). It goes beyond the scope of this work to analyse and implement an appropriate supervisory control of the integrated energy system, and only the effect of the forecasting window on the AD system operation is evaluated.

Three different demand matching strategies based on differing timescales of prediction (1 day, 2 day and 7 day) were assessed against the same three biogas demand cases as in Section 6.2.1. The predictions in this case were the actual demand profiles as supplied from HOMER, with forward averages over the timescales of the prediction. In reality there would be some expected variation between the predicted demand and the actual demand which is not accounted for in this modelling. An example of the load profile calculated from the Case 3 biogas demand profile is shown in Figure 6.14. The contrast between the loading profiles based on 1 and 7 day predictions is shown: the 1 day prediction loading tracks the biogas demand closely, with a phase shift of 1 day; whereas the 7 day prediction loading profile has the effect of smoothing the day to day variation of the biogas demand.

The results from a year round simulation of the AD system for the three demand profile Case 1, 3 and 5 and applying the three different prediction timescales are summarised in Table 6.8. Figure 6.15 focuses on the results of the demand profile case 3 using prediction timescales of 1 and 7 days: substrate loading profile, VFA concentration and required storage of biogas.

Some comments can be made regarding the effect of the different prediction timescales. For the demand profiles Cases 1 and 3:

- All prediction timescales were able to satisfy the biogas demand.
- The length of prediction gave several benefits:

- A reduction of the stress indicators, especially in Case 3, where the VFA concentration is highest for the 1 day prediction timescale at 1.72 gCOD L^{-1} d^{-1} and decreases to 1.43 gCOD L^{-1} d^{-1} for the 7 day timescale. This can be attributed to the smoothing of the loading rate variations when applying a longer timescale, while rapid changes in loading rate cause short term accumulations of VFA in the AD system, as can be seen in Figure 6.15.
- A slight reduction in biogas storage size: for the biogas demand Case 1 the volume is 29 m^3 for the 1 day prediction timescale, 27 m^3 for the 2 days prediction and 23 m^3 for the 7 days prediction; for the biogas demand Case 3 the volume is 50 m^3 for the 1 day prediction timescale, 47 m^3 for the 2 days prediction and 47 m^3 for the 7 days prediction. Although the differences are narrow, these results are an indication that too short a timescale does not correspond to a better following of the biogas demand. This can be further explained by considering the time constant for the AD system which, for a simpler case of hydrolysis limited system, corresponds to the inverse of the hydrolysis rate constant. The time constant represents the time it takes a system's step response to reach 63.2% of its final (asymptotic) value (Ljung, 1998), which for the AD system would correspond to the complete substrate methanisation after its step loading. In the case of FW and GW, it results in a time constant of approximately 5 days for the slowly degradable fraction and 5 hours for the readily degradable fraction. It is therefore clear how a too short timescale prediction would neglect the dynamics of the slow degrading fraction, which eventually could be overloaded and produce unnecessary biogas beyond the forecasting window, therefore resulting in an increased biogas storage.

- Compared with the monthly adapted strategy analysed in Section 6.3.1, it is evident how a better forecast of the biogas demand leads to significant reductions in the required biogas storage. While monthly adapted loading required 38 m^3 (Case 1) and 84 m^3 (Case 3) of storage, the 7 days predictive strategy is able to decrease the requirement down to 23 m^3 (Case 1) and 47 m^3 (Case 3), equal to 104% and 191% of the daily biogas demand. Moreover this benefit does not correspond to a significant increase of the stress indicators, with a maximum VFA concentration in the case 3 of 1.43 gCOD L^{-1} d^{-1} for the predictive strategy, compared to 0.59 gCOD L^{-1} d^{-1} for the monthly adapted.

The demand profile Case 5 shows some differences in the results:

- The predictive strategy was unsuccessful in meeting the biogas demand of Case 5 and in all three prediction timescales the temporal variability of the loading rate caused instability and eventual process failure.
- The failure time occurs later for the 7 day prediction (July), compared with the 1 and 2 day prediction, another indication the smoothing reduces excessive (and unnecessary) changes in loading.
- A further investigation was realized to analyse the effect of the digester size on the benchmark indicators for the 7 day prediction and demand profile Case 5. Figure 6.16 shows that the for safe operation the digester, the volume should be increased from 14.1 m^3 to above 15.9 m^3 where the biogas storage requirement is reduced to 140 m^3 with maximum and mean VFA concentration of 6.39 gCOD L^{-1} and 1.15 gCOD L^{-1}, respectively. Increasing the digester volume further decreases the storage requirement and VFA concentration e.g. at 20 m^3 digester size the storage requirement is 120 m^3 and maximum and mean VFA are 2.86 and 0.42 kg m^{-3}, respectively. This analysis points out how the AD system dynamics are highly non-linear, and a small variation is one variable (e.g. volume) greatly influences the values of other variables (e.g. VFA concentration). It also highlights the usefulness of model-based design in showing complex relationships between the various design parameters of an AD system.

From the analysis presented in this section, it can be concluded that a prediction based operational strategy achieves a better performance than the simpler operating strategies analysed in section 6.3.1, achieving smaller biogas storages with acceptable stress indicators. The prediction horizon should be chosen considering the time constants of the AD system, which in a first approximation can be obtained from the hydrolysis rate constants. However, this operational strategy does not perform satisfactorily with challenging demand profiles as in the case 5. The controller would impose excessive changes in the loading profile to follow the variations in the biogas demand, leading to process imbalances (as also happened in the case of the feedback controller examined in section 6.2.1). Again, a possible improvement in the performance of the controller could come from a knowledge of the state of the digester, and this will be explored in the next section.

It was shown how the volume of the digester is a highly sensitive design parameter on the ability of the system to cope with the challenging dynamics. For this analysis, the size of the digester was calculated based on the possibility of satisfying the overall yearly demand, using a conservative volumetric productivity value. However

this approach cannot take into account the effect of varying loading rates. Therefore, model based design should be used to achieve a better initial design of the digester, which takes into account the possible dynamics of the biogas demand.

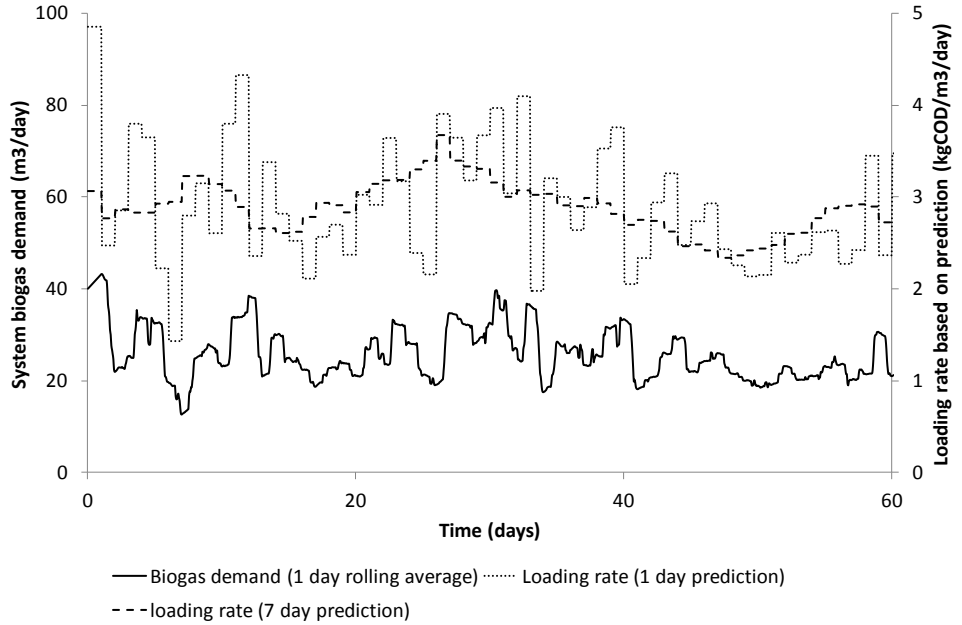

Figure 6.14 Example of the loading rate profiles for the 1 and 7 day predictions calculated from the case 3 biogas demand of the period 0-60 days.

Demand profile	Prediction (rolling average)	Biogas storage	VFA (max)	VFA (average)	Demand met	HRT (max)	HRT (min)	Process failure day
#	days	m^3	kg m^{-3}	kg m^{-3}	Yes/No	days	days	#
1	1	29	0.59	0.39	Yes	94	63	NA
	2	27	0.59	0.39	Yes	91	65	NA
	7	23	0.61	0.39	Yes	89	65	NA
3	1	50	1.72	0.47	Yes	145	39	NA
	2	47	1.62	0.46	Yes	114	45	NA
	7	47	1.43	0.43	Yes	104	45	NA
5	1	NA	21.59	11.53	No	77	77	April
	2	NA	21.42	11.02	No	91	61	April
	7	NA	21.76	6.96	No	166	51	July

Table 6.8 Summary of system performance characteristics using prediction based loading strategies for biogas demand matching in cases 1, 3 and 5.

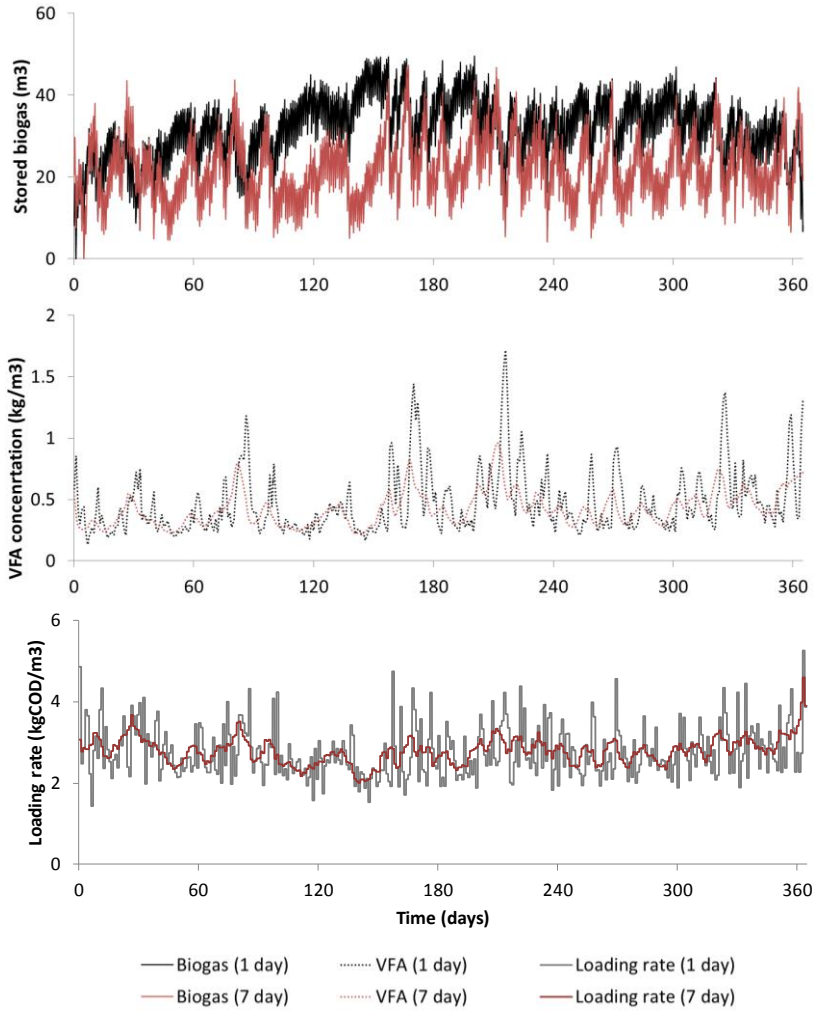

Figure 6.15 Biogas storage requirements, VFA concentration and loading rate profile for biogas demand from the Case 3 using 1 and 7 day prediction based loading profiling.

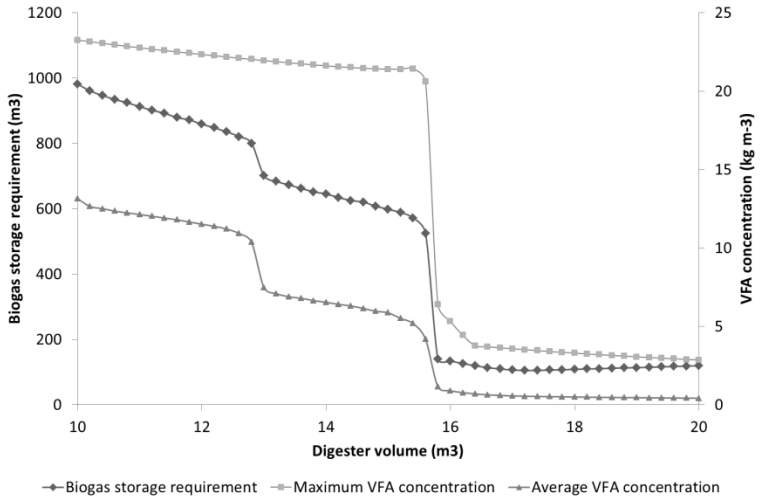

Figure 6.16 Variations in biogas storage requirement and VFA concentration with digester working volume in meeting the Case 5 biogas demand using 7 day prediction based loading.

6.3.3 Expert control for AD demand matching

As was seen in previous sections, when the operation of the digester is driven by a highly variable biogas demand, process imbalances easily occur and both the simple operational strategies from Section 6.3.1 and the prediction based load profiling from Section 6.3.2 could not avoid process collapse or otherwise required unsustainable gas storages.

Therefore a further controller was developed which includes an evaluation of the state of the AD systems and which mimics the kind of 'feedback control' that an expert operator may perform based on 3 objectives:

- Maintaining the storage of biogas in the central position (half full) to avoid possible waste of production, or inability to meet demand by changing the loading rate.
- Matching the supply of biogas with the demands of the system by changing the loading rate.
- Use pH measurements as a proxy of the stability of the process, due to its link with VFA concentration, and to reduce the loading rate when pH drops.

The proposed controller architecture is shown in Figure 6.17 and the control algorithm therefore can be summarised as follows:

1) *Check the stored biogas volume and generate a gain equal to the difference between the stored biogas volume and the storage set point multiplied by a gain coefficient p1.*
2) *Check the biogas production rate and generate a gain equal to the difference between the biogas production rate and the set-point for the biogas demand, multiplied by a gain coefficient p2. The biogas demand set-point can be the current demand of the system (e.g. the MT biogas usage) or estimated from prediction over a certain horizon time.*
3) *Sum the gains from 1 and 2.*
4) *Check the pH of the digester and apply a "soft switch" as follows;*
    a. *If the pH is greater than a previously established pH upper safety point (pHs) then generate a gain of 1.*
    b. *If the pH is below a pHs – 0.1 then generate a gain of 0.*
    c. *If the pH is between a) and b) then interpolate to generate a gain between 0 and 1.*

5) *Multiply the results of 3) and 4) and add to the loading bias (lb), which represents the approximate loading rate to meet the average biogas demand of the system.*
6) *Limit the result to an established maximum value to simulate the pumping capacity of the feed pump.*
7) *Pass the resulting value to the digester feeding pump as the required flow rate in m^3 day^{-1}.*

The value pH safety point depends mainly on the substrate characteristics and its charge balance and buffer characteristics, as explored in previous Chapters 3 and 4. The maximum limit of the flow rate as applied in point 6 depends as well on the substrate characteristics and on the size of the digester. After some preliminary testing and manual tuning of the controller, the values given in Table 6.9 were selected for the benchmark study. The biogas demand set-point can be ideally derived from a prior knowledge of the energy system or otherwise from a hypothetical supervisory controller. Three examples were chosen for this analysis:

- 'Monthly' – the biogas demand input to the controller is equivalent to the known monthly average demand, which was used to calculate the feeding rate in Section 6.2.1, i.e. a step change in loading rate for each calendar month.
- '7 day' – the biogas demand input to the controller was equivalent to the weekly rolling average demand (i.e. prediction based as per Section 6.3.2) .
- 'Responsive' – the controller was supplied with the current biogas demand (i.e. the MT usage).

The results of the simulations are shown in Table 6.10, while Figure 6.18 shows storage volume, VFA concentration and loading rate profile for the 3 demand controller input signals. Some observations can be made as follows:

- When using monthly predictions, compared with the results from Section 6.3.1, resulted in only a marginal reduction in storage requirement (254 to 252 m^3). This can be expected since the controller is simply attempting to meet the monthly average demand. The process remained stable, similarly as it occurred previously in section 6.3.1. The peak VFA was slightly higher (3.65 cf. 2.67 gCOD L^{-1} day^{-1}, see Table 6.10 and the profile in Figure 6.18) due to the a higher fluctuations in loading rate caused by the response of the controller to the current stored biogas volume.
- Supplying the controller with 7 day predictions resulted in the system successfully meeting the biogas demand, in contrast to the system failure using

the prediction based loading as described in Section 6.2.2. This is due to the expert element of the controller and as can be seen in Figure 6.18, the controller sacrifices biogas demand matching in order to avoid the organic overload condition. This is especially noticeable in August, where the increased demand produces an initial increase in VFA concentration. The increase in VFA concentration results in a drop in the pH which stabilises the loading rate. Although the storage gets depleting during August, this not results in an increase in the loading rate; instead the controller maintains a steady loading which eventually allows the system to recover from the VFA accumulation. The required biogas storage is the smallest amongst the three scenario analysed at 174 m^3.

- The responsive mode scenario again shows the strength of the controller to balance the demand matching capability with the organic stress condition, with a similar behaviour during the month of August as explored above. The total storage requirement is at 256 m^3, similar to the "monthly" scenario (c.f. 254 m^3).

The controller relies on accurate pH measurements – which may have cost and O&M implications. Biogas storage and flow rate are not so difficult. This is why pH controllers are not favoured in practice and even in the literature. However the point of this section was to demonstrate the application of the model rather than propose a control architecture that was appropriate for rural systems.

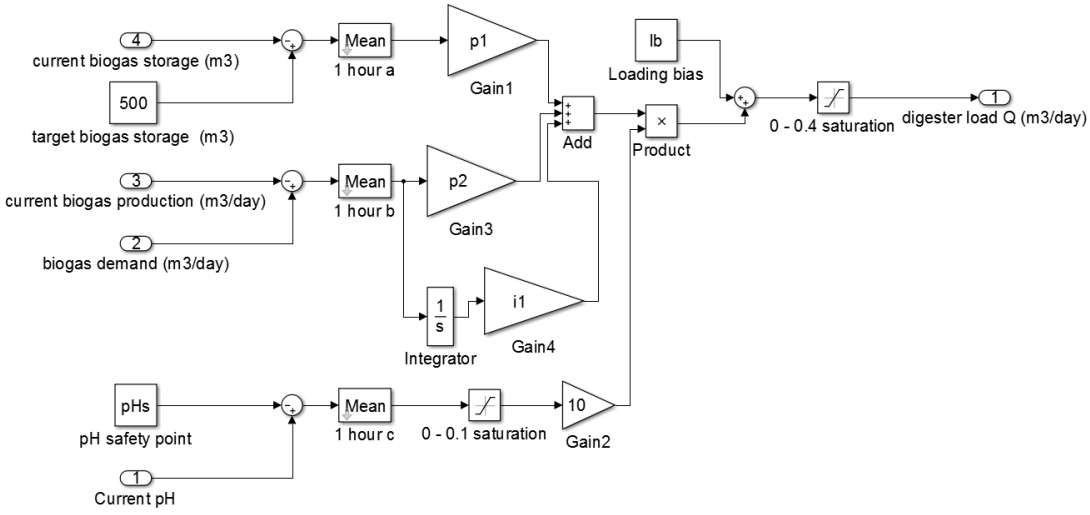

Figure 6.17 Proposed expert controller architecture.

Parameter	Description	Default value
p1	Storage proportional gain	0.0025
p2	Biogas production/demand proportional gain	0.01
i1	Biogas production/demand integrated gain	0
pHs	pH safety value	7.75
lb	Load bias	0.18

Table 6.9 Default parameters of the controller using manual tuning.

Demand signal supplied to controller	Biogas storage	VFA (max)	VFA (average)	Demand met	HRT (max)	HRT (min)
	m^3	kg m^{-3}	kg m^{-3}	Yes/No	days	days
Monthly prediction	252	3.65	0.83	Yes	162	56
7 day prediction	174	2.61	0.58	Yes	150	51
Current demand (responsive)	256	3.87	1.24	Yes	364	42

Table 6.10 Performance of controller in matching Case 5 system biogas demand with monthly predicative, 7 day predictive and current demand (responsive) biogas demand controller input.

Controller optimisation

As well as controller testing and benchmarking, it is also possible to use the developed ADM1 implementation in Simulink in order to tune, or optimise, the control parameters to meet a particular control objective in the chosen scenario. In order to demonstrate this, the Simulink Design Optimisation toolbox (Least square non-linear search algorithm) was used to minimise the required biogas storage requirement in the same three scenarios presented in this section; namely the controller input biogas demand was ‘Monthly’, ‘7 day’ or ‘responsive’. The control architecture was maintained as per Figure 6.17 but the 5 parameters were allowed to vary as per the optimisation algorithm.

In each of the three scenarios, a different optimised parameter set was found, and these are given in Table 6.11 and in each case, significant benefits were demonstrated in the reduction of the storage requirements of 7-32% as shown in Table 6.12. Interestingly, in all cases this reduction in demand was paired with an increase in the stress indicators, which demonstrated that increasing the demand matching responsiveness of the controller in general led to more rapid changes in loading rate which in turn caused an increase in stress indicators.

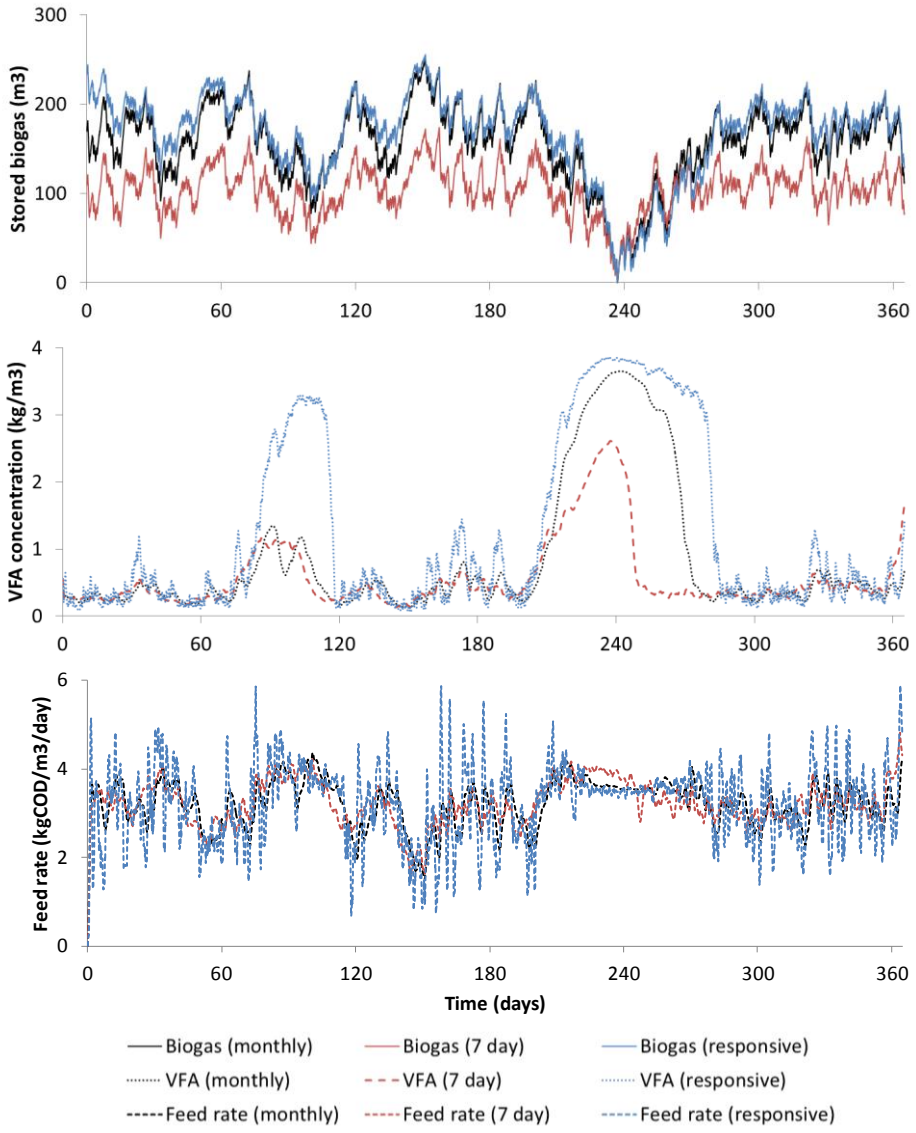

Figure 6.18 Biogas storage requirements, VFA concentration and feed rate variation for the AD and controller with Case 5 system biogas demand using monthly predicative, 7 day predictive and current demand (responsive) biogas demand controller input.

In each case, the parameters were tuned to a particular demand profile (supplied to the controller) and therefore there is again the question of the sensitivity of the optimised parameter set to the conditions of the optimisation, which has not been explored. It is worth mentioning that in all cases, the optimised parameter set were of the same order of magnitude as the original manually tuned parameters, and in the case of pHs and lb varied by less than 1 and 6%, respectively. This could indicate that either the original parameters were a good estimate of an optimal solution, due to expert knowledge of the modeller, or that the parameters were close to a local minima in the objective function and therefore may not represent a true optimal solution.

Parameter	Default value (manual tuning)	Optimised controllers		
		Monthly	7 day	Responsive
p1	0.0025	0.0052	0.0029	0.0020
p2	0.0100	0.0101	0.0201	0.0045
i1	0.0000	0.0053	0.0000	0.0000
pHs	7.7500	7.7354	7.7408	7.7667
lb	0.1800	0.1695	0.1885	0.1886

Table 6.11 Optimised controller parameters using monthly and 7 day predictive, and current demand (responsive) biogas demand controller input of the case 5 biogas demand.

Demand supplied to controller	Biogas storage	c.f. default	VFA (max)	c.f. default	VFA (average)	c.f. default
	m^3	%	kg m^{-3}	%	kg m^{-3}	%
Monthly demand prediction	170	-32%	4.33	+19%	0.94	+13%
7 day demand prediction	162	-7%	3.18	+22%	0.63	+8%
Current demand (responsive)	207	-19%	2.26	-42%	0.62	-50%

Table 6.12 Performance of optimised controller in matching case 5 system biogas demand with monthly predicative, 7 day predictive and current demand (responsive) biogas demand controller input and comparison with default controller parameters.

6.4 Conclusion

This chapter has explored the role that AD can play in off grid hybrid energy systems for rural electrification. The modelling software HOMER was used to design an optimal (economically) system containing several elements such as PV, MT CHP, AC/DC converter; because the modelling of AD and biogas storage is beyond the scope of HOMER, the ADM1 model developed in previous chapters 3-5 was used to investigate the operation and design of this system component. In order to do this additional demand profiles were developed with varying levels of challenge in terms of temporal variations in biogas demanded by the hybrid energy system.

For biogas demand profiles with small day to day variations it was found that simple operating procedures, such as monthly variations in loading rates based on expected overall demand, were sufficient although resulted in relatively large biogas storage requirements. Improvements were found by introducing biogas demand predictions over a timescales from 1 to 7 days, which resulted in a large reduction

in the requirements for stored biogas since the AD system was able to meet the biogas demand more closely.

For more challenging biogas demand profiles, a different approach was required since simple operating and prediction based strategies either resulted in huge biogas storage requirements, or failure of the AD system due to organic overload. In this case the calibrated ADM1 model allows exploration of the feasibility of a variety of options in meeting the system demand, e.g. system scale (digester vs. storage requirement) and control/operational strategies. It was found that adding an expert control, as well as increasing the size of the digester, both allowed better demand matching and reduced organic stress on the AD system.

The work performed in this chapter demonstrates that the developed ADM1 model could allow short-listing of best options which could go forward for techno-economic assessment and therefore be used as a decision making tool during the system design stage:

- in particular increasing the size of the digester yielded a reduction in biogas storage and vice-versa.
- Controller optimisation allowed a reduction in biogas storage which was even more marked when combined with demand forecasting.

However there are several weaknesses to this approach including;

- The modelling (neither HOMER or ADM1) does not take into account feedstock variability or any other variation that can occur in real AD systems (e.g. flow rate control may be difficult – this can be resolved by having a fixed flow rate and timed pulses for loading – this also could be investigated in the model).
- The current demonstration does not take into account biogas composition changes which occur during the transient conditions of loading rate. Biogas demand from HOMER uses a constant composition of 62% methane in biogas to calculate the energy output from MT. This could be addressed with more time but the main point of this chapter is to demonstrate application rather than to produce definitive results.
- Tuned controller, or design decisions, could be very sensitive to a variety of model parameters in both HOMER and ADM1 – this would need to be further understood using local or global sensitivity analysis

Using both the developed ADM1 model and HOMER micro-grid modelling it should be possible to perform more in depth analysis of a variety of design and operational decisions, and even to incorporate economic analysis into the model and decision making process.

7 Conclusions and future work

7.1 Conclusions

This thesis has explored new developments of ADM1 in order to better describe the kinetics of biogas production in an AD system with particular focus on substrate characterisation, codigestion and the mechanisms of inhibition. The resulting model was used to explore the possible role of AD in microgrid systems for rural electrification.

Chapter 4 explored a novel biochemical and kinetic fractionation method which was used to characterise feedstock inputs for ADM1 using different hydrolysis model structures. It was shown that the required fractionation complexity (i.e. number of distinct kinetic fractions) is a reflection of the substrate complexity and a range of 4 feedstocks were characterised including food waste (FW), green waste (GW), pig manure (PM) and oat residues (OAT) . The proposed method of estimating the kinetic parameters, using experimental data and explicit numerical calibration and uncertainty estimation, constitutes an improvement on the fractionation methods employed by Girault et al. (2012) and García-Gen et al. (2015), which were based on ambiguous visual interpretations of the methane flow rate.

A key result was that the extent of degradation (and therefore methane production) is rather independent of the testing platform and batch tests (simpler to implement than semi-continuous tests) can be safely used when planning and designing AD systems. However the kinetic parameters showed significant differences between batch and semi-continuous testing and therefore the latter is required for an accurate kinetic description.

Experimental data were used to successfully validate both the codigestion modelling methodology and the substrate fractionation method. The model (with default inhibition parameters) was able to predict the behaviour of the experimental system including the effect of water dilution, but excluding the periods of high organic loadings. Another application of the model was to perform a model based assessment of the synergistic/antagonistic effects of codigestion. In the examined case of FW and GW, a slight synergistic effect was detected in terms of increased overall methane production; although it was not possible to ascertain whether the effect was due to a higher degradability of the substrate or a faster rate of degradation of the slowly degrading fraction. The investigation into the important

inhibition mechanisms found that the best model fit of the experimental data included inhibition by LCFA on acetoclastic methanogens, and of undissociated VFA on fermentation, acetogenesis and both types of methanogens. When validated against the whole experimental datasets the model with the selected inhibition parameter set showed poor agreement and predicted inaccurate process collapse.

Chapter 6 demonstrated the use of the updated version of ADM1 (developed in Chapters 3-5) for *in silico* benchmarking of operation and control strategies for an AD system meeting the variable biogas demand of microgrid system. Microgrid modelling software HOMER was used to develop realistic biogas demand profiles with varying levels of challenge to the AD system in terms of daily and seasonal variation in demand. In the simplest case of a biogas demand profile with low variability, simple rule-based operational strategies could be used without requiring huge quantities of storage of biogas or causing process instabilities. With more variable demand profiles the situation changed and in order to reduce biogas storage requirements and guarantee stability either an over-dimensioned digester or an expert control system is required.

7.2 Future work

7.2.1 Improvement in kinetic fractionation methods

As was shown in this work, batch tests offer a simple way of describing substrate characteristics, however this is highly sensitive to the accuracy of the initial conditions and adaptation of the inoculum to the substrate. Therefore repeated semi-continuous experiments may offer advantages. In this regard, repetition of feedings increases the amount of data and therefore improve the identifiability of the parameters. Optimal design of experiments can be performed prior to the experiment to evaluate the adequate amplitude and number of feedings that will achieve a satisfactory uncertainty in estimated parameters; the influence of uncertainty on the initial biomass condition could also be evaluated. Also, it will be possible to evaluate the effect of biomass concentration and its uncertainty and therefore select an appropriate inoculum/substrate ratio which will limit the accumulation of intermediates.

Multivariate estimation, including further measurements (in addition to methane flow) could lead to the calibration of further parameters; promising would be the on-

line measurement of gas composition, which could allow to differentiate between the hydrolysis of carbohydrates, proteins and lipids. In this work a cost-effective methane analyser was developed and implemented and could be an easy add-on to laboratory scale experiments.

7.2.2 Comprehensive AD integration into microgrid

As an extension to the work presented in Chapter 6 of this thesis it is suggested that many improvements could be made to make the results more comprehensive and realistic, specifically the follow items would improve the work:

- Incorporation of all forms of uncertainty into the modelling, such as:
    - Substrate variations (composition, moisture content).
    - Substrate availability/shortage/alternatives.
    - Feeding rate variations.
- Techno-economic assessment of the AD model, including the potential control systems and feedstock costs.
- Effect of changing biogas quality due to feeding rate fluctuations, changes in the feedstocks, on the downstream applications.
- Extending the control architecture to include the whole microgrid operation. In fact the control strategy of the mini-grid should, at one level (primary control), maintain grid stability and, at the other level (secondary, or supervisory, control), optimize the operation of the power sources, energy storage units and controllable loads.

7.2.3 Advanced control systems

A natural progression from the work on microgrid modelling is to investigate the applicability of advanced controllers to the problem of demand matching for AD systems. There is support in the literature that model predictive control (MPC) can oversee the operation of an AD system and maintain productivity and stability in the face of disturbances and changes in methane production setpoint (Ordace et al., 2012). Model based predictive controllers take into account not only the past information, but also predictions of the future behaviour of the system, and are indicated when dealing with time varying setpoints (Haugen et al., 2014). However this type of controller still needs further development and testing in the following ways:

- Using validated complex models (ADM1) calibrated on data collected from AD experiments, thereby ensuring that the reduced model used by the MPC represents the real AD process effectively, thus leading to a better control design and performance.
- Implementation on systems fed on a solid waste, such as those in this thesis, with continuous monitoring of simple variables such as biogas flow, biogas composition and pH.
- Implementation on full or pilot scale systems.
- Under a demand matching regime i.e. with a variable methane production setpoint to compensate the energy fluctuations of the larger system.

The work could be kick-started with an initial *in silico* testing of the MPC controller using the modified ADM1 model developed as part of this work. This would allow evaluation of the influence of the controller parameters (e.g. control and prediction horizon) on the controller performance. MPC development could make use of MATLAB MPC toolbox and the whole simulation could implemented in the Simulink environment.

References

ABBASSI-GUENDOUZ, A., BROCKMANN, D., TRABLY, E., DUMAS, C., DELGENÈS, J.-P., STEYER, J.-P. & ESCUDIÉ, R. 2012a. Total solids content drives high solid anaerobic digestion via mass transfer limitation. *Bioresource Technology,* 111**,** 55-61.

ABBASSI-GUENDOUZ, A., BROCKMANN, D., TRABLY, E., DUMAS, C., DELGENÈS, J.-P., STEYER, J.-P. & ESCUDIÉ, R. 2012b. Total solids content drives high solid anaerobic digestion via mass transfer limitation. *Bioresource Technology,* 111**,** 55-61.

AHRING, B. K., SANDBERG, M. & ANGELIDAKI, I. 1995. Volatile fatty acids as indicators of process imbalance in anaerobic digestors. *Applied Microbiology and Biotechnology,* 43**,** 559-565.

AICHINGER, P., KUPRIAN, M., PROBST, M., INSAM, H. & EBNER, C. 2015. Demand-driven energy supply from stored biowaste for biomethanisation. *Bioresource Technology,* 194**,** 389-393.

ALFERES, J. 2012. Evaluation of performance robustness of anaerobic digestion. *3rd IWA/WEF Wastewater Treatment Modelling Seminar.* Quebec, Canada: IWA publisher.

ALFERES, J., VANROLLEGHEM, P. & IRIZAR, I. Design procedure for anaerobic digestion controllers aimed at feasible full-scale application. Proceedings IWA World Water Congress 2012, 2012 Busan, South Korea.

ANGELIDAKI, I., ALVES, M., BOLZONELLA, D., BORZACCONI, L., CAMPOS, J., GUWY, A., KALYUZHNYI, S., JENICEK, P. & LIER, J. B. 2009. Defining the biomethane potential (BMP) of solid organic wastes and energy crops: a proposed protocol for batch assays. *Water Science and Technology,* 59**,** 927-34.

ANGELIDAKI, I., KARAKASHEV, D., BATSTONE, D., PLUGGE, C. & STAMS, A. 2011. Biomethanation and its potential. *Methods in enzymology,* 494**,** 327.

ANGELIDAKI, I. & SANDERS, W. 2004. Assessment of the anaerobic biodegradability of macropollutants. *Reviews in Environmental Science and Biotechnology,* 3**,** 117-129.

ANTONOPOULOU, G., GAVALA, H. N., SKIADAS, I. V. & LYBERATOS, G. 2012a. ADM1-based modeling of methane production from acidified sweet sorghum extract in a two stage process. *Bioresource Technology,* 106**,** 10-19.

ANTONOPOULOU, G., GAVALA, H. N., SKIADAS, I. V. & LYBERATOS, G. 2012b. Modeling of fermentative hydrogen production from sweet sorghum extract based on modified ADM1. *International Journal of Hydrogen Energy,* 37**,** 191-208.

APHA 1998. *Standard methods for the examination of water and wastewater,* Washington, DC, American Public Health Association.

APHA 2005. Standard methods for the examination of water and wastewater. Washington, DC, USA: American Public Health Association (APHA).

ARTHUR THOMAS, T. 2006. An automated procedure for the determination of soluble carbohydrates in herbage. *Journal of the Science of Food and Agriculture,* 28**,** 639-642.

ASTALS, S., ARISO, M., GALÍ, A. & MATA-ALVAREZ, J. 2011. Co-digestion of pig manure and glycerine: Experimental and modelling study. *Journal of Environmental Management,* 92**,** 1091-1096.

ASTALS, S., ESTEBAN-GUTIÉRREZ, M., FERNÁNDEZ-ARÉVALO, T., AYMERICH, E., GARCÍA-HERAS, J. L. & MATA-ALVAREZ, J. 2013. Anaerobic digestion of seven different sewage sludges: A biodegradability and modelling study. *Water Research,* 47**,** 6033-6043.

BAJPAI, P. & DASH, V. 2012. Hybrid renewable energy systems for power generation in stand-alone applications: A review. *Renewable and Sustainable Energy Reviews,* 16**,** 2926-2939.

BAKER, J. R., MILKE, M. W. & MIHELCIC, J. R. 1999. Relationship between chemical and theoretical oxygen demand for specific classes of organic chemicals. *Water Research,* 33**,** 327-334.

BANKS, C. J., CHESSHIRE, M., HEAVEN, S. & ARNOLD, R. 2011. Anaerobic digestion of source-segregated domestic food waste: Performance assessment by mass and energy balance. *Bioresource Technology,* 102**,** 612-620.

BANKS, C. J., ZHANG, Y., JIANG, Y. & HEAVEN, S. 2012. Trace element requirements for stable food waste digestion at elevated ammonia concentrations. *Bioresource Technology,* 104**,** 127-135.

BATSTONE, D. & KELLER, J. 2003. Industrial applications of the IWA anaerobic digestion model No. 1 (ADM1). *Water Science & Technology,* 47**,** 199-206.

BATSTONE, D., KELLER, J., ANGELIDAKI, R., KALYUZHNYI, S., PAVLOSTATHIS, S., ROZZI, A., SANDERS, W., SIEGRIST, H. & VAVILIN, V. 2002. Anaerobic Digestion Model No. 1 (ADM1), Scientific and Technical Report No. 13.

BATSTONE, D., KELLER, J. & STEYER, J. 2006. A review of ADM1 extensions, applications, and analysis: 2002-2005. *Water Science & Technology,* 54**,** 1-10.

BATSTONE, D., PUYOL, D., FLORES-ALSINA, X. & RODRÍGUEZ, J. 2015. Mathematical modelling of anaerobic digestion processes: applications and future needs. *Reviews in Environmental Science and Bio/Technology***,** 1-19.

BATSTONE, D. & STEYER, J. 2007. Use of modelling to evaluate best control practice for winery-type wastewaters. *Water Sci. Technol,* 56**,** 147.

BATSTONE, D., TORRIJOS, M., RUIZ, C. & SCHMIDT, J. 2004. Use of an anaerobic sequencing batch reactor for parameter estimation in modelling of anaerobic digestion. *Water Science & Technology,* 50**,** 295-303.

BATSTONE, D. J., HERNANDEZ, J. & SCHMIDT, J. E. 2005. Hydraulics of laboratory and full-scale upflow anaerobic sludge blanket (UASB) reactors. *Biotechnology and Bioengineering,* 91**,** 387-391.

BATSTONE, D. J. & JENSEN, P. D. 2011. Anaerobic Processes. *In:* EDITOR-IN-CHIEF: PETER, W. (ed.) *Treatise on Water Science.* Oxford: Elsevier.

BATSTONE, D. J., PIND, P. F. & ANGELIDAKI, I. 2003. Kinetics of thermophilic, anaerobic oxidation of straight and branched chain

butyrate and valerate. *Biotechnology and Bioengineering,* 84**,** 195-204.

BATSTONE, D. J., TAIT, S. & STARRENBURG, D. 2009. Estimation of hydrolysis parameters in full-scale anerobic digesters. *Biotechnology and Bioengineering,* 102**,** 1513-1520.

BELLO-MENDOZA, R. & SHARRATT, P. N. 1999. Analysis of retention time distribution (RTD) curves in an anaerobic digester with confined-gas mixing using a compartment model. *Water science and technology,* 40**,** 49-56.

BENSMANN, A., HANKE-RAUSCHENBACH, R. & SUNDMACHER, K. 2013. Reactor configurations for biogas plants–a model based analysis. *Chemical Engineering Science,* 104**,** 413-426.

BERNARD, O., CHACHUAT, B., HELIAS, A. & RODRIGUEZ, J. 2006. Can we assess the model complexity for a bioprocess: theory and example of the anaerobic digestion process. *Water science and technology,* 53**,** 85-92.

BIERNACKI, P., STEINIGEWEG, S., BORCHERT, A. & UHLENHUT, F. 2013. Application of Anaerobic Digestion Model No. 1 for describing anaerobic digestion of grass, maize, green weed silage, and industrial glycerine. *Bioresource Technology,* 127**,** 188-194.

BOE, K., BATSTONE, D. J., STEYER, J.-P. & ANGELIDAKI, I. 2010. State indicators for monitoring the anaerobic digestion process. *Water Research,* 44**,** 5973-5980.

BOLLON, J., LE-HYARIC, R., BENBELKACEM, H. & BUFFIERE, P. 2011. Development of a kinetic model for anaerobic dry digestion processes: Focus on acetate degradation and moisture content. *Biochemical Engineering Journal,* 56**,** 212-218.

BOUBAKER, F. & RIDHA, B. C. 2008. Modelling of the mesophilic anaerobic co-digestion of olive mill wastewater with olive mill solid waste using anaerobic digestion model No. 1 (ADM1). *Bioresource Technology,* 99**,** 6565-6577.

BUFFIERE, P., FREDERIC, S., MARTY, B. & DELGENES, J. P. 2008. A comprehensive method for organic matter characterization in solid wastes in view of assessing their anaerobic biodegradability. *Water science and technology,* 58**,** 1783-1788.

BUFFIERE, P., LOISEL, D., BERNET, N. & DELGENES, J. P. 2006. Towards new indicators for the prediction of solid waste anaerobic digestion properties. *Water science and technology,* 53**,** 233-241.

BUSWELL, A. & MUELLER, H. 1952. Mechanism of methane fermentation. *Industrial & Engineering Chemistry,* 44**,** 550-552.

CAPELA, I., BILÉ, M. J., SILVA, F., NADAIS, H., PRATES, A. & ARROJA, L. 2009. Hydrodynamic behaviour of a full-scale anaerobic contact reactor using residence time distribution technique. *Journal of Chemical Technology & Biotechnology,* 84**,** 716-724.

CASTELLANOS, J., NIMMO, W., WALKER, M., POGGIO, D. & POURKASHANIAN, M. 2014. Modelling an off-grid integrated renewable energy system for rural electrification in India using photovoltaics and anaerobic digestion. *Renewable Energy*.

CHEN, C., DUAN, S., CAI, T., LIU, B. & HU, G. 2011. Smart energy management system for optimal microgrid economic operation. *IET renewable power generation,* 5**,** 258-267.

CHEN, Y., CHENG, J. J. & CREAMER, K. S. 2008. Inhibition of anaerobic digestion process: A review. *Bioresource Technology,* 99**,** 4044-4064.

CONFER, D. R. & LOGAN, B. E. 1998. A conceptual model describing macromolecule degradation by suspended cultures and biofilms. *Water science and technology,* 37**,** 231-234.

CONRAD, R., BAK, F., SEITZ, H., THEBRATH, B., MAYER, H. & SCHÜTZ, H. 1989. Hydrogen turnover by psychrotrophic homoacetogenic and mesophilic methanogenic bacteria in anoxic paddy soil and lake sediment. *FEMS Microbiology Letters,* 62**,** 285-293.

COSTELLO, D. J., GREENFIELD, P. F. & LEE, P. L. 1991. Dynamic modelling of a single-stage high-rate anaerobic reactor—I. Model derivation. *Water Research,* 25**,** 847-858.

DE VRIEZE, J., VERSTRAETE, W. & BOON, N. 2013. Repeated pulse feeding induces functional stability in anaerobic digestion. *Microbial Biotechnology***,** n/a-n/a.

DELUCCHI, M. A. & JACOBSON, M. Z. 2011. Providing all global energy with wind, water, and solar power, Part II: Reliability, system and transmission costs, and policies. *Energy Policy,* 39**,** 1170-1190.

DERBAL, K., BENCHEIKH-LEHOCINE, M., CECCHI, F., MENIAI, A. H. & PAVAN, P. 2009. Application of the IWA ADM1 model to simulate anaerobic co-digestion of organic waste with waste activated sludge in mesophilic condition. *Bioresource Technology,* 100**,** 1539-1543.

DIAGNE, M., DAVID, M., LAURET, P., BOLAND, J. & SCHMUTZ, N. 2013. Review of solar irradiance forecasting methods and a proposition for small-scale insular grids. *Renewable and Sustainable Energy Reviews,* 27**,** 65-76.

DOCHAIN, D. & VANROLLEGHEM, P. 2001. *Dynamical modelling and estimation in wastewater treatment processes*, IWA Publishing.

DONOSO-BRAVO, A., MAILIER, J., MARTIN, C., RODRÍGUEZ, J., ACEVES-LARA, C. A. & WOUWER, A. V. 2011. Model selection, identification and validation in anaerobic digestion: A review. *Water Research,* 45**,** 5347-5364.

DONOSO-BRAVO, A., MAILIER, J., RUIZ-FILIPPI, G. & VANDE WOUWER, A. 2012. Identification in an anaerobic batch system: global sensitivity analysis, multi-start strategy and optimization criterion selection. *Bioprocess and Biosystems Engineering***,** 1-9.

DONOSO-BRAVO, A. & MAIRET, F. 2012. Determining the limiting reaction in anaerobic digestion processes. How has this been tackled? *Journal of Chemical Technology & Biotechnology***,** n/a-n/a.

EASTMAN, J. A. & FERGUSON, J. F. 1981. Solubilization of particulate organic carbon during the acid phase of anaerobic digestion. *Journal (Water Pollution Control Federation)***,** 352-366.

ECN/PHYLLIS n.d. Phyllis, database for biomass and waste. Energy research Centre of the Netherlands.

ELMITWALLI, T., SAYED, S., GROENDIJK, L., VAN LIER, J., ZEEMAN, G. & LETTINGA, G. 2003. Decentralised treatment of concentrated sewage at low temperature in a two-step anaerobic system: two upflow-hybrid septic tanks. *Water Science & Technology,* 48**,** 219-226.

FACCHIN, V., CAVINATO, C., FATONE, F., PAVAN, P., CECCHI, F. & BOLZONELLA, D. 2013. Effect of trace element supplementation on

the mesophilic anaerobic digestion of foodwaste in batch trials: The influence of inoculum origin. *Biochemical Engineering Journal,* 70**,** 71-77.

FAO/INFODOS 2012. FAO/INFODOS Food composition database for biodiversity version 2.0 - BioFoodComp2.0 Rome: FAO.

FEDOROVICH, V., LENS, P. & KALYUZHNYI, S. 2003. Extension of Enaerobic Digestion Model No. 1 with processes of sulfate reduction. *Applied Biochemistry and Biotechnology,* 109**,** 33-45.

FENG, Y., BEHRENDT, J., WENDLAND, C. & OTTERPOHL, R. 2006. Parameter analysis of the IWA Anaerobic Digestion Model No. 1 for the anaerobic digestion of blackwater with kitchen refuse. *Water science and technology: a journal of the International Association on Water Pollution Research,* 54**,** 139.

FLORES-ALSINA, X., SOLON, K., KAZADI MBAMBA, C., TAIT, S., GERNAEY, K. V., JEPPSSON, U. & BATSTONE, D. J. 2016. Modelling phosphorus (P), sulfur (S) and iron (Fe) interactions for dynamic simulations of anaerobic digestion processes. *Water Research*.

FLOTATS, X., PALATSI, J., AHRING, B. & ANGELIDAKI, I. 2006. Identifiability study of the proteins degradation model, based on ADM1, using simultaneous batch experiments. *Water Science & Technology,* 54**,** 31-39.

FRANCESCHINI, G. & MACCHIETTO, S. 2008. Model-based design of experiments for parameter precision: State of the art. *Chemical Engineering Science,* 63**,** 4846-4872.

FUENTES, M., MUSSATI, M. C., SCENNA, N. J. & AGUIRRE, P. A. 2009. Global modeling and simulation of a three-phase fluidized bed bioreactor. *Computers & Chemical Engineering,* 33**,** 359-370.

GAIDA, D., WOLF, C., MEYER, C., STUHLSATZ, A., LIPPEL, J., BÄCK, T., BONGARDS, M. & MCLOONE, S. 2012. State estimation for anaerobic digesters using the ADM1. *Water science and technology: a journal of the International Association on Water Pollution Research,* 66**,** 1088.

GALÍ, A., BENABDALLAH, T., ASTALS, S. & MATA-ALVAREZ, J. 2009. Modified version of ADM1 model for agro-waste application. *Bioresource Technology,* 100**,** 2783-2790.

GAO, X., LIU, X. & WANG, W. Biodegradation of particulate organics and its enhancement during anaerobic co-digestion of municipal biowaste and waste activated sludge. *Renewable Energy*.

GARCÍA-GEN, S., SOUSBIE, P., RANGARAJ, G., LEMA, J. M., RODRÍGUEZ, J., STEYER, J.-P. & TORRIJOS, M. 2015. Kinetic modelling of anaerobic hydrolysis of solid wastes, including disintegration processes. *Waste Management,* 35**,** 96-104.

GAVALA, H., ANGELIDAKI, I. & AHRING, B. 2003. Kinetics and Modeling of Anaerobic Digestion Process. . *In:* AHRING, B., ANGELIDAKI, I., DE MACARIO, E., GAVALA, H., HOFMAN-BANG, J., MACARIO, A., ELFERINK, S., RASKIN, L., STAMS, A., WESTERMANN, P. & ZHENG, D. (eds.) *Biomethanation I.* Springer Berlin / Heidelberg.

GERLOFF, E. D., LIMA, I. H. & STAHMANN, M. A. 1965. Leaf Proteins as Foodstuffs, Amino Acid Composition of Leaf Protein Concentrates. *Journal of Agricultural and Food Chemistry,* 13**,** 139-143.

GERNAEY, K. V., LANTZ, A. E., TUFVESSON, P., WOODLEY, J. M. & SIN, G. 2010. Application of mechanistic models to fermentation and biocatalysis for next-generation processes. *Trends in Biotechnology,* 28**,** 346-354.

GIRAULT, R., BRIDOUX, G., NAULEAU, F., POULLAIN, C., BUFFET, J., STEYER, J. P., SADOWSKI, A. G. & BÉLINE, F. 2012. A waste characterisation procedure for ADM1 implementation based on degradation kinetics. *Water Research,* 46**,** 4099-4110.

GIRAULT, R., ROUSSEAU, P., STEYER, J., BERNET, N. & BELINE, F. 2011. Combination of batch experiments with continuous reactor data for ADM1 calibration: application to anaerobic digestion of pig slurry. *Water science and technology,* 63**,** 2575-2582.

GLOVER, G., PRINTEMPS, C., ESSEMIANI, K. & MEINHOLD, J. 2006. Modelling of wastewater treatment plants how far shall we go with sophisticated modelling tools? *Water Science & Technology,* 53**,** 79-89.

GUJER, W. 2008. *Systems analysis for water technology*, Springer Science & Business Media.

GUJER, W. & ZEHNDER, A. 1983. Conversion processes in anaerobic digestion. *Water Science & Technology,* 15**,** 127-167.

GUNASEELAN, V. N. 1997. Anaerobic digestion of biomass for methane production: A review. *Biomass and Bioenergy,* 13**,** 83-114.

HAHN, H., KRAUTKREMER, B., HARTMANN, K. & WACHENDORF, M. 2014. Review of concepts for a demand-driven biogas supply for flexible power generation. *Renewable and Sustainable Energy Reviews,* 29**,** 383-393.

HAUGEN, F., BAKKE, R. & LIE, B. 2014. State Estimation and Model-Based Control of a Pilot Anaerobic Digestion Reactor. *Journal of Control Science and Engineering,* 2014**,** 19.

HE, P.-J., LÜ, F., SHAO, L.-M., PAN, X.-J. & LEE, D.-J. 2006. Enzymatic hydrolysis of polysaccharide-rich particulate organic waste. *Biotechnology and Bioengineering,* 93**,** 1145-1151.

HENTZ, L. H. & BALCHUNAS, B. M. 2000. Chemical and physical processes associated with mass transfer in odor control scrubbers. *Proceedings of the Water Environment Federation,* 2000**,** 1013-1030.

HOLMES, W. 1980. *Grass, its production and utilization*, Blackwell Scientific Publications.

HORIUCHI, J. I., SHIMIZU, T., TADA, K., KANNO, T. & KOBAYASHI, M. 2002. Selective production of organic acids in anaerobic acid reactor by pH control. *Bioresource Technology,* 82**,** 209-213.

HUETE, E., DE GRACIA, M., AYESA, E. & GARCIA-HERAS, J. 2006. ADM1-based methodology for the characterisation of the influent sludge in anaerobic reactors. *Water science and technology: a journal of the International Association on Water Pollution Research,* 54**,** 157.

JABŁOŃSKI, S. J. & ŁUKASZEWICZ, M. 2014. Mathematical modelling of methanogenic reactor start-up: Importance of volatile fatty acids degrading population. *Bioresource Technology,* 174**,** 74-80.

JAKEMAN, A. J., LETCHER, R. A. & NORTON, J. P. 2006. Ten iterative steps in development and evaluation of environmental models. *Environmental Modelling & Software,* 21**,** 602-614.

JENKINS, S. R., MORGAN, J. M. & SAWYER, C. L. 1983. Measuring Anaerobic Sludge Digestion and Growth by a Simple Alkalimetric Titration. *Journal (Water Pollution Control Federation),* 55**,** 448-453.

JENSEN, P., GE, H. & BATSTONE, D. J. 2011. Assessing the role of biochemical methane potential tests in determining anaerobic degradability rate and extent. *Water science and technology,* 64**,** 880.

JENSEN, P., HARDIN, M. & CLARKE, W. 2008. Measurement and quantification of sessile and planktonic microbial populations during the anaerobic digestion of cellulose. *Water Science & Technology,* 4**,** 465-9.

JENSEN, P. D., HARDIN, M. T. & CLARKE, W. P. 2009. Effect of biomass concentration and inoculum source on the rate of anaerobic cellulose solubilization. *Bioresource Technology,* 100**,** 5219-5225.

JEONG, H.-S., SUH, C.-W., LIM, J.-L., LEE, S.-H. & SHIN, H.-S. 2005. Analysis and application of ADM1 for anaerobic methane production. *Bioprocess and Biosystems Engineering,* 27**,** 81-89.

JUŽNIČ-ZONTA, Ž., KOCIJAN, J., FLOTATS, X. & VREČKO, D. in press. Multi-criteria analyses of wastewater treatment bio-processes under an uncertainty and a multiplicity of steady states. *Water Research*.

KALFAS, H., SKIADAS, I., GAVALA, H., STAMATELATOU, K. & LYBERATOS, G. 2006a. Application of ADM1 for the simulation of anaerobic digestion of olive pulp under mesophilic and thermophilic conditions. *Water Science & Technology,* 54**,** 149-156.

KALFAS, H., SKIADAS, I., GAVALA, H., STAMATELATOU, K. & LYBERATOS, G. 2006b. Application of ADM 1 for the simulation of anaerobic digestion of olive pulp under mesophilic and thermophilic conditions. *Water Science & Technology,* 54**,** 149-156.

KANASE-PATIL, A. B., SAINI, R. P. & SHARMA, M. P. 2010. Integrated renewable energy systems for off grid rural electrification of remote area. *Renewable Energy,* 35**,** 1342-1349.

KLEEREBEZEM, R. & VAN LOOSDRECHT, M. 2006. Waste characterization for implementation in ADM1. *Water science and technology: a journal of the International Association on Water Pollution Research,* 54**,** 167.

KLEEREBEZEM, R. & VAN LOOSDRECHT, M. C. 2010. A generalized method for thermodynamic state analysis of environmental systems. *Critical Reviews in Environmental Science and Technology,* 40**,** 1-54.

KOCH, K., LUBKEN, M., GEHRING, T., WICHERN, M. & HORN, H. 2010a. Biogas from grass silage - Measurements and modeling with ADM1. *Bioresource Technology,* 101**,** 8158-8165.

KOCH, K., LÜBKEN, M., GEHRING, T., WICHERN, M. & HORN, H. 2010b. Biogas from grass silage – Measurements and modeling with ADM1. *Bioresource Technology,* 101**,** 8158-8165.

LAUWERS, J., APPELS, L., THOMPSON, I. P., DEGRÈVE, J., VAN IMPE, J. F. & DEWIL, R. 2013. Mathematical modelling of anaerobic digestion of biomass and waste: Power and limitations. *Progress in Energy and Combustion Science,* 39**,** 383-402.

LEITAO, R. C., VAN HAANDEL, A. C., ZEEMAN, G. & LETTINGA, G. 2006. The effects of operational and environmental variations on anaerobic wastewater treatment systems: A review. *Bioresource Technology,* 97**,** 1105-1118.

LIAO, W., FREAR, C. & CHEN, S. 2007. Biomass Inventory Technology and Economics Assessment. *Ecology Publication* Olympia, WA: Washington State University, Center for Bioproducts and Bioenergy

LIZARRALDE, I., FERNÁNDEZ-ARÉVALO, T., BROUCKAERT, C., VANROLLEGHEM, P., IKUMI, D. S., EKAMA, G. A., AYESA, E. & GRAU, P. 2015. A new general methodology for incorporating physico-chemical transformations into multi-phase wastewater treatment process models. *Water Research,* 74**,** 239-256.

LJUNG, L. 1998. *System identification*, Springer.

LOW, A. 1979. Studies on digestion and absorption in the intestines of growing pigs. *British journal of nutrition,* 41**,** 147-156.

LÜBKEN, M., WICHERN, M., SCHLATTMANN, M., GRONAUER, A. & HORN, H. 2007. Modelling the energy balance of an anaerobic digester fed with cattle manure and renewable energy crops. *Water Research,* 41**,** 4085-4096.

MAIRET, F., BERNARD, O., RAS, M., LARDON, L. & STEYER, J.-P. 2011. Modeling anaerobic digestion of microalgae using ADM1. *Bioresource Technology,* 102**,** 6823-6829.

MALLICK, T., SARMAH, N., BANERJEE, S., MICHELI, L., REDDY, K., GHOSH, P., WALKER, G., CHOUDHURY, S., POURKASHANIAN, M. & HAMILTON, J. Design concept and configuration of a hybrid renewable energy system for rural electrification in India through BioCPV project. International Conference on Advances in Energy Research, 2013 Indian Institute of Technology Bombay, Mumbai.

MARTENSEN, N., KUWAHATA, R. & ACKERMANN, T. 2012. "e[r] cluster" for a smart energy access. The role of microgrids in promoting the integration of renewable energy in India. A Greenpeace report for a smart energy access http://www.greenpeace.org/india/Global/india/report/Bihar-Smart-Energy-Access.pdf.

MATA-ALVAREZ, J., DOSTA, J., MACÉ, S. & ASTALS, S. 2011. Codigestion of solid wastes: A review of its uses and perspectives including modeling. *Critical Reviews in Biotechnology***,** 1-13.

MATTHIESSEN, M. K., LARNEY, F. J., BRENT SELINGER, L. & OLSON, A. F. 2005. Influence of Loss-on-Ignition Temperature and Heating Time on Ash Content of Compost and Manure. *Communications in soil science and plant analysis,* 36**,** 2561-2573.

MELLIT, A. & PAVAN, A. M. 2010. A 24-h forecast of solar irradiance using artificial neural network: Application for performance prediction of a grid-connected PV plant at Trieste, Italy. *Solar Energy,* 84**,** 807-821.

MERKEL, W. & KRAUTH, K. 1999. Mass transfer of carbon dioxide in anaerobic reactors under dynamic substrate loading conditions. *Water Research,* 33**,** 2011-2020.

MORGENROTH, E., KOMMEDAL, R. & HARREMOËS, P. 2002. Processes and modeling of hydrolysis of particulate organic matter in aerobic wastewater treatment--a review. *Water science and technology: a journal of the International Association on Water Pollution Research,* 45**,** 25.

MOSEY, F. 1983. Mathematical modelling of the anaerobic digestion process: regulatory mechanisms for the formation of short-chain

volatile acids from glucose. *Water Science & Technology,* 15**,** 209-232.

MOTTET, A., RAMIREZ, I., CARRÈRE, H., DÉLÉRIS, S., VEDRENNE, F., JIMENEZ, J. & STEYER, J. P. 2013. New fractionation for a better bioaccessibility description of particulate organic matter in a modified ADM1 model. *Chemical Engineering Journal,* 228**,** 871-881.

MU, S. J., ZENG, Y., WU, P., LOU, S. J. & TARTAKOVSKY, B. 2008. Anaerobic digestion model no. 1-based distributed parameter model of an anaerobic reactor: I. Model development. *Bioresource Technology,* 99**,** 3665-3675.

MUSVOTO, E. V., WENTZEL, M. C., LOEWENTHAL, R. E. & EKAMA, G. A. 2000. Integrated chemical–physical processes modelling—I. Development of a kinetic-based model for mixed weak acid/base systems. *Water Research,* 34**,** 1857-1867.

MYER, R., BRENDEMUHL, J. & JOHNSON, D. 2000. Dehydrated Restaurant Food Waste as Swine Feed. *Food Waste to Animal Feed***,** 113-144.

NIZAMI, A. S. & MURPHY, J. D. 2010. What type of digester configurations should be employed to produce biomethane from grass silage? *Renewable & Sustainable Energy Reviews,* 14**,** 1558-1568.

NOGUEROL-ARIAS, J., RODRÍGUEZ-ABALDE, A., ROMERO-MERINO, E. & FLOTATS, X. 2012. Determination of Chemical Oxygen Demand in Heterogeneous Solid or Semisolid Samples Using a Novel Method Combining Solid Dilutions as a Preparation Step Followed by Optimized Closed Reflux and Colorimetric Measurement. *Analytical Chemistry,* 84**,** 5548-5555.

NOPENS, I., BATSTONE, D. J., COPP, J. B., JEPPSSON, U., VOLCKE, E., ALEX, J. & VANROLLEGHEM, P. A. 2009. An ASM/ADM model interface for dynamic plant-wide simulation. *Water Research,* 43**,** 1913-1923.

O'SULLIVAN, C. A., BURRELL, P. C., CLARKE, W. P. & BLACKALL, L. L. 2005. Structure of a cellulose degrading bacterial community during anaerobic digestion. *Biotechnology and Bioengineering,* 92**,** 871-878.

OAKLEY, J. E. & O'HAGAN, A. 2004. Probabilistic sensitivity analysis of complex models: a Bayesian approach. *Journal of the Royal Statistical Society: Series B (Statistical Methodology),* 66**,** 751-769.

ORDACE, A., IONESCU, C. M., VANNECKE, T., VOLCKE, E., NASCU, I. & DE KEYSER, R. Predictive control of anaerobic digestion of wastewater sludge: a feasibility study. 16th International Conference on System Theory, Control and Computing (ICSTCC-2012), 2012. IEEE.

PAGE, D., HICKEY, K., NARULA, R., MAIN, A. & GRIMBERG, S. 2008. Modeling anaerobic digestion of dairy manure using the IWA Anaerobic Digestion Model no. 1 (ADM1). *Water science and technology,* 58**,** 689-95.

PALATSI, J., ILLA, J., PRENAFETA-BOLDÚ, F. X., LAURENI, M., FERNANDEZ, B., ANGELIDAKI, I. & FLOTATS, X. 2010. Long-chain fatty acids inhibition and adaptation process in anaerobic thermophilic digestion: Batch tests, microbial community structure and mathematical modelling. *Bioresource Technology,* 101**,** 2243-2251.

PALMA-BEHNKE, R., BENAVIDES, C., ARANDA, E., LLANOS, J. & SÁEZ, D. Energy management system for a renewable based microgrid with a demand side management mechanism. Computational intelligence applications in smart grid (CIASG), 2011 IEEE symposium on, 2011. IEEE, 1-8.

PALMA-BEHNKE, R., BENAVIDES, C., LANAS, F., SEVERINO, B., REYES, L., LLANOS, J. & SAEZ, D. 2013. A Microgrid Energy Management System Based on the Rolling Horizon Strategy. *Smart Grid, IEEE Transactions on,* PP**,** 1-11.

PARAWIRA, W., MURTO, M., READ, J. S. & MATTIASSON, B. 2005. Profile of hydrolases and biogas production during two-stage mesophilic anaerobic digestion of solid potato waste. *Process Biochemistry,* 40**,** 2945-2952.

PAUL, E., OCHOA, J. C., PECHAUD, Y., LIU, Y. & LINÉ, A. 2012. Effect of shear stress and growth conditions on detachment and physical properties of biofilms. *Water Research,* 46**,** 5499-5508.

PAVLOSTATHIS, S. & GIRALDO-GOMEZ, E. 1991. Kinetics of anaerobic treatment: a critical review. *Critical Reviews in Environmental Science and Technology,* 21**,** 411-490.

PENUMATHSA, B. K. V., PREMIER, G. C., KYAZZE, G., DINSDALE, R., GUWY, A. J., ESTEVES, S. & RODRÍGUEZ, J. 2008. ADM1 can be applied to continuous bio-hydrogen production using a variable stoichiometry approach. *Water Research,* 42**,** 4379-4385.

PÉREZ-ARRIAGA, I. & BATLLE, C. 2012. Impacts of intermittent renewables on electricity generation system operation. *Economics of Energy and Environmental Policy,* 1.

POBEHEIM, H., MUNK, B., MÜLLER, H., BERG, G. & GUEBITZ, G. M. 2010. Characterization of an anaerobic population digesting a model substrate for maize in the presence of trace metals. *Chemosphere,* 80**,** 829-836.

POGGIO, D., WALKER, M., NIMMO, W. & POURKASHANIAN, M. 2013. Model based evaluation of control strategies for the operation of anaerobic digesters in a microgrid with variable biogas demand. *13th World Congress on Anaerobic Digestion (AD13).* Santiago de Compostela, Spain.

POMERANZ, Y., YOUNGS, V. & ROBBINS, G. 1973. Protein content and amino acid composition of oat species and tissues. *Cereal chemistry*.

POMMIER, S., CHENU, D., QUINTARD, M. & LEFEBVRE, X. 2007. A logistic model for the prediction of the influence of water on the solid waste methanization in landfills. *Biotechnology and Bioengineering,* 97**,** 473-482.

RAE, C. & BRADLEY, F. 2012. Energy autonomy in sustainable communities—A review of key issues. *Renewable and Sustainable Energy Reviews,* 16**,** 6497-6506.

RALSTON, M. L. & JENNRICH, R. I. 1978. DUD, A derivative-free algorithm for nonlinear least squares. *Technometrics,* 20**,** 7-14.

RAMIREZ, I., MOTTET, A., CARRÈRE, H., DÉLÉRIS, S., VEDRENNE, F. & STEYER, J.-P. 2009. Modified ADM1 disintegration/hydrolysis structures for modeling batch thermophilic anaerobic digestion of thermally pretreated waste activated sludge. *Water Research,* 43**,** 3479-3492.

RAMSAY, I. R. & PULLAMMANAPPALLIL, P. C. 2001. Protein degradation during anaerobic wastewater treatment: derivation of stoichiometry. *Biodegradation,* 12**,** 247-256.

RAPOSO, F., DE LA RUBIA, M. A., BORJA, R. & ALAIZ, M. 2008. Assessment of a modified and optimised method for determining chemical oxygen demand of solid substrates and solutions with high suspended solid content. *Talanta,* 76**,** 448-453.

RAPOSO, F., DE LA RUBIA, M. A., FERNANDEZ-CEGRI, V. & BORJA, R. 2012. Anaerobic digestion of solid organic substrates in batch mode: An overview relating to methane yields and experimental procedures. *Renewable and Sustainable Energy Reviews,* 16**,** 861-877.

REICHERT, P. 1998. AQUASIM 2.0–user manual. *Swiss Federal Institute for Environmental Science and Technology. Dubendorf, Switzerland*.

REICHERT, P. & OMLIN, M. 1997. On the usefulness of overparameterized ecological models. *Ecological Modelling,* 95**,** 289-299.

RIPLEY, L. E., BOYLE, W. C. & CONVERSE, J. C. 1986. Improved Alkalimetric Monitoring for Anaerobic Digestion of High-Strength Wastes. *Journal (Water Pollution Control Federation),* 58**,** 406-411.

RITTMANN, B. E. & MCCARTY, P. L. 2001. *Environmental biotechnology*, McGraw-Hill Boston.

RODRIGUEZ, J., LEMA, J., VAN LOOSDRECHT, M. & KLEEREBEZEM, R. 2006. Variable stoichiometry with thermodynamic control in ADM1. *Water science and technology: a journal of the International Association on Water Pollution Research,* 54**,** 101.

RODRÍGUEZ, J., ROCA, E., LEMA, J. M. & BERNARD, O. 2008. Determination of the adequate minimum model complexity required in anaerobic bioprocesses using experimental data. *Journal of Chemical Technology & Biotechnology,* 83**,** 1694-1702.

RÖNNER-HOLM, S., ZAK, A. & HOLM, N. 2012. Comparison of different conditions, substrates and operation modes by dynamic simulation of a full-scale anaerobic SBR plant. *Water science and technology: a journal of the International Association on Water Pollution Research,* 65**,** 558.

ROSEN, C. & JEPPSSON, U. 2006. Aspects on ADM1 Implementation within the BSM2 Framework. *Department of Industrial Electrical Engineering and Automation, Lund University, Lund, Sweden*.

SANDERS, W. T. M. 2001. *Anaerobic hydrolysis during digestion of complex substrates.* Proefschrift Wageningen, s.n.].

SCHINK, B. 1997. Energetics of syntrophic cooperation in methanogenic degradation. *Microbiology and molecular biology reviews,* 61**,** 262-280.

SCHNÜRER, A. & NORDBERG, A. 2008. Ammonia, a selective agent for methane production by syntrophic acetate oxidation at mesophilic temperature. *Water science and technology: a journal of the International Association on Water Pollution Research,* 57**,** 735.

SIEGRIST, H., VOGT, D., GARCIA-HERAS, J. L. & GUJER, W. 2002. Mathematical model for meso-and thermophilic anaerobic sewage sludge digestion. *Environmental Science & Technology,* 36**,** 1113-1123.

SIN, G., GERNAEY, K. V. & LANTZ, A. E. 2009a. Good modeling practice for PAT applications: Propagation of input uncertainty and sensitivity analysis. *Biotechnology Progress,* 25**,** 1043-1053.

SIN, G., GERNAEY, K. V., NEUMANN, M. B., VAN LOOSDRECHT, M. C. M. & GUJER, W. 2009b. Uncertainty analysis in WWTP model applications: A critical discussion using an example from design. *Water Research,* 43**,** 2894-2906.

SIN, G., VAN HULLE, S. W. H., DE PAUW, D. J. W., VAN GRIENSVEN, A. & VANROLLEGHEM, P. A. 2005. A critical comparison of systematic calibration protocols for activated sludge models: A SWOT analysis. *Water Research,* 39**,** 2459-2474.

SIRIWONGRUNGSON, V., ZENG, R. J. & ANGELIDAKI, I. 2007. Homoacetogenesis as the alternative pathway for H2 sink during thermophilic anaerobic degradation of butyrate under suppressed methanogenesis. *Water Research,* 41**,** 4204-4210.

SMITH, S. A. & STÖCKLE, C. O. 2010. Self-consistent liquid-to-gas mass transfer calculations. *Bioresource Technology,* 101**,** 9361-9365.

SOMAN, S. S., ZAREIPOUR, H., MALIK, O. & MANDAL, P. A review of wind power and wind speed forecasting methods with different time horizons. North American Power Symposium (NAPS), 2010, 2010. IEEE, 1-8.

SONG, H., CLARKE, W. P. & BLACKALL, L. L. 2005. Concurrent microscopic observations and activity measurements of cellulose hydrolyzing and methanogenic populations during the batch anaerobic digestion of crystalline cellulose. *Biotechnology and Bioengineering,* 91**,** 369-378.

SOUTH, C. R., HOGSETT, D. A. L. & LYND, L. R. 1995. Modeling simultaneous saccharification and fermentation of lignocellulose to ethanol in batch and continuous reactors. *Enzyme and Microbial Technology,* 17**,** 797-803.

SOUZA, T. S., CARVAJAL, A., DONOSO-BRAVO, A., PENA, M. & FDZ-POLANCO, F. 2013. ADM1 calibration using BMP tests for modeling the effect of autohydrolysis pretreatment on the performance of continuous sludge digesters. *Water Research,* 47**,** 3244-3254.

STEYER, J., BERNARD, O., BATSTONE, D. & ANGELIDAKI, I. 2006. Lessons learnt from 15 years of ICA in anaerobic digesters. *Water Science & Technology,* 53**,** 25-33.

STRÖMBERG, S., NISTOR, M. & LIU, J. 2014. Towards eliminating systematic errors caused by the experimental conditions in Biochemical Methane Potential (BMP) tests. *Waste Management,* 34**,** 1939-1948.

STRÖMBERG, S., NISTOR, M. & LIU, J. 2015. Early prediction of Biochemical Methane Potential through statistical and kinetic modelling of initial gas production. *Bioresource Technology,* 176**,** 233-241.

STROOT, P. G., MCMAHON, K. D., MACKIE, R. I. & RASKIN, L. 2001. Anaerobic codigestion of municipal solid waste and biosolids under various mixing conditions—I. digester performance. *Water Research,* 35**,** 1804-1816.

STUMM, W. & MORGAN, J. 1996. Aquatic chemistry: chemical equilibrium and rates in natural waters. *John Wiley, New York*.

SUGANTHI, L. & SAMUEL, A. A. 2012. Energy models for demand forecasting—A review. *Renewable and Sustainable Energy Reviews,* 16**,** 1223-1240.

TAYLOR, J. R. 1996. *An Introduction To Error Analysis: The Study Of Uncertainties In Physical Measurements* Sausalito, California, University Science Books.

TCHOBANOGLOUS, G., BURTON, F. & STENSEL, H. 2003. *Wastewater Engineering Treatment and Reuse*, McGraw-Hill Company.

TCHOBANOGLOUS, G. & BURTON, F. L. 1991. Wastewater engineering. *Management,* 7**,** 1-4.

THAMSIRIROJ, T. & MURPHY, J. D. 2011. Modelling mono-digestion of grass silage in a 2-stage CSTR anaerobic digester using ADM1. *Bioresource Technology,* 102**,** 948-959.

THAMSIRIROJ, T., NIZAMI, A. S. & MURPHY, J. D. 2012. Why does mono-digestion of grass silage fail in long term operation? *Applied Energy,* 95**,** 64-76.

THERMO FISHER SCIENTIFIC INC. 2008. Organic Elemental Analysis: Flash 2000 Elemental Analyzer Operating Manual. P/N 31712052, Revision B September 2009 ed. Cambridge, United Kingdom: Thermo Fisher Scientific.

TRIOLO, J. M., SOMMER, S. G., MØLLER, H. B., WEISBJERG, M. R. & JIANG, X. Y. 2011. A new algorithm to characterize biodegradability of biomass during anaerobic digestion: Influence of lignin concentration on methane production potential. *Bioresource Technology,* 102**,** 9395-9402.

VAN SOEST, P. & WINE, R. 1967. Use of detergents in the analysis of fibrous feeds. IV. Determination of plant cell-wall constituents. *Journal of the Association of Official Analytical Chemists,* 50**,** 5.

VAVILIN, V. A., FERNANDEZ, B., PALATSI, J. & FLOTATS, X. 2008. Hydrolysis kinetics in anaerobic degradation of particulate organic material: An overview. *Waste Management,* 28**,** 939-951.

VEEKEN, A., KALYUZHNYI, S., SCHARFF, H. & HAMELERS, B. 2000. Effect of pH and VFA on hydrolysis of organic solid waste. *Journal of environmental engineering,* 126**,** 1076-1081.

VETTER, Y. A., DEMING, J. W., JUMARS, P. A. & KRIEGER-BROCKETT, B. B. 1998. A Predictive Model of Bacterial Foraging by Means of Freely Released Extracellular Enzymes. *Microbial Ecology,* 36**,** 75-92.

VON STOCKAR, U., MASKOW, T., LIU, J., MARISON, I. W. & PATIÑO, R. 2006. Thermodynamics of microbial growth and metabolism: An analysis of the current situation. *Journal of Biotechnology,* 121**,** 517-533.

WELLINGER, A. 1999. Process design of agricultural digesters. Ettenhausen: Nova Energie GmbH.

WICHERN, M., GEHRING, T., FISCHER, K., ANDRADE, D., LÜBKEN, M., KOCH, K., GRONAUER, A. & HORN, H. 2009. Monofermentation of grass silage under mesophilic conditions: Measurements and mathematical modeling with ADM 1. *Bioresource Technology,* 100**,** 1675-1681.

YASUI, H., GOEL, R., LI, Y. Y. & NOIKE, T. 2008. Modified ADM1 structure for modelling municipal primary sludge hydrolysis. *Water Research,* 42**,** 249-259.

YU, L., ZHAO, Q., MA, J., FREAR, C. & CHEN, S. 2012. Experimental and modeling study of a two-stage pilot scale high solid anaerobic digester system. *Bioresource Technology,* 124**,** 8-17.

YUAN, X.-Z., SHI, X.-S., YUAN, C.-X., WANG, Y.-P., QIU, Y.-L., GUO, R.-B. & WANG, L.-S. 2014. Modeling anaerobic digestion of blue algae: Stoichiometric coefficients of amino acids acidogenesis and thermodynamics analysis. *Water Research,* 49**,** 113-123.

ZAHER, U., LI, R., JEPPSSON, U., STEYER, J.-P. & CHEN, S. 2009. GISCOD: General Integrated Solid Waste Co-Digestion model. *Water Research,* 43**,** 2717-2727.

ZAHER, U., RODRÍGUEZ, J., FRANCO, A. & VANROLLEGHEM, P. Application of the IWA ADM1 model to simulate anaerobic digester dynamics using a concise set of practical measurements. *In:* UJANG, Z. & HENZE, M., eds. Environmental Biotechnology: Advancement in Water and Wastewater Application in the Tropics, 2003 Kuala Lumpur, Malaysia. IWA Publishing

ZAMANZADEH, M., PARKER, W. J., VERASTEGUI, Y. & NEUFELD, J. D. 2013. Biokinetics and bacterial communities of propionate oxidizing bacteria in phased anaerobic sludge digestion systems. *Water Research*.

ZHANG, B., HE, P.-J., LÜ, F., SHAO, L.-M. & WANG, P. 2007. Extracellular enzyme activities during regulated hydrolysis of high-solid organic wastes. *Water Research,* 41**,** 4468-4478.

ZHAO, B.-H., YUE, Z.-B., NI, B.-J., MU, Y., YU, H.-Q. & HARADA, H. 2009. Modeling anaerobic digestion of aquatic plants by rumen cultures: Cattail as an example. *Water Research,* 43**,** 2047-2055.

ZHOU, H., LÖFFLER, D. & KRANERT, M. 2011. Model-based predictions of anaerobic digestion of agricultural substrates for biogas production. *Bioresource Technology,* 102**,** 10819-10828.

Appendix 1 – ADM1 Aquasim Implementation

```
************************************************************************

AQUASIM Version 2.1d (win/mfc) - Listing of System Definition

************************************************************************

Date and time of listing:  10/30/2015  05:51:15



************************************************************************
Variables
************************************************************************
alkalinity:    S_hco3_ion*50000
Ammonia_free:  S_nh3*17*1000
Ammonia_TAN:   S_IN*18*1000
blanace_COD_acc:
               V_fedCOD-V_outVFA-V_gasCH4COD_exp-V_outCOD
CODVS_biomass: 1.415
CODVS_ch:      1.184
CODVS_FW:      1.6048
CODVS_GW:      1.3902
CODVS_I:       1.4
CODVS_INO:     1.3966
CODVS_li:      2.874
CODVS_pr_avg:  1.263
CODVS_pr_FW:   1.221
CODVS_pr_GW:   1.285
CODVS_pr_INO:  1.415
CODVS_Xc:      1.415
COD_S:         S_aa+S_ac+S_bu+S_ch4+S_fa+S_h2+S_I+S_pro+S_su+S_va
COD_unconverted:
               X_ch_INO+X_ch_r_FW+X_ch_s_FW+X_ch_r_GW+X_ch_s_GW+X_ch_r_A
               LA+X_ch_s_ALA+X_ch_r_PM+X_ch_s_PM+S_su+X_li_INO+X_li_r_FW
               +X_li_s_FW+X_li_r_GW+X_li_s_GW+X_li_r_PM+X_li_s_PM+X_li_r
               _ALA+X_li_s_ALA+S_fa+X_pr_INO+X_pr_s_FW+X_pr_r_FW+X_pr_s_
               GW+X_pr_r_GW+X_pr_s_ALA+X_pr_r_ALA+X_pr_s_PM+X_pr_r_PM+S_
               aa
COD_unc_probe: COD_unconverted(reactor,Bulk Volume,0)
C_aa_avg:      0.03036
C_aa_FW:       0.0307
C_aa_GW:       0.0301
C_aa_INO:      0.02994
C_ac:          2/64
C_biom:        0.03125
C_bu:          4/160
C_ch4:         1/64
C_fa:          0.0217
C_li:          0.02198
C_pro:         3/112
C_SI:          0.03
C_su:          6/192
C_va:          5/208
C_Xc:          0.0278329
C_Xc_INO:      0.0278329
C_XI:          0.03
deltaH0_Ka_co2:7646
deltaH0_Ka_h2o:55900
deltaH0_Ka_nh4:51965
deltaH0_KH_ch4:
              -14240
deltaH0_KH_co2:
              -19410
deltaH0_KH_h2:-4180
exp_BMPflow_FW1:
               Real List Variable (t)
exp_BMPflow_FW2:
               Real List Variable (t)
exp_BMPflow_FW3:
               Real List Variable (t)
exp_BMPflow_FW4:
               Real List Variable (t)
exp_BMPflow_I1:Real List Variable (t)
```

```
exp_BMPflow_I2:Real List Variable (t)
exp_BMPflow_I3:Real List Variable (t)
exp_BMPpmal_ALA1:
               Real List Variable (t)
exp_BMPpmal_ALA2:
               Real List Variable (t)
exp_BMPpmal_I1:Real List Variable (t)
exp_BMPpmal_I2:Real List Variable (t)
exp_BMPpmal_I3:Real List Variable (t)
exp_BMPpmal_PM1:
               Real List Variable (t)
exp_BMPpmal_PM2:
               Real List Variable (t)
exp_BMP_FW1:   Real List Variable (t)
exp_BMP_FW2:   Real List Variable (t)
exp_BMP_FW3:   Real List Variable (t)
exp_BMP_FW4:   Real List Variable (t)
exp_BMP_I1:    Real List Variable (t)
exp_BMP_I2:    Real List Variable (t)
exp_BMP_I3:    Real List Variable (t)
exp_C_Ac_FW1:  Real List Variable (t)
exp_C_Ac_FW1_I1:
               Real List Variable (t)
exp_C_Ac_FW1_I2:
               Real List Variable (t)
exp_C_Ac_FW1_I3:
               Real List Variable (t)
exp_C_Ac_FW2:  Real List Variable (t)
exp_C_Ac_R1:   Real List Variable (t)
exp_C_Ac_R1_138:
               Real List Variable (t)
exp_C_Ac_R1_inh1:
               Real List Variable (t)
exp_C_Ac_R2:   Real List Variable (t)
exp_C_Ac_R3:   Real List Variable (t)
exp_C_Ac_R4:   Real List Variable (t)
exp_C_Ac_R5:   Real List Variable (t)
exp_C_Ac_R6:   Real List Variable (t)
exp_C_Alk_FW1: Real List Variable (t)
exp_C_Alk_FW2: Real List Variable (t)
exp_C_Alk_R1:  Real List Variable (t)
exp_C_Alk_R2:  Real List Variable (t)
exp_C_Alk_R3:  Real List Variable (t)
exp_C_Alk_R4:  Real List Variable (t)
exp_C_Alk_R5:  Real List Variable (t)
exp_C_Alk_R6:  Real List Variable (t)
exp_C_Bu_FW1:  Real List Variable (t)
exp_C_Bu_FW1_I1:
               Real List Variable (t)
exp_C_Bu_FW1_I2:
               Real List Variable (t)
exp_C_Bu_FW1_I3:
               Real List Variable (t)
exp_C_Bu_FW2:  Real List Variable (t)
exp_C_Bu_R1:   Real List Variable (t)
exp_C_Bu_R1_138:
               Real List Variable (t)
exp_C_Bu_R1_inh1:
               Real List Variable (t)
exp_C_Bu_R2:   Real List Variable (t)
exp_C_Bu_R3:   Real List Variable (t)
exp_C_Bu_R4:   Real List Variable (t)
exp_C_Bu_R5:   Real List Variable (t)
exp_C_Bu_R6:   Real List Variable (t)
exp_C_flow_R1_138:
               Real List Variable (t)
exp_C_flow_R1_2pts_all:
               Real List Variable (t)
exp_C_flow_R1_all:
               Real List Variable (t)
exp_C_flow_R1_inh1:
               Real List Variable (t)
exp_C_flow_R2_all:
               Real List Variable (t)
exp_C_flow_R3_all:
               Real List Variable (t)
exp_C_flow_R4_all:
               Real List Variable (t)
exp_C_flow_R5_all:
```

```
                Real List Variable (t)
exp_C_flow_R6_all:
                Real List Variable (t)
exp_C_f_FW1_1: Real List Variable (t)
exp_C_f_FW1_10:Real List Variable (t)
exp_C_f_FW1_11:Real List Variable (t)
exp_C_f_FW1_12:Real List Variable (t)
exp_C_f_FW1_13:Real List Variable (t)
exp_C_f_FW1_14:Real List Variable (t)
exp_C_f_FW1_15:Real List Variable (t)
exp_C_f_FW1_2: Real List Variable (t)
exp_C_f_FW1_3: Real List Variable (t)
exp_C_f_FW1_4: Real List Variable (t)
exp_C_f_FW1_5: Real List Variable (t)
exp_C_f_FW1_6: Real List Variable (t)
exp_C_f_FW1_7: Real List Variable (t)
exp_C_f_FW1_8: Real List Variable (t)
exp_C_f_FW1_9: Real List Variable (t)
exp_C_NH4_FW1: Real List Variable (t)
exp_C_NH4_FW2: Real List Variable (t)
exp_C_NH4_R1:  Real List Variable (t)
exp_C_NH4_R2:  Real List Variable (t)
exp_C_NH4_R3:  Real List Variable (t)
exp_C_NH4_R4:  Real List Variable (t)
exp_C_NH4_R5:  Real List Variable (t)
exp_C_NH4_R6:  Real List Variable (t)
exp_C_pHc_FW1: Real List Variable (t)
exp_C_pHc_FW2: Real List Variable (t)
exp_C_pH_FW1:  Real List Variable (t)
exp_C_pH_R1:   Real List Variable (t)
exp_C_pH_R2:   Real List Variable (t)
exp_C_pH_R3:   Real List Variable (t)
exp_C_pH_R4:   Real List Variable (t)
exp_C_pH_R5:   Real List Variable (t)
exp_C_pH_R6:   Real List Variable (t)
exp_C_Pro_FW1: Real List Variable (t)
exp_C_Pro_FW1_I1:
                Real List Variable (t)
exp_C_Pro_FW1_I2:
                Real List Variable (t)
exp_C_Pro_FW1_I3:
                Real List Variable (t)
exp_C_Pro_FW2: Real List Variable (t)
exp_C_Pro_R1:  Real List Variable (t)
exp_C_Pro_R1_138:
                Real List Variable (t)
exp_C_Pro_R1_inh1:
                Real List Variable (t)
exp_C_Pro_R2:  Real List Variable (t)
exp_C_Pro_R3:  Real List Variable (t)
exp_C_Pro_R4:  Real List Variable (t)
exp_C_Pro_R5:  Real List Variable (t)
exp_C_Pro_R6:  Real List Variable (t)
exp_C_SVFA_R1: Real List Variable (t)
exp_C_SVFA_R2: Real List Variable (t)
exp_C_SVFA_R3: Real List Variable (t)
exp_C_SVFA_R4: Real List Variable (t)
exp_C_SVFA_R5: Real List Variable (t)
exp_C_SVFA_R6: Real List Variable (t)
exp_C_TS_FW1:  Real List Variable (t)
exp_C_TS_R1:   Real List Variable (t)
exp_C_TS_R2:   Real List Variable (t)
exp_C_TS_R3:   Real List Variable (t)
exp_C_TS_R4:   Real List Variable (t)
exp_C_TS_R5:   Real List Variable (t)
exp_C_TS_R6:   Real List Variable (t)
exp_C_Va_FW1:  Real List Variable (t)
exp_C_Va_FW1_I1:
                Real List Variable (t)
exp_C_Va_FW1_I2:
                Real List Variable (t)
exp_C_Va_FW1_I3:
                Real List Variable (t)
exp_C_Va_FW2:  Real List Variable (t)
exp_C_Va_R1:   Real List Variable (t)
exp_C_Va_R1_138:
                Real List Variable (t)
exp_C_Va_R1_inh1:
                Real List Variable (t)
```

```
exp_C_Va_R2:   Real List Variable (t)
exp_C_Va_R3:   Real List Variable (t)
exp_C_Va_R4:   Real List Variable (t)
exp_C_Va_R5:   Real List Variable (t)
exp_C_Va_R6:   Real List Variable (t)
exp_C_VFA_FW1_I2:
               Real List Variable (t)
exp_C_VFA_FW1_I3:
               Real List Variable (t)
exp_C_Volume_FW1:
               Real List Variable (t)
exp_C_Volume_R1:
               Real List Variable (t)
exp_C_Volume_R1_raw:
               Real List Variable (t)
exp_C_Volume_R2:
               Real List Variable (t)
exp_C_Volume_R3:
               Real List Variable (t)
exp_C_Volume_R4:
               Real List Variable (t)
exp_C_Volume_R5:
               Real List Variable (t)
exp_C_Volume_R6:
               Real List Variable (t)
exp_C_VS_FW1:  Real List Variable (t)
exp_C_VS_R1:   Real List Variable (t)
exp_C_VS_R2:   Real List Variable (t)
exp_C_VS_R3:   Real List Variable (t)
exp_C_VS_R4:   Real List Variable (t)
exp_C_VS_R5:   Real List Variable (t)
exp_C_VS_R6:   Real List Variable (t)
exp_p_ch4:     Real List Variable (t)
exp_p_co2:     Real List Variable (t)
exp_VS_I2:     Real List Variable (t)
exp_VS_I3:     Real List Variable (t)
fbio_checksum: fbio_Xsu+fbio_Xaa+fbio_Xfa+fbio_Xc4+fbio_Xpro+fbio_Xac+fb
               io_Xh2
fbio_Xaa:      0.33795
fbio_Xac:      0.217977
fbio_Xc4:      0.123789
fbio_Xfa:      0.0696539
fbio_Xh2:      0.0908587
fbio_Xpro:     0.0393518
fbio_Xsu:      0.120419
fCarbs_ALA:    0.6272
fCarbs_FW:     0.3629
fCarbs_GW:     0.5471
fCarbs_PM:     0.6245
fd_ALA:        1.0806657
fd_FW:         0.9
fd_GW:         0.38
fd_PM:         0.682
fLipid_ALA:    1-fProtein_ALA-fCarbs_ALA
fLipid_FW:     1-fProtein_FW-fCarbs_FW
fLipid_GW:     1-fProtein_GW-fCarbs_GW
fLipid_PM:     1-fProtein_PM-fCarbs_PM
fProtein_ALA:  0.335
fProtein_FW:   0.202
fProtein_GW:   0.19
fProtein_PM:   0.238
fS_ALA:        0
fS_FW:         0
fS_GW:         0
fS_PM:         0
fXr_ALA:       0.05
fXr_FW:        0.34
fXr_GW:        0.51
fXr_PM:        0.245
f_ac_aa:       0.32486
f_ac_su:       0.67*nue_1_su+0.22*nue_2_su
f_bu_aa:       0.26301
f_bu_su:       0.83*nue_3_su
f_ch_xc:       0.2
f_ch_xc_INO:   0.2
f_fa_li:       0.95
f_h2_aa:       0.08368
f_h2_su:       0.33*nue_1_su+0.17*nue_3_su
f_li_xc:       1-f_ch_xc-f_pr_xc-f_SI_xc-f_XI_xc
```

```
f_li_xc_INO:    1-f_ch_xc_INO-f_pr_xc_INO-f_SI_xc-f_XI_xc
f_pro_aa:       0.06291
f_pro_su:       0.78*nue_2_su
f_pr_xc:        0.2
f_pr_xc_INO:    0.2
f_SI_xc:        0.1
f_va_aa:        0.26555
f_XI_xc:        0.2
gasCH4flow:      if P_headspace<P_atm then 0 else (p_ch4_percentage/100)*
                V*(P_headspace-P_atm)/P_atm*(T_ref_gas/T)*(P_headspace/P_
                ref_gas)*gas_coef endif
gasCH4flow_probe:
                gasCH4flow(headspace,Bulk Volume,0)
gasCO2flow:      if P_headspace<P_atm then 0 else (p_co2_percentage/100)*
                V*(P_headspace-P_atm)/P_atm*(T_ref_gas/T)*(P_headspace/P_
                ref_gas)*gas_coef endif
gasCO2flow_probe:
                gasCO2flow(headspace,Bulk Volume,0)
gasflow:         if P_headspace<P_atm then 0 else V*(P_headspace-P_atm)/P
                _atm*gas_coef endif
gasflow_probe: gasflow(headspace,Bulk Volume,0)
gasH2flow:       if P_headspace<P_atm then 0 else (p_h2_percentage/100)*V
                *(P_headspace-P_atm)/P_atm*(T_ref_gas/T)*(P_headspace/P_r
                ef_gas)*gas_coef endif
gasH2flow_probe:
                gasH2flow(headspace,Bulk Volume,0)
gasH2Oflow:      if P_headspace<P_atm then 0 else (p_h2o_percentage/100)*
                V*(P_headspace-P_atm)/P_atm*(T_ref_gas/T)*(P_headspace/P_
                ref_gas)*gas_coef endif
gas_coef:       3000
HRT:            V_reactor/(V_inflow/t)
hydCNT_ch_s_GW:10
INI_COD_Tot:    INI_VS*CODVS_INO
INI_San:        0
INI_Scat:       0.056846502
INI_S_aa:       INI_S_TOT*INI_S_aa_alpha
INI_S_aa_alpha:0.0458598
INI_S_ac:       0.065805
INI_S_ac_ion:   0.01923522
INI_S_bu:       1.82e-005
INI_S_bu_ion:   1.81842e-005
INI_S_fa:       INI_S_TOT*INI_S_fa_alpha
INI_S_fa_alpha:0.850984
INI_S_hco3_ion:0.12718351
INI_S_h_ion:    1.25893e-008
INI_S_I:        0.328698
INI_S_IN:       0.077777778
INI_S_nh3:      0.006365177
INI_S_nh4_ion:  0.071412601
INI_S_oh_ion:   1.67015e-006
INI_S_pro:      1.51e-005
INI_S_pro_ion:  1.50856e-005
INI_S_su:       INI_S_TOT*INI_S_su_alpha
INI_S_su_alpha:0.103156
INI_S_TOT:      0.1
INI_S_va:       0.0096237
INI_S_va_ion:   0.009616062
INI_TS:         16.2
INI_VS:         0.51*INI_TS
INI_X_ash:      INI_TS-INI_VS
INI_X_biomass:  1
INI_X_ch_alpha_INO:
                0.174665
INI_X_ch_INO:   INI_X_TOT_INO*INI_X_ch_alpha_INO
INI_X_c_INO:    0.29639796
INI_X_I:        INI_COD_Tot-INI_S_I-INI_X_biomass-INI_X_c_INO-INI_X_li_IN
                O-INI_X_pr_INO-INI_X_ch_INO-INI_S_aa-INI_S_fa-INI_S_su-IN
                I_S_ac-INI_S_ac_ion-INI_S_pro-INI_S_pro_ion-INI_S_bu-INI_
                S_bu_ion-INI_S_va-INI_S_va_ion
INI_X_li_alpha_INO:
                0.184264
INI_X_li_INO:   INI_X_TOT_INO*INI_X_li_alpha_INO
INI_X_pr_alpha_INO:
                1-INI_X_li_alpha_INO-INI_X_ch_alpha_INO
INI_X_pr_INO:   INI_X_TOT_INO*INI_X_pr_alpha_INO
INI_X_TOT_INO: 0.1
input_AN_ALA:   0
input_AN_FW:    0
input_AN_GW:    0.002098853
```

```
input_AN_PM:   0
input_CAT_ALA: 0.075577189
input_CAT_FW:  0.013
input_CAT_GW:  0
input_CAT_PM:  0.18198176
input_CODin_ALA:
               1107.2597
input_CODin_FW:440.3
input_CODin_GW:391.4
input_CODin_PM:317.72663
input_Qin_ALA: input_Qin_dyn_ALA_R1
input_Qin_dyn_ALA_R1:
               Real List Variable (t)
input_Qin_dyn_ALA_R3:
               Real List Variable (t)
input_Qin_dyn_ALA_R5:
               Real List Variable (t)
input_Qin_dyn_FW_R1:
               Real List Variable (t)
input_Qin_dyn_FW_R3:
               Real List Variable (t)
input_Qin_dyn_FW_R5:
               Real List Variable (t)
input_Qin_dyn_GW_R1:
               Real List Variable (t)
input_Qin_dyn_GW_R3:
               Real List Variable (t)
input_Qin_dyn_GW_R5:
               Real List Variable (t)
input_Qin_dyn_PM_R1:
               Real List Variable (t)
input_Qin_dyn_PM_R3:
               Real List Variable (t)
input_Qin_dyn_PM_R5:
               Real List Variable (t)
input_Qin_dyn_WATER_R1:
               Real List Variable (t)
input_Qin_dyn_WATER_R3:
               Real List Variable (t)
input_Qin_dyn_WATER_R5:
               Real List Variable (t)
input_Qin_FW:  input_Qin_dyn_FW_R1
input_Qin_GW:  input_Qin_dyn_GW_R1
input_Qin_PM:  input_Qin_dyn_PM_R1
input_Qin_WATER:
               input_Qin_dyn_WATER_R1
input_Qout:    input_Qout_dyn_R1
input_Qout_dyn_R1:
               Real List Variable (t)
input_Qout_dyn_R3:
               Real List Variable (t)
input_Qout_dyn_R5:
               Real List Variable (t)
input_SIC_ALA: 0.0985564
input_SIC_FW:  0
input_SIC_GW:  0
input_SIC_PM:  0.144937
input_SIN_ALA: 0
input_SIN_FW:  0.038
input_SIN_GW:  0.045
input_SIN_PM:  0.155575
input_S_ac_ALA:0
input_S_ac_FW: 3.241
input_S_ac_GW: 4.465
input_S_ac_PM: 10.680272
input_S_bu_ALA:0
input_S_bu_FW: 9.369
input_S_bu_GW: 0.878
input_S_bu_PM: 8.4234549
input_S_h_ion_ALA:
               1.3e-007
input_S_h_ion_FW:
               1.82e-005
input_S_h_ion_GW:
               1.41e-005
input_S_h_ion_PM:
               5.01187e-007
input_S_OH_ion_ALA:
               6.10074e-008
```

```
input_S_OH_ion_FW:
                4.42e-010
input_S_OH_ion_GW:
                5.69e-010
input_S_OH_ion_PM:
                1.60466e-008
input_S_pro_ALA:
                0
input_S_pro_FW:0.04
input_S_pro_GW:0.337
input_S_pro_PM:4.7819259
input_S_va_ALA:0
input_S_va_FW: 0.004
input_S_va_GW: 0.068
input_S_va_PM: 3.4274076
input_S_Xd_ALA:input_Xd_ALA*fS_ALA
input_S_Xd_FW: input_Xd_FW*fS_FW
input_S_Xd_GW: input_Xd_GW*fS_GW
input_S_Xd_PM: input_Xd_PM*fS_PM
input_Xd_ALA:  input_CODin_ALA*fd_ALA
input_Xd_FW:   input_CODin_FW*fd_FW
input_Xd_GW:   input_CODin_GW*fd_GW
input_Xd_PM:   input_CODin_PM*fd_PM
input_XI_ALA:  input_CODin_ALA*(1-fd_ALA)
input_XI_FW:   input_CODin_FW*(1-fd_FW)
input_XI_GW:   input_CODin_GW*(1-fd_GW)
input_XI_PM:   input_CODin_PM*(1-fd_PM)
input_X_ash_ALA:
                35.9313
input_X_ash_FW:32.85
input_X_ash_GW:137.97
input_X_ash_PM:36.8
input_X_Xd_ALA:input_Xd_ALA*(1-fS_ALA)
input_X_Xd_FW: input_Xd_FW*(1-fS_FW)
input_X_Xd_GW: input_Xd_GW*(1-fS_GW)
input_X_Xd_PM: input_Xd_PM*(1-fS_PM)
I_ac_ac:       1
I_ac_h2:       1
I_ac_pro:      1
I_fa_ac:       1/(1+S_fa/KI_fa_ac)
I_fa_fa:       1/(1+S_fa/KI_fa_fa)
I_h2_acox:     1/(S_h2/KI_h2_acox+1)
I_h2_c4:       1/(S_h2/KI_h2_c4+1)
I_h2_fa:       1/(S_h2/KI_h2_fa+1)
I_h2_pro:      1/(S_h2/KI_h2_pro+1)
I_Hac_ac_mM:   1/(1+S_Hac_mM/KI_Hac_ac_mM)
I_Hac_H2:      1/(1+S_Hac/KI_Hac_H2_mM)
I_Hac_VFAs:    1/(1+S_Hac/KI_Hac_VFAs)
I_HVFA_ac_h2:  1/(1+S_HVFA_mM/KI_HVFA_ac_h2)
I_HVFA_ac_h2_mM:
                1/(1+S_HVFA_mM/KI_HVFA_ac_h2_mM)
I_HVFA_ac_mM:  1/(1+S_HVFA_mM/KI_HVFA_ac_mM)
I_HVFA_bac_mM: 1/(1+S_HVFA_mM/KI_HVFA_bac_mM)
I_HVFA_bu_mM:  1/(1+S_HVFA_mM/KI_HVFA_bu_mM)
I_HVFA_fa_mM:  1/(1+S_HVFA_mM/KI_HVFA_fa_mM)
I_HVFA_fer_mM: 1/(1+S_HVFA_mM/KI_HVFA_fer_mM)
I_HVFA_h2_mM:  1/(1+S_HVFA_mM/KI_HVFA_h2_mM)
I_HVFA_meth_mM:1/(1+S_HVFA_mM/KI_HVFA_meth_mM)
I_HVFA_pro_mM: 1/(1+S_HVFA_mM/KI_HVFA_pro_mM)
I_HVFA_va_mM:  1/(1+S_HVFA_mM/KI_HVFA_va_mM)
I_HVFA_VFAs_mM:1/(1+S_HVFA_mM/KI_HVFA_VFAs_mM)
I_nh3_ac:      1/(S_nh3/KI_nh3_ac+1)
I_nh3_acox:    1/(S_nh3/KI_nh3_acox+1)
I_nh3_acox_W:  1/(1+exp(-KI_nh3_acox_sl*(KI_nh3_acox-S_nh3)))
I_nh3_ac_W:    1/(1+exp(-KI_nh3_ac_sl*(KI_nh3_ac-S_nh3)))
I_NH_limit:     if S_IN<0 then 0 else 1/(Ks_IN/S_IN+1) endif
I_ph_ac:        if pH<I_ph_ac_ul then exp(-3*((pH-I_ph_ac_ul)/(I_ph_ac_u
                l-I_ph_ac_ll))^2) else 1 endif
I_ph_ac_ll:    6
I_ph_ac_ul:    7
I_ph_bac:       if pH<I_ph_bac_ul then exp(-3*((pH-I_ph_bac_ul)/(I_ph_ba
                c_ul-I_ph_bac_ll))^2) else 1 endif
I_ph_bac_ll:   4
I_ph_bac_ul:   5.5
I_ph_h2:       1
I_ph_h2_ll:    5
I_ph_h2_ul:    6
I_VFA_ac:      1/(1+S_VFA/KI_VFA_ac)
I_VFA_bu:      1
```

```
I_VFA_fer:      if S_VFA>KI_VFA_fer then 0 else 1-(S_VFA/KI_VFA_fer) end
                if
I_VFA_H2:       1/(1+S_VFA/KI_VFA_H2)
I_VFA_pro:      1
I_VFA_va:       1
kAB_co2:        1e+014
Ka_ac:          10^(-pKa_ac)
Ka_bu:          10^(-pKa_bu)
Ka_co2:         10^(-pKa_co2)*exp(deltaH0_Ka_co2/(R*100)*(1/298-1/T))
Ka_fa:          10^(-pKa_fa)
Ka_h2o:         10^(-pKa_h2o)*exp(deltaH0_Ka_h2o/(R*100)*(1/298-1/T))
Ka_nh4:         10^(-pKa_nh3)*exp(deltaH0_Ka_nh4/(R*100)*(1/298-1/T))
Ka_pro:         10^(-pKa_pro)
Ka_va:          10^(-pKa_va)
kdec_xaa:       0.02
kdec_xac:       0.02
kdec_xc4:       0.02
kdec_xfa:       0.02
kdec_xh2:       0.02
kdec_xpro:      0.02
kdec_xsu:       0.02
kdis:           0.5
khyd_INO:       0.20663267
khyd_li_INO:    khyd_INO
khyd_li_r_ALA:  khyd_r_ALA
khyd_li_r_FW:   khyd_r_FW
khyd_li_r_GW:   khyd_r_GW
khyd_li_r_PM:   khyd_r_PM
khyd_li_s_ALA:  khyd_s_ALA
khyd_li_s_FW:   khyd_s_FW
khyd_li_s_GW:   khyd_s_GW
khyd_li_s_PM:   khyd_s_PM
khyd_pr_INO:    khyd_INO
khyd_pr_r_ALA:  khyd_r_ALA
khyd_pr_r_FW:   khyd_r_FW
khyd_pr_r_GW:   khyd_r_GW
khyd_pr_r_PM:   khyd_r_PM
khyd_pr_s_ALA:  khyd_s_ALA
khyd_pr_s_FW:   khyd_s_FW
khyd_pr_s_GW:   khyd_s_GW
khyd_pr_s_PM:   khyd_s_PM
khyd_r_ALA:     0.9
khyd_r_FW:      18.91
khyd_r_GW:      5.72
khyd_r_PM:      2.085
khyd_s_ALA:     0.724
khyd_s_FW:      0.68
khyd_s_GW:      0.21
khyd_s_PM:      0.13
KH_ch4:         0.0014*R*T*exp(deltaH0_KH_ch4/(R*100)*(1/298-1/T))
KH_co2:         0.035*R*T*exp(deltaH0_KH_co2/(R*100)*(1/298-1/T))
KH_h2:          0.00078*R*T*exp(deltaH0_KH_h2/(R*100)*(1/298-1/T))
KI_ac_ac:       1.6211151
KI_ac_pro:      1.6211151
KI_fa_ac:       0.90563403
KI_fa_fa:       KI_fa_ac*7
KI_h2_acox:     3e-006*KI_h2_alpha
KI_h2_alpha:    1
KI_h2_c4:       1e-005*KI_h2_alpha
KI_h2_fa:       5e-006*KI_h2_alpha
KI_h2_pro:      3.5e-006*KI_h2_alpha
KI_Hac_ac_mM:   0.5
KI_Hac_H2_mM:   0.46
KI_Hac_VFAs:    0.01
KI_HVFA_ac_h2:  0.017357102
KI_HVFA_ac_h2_mM:
                0.1
KI_HVFA_ac_mM:  0.13284142
KI_HVFA_bac_mM:0.4
KI_HVFA_bu_mM:  KI_HVFA_VFAs_mM
KI_HVFA_fa_mM:  2.56
KI_HVFA_fer_mM:0.008200509
KI_HVFA_h2_mM:  0.11812046
KI_HVFA_meth_mM:
                0.12719036
KI_HVFA_pro_mM:KI_HVFA_VFAs_mM
KI_HVFA_va_mM:  KI_HVFA_VFAs_mM
KI_HVFA_VFAs_mM:
                0.017813168
```

```
KI_nh3_ac:      0.0032
KI_nh3_acox:    0.004877952
KI_nh3_acox_sl:180
KI_nh3_ac_sl:   360
KI_VFA_ac:      5.2
KI_VFA_bu:      KI_VFA_ac
KI_VFA_fer:     15
KI_VFA_H2:      KI_VFA_ac
KI_VFA_pro:     KI_VFA_ac
KI_VFA_va:      KI_VFA_ac
KLa:            V_reactor*kLa
kLa:            100
km_aa:          50
km_ac:          8
km_acox:        6.9
km_c4:          20
km_fa:          6
km_h2:          35
km_pro:         13
km_su:          30
Ks_aa:          0.3
Ks_ac:          0.15
Ks_c4:          0.2
Ks_fa:          0.4
Ks_h2:          7e-006
Ks_IN:          0.0001
Ks_pro:         0.15
Ks_su:          0.5
mue_X_aa:       km_aa*X_aa*S_aa/(Ks_aa+S_aa)*I_ph_bac*I_NH_limit*Y_aa*I_V
                FA_fer
mue_X_ac:       km_ac*X_ac*S_ac/(Ks_ac+S_ac)*I_ph_ac*I_nh3_ac*I_NH_limit*
                Y_ac*I_VFA_ac
mue_X_c4:       km_c4*X_c4*S_bu/(Ks_c4+S_bu)*S_bu/(S_bu+S_va+0.1)*I_ph_ba
                c*I_h2_c4*I_NH_limit*Y_c4+km_c4*X_c4*S_va/(Ks_c4+S_va)*S_
                va/(S_va+S_bu+0.1)*I_ph_bac*I_h2_c4*I_NH_limit*Y_c4
mue_X_fa:       km_fa*X_fa*S_fa/(Ks_fa+S_fa)*I_ph_bac*I_h2_c4*Y_fa
mue_X_h2:       km_h2*X_h2*S_h2/(Ks_h2+S_h2)*I_ph_h2*I_NH_limit*Y_h2*I_ac
                _h2
mue_X_pro:      km_pro*X_pro*S_pro/(Ks_pro+S_pro)*I_ph_bac*I_h2_pro*I_NH_
                limit*Y_h2*I_ac_pro
mue_X_su:       km_su*X_su*S_su/(Ks_su+S_su)*I_ph_bac*I_NH_limit*Y_su*I_V
                FA_fer
nue_1_su:       0.495
nue_2_su:       0.345
nue_3_su:       1-nue_1_su-nue_2_su
N_aa_avg:       0.00768
N_aa_FW:        0.007965
N_aa_GW:        0.007613
N_aa_INO:       0.00748503
N_biom:         0.00625
N_SI:           0.00428571
N_Xc:           0.00278272
N_Xc_INO:       0.00278272
N_XI:           0.00428571
pH:             -log10(S_h_ion)
pH_reactor:     pH(reactor,Bulk Volume,0)
pKa_ac:         4.76
pKa_bu:         4.84
pKa_co2:        6.35
pKa_fa:         4.78
pKa_h2o:        14
pKa_nh3:        9.25
pKa_pro:        4.88
pKa_va:         4.8
P_atm:          1.013
p_ch4:          S_ch4/64*R*T
p_ch4_dry:      p_ch4/(p_ch4+p_co2)*100
p_ch4_percentage:
                p_ch4/P_headspace*100
p_ch4_probe:    p_ch4_percentage(headspace,Bulk Volume,0)
p_co2:          S_co2*R*T
p_co2_dry:      p_co2/(p_ch4+p_co2)*100
p_co2_percentage:
                p_co2/P_headspace*100
p_h2:           S_h2/16*R*T
p_h2o:          0.0313*exp(5290*(1/298-1/T))
p_h2o_percentage:
                p_h2o/P_headspace*100
p_h2_percentage:
```

```
                p_h2/P_headspace*100
P_headspace:    p_co2+p_h2+p_ch4+p_h2o
P_ref_gas:      1
Qout:           Discharge
R:              0.08314
SX_ratio:       VS_hydrolizableGW/VS_biomass
S_aa:           Dyn. Volume State Var.
S_ac:           Dyn. Volume State Var.
S_ac_ion:       Eq. State Variable
S_an:           Dyn. Volume State Var.
S_bu:           Dyn. Volume State Var.
S_bu_ion:       Eq. State Variable
S_cat:          Dyn. Volume State Var.
S_ch4:          Dyn. Volume State Var.
S_co2:          Dyn. Volume State Var.
S_fa:           Dyn. Volume State Var.
S_fa_ion:       Eq. State Variable
S_h2:           Dyn. Volume State Var.
S_Hac:          S_ac-S_ac_ion
S_Hac_mM:       S_Hac*1000/64
S_Hbu:          S_bu-S_bu_ion
S_hco3_ion:     Dyn. Volume State Var.
S_Hpro:         S_pro-S_pro_ion
S_Hva:          S_va-S_va_ion
S_HVFA_mM:      S_Hac*1000/64+S_Hpro*1000/112+S_Hbu*1000/160+S_Hva*1000/2
                08
S_h_ion:        Eq. State Variable
S_I:            Dyn. Volume State Var.
S_IN:           Dyn. Volume State Var.
S_nh3:          Eq. State Variable
S_nh4_ion:      Eq. State Variable
S_oh_ion:       Eq. State Variable
S_pro:          Dyn. Volume State Var.
S_pro_ion:      Eq. State Variable
S_su:           Dyn. Volume State Var.
S_va:           Dyn. Volume State Var.
S_va_ion:       Eq. State Variable
S_VFA:          S_ac+S_pro+S_bu+S_va
T:              308.15
t:              Time
TS:             VS_R1+X_ash
T_headspace_gas:
                298.15
T_ref_gas:      273.15
uM_aa:           if X_aa>0 then u_aa/X_aa else 0 endif
uM_ac:           if X_ac>0 then u_ac/X_ac else 0 endif
uM_bu:           if X_c4>0 then u_bu/X_c4 else 0 endif
uM_fa:           if X_fa>0 then u_fa/X_fa else 0 endif
uM_h2:           if X_h2>0 then u_h2/X_h2 else 0 endif
uM_pro:          if X_pro>0 then u_pro/X_pro else 0 endif
uM_su:           if X_su>0 then u_su/X_su else 0 endif
uM_va:           if X_c4>0 then u_va/X_c4 else 0 endif
u_aa:           km_aa*X_aa*S_aa/(Ks_aa+S_aa)*I_NH_limit*I_HVFA_fer_mM
u_ac:           km_ac*X_ac*S_ac/(Ks_ac+S_ac)*I_nh3_ac*I_NH_limit*I_HVFA_a
                c_mM*I_fa_ac
u_acox:         km_acox*X_acox*S_ac/(Ks_ac+S_ac)*I_nh3_acox_W*I_NH_limit*
                I_HVFA_ac_h2
u_bu:           km_c4*X_c4*S_bu/(Ks_c4+S_bu)*1/(1+S_va/S_bu)*I_h2_c4*I_NH
                _limit*I_HVFA_VFAs_mM
u_fa:           km_fa*X_fa*S_fa/(Ks_fa+S_fa)*I_h2_fa*I_NH_limit*I_ph_bac
u_h2:           km_h2*X_h2*S_h2/(Ks_h2+S_h2)*I_NH_limit*I_HVFA_h2_mM
u_pro:          km_pro*X_pro*S_pro/(Ks_pro+S_pro)*I_h2_pro*I_NH_limit*I_p
                h_bac*I_HVFA_VFAs_mM
u_su:           km_su*X_su*S_su/(Ks_su+S_su)*I_NH_limit*I_HVFA_fer_mM
u_va:           km_c4*X_c4*S_va/(Ks_c4+S_va)*1/(1+S_bu/S_va)*I_h2_c4*I_NH
                _limit*I_HVFA_VFAs_mM
V:              Reactor Volume
VS_biomass:     (X_aa+X_ac+X_c4+X_fa+X_h2+X_pro+X_su)/CODVS_biomass
VS_hydrolizableGW:
                (X_c+X_c_INO)/CODVS_Xc+(X_ch_INO+X_ch_r_GW+X_ch_s_GW)/COD
                VS_ch+(X_li_INO+X_li_r_GW+X_li_s_GW)/CODVS_li+(X_pr_INO+X
                _pr_s_GW+X_pr_r_GW)/CODVS_pr_GW
VS_inconv_GWFW:(X_ch_INO+X_ch_r_FW+X_ch_s_FW+X_ch_r_GW+X_ch_s_GW+S_su)/C
                ODVS_ch+(X_li_INO+X_li_r_FW+X_li_s_FW+X_li_r_GW+X_li_s_GW
                +S_fa)/CODVS_li+(X_pr_INO+X_pr_s_FW+X_pr_r_FW+X_pr_s_GW+X
                _pr_r_GW+S_aa)/CODVS_pr_GW+S_va/2.04+S_bu/1.82+S_pro/1.51
                +S_ac/1.07
VS_inconv_R1:   (X_ch_INO+X_ch_r_FW+X_ch_s_FW+X_ch_r_GW+X_ch_s_GW+X_ch_r_
                ALA+X_ch_s_ALA+X_ch_r_PM+X_ch_s_PM+S_su)/CODVS_ch+(X_li_I
```

```
                NO+X_li_r_FW+X_li_s_FW+X_li_r_GW+X_li_s_GW+X_li_r_PM+X_li
                _s_PM+X_li_r_ALA+X_li_s_ALA+S_fa)/CODVS_li+(X_pr_INO+X_pr
                _s_FW+X_pr_r_FW+X_pr_s_GW+X_pr_r_GW+X_pr_s_ALA+X_pr_r_ALA
                +X_pr_s_PM+X_pr_r_PM+S_aa)/CODVS_pr_GW
VS_inerts:      (X_I+S_I)/CODVS_I
VS_R1:          (X_ch_INO+X_ch_r_FW+X_ch_s_FW+X_ch_r_GW+X_ch_s_GW+X_ch_r_
                ALA+X_ch_s_ALA+X_ch_r_PM+X_ch_s_PM+S_su)/CODVS_ch+(X_li_I
                NO+X_li_r_FW+X_li_s_FW+X_li_r_GW+X_li_s_GW+X_li_r_PM+X_li
                _s_PM+X_li_r_ALA+X_li_s_ALA+S_fa)/CODVS_li+(X_pr_INO+X_pr
                _s_FW+X_pr_r_FW+X_pr_s_GW+X_pr_r_GW+X_pr_s_ALA+X_pr_r_ALA
                +X_pr_s_PM+X_pr_r_PM+S_aa)/CODVS_pr_avg+S_va/2.04+S_bu/1.
                82+S_pro/1.51+S_ac/1.07+(X_I+S_I)/CODVS_I+(X_aa+X_ac+X_c4
                +X_fa+X_h2+X_pro+X_su)/CODVS_biomass
VS_XC:          (X_c+X_c_INO)/CODVS_Xc
V_fedCOD:       V(inCOD_degradable,Bulk Volume,0)
V_gasCH4COD_exp:
                exp_C_Volume_R1*2.82
V_gasCH4COD_sim:
                V_gasCH4_sim*2.82
V_gasCH4_sim:   V(gasCH4,Bulk Volume,0)
V_inflow:       V(inflow,Bulk Volume,0)
V_outCOD:       V(outCOD_sim,Bulk Volume,0)
V_outflow:      V(outflow,Bulk Volume,0)
V_outVFA:       V(outVFA_exp,Bulk Volume,0)
V_reactor:      V(reactor,Bulk Volume,0)
X_aa:           Dyn. Volume State Var.
X_aa_ini:       fbio_Xaa*INI_X_biomass
X_ac:           Dyn. Volume State Var.
X_acox:         Dyn. Volume State Var.
X_acox_ini:     0
X_ac_ini:       fbio_Xac*INI_X_biomass
X_ash:          Dyn. Volume State Var.
X_biomass:      X_aa+X_ac+X_c4+X_fa+X_h2+X_pro+X_su
X_c:            Dyn. Volume State Var.
X_c4:           Dyn. Volume State Var.
X_c4_ini:       fbio_Xc4*INI_X_biomass
X_ch_INO:       Dyn. Volume State Var.
X_ch_r_ALA:     Dyn. Volume State Var.
X_ch_r_FW:      Dyn. Volume State Var.
X_ch_r_GW:      Dyn. Volume State Var.
X_ch_r_PM:      Dyn. Volume State Var.
X_ch_s_ALA:     Dyn. Volume State Var.
X_ch_s_FW:      Dyn. Volume State Var.
X_ch_s_GW:      Dyn. Volume State Var.
X_ch_s_PM:      Dyn. Volume State Var.
X_c_INO:        Dyn. Volume State Var.
X_fa:           Dyn. Volume State Var.
X_fa_ini:       fbio_Xfa*INI_X_biomass
X_h2:           Dyn. Volume State Var.
X_h2_ini:       fbio_Xh2*INI_X_biomass
X_I:            Dyn. Volume State Var.
X_li_INO:       Dyn. Volume State Var.
X_li_r_ALA:     Dyn. Volume State Var.
X_li_r_FW:      Dyn. Volume State Var.
X_li_r_GW:      Dyn. Volume State Var.
X_li_r_PM:      Dyn. Volume State Var.
X_li_s_ALA:     Dyn. Volume State Var.
X_li_s_FW:      Dyn. Volume State Var.
X_li_s_GW:      Dyn. Volume State Var.
X_li_s_PM:      Dyn. Volume State Var.
X_pro:          Dyn. Volume State Var.
X_pro_ini:      fbio_Xpro*INI_X_biomass
X_pr_INO:       Dyn. Volume State Var.
X_pr_r_ALA:     Dyn. Volume State Var.
X_pr_r_FW:      Dyn. Volume State Var.
X_pr_r_GW:      Dyn. Volume State Var.
X_pr_r_PM:      Dyn. Volume State Var.
X_pr_s_ALA:     Dyn. Volume State Var.
X_pr_s_FW:      Dyn. Volume State Var.
X_pr_s_GW:      Dyn. Volume State Var.
X_pr_s_PM:      Dyn. Volume State Var.
X_su:           Dyn. Volume State Var.
X_su_ini:       fbio_Xsu*INI_X_biomass
Y_aa:           0.08
Y_ac:           0.05
Y_acox:         0.04
Y_c4:           0.06
Y_fa:           0.06
Y_h2:           0.06
```

```
Y_pro:          0.04
Y_su:           0.1
ZZ_V_gasometer:V(gasTOT,Bulk Volume,0)
ZZ_V_gasometer_oldCH4:
                ZZ_V_gasometer*p_ch4_percentage/100*(T_ref_gas/T)*(P_atm/
                P_ref_gas)



*****************************************************************************
Processes
*****************************************************************************
decay_aa:       kdec_xaa*X_aa
                   X_c : 1
                   X_aa : -1
                   S_co2 : C_biom-C_Xc
                   S_IN : N_biom-N_Xc
decay_ac:       X_ac*kdec_xac
                   X_ac : -1
                   X_c : 1
                   S_co2 : C_biom-C_Xc
                   S_IN : N_biom-N_Xc
decay_acox:     X_acox*kdec_xac
                   X_acox : -1
                   X_c : 1
                   S_co2 : C_biom-C_Xc
                   S_IN : N_biom-N_Xc
decay_c4:       X_c4*kdec_xc4
                   X_c4 : -1
                   X_c : 1
                   S_co2 : C_biom-C_Xc
                   S_IN : N_biom-N_Xc
decay_fa:       X_fa*kdec_xfa
                   X_fa : -1
                   X_c : 1
                   S_co2 : C_biom-C_Xc
                   S_IN : N_biom-N_Xc
decay_h2:       X_h2*kdec_xh2
                   X_c : 1
                   X_h2 : -1
                   S_co2 : C_biom-C_Xc
                   S_IN : N_biom-N_Xc
decay_pro:      X_pro*kdec_xpro
                   X_pro : -1
                   X_c : 1
                   S_co2 : C_biom-C_Xc
                   S_IN : N_biom-N_Xc
decay_su:       X_su*kdec_xsu
                   X_su : -1
                   X_c : 1
                   S_co2 : C_biom-C_Xc
                   S_IN : N_biom-N_Xc
disintegration:kdis*X_c
                   X_c : -1
                   X_ch_INO : f_ch_xc
                   S_I : f_SI_xc
                   X_pr_INO : f_pr_xc
                   X_I : f_XI_xc
                   X_li_INO : f_li_xc
                   S_IN : N_Xc-f_XI_xc*N_XI-f_SI_xc*N_SI-f_pr_xc*N_aa_INO
                   S_co2 : C_Xc-f_XI_xc*C_XI-f_SI_xc*C_SI-f_pr_xc*C_aa_IN
                   O-f_ch_xc*C_su-f_li_xc*C_li
disintegration_INO:
                kdis*X_c_INO
                   X_c_INO : -1
                   X_ch_INO : f_ch_xc_INO
                   S_I : f_SI_xc
                   X_pr_INO : f_pr_xc_INO
                   X_I : f_XI_xc
                   X_li_INO : f_li_xc_INO
                   S_IN : N_Xc_INO-f_XI_xc*N_XI-f_SI_xc*N_SI-f_pr_xc_INO*
                   N_aa_INO
                   S_co2 : C_Xc_INO-f_XI_xc*C_XI-f_SI_xc*C_SI-f_pr_xc*C_a
                   a_INO-f_ch_xc_INO*C_su-f_li_xc_INO*C_li
dyn_acid_base_co2:
                kAB_co2*(S_hco3_ion*S_h_ion-Ka_co2*S_co2)
                   S_co2 : 1
                   S_hco3_ion : -1
```

```
equilib_ac:    S_ac_ion : 0 = Ka_ac*S_ac-(Ka_ac+S_h_ion)*S_ac_ion
equilib_bu:    S_bu_ion : 0 = Ka_bu*S_bu-(Ka_bu+S_h_ion)*S_bu_ion
equilib_charge:S_h_ion : 0 = S_h_ion+S_cat-S_an-S_oh_ion-S_hco3_ion+S_nh
               4_ion-S_ac_ion/64-S_pro_ion/112-S_bu_ion/160-S_va_ion/208
               -S_fa_ion/736
equilib_fa:    S_fa_ion : 0 = Ka_fa*S_fa-(Ka_fa+S_h_ion)*S_fa_ion
equilib_h2o:   S_oh_ion : 0 = S_oh_ion-Ka_h2o/S_h_ion
equilib_IN:    S_nh4_ion : 0 = S_IN*S_h_ion-(Ka_nh4+S_h_ion)*S_nh4_ion
equilib_IN_bal:S_nh3 : 0 = S_nh3+S_nh4_ion-S_IN
equilib_prop:  S_pro_ion : 0 = Ka_pro*S_pro-(Ka_pro+S_h_ion)*S_pro_ion
equilib_va:    S_va_ion : 0 = Ka_va*S_va-(Ka_va+S_h_ion)*S_va_ion
hyd_ch_INO:    khyd_INO*X_ch_INO
                  S_su : 1
                  X_ch_INO : -1
hyd_ch_r_ALA:  khyd_r_ALA*X_ch_r_ALA
                  S_su : 1
                  X_ch_r_ALA : -1
hyd_ch_r_FW:   khyd_r_FW*X_ch_r_FW
                  S_su : 1
                  X_ch_r_FW : -1
hyd_ch_r_GW:   khyd_r_GW*X_ch_r_GW
                  S_su : 1
                  X_ch_r_GW : -1
hyd_ch_r_PM:   khyd_r_PM*X_ch_r_PM
                  S_su : 1
                  X_ch_r_PM : -1
hyd_ch_s_ALA:  khyd_s_ALA*X_ch_s_ALA
                  S_su : 1
                  X_ch_s_ALA : -1
hyd_ch_s_FW:   khyd_s_FW*X_ch_s_FW
                  S_su : 1
                  X_ch_s_FW : -1
hyd_ch_s_GW:   khyd_s_GW*X_ch_s_GW
                  S_su : 1
                  X_ch_s_GW : -1
hyd_ch_s_PM:   khyd_s_PM*X_ch_s_PM
                  S_su : 1
                  X_ch_s_PM : -1
hyd_li_INO:    khyd_li_INO*X_li_INO
                  S_su : (1-f_fa_li)
                  S_fa : f_fa_li
                  X_li_INO : -1
hyd_li_r_ALA:  khyd_li_r_ALA*X_li_r_ALA
                  S_su : (1-f_fa_li)
                  S_fa : f_fa_li
                  X_li_r_ALA : -1
hyd_li_r_FW:   khyd_li_r_FW*X_li_r_FW
                  S_su : (1-f_fa_li)
                  S_fa : f_fa_li
                  X_li_r_FW : -1
hyd_li_r_GW:   khyd_li_r_GW*X_li_r_GW
                  S_su : (1-f_fa_li)
                  S_fa : f_fa_li
                  X_li_r_GW : -1
hyd_li_r_PM:   khyd_li_r_PM*X_li_r_PM
                  S_su : (1-f_fa_li)
                  S_fa : f_fa_li
                  X_li_r_PM : -1
hyd_li_s_ALA:  khyd_li_s_ALA*X_li_s_ALA
                  S_su : (1-f_fa_li)
                  S_fa : f_fa_li
                  X_li_s_ALA : -1
hyd_li_s_FW:   khyd_li_s_FW*X_li_s_FW
                  S_su : (1-f_fa_li)
                  S_fa : f_fa_li
                  X_li_s_FW : -1
hyd_li_s_GW:   khyd_li_s_GW*X_li_s_GW
                  S_su : (1-f_fa_li)
                  S_fa : f_fa_li
                  X_li_s_GW : -1
hyd_li_s_PM:   khyd_li_s_PM*X_li_s_PM
                  S_su : (1-f_fa_li)
                  S_fa : f_fa_li
                  X_li_s_PM : -1
hyd_pr_INO:    khyd_pr_INO*X_pr_INO
                  S_aa : 1
                  X_pr_INO : -1
hyd_pr_r_ALA:  khyd_pr_r_ALA*X_pr_r_ALA
                  S_aa : 1
```

```
                  X_pr_r_ALA : -1
hyd_pr_r_FW:   khyd_pr_r_FW*X_pr_r_FW
                  S_aa : 1
                  X_pr_r_FW : -1
hyd_pr_r_GW:   khyd_pr_r_GW*X_pr_r_GW
                  S_aa : 1
                  X_pr_r_GW : -1
hyd_pr_r_PM:   khyd_pr_r_PM*X_pr_r_PM
                  S_aa : 1
                  X_pr_r_PM : -1
hyd_pr_s_ALA:  khyd_pr_s_ALA*X_pr_s_ALA
                  S_aa : 1
                  X_pr_s_ALA : -1
hyd_pr_s_FW:   khyd_pr_s_FW*X_pr_s_FW
                  S_aa : 1
                  X_pr_s_FW : -1
hyd_pr_s_GW:   khyd_pr_s_GW*X_pr_s_GW
                  S_aa : 1
                  X_pr_s_GW : -1
hyd_pr_s_PM:   khyd_pr_s_PM*X_pr_s_PM
                  S_aa : 1
                  X_pr_s_PM : -1
uptake_aa:     u_aa
                  S_h2 : (1-Y_aa)*f_h2_aa
                  S_co2 : C_aa_avg-(1-Y_aa)*f_ac_aa*C_ac-(1-Y_aa)*f_bu_a
                  a*C_bu-(1-Y_aa)*f_pro_aa*C_pro-(1-Y_aa)*f_va_aa*C_va-Y
                  _aa*C_biom
                  S_ac : (1-Y_aa)*f_ac_aa
                  S_bu : (1-Y_aa)*f_bu_aa
                  S_aa : -1
                  S_pro : (1-Y_aa)*f_pro_aa
                  S_va : (1-Y_aa)*f_va_aa
                  S_IN : N_aa_avg-Y_aa*N_biom
                  X_aa : Y_aa
uptake_ac:     u_ac
                  S_ac : -1
                  X_ac : Y_ac
                  S_IN : -(N_biom)*Y_ac
                  S_ch4 : (1-Y_ac)
                  S_co2 : C_ac-Y_ac*C_biom-(1-Y_ac)*C_ch4
uptake_ac_acox:km_acox*X_acox*S_ac/(Ks_ac+S_ac)*I_nh3_acox_W*I_NH_limit*
               I_HVFA_ac_h2*I_h2_acox
                  S_ac : -1
                  X_acox : Y_acox
                  S_IN : -(N_biom)*Y_ac
                  S_h2 : (1-Y_acox)
                  S_co2 : C_ac-Y_acox*C_biom
uptake_bu:     u_bu
                  S_h2 : (1-Y_c4)*0.2
                  S_ac : (1-Y_c4)*0.8
                  X_c4 : Y_c4
                  S_IN : -(N_biom)*Y_c4
                  S_bu : -1
uptake_fa:     u_fa
                  S_h2 : (1-Y_fa)*0.3
                  S_ac : (1-Y_fa)*0.7
                  X_fa : Y_fa
                  S_IN : -(N_biom)*Y_fa
                  S_fa : -1
uptake_h2:     u_h2
                  S_h2 : -1
                  X_h2 : Y_h2
                  S_IN : -(N_biom)*Y_h2
                  S_ch4 : (1-Y_h2)
                  S_co2 : -Y_h2*C_biom-(1-Y_h2)*C_ch4
uptake_pro:    u_pro
                  S_h2 : (1-Y_pro)*0.43
                  S_ac : (1-Y_pro)*0.57
                  X_pro : Y_pro
                  S_IN : -(N_biom)*Y_pro
                  S_pro : -1
                  S_co2 : C_pro-(1-Y_pro)*0.57*C_ac-Y_pro*C_biom
uptake_su:     u_su
                  S_h2 : (1-Y_su)*(f_h2_su)
                  S_co2 : C_su-(1-Y_su)*(f_ac_su)*C_ac-(1-Y_su)*f_pro_su
                  *C_pro-(1-Y_su)*f_bu_su*C_bu-Y_su*C_biom
                  S_ac : (1-Y_su)*(f_ac_su)
                  X_su : Y_su
                  S_IN : -(N_biom)*Y_su
```

```
                  S_su : -1
                  S_bu : (1-Y_su)*f_bu_su
                  S_pro : (1-Y_su)*f_pro_su
uptake_va:     u_va
                  S_h2 : (1-Y_c4)*0.15
                  S_ac : (1-Y_c4)*0.31
                  X_c4 : Y_c4
                  S_IN : -(N_biom)*Y_c4
                  S_va : -1
                  S_pro : (1-Y_c4)*0.54



************************************************************************
Compartments
************************************************************************
gasCH4:        Mixed Reactor Compartment
               Active Variables:
               Active Processes:
gasTOT:        Mixed Reactor Compartment
               Active Variables:     S_ch4, S_co2, S_h2
               Active Processes:
headspace:     Mixed Reactor Compartment
               Active Variables:     S_ch4, S_co2, S_h2
               Active Processes:
inCOD_degradable:
               Mixed Reactor Compartment
               Active Variables:
               Active Processes:
inflow:        Mixed Reactor Compartment
               Active Variables:
               Active Processes:
outCOD_sim:    Mixed Reactor Compartment
               Active Variables:
               Active Processes:
outflow:       Mixed Reactor Compartment
               Active Variables:
               Active Processes:
outVFA_exp:    Mixed Reactor Compartment
               Active Variables:
               Active Processes:
reactor:       Mixed Reactor Compartment
               Active Variables:     S_ac_ion, S_bu_ion, S_cat, S_h_ion,
                                      S_nh3, S_nh4_ion, S_oh_ion, S_pro_
                                     ion, S_va_ion, S_aa, S_ac, S_bu, S_
                                     ch4, S_co2, S_fa, S_h2, S_hco3_ion,
                                      S_I, S_IN, S_pro, S_su, S_va, X_aa
                                     , X_ac, X_c, X_c4, X_ch_s_FW, X_fa,
                                      X_h2, X_I, X_pr_s_FW, X_pro, X_su,
                                      S_an, X_ash, X_li_r_FW, X_li_s_FW,
                                      X_pr_r_FW, X_ch_r_FW, X_biomass, a
                                     lkalinity, gasCH4flow, gasflow, gas
                                     flow_probe, pH, pH_reactor, T, t, V
                                     , V_reactor, X_ch_INO, X_c_INO, X_l
                                     i_INO, X_pr_INO, S_fa_ion, X_ch_r_A
                                     LA, X_ch_r_PM, X_ch_s_ALA, X_ch_s_P
                                     M, X_fa_ini, X_h2_ini, X_li_r_ALA,
                                     X_li_r_PM, X_li_s_ALA, X_li_s_PM, X
                                     _pro_ini, X_pr_r_ALA, X_pr_r_PM, X_
                                     pr_s_ALA, X_pr_s_PM, X_ch_r_GW, X_c
                                     h_s_GW, X_li_r_GW, X_li_s_GW, X_pr_
                                     r_GW, X_pr_s_GW
               Active Processes:     dyn_acid_base_co2, decay_aa, decay_
                                     ac, decay_c4, decay_h2, decay_fa, d
                                     ecay_pro, decay_su, equilib_ac, equ
                                     ilib_bu, equilib_charge, equilib_h2
                                     o, equilib_IN, equilib_IN_bal, equi
                                     lib_prop, equilib_va, hyd_ch_s_FW,
                                     hyd_li_s_FW, hyd_pr_s_FW, uptake_aa
                                     , uptake_ac, uptake_bu, uptake_h2,
                                     uptake_fa, uptake_pro, uptake_su, u
                                     ptake_va, disintegration, hyd_ch_r_
                                     FW, hyd_li_r_FW, hyd_pr_r_FW, disin
                                     tegration_INO, hyd_ch_INO, hyd_li_I
                                     NO, hyd_pr_INO, equilib_fa, hyd_ch_
                                     r_ALA, hyd_ch_r_PM, hyd_ch_s_ALA, h
                                     yd_ch_s_PM, hyd_li_r_ALA, hyd_li_r_
                                     PM, hyd_li_s_ALA, hyd_li_s_PM, hyd_
```

```
                                        pr_r_ALA, hyd_pr_r_PM, hyd_pr_s_ALA
                                        , hyd_pr_s_PM, hyd_ch_r_GW, hyd_ch_
                                        s_GW, hyd_li_r_GW, hyd_li_s_GW, hyd
                                        _pr_r_GW, hyd_pr_s_GW


*****************************************************************************
Links
*****************************************************************************
gas_trans:     headspace <-> reactor
```